UNIVERSITY OF SOUTHAMPTON

FACULTY OF ENGINEERING, SCIENCE & MATHEMATICS

School of Ocean & Earth Sciences

Trace metals and nutrients in aerosols over the tropical and subtropical North Atlantic Ocean

by

Matthew David Patey

Thesis for the degree of Doctor of Philosophy

September 2010

UNIVERSITY OF SOUTHAMPTON

ABSTRACT

FACULTY OF ENGINEERING, SCIENCE & MATHEMATICS

SCHOOL OF OCEAN & EARTH SCIENCES

Doctor of Philosophy

Trace metals and nutrients in aerosols over the tropical and subtropical North Atlantic Ocean

by Matthew David Patey

In the first part of this thesis an overview is given of methods available for the analysis of nanomolar nitrate and phosphate in seawater before going on to describe in more detail a system built in our laboratory comprising liquid waveguide capillary cells connected to a conventional segmented-flow autoanalyser. This approach is suitable for routine field measurements of nitrate and phosphate and achieves detection limits of < 1 nM phosphate and nitrate. Investigations were conducted into interferences of silicate and arsenate with the analysis of nanomolar concentrations of SRP, the effect of sample filtration on the measurement of nanomolar nitrate + nitrite and SRP concentrations, and the stability of samples during storage are described. Arsenate interference scaled linearly with phosphate concentrations of up to 50 nM, resulting in an overestimation of SRP concentrations of 4.6 ± 1.4% for an assumed arsenate concentration of 20 nM. The interference effect of added $Si(OH)_4$ on the measured SRP signal is small at the dissolved silicon concentrations typically found in oligotrophic waters. Filtration of surface seawater samples resulted in a decrease in concentration of 1.7 – 2.7 nM (±0.5 nM) SRP, and a small decrease in nitrate concentrations which was within the precision of the method (±0.6 nM). A stability study indicated that storage of very low concentration nutrient samples in the dark at 4°C for less than 24 h resulted in no statistically significant changes in nutrient concentrations.

The second half of this thesis presents a dataset from aerosols collected at the Cape Verde Atmospheric Observatory (CVAO) between July 2007 and July 2008 and collected during a research cruise in the (sub-) tropical North Atlantic Ocean in January 2008. Total acid digestion followed by ICP-MS analysis reveals that the total elemental composition of the dust is close to average crustal composition and shows a high degree of consistency. Based on elemental composition data alone, dust collected on the cruise appears similar to dust collected at the CVAO. Zn and Pb are elevated above crustal values indicating an anthropogenic source, but show an association with periods of high mineral dust concentration. Ultrapure water leaches of dust samples combined with analysis for nutrients and trace metals show a picture of atmospheric concentrations of soluble trace metals and nutrients throughout the year in the study region. Estimated dry deposition fluxes for Fe, and inorganic N and P show a marked difference between summer and winter, with higher Fe and P deposition during winter when mineral dust concentrations are at their greatest, while N inputs are more constant throughout the year. Relative to Redfield ratios, atmospheric inputs are greatly enriched in Fe relative to N and P.

Contents

List of figures

List of tables

List of accompanying material

CDROM containing raw data (in PDF format)

Nanomolar nutrient data from surface (towed fish) and depth profiles (CTD) for 2 cruises:

- PO332 Nutrients Surface
- PO332 CTD
- D326 Nutrients Surface
- D326 CTD

Aerosol measurements from cruise (D326) and Cape Verde Observatory (CVAO) :

- Blank and reference material info
- D326 Totals
- D326 MQ Soluble
- CVAO Totals
- CVAO MQ Soluble

Declaration of authorship

I, Matthew David Patey, declare that the thesis entitled *Aerosol-derived trace metals and nutrients in the tropical and subtropical North Atlantic Ocean* and the work presented in the thesis are both my own, and have been generated by me as the result of my own original research. I confirm that:

- this work was done wholly or mainly while in candidature for a research degree at this University;
- where any part of this thesis has previously been submitted for a degree or any other qualification at this University or any other institution, this has been clearly stated;
- where I have consulted the published work of others, this is always clearly attributed;
- where I have quoted from the work of others, the source is always given. With the exception of such quotations, this thesis is entirely my own work;
- I have acknowledged all main sources of help;
- where the thesis is based on work done by myself jointly with others, I have made clear exactly what was done by others and what I have contributed myself;
- parts of this work have been published as:

  Patey, M. D., Rijkenberg, M. J. A., et al. (2008). Determination of nitrate and phosphate in seawater at nanomolar concentrations. TrAC Trends in Analytical Chemistry 27(2): 169-182

  Patey, M. D., Achterberg, E. P., et al. (2010). Interferences in the analysis of nanomolar concentrations of nitrate and phosphate in oceanic waters. Analytica Chimica Acta 673(2): 109-116.

Signed: ……

Date:……

Acknowledgements

I am grateful to many people whose advice, support and encouragement has made this work possible. First, I must thank my supervisor, Eric Achterberg, whose efforts gave direction to my PhD and made possible all the opportunities for the field work. Second, I received significant help from my co-supervisor, Peter Statham, and Micha Rijkenberg, with whom I had many useful discussions about my research and the data generated. My supervisors and Micha also proof-read chapters of this thesis and gave valuable advice on its content. It is also important to mention that this work has been made possible by the NERC-funded UK SOLAS programme, which funded my studentship and all the research described in this thesis.

Assistance with field work and in the laboratory has also been given by a number of individuals: Paul Gooddy helped to wash bottles for trace-metal sampling in preparation for research cruises. Brian Dickie conducted the ammonium analyses for ultrapure water and seawater leach samples. Mark Stinchcombe gave advice and some help with the construction of the manifold for the nutrient autoanalyser. Matt Mowlem provided advice on processing the data signals from the spectrometers used for nutrient analysis. During the two research cruises Mark Stinchcombe, Claire Powell and Claire Mahaffey helped me on numerous occasions with the soul-destroying task of changing the samples for the nutrient analysis. Neil Jenkinson carried out all the necessary electrical work for the two aerosol samplers, while Nigel Eastwood designed, assembled and programmed the automatic control system for the ship-board aerosol sampler. Ray Collins and John Hewitt prepared the housings for the two aerosol collection systems, and made numerous repairs to the aerosol pumps and other equipment, often at very short notice. Luis Mendes Neves and his brother Paulo changed the filters at the Atmospheric Observatory in Cape Verde then packaged and stored them prior to their transport back to the UK. Thanks are due to Katie Read and her colleagues at the University of York for carrying samples with them on their return from the Cape Verde Atmospheric Observatory. Assistance with preparing over 200 ultra-pure water and seawater leaches from the filters was provided by Pornsri Mingkwan, Sebastian Steigenberger and Patricia López García. Matt Cooper gave a great deal of advice and help with the development of the method for the filter digestions, a process that turned out to be a lot more challenging than anticipated. Andy Milton spent significant amounts of his time giving advice on preparing the samples for ICP-MS determination and calibration issues, not to mention the hours spent setting up the instrument and monitoring the analytical runs for me.

I would also like to mention my parents, Carolyn and David, my brothers, Martin and James, and many friends whose continuous support helped to keep me sane during my long period of candidature. Finally I must thank Patricia, who proof read draft chapters of this thesis and with whom I had many valuable discussions about the data within it. Without her support and encouragement this work might never have been completed.

1. Introduction

1.1 Background

Desert regions cover about one-third of global land area and are the dominant source for an estimated 1700 Tg.year^{-1} (1 Tg ≡ 10^6 tonnes) of dust produced globally (Jickells et al., 2005). Once uplifted, dust particles can remain airborne for periods ranging from a few hours (for particles larger than 10 µm) to several weeks (for particles in the sub-micrometre size range), during which time particles may be transported thousands of kilometres from their source (Mahowald et al., 2005). The Sahara and Sahel desert regions in Africa are the world's largest sources of dust and trade winds transport vast quantities of dust westwards over the North Atlantic Ocean, in turn making it the dustiest ocean region in the world with an estimated 195 Tg of annual dust deposition (Jickells et al., 2005) (see Figure 1.1).

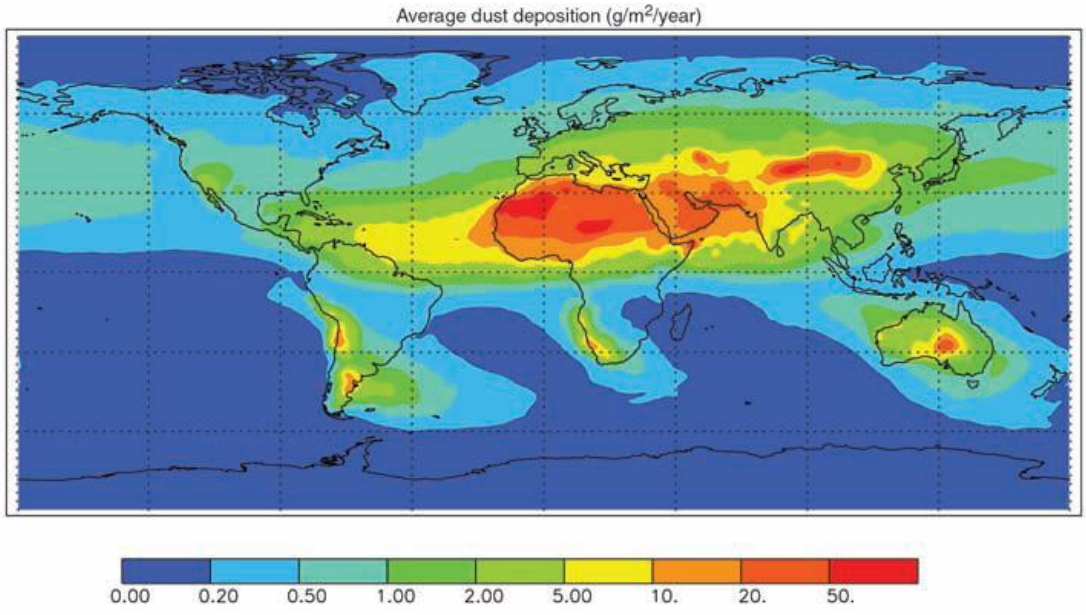

Figure 1.1 Global map of average dust deposition; a composite image based on the output of three modelling studies. Taken from Jickells et al. (2005).

Recorded observations of dust far from land in the North Atlantic go back many centuries; however the first written reports of the phenomenon in the scientific literature were published in the 18th century by Matthew Dobson (Dobson and Fothergill, 1781) and later in the 19th century by Charles Darwin during an

expedition aboard *The Beagle* (Darwin, 1846). In recent decades, research into dust emissions and transport has intensified, due in part to recognition of its important role in the climate system through the scattering and absorption of solar radiation and through the modification of the physical and radiative properties of clouds (Kaufman et al., 2002), but also due to the realisation of the potential role of dust in biogeochemical nutrient cycling in the oceans (Jickells et al., 2005).

1.1.1 Dust as a source of nutrients

Interest in aeolian transport of nutrients was raised following the proposed hypothesis that iron was the limiting nutrient in certain high-nutrient, low-chlorophyll (HNLC) regions of the world's oceans (Martin and Gordon, 1988). This highlighted the potential role of dust-derived nutrients in regulating climate and since then, a great deal of effort has been spent on quantifying aeolian inputs of nutrients, particularly iron, to the world's oceans. The atmosphere is now recognised as a major pathway by which nutrients enter the ocean (Jickells, 1995) and a great deal of work has focussed on quantifying dust emissions, transport and solubility (Jickells et al., 2005; Engelstaedter et al., 2006).

In the eastern tropical and sub-tropical North Atlantic, surface nutrient concentrations are extremely low and it is not possible to identify a single limiting nutrient from standing stock concentrations alone. Nutrient addition bio-assay experiments have shown that while primary production is co-limited by N and P in this region, nitrogen fixation is co-limited by Fe and P (Mills et al., 2004); thus dust inputs may potentially control nitrogen fixation in this ocean region (Moore et al., 2009).

1.1.2 The difficulties in assessing aerosol solubility

A key limitation in assessing the biogeochemical effects of dust inputs into the oceans is the large uncertainty in aerosol solubility. This uncertainty stems from the complexity and number of possible processes occurring between dust production and biological uptake of its nutrient content in the ocean. After becoming air-borne, a dust particle is subjected to a variety of physical and chemical changes,

particularly photochemical induced redox reactions and changes in pH during transport within clouds (Spokes and Jickells, 1995; Mackie et al., 2005). Mineral aerosols may combine with acid species such as sulphuric acid, altering the solubility of contained nutrients. When the dust particle reaches the ocean, another equally complex set of possibilities must be considered. If deposited into the ocean on a calm day, it may pass through a well-established sea-surface micro-layer, collecting a coat of adsorbed organic surfactants on the way (Carrasco et al., 2007). Once in the water column, it may also pass through the gut of zooplankton, potentially increasing the solubility of its constituents (Barbeau et al., 1996). Once dissolved, constituents with very low solubility, such as iron, may be removed from solution by re-precipitation or adsorption to water column particles. In addition to all of this, organic complexation and active biological uptake by phytoplankton may aid dissolution by increasing the solution capacity of the seawater. All of these competing processes will continue for the residence time of the dust particle in the surface layers (Jickells, 1999). It is impossible to design a single experiment that can untangle this complex array of competing processes.

Of the nutrient leaching experiments conducted on dust, the most data exist for iron solubility. Table 1.1 lists some recent estimates of iron solubility from dust, including the methods used. Values ranging from 0.001% to 87% solubility can be found in the literature. Some of this variability is due to the wide variety of dissolution media and analytical techniques used; however it appears that most of the variability is caused by differences in the dust itself (Aguilar-Islas et al., 2010). There is a need for a mechanistic understanding of the factors that affect particle solubility. Differences in iron dissolution can only be understood when the effect of individual parameters on the dissolution process is investigated.

Table 1.1 Recent estimates of Fe solubility from dust in the literature.

Reference	Summary of employed method	Location of sample collection	Types of aerosol sample	Fe solubility % total Fe (range)
Hand et al. (2004)	Fe(II) measurement after aerosol extraction with 0.5mM formate-acetate buffer , pH = 4.5	Atlantic and Pacific Oceans	open ocean	fine mode = 4 ± 9 (0-45) coarse mode = 2 ± 10 (0-87)
Bonnet and Guieu (2004)	seawater pH=8		Saharan anthropogenic	0.001 – 1.6 0.2 – 2.2
Sedwick et al. (2005)	estimated by comparing increase in the DFe inventory of the surface mixed layer with total aeolian Fe deposition.	Bermuda – Atlantic	open ocean	3 – 30
Desboeufs et al. (2005)	aqueous solution, pH = 4.7 for 120 minutes	Cape Verde	loess urban	0.04 – 3
Kocak et al. (2006)	"exchangeable" - 1M ammonium acetate - 15 minutes – pH 7 "oxide / carbonate" 25% acetic acid and 1M hydroxylamine hydrochloride	Eastern Mediterranean	anthropogenic Saharan anthropogenic Saharan	0.8 0.3 8.9 3.5
Buck et al. (2006)	100 ml ultrapure water / seawater drawn through sample filter	North Pacific ocean	Asian dust events	SW = 6 ± 5 H_20 = 9 ± 8
Baker et al. (2006b)	1M ammonium acetate pH =4.7 for 1-2 h	Atlantic Ocean	North Atlantic / remote Saharan	median = 7.8 (4.0-19) median = 1.7 (1.4-4.1)
Chen. (2006)	water Sargasso Sea	Gulf of Aqaba	crustal	water; mean = 5 (0.5 – 19) seawater; mean= 0.7 (0.003 – 2)
Wu et al. (2007)	exposure of sample to successive batches of filtered seawater	Atlantic and Pacific Oceans	Open ocean	1.5 – 6 (N Atlantic) 2.2 – 9.5 (N Pacific)
Aguilar-Islas et al. (2010)	As for Wu et al., (2007)	Alaska California Pacific Ocean	Urban and open ocean	~1 (Urban) 6 – 13 (Open Ocean)
Sedwick et al. (2007)	250 ml ultrapure water / seawater drawn through sample filter	Sargasso Sea - Atlantic	Marine Urban Saharan	0.85 – 2.58 3.93 – 19 0.44 – 2.45

1.1.3 Solubility of macro-nutrients

In dust-influenced areas of the ocean, such as the tropical and sub-tropical North Atlantic Ocean, where primary productivity is not limited solely by Fe, it is essential to consider also nitrogen and phosphorus, since the balance of these nutrients will influence the community structure and may determine whether diazotrophy is enhanced or suppressed (Moore et al., 2009). Saharan aerosols generally contain between 0.06 and 0.2 %wt phosphorus (Ridame and Guieu, 2002). The solubility of phosphate has been investigated using leaching experiments with aerosols

collected by high-volume sampling methods (Herut et al., 2002; Baker et al., 2006b; Chen et al., 2007). However, leaching experiments conducted in bottles have used either unrealistically high concentrations of dust (Ridame and Guieu, 2002) or the phosphate concentrations have been below the detection limit of conventional methods of analysis (Bonnet et al., 2005).

Fewer data are available for the nitrogen content of Saharan aerosols, although Eglinton et al. measured a mean value of 1% total organic carbon (TOC) with a C_{org}/N_{org} ratio of 11.45 in samples collected on a buoy off the west coast of Africa (Eglinton et al., 2002). Experiments conducted with dust concentrations likely to be encountered in the ocean produce concentrations below conventional detection limits (Bonnet et al., 2005). Therefore, in order to measure detectable nitrate concentrations leaching experiments conducted with aerosol samples collected using high-volume samplers (Herut et al., 2002; Baker et al., 2006a) and bottle experiments conducted using very high dust concentrations have been performed (Herut et al., 2005).

In order to quantify the very low, yet possibly significant increase in concentrations of phosphate and nitrate in nutrient-depleted surface seawater after deposition of Saharan aerosols it is necessary to measure these nutrients at nanomolar concentrations.

1.1.4 Studies of dust at Cape Verde

Situated within the main transport area of dust over the tropical North Atlantic, the Cape Verde Islands are an ideal location to study dust inputs to this ocean region. Two main modes of dust transport over the tropical Atlantic Ocean have been identified. During the summer, most of the dust is transported at high altitudes (typically 5 – 6 km) within the so-called Saharan Air Layer. This transport mechanism carries dust as far as the United States and results in a seasonal cycle with maximum dust concentrations between April and October in the western North Atlantic Ocean (Prospero and Lamb, 2003). During the winter, dust transport is restricted to the trade-wind layer, below 1.5 – 3 km altitude, and affects only the

eastern tropical and subtropical North Atlantic. Thus, dust concentrations around the Cape Verde Islands are at a maximum between November and April, while during the summer most of the dust passes over the islands at altitude and concentrations at sea-level are much lower (Chiapello et al., 1995). Figure 1.2 illustrates the principal winds which transport African dust over the Atlantic Ocean.

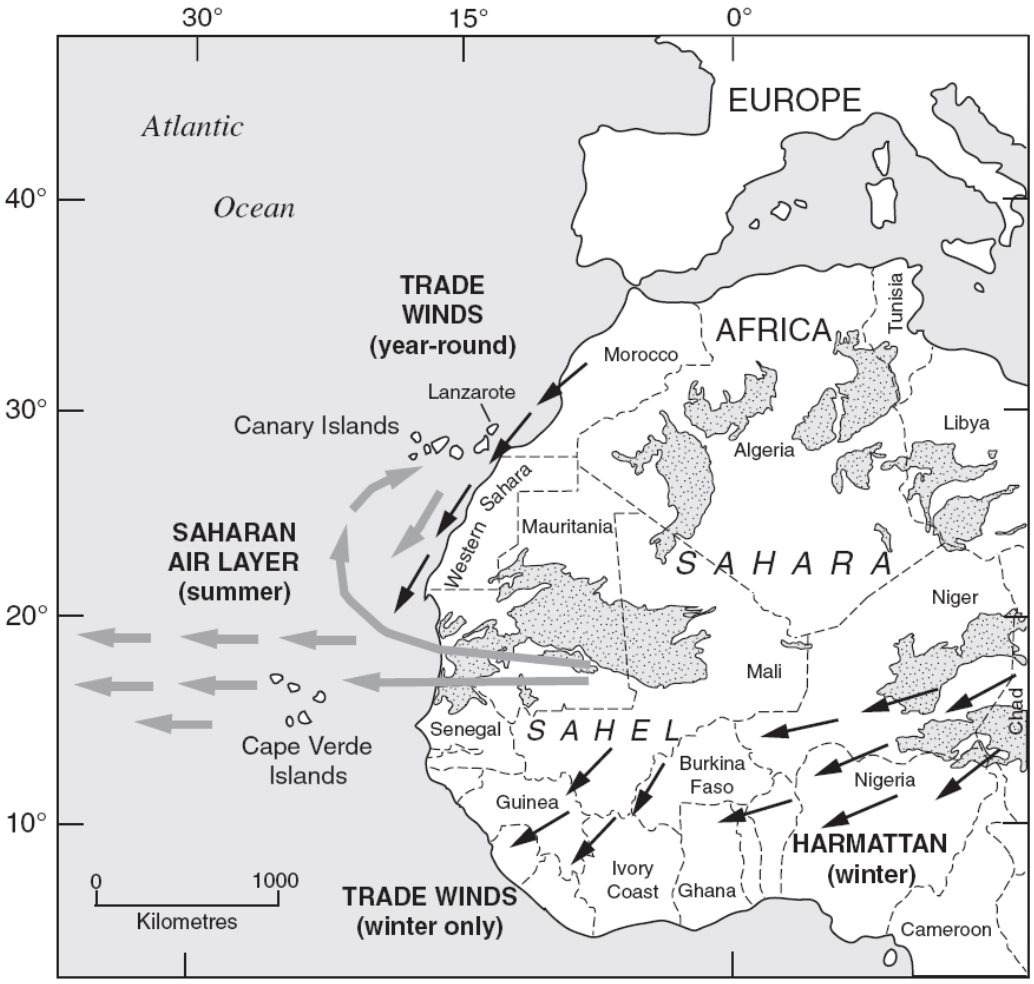

Figure 1.2 Map of north-western Africa showing the principal dust-transporting winds. Taken from Muhs et al. (2010).

Chiapello et al. (1997) collected dust samples on the island of Sal, Cape Verde between 1991 and 1994. Using a combination of geochemical analysis and air-mass back trajectory calculations they identified three distinct source regions with characteristic geochemical signatures: north and west Sahara; south and central Sahara; and the Sahel. Dust originating from north and west Sahara contains relatively high amounts of calcite in comparison with regions to the south and this is

manifested in the elemental ratios Ca/Al, K/Ca and Fe/Ca. Mineralogy measurements as determined by X-ray diffraction forms a key tool for the identification of dust source regions (Caquineau et al., 2002). In particular, the ratio of the clay minerals illite/kaolinite provides a good indicator of dust source, due to the higher abundance of kaolinite in the Sahel than in the Sahara. Strontium isotopes and REE (rare earth element) patterns have also been used to fingerprint source regions of African dust (Chavagnac et al., 2007).

Recent work has highlighted the potentially critical importance of mineralogy and therefore dust source in trace metal solubility (Journet et al., 2008; Schroth et al., 2009). An improved understanding of the composition and source of aerosol dust over the North Atlantic coupled with an understanding of how this relates to trace metal and nutrient solubility would be of great value to modellers wishing to constrain atmospheric nutrient inputs to the ocean in this region.

1.2 Aims and objectives

The principal research aims of this project are to improve knowledge of the composition and variability of dust over the tropical and subtropical eastern North Atlantic Ocean and to investigate its potential impact on dissolved trace metals and nutrients in surface waters of the region. To this end we had the following objectives:

- To construct instruments for nanomolar nitrate and phosphate analysis, and to use this technology on research cruises to obtain precise and accurate measurements of dissolved inorganic nutrients in the surface waters of oligotrophic marine environments.
- To characterise the interference of arsenate and dissolved silicon on phosphate measurements made with our nanomolar nutrient instrument and to investigate other factors (sample filtration and sample storage protocol) that can affect nitrate and phosphate measurements, particularly at ultra-low concentrations.

- To install an aerosol sampler at the Cape Verde Atmospheric Observatory (CVAO) on the Cape Verde Islands and collect a time-series of samples. A combination of total acid digestion, XRD and a simple leaching protocol applied to the samples will give a picture of aerosol composition and solubility and temporal variability over a full seasonal cycle.
- To use a similar sampler to that installed at the CVAO to collect aerosols during a research cruise in the tropical and sub-tropical eastern North Atlantic in January 2008. This data will complement the data from the CVAO and allow assessment of any spatial variations in the dust composition.
- To identify correlations between air-mass source regions and aerosol composition. Furthermore to identify any relationships between the aerosol source and composition that can be used to predict solubility variations.
- To produce an estimate of soluble metal and nutrient fluxes to the ocean and estimate the relative balance of nutrients supplied by dust to the tropical and sub-tropical North Atlantic.

1.3 This study

A massive and increasing amount of research effort is focussed on aerosol inputs to the oceans and their impact on marine biogeochemistry. A literature search using the keywords “dust” and “ocean(s)” yields over 2200 peer-reviewed articles published since 1990 (correct as of March 2011). To further progress in this important field of research there is a pressing need for more aerosol measurements in remote ocean regions. The tropical and sub-tropical North Atlantic receive greater inputs of dust than any other ocean region yet direct measurements of dust are limited to just a few long-term monitoring sites in Barbados, Miami and the Canary Islands, as well as occasional short-term measurements during research cruises. Such measurements are essential to quantify atmospheric aerosol transport, deposition and composition and to characterise particle solubility. The aerosol measurements described in this thesis will make a valuable addition to the few aerosol datasets available in the study region and be of particular use to other researchers interested in nutrient cycling and nitrogen fixation.

Nanomolar nutrient analysis is closely linked with the study of aerosol inputs to the marine environment, since many vast ocean regions that receive significant inputs of dust are oligotrophic environments containing very low surface nutrient concentrations. To assess the impact of dust in such areas, a complete picture of nutrient cycling in the marine environment is essential and this is impossible without accurate measurements of nutrient concentrations. Despite the importance of nanomolar techniques, the necessary analytical methods and sampling procedures have received far less attention than has been given to trace metal analysis and nanomolar nutrient analysis is still some way from becoming the routine oceanographic measurement that it should be. As such, the nutrient development work presented in this thesis will benefit not only those working directly in the field of nanomolar nutrient analysis and instrument development, but also those looking to address questions related to nutrient cycling in oligotrophic environments.

This research has been funded by the Natural Environment Research Council (NERC) through the UK SOLAS programme. SOLAS (Surface Ocean Lower Atmosphere Study) is an international research initiative involving more than 1500 scientists in 23 countries. One of its key aims is to further understanding of key biogeochemical interactions and feedbacks between the ocean and the atmosphere.

1.4 Thesis structure

Chapter 2 describes the instrumental methods associated with aerosol sampling at the Cape Verde Atmospheric Observatory (CVAO) and during a cruise aboard RRS Discovery during January 2008. It describes the instrumentation and sampling approach. The chapter also descibes the chemical methods used to derive total and soluble chemical composition of the dust samples before finally discussing the various analytical methods used with the dust samples and dust extract solutions produced.

Chapter 3 is concerned with the analysis of nanomolar concentrations of nitrate and phosphate in seawater. The chapter begins with a review of the field and compares the relative merits of all the available methods for nanomolar nitrate and phosphate analysis. An instrument for the ship-board measurement of nanomolar nitrate and phosphate that was developed in our laboratory is described in detail. Field data is presented that was collected with the instrument in the tropical and sub-tropical eastern North Atlantic during a research cruise aboard *RV Poseidon* in January and February 2006 (PO332).

Chapter 4 discusses various interferences with the measurement of nanomolar nitrate and phosphate at nanomolar concentrations. Using the system built in our laboratory, experiments were conducted to determine the interference of dissolved silicon ($Si(OH)_4$) and arsenate (AsO_4^{3-}) with phosphate measurement, and to determine the effect of sample filtration on measured nitrate and phosphate concentrations. The results show that the artefacts produced can become very significant when working in this concentration range and highlight the need for careful characterisation of individual systems. Additionally, the issue of sample storage was investigated.

Chapters 5 and 6 present an analysis of dust samples collected at the Cape Verde Atmospheric Observatory and during a research cruise in the tropical and sub-tropical eastern North Atlantic aboard *RRS Discovery* (D326). In Chapter 5 total elemental composition data is presented. An analysis of correlations between concentrations of different elements within the dust reveals three groups of elements associated with crustal, marine and anthropogenic sources. Elemental composition is compared with air-mass source regions. Chapter 6 focuses on the solubility data from ultrapure water and seawater leaching experiments. Correlations between the various elements measured are investigated using multivariate statistical techniques to reveal information about the different sources contributing to the soluble fraction of the dust. Estimates are calculated of soluble nutrient fluxes to the tropical and sub-tropical eastern North.

Chapter 7 attempts to bring together the principal findings from this work described in this thesis and describes further work to be carried out on the datasets from the dust samples collected. Finally, this work is put in the more general context of future research directions in marine biogeochemistry.

1.5 References

Aguilar-Islas, A. M., et al. (2010). Dissolution of aerosol-derived iron in seawater: Leach solution chemistry, aerosol type, and colloidal iron fraction. *Marine Chemistry* 120(1-4): 25-33.

Baker, A. R., et al. (2006a). Nutrients in atmospheric aerosol particles along the Atlantic Meridional Transect. *Deep Sea Research Part II: Topical Studies in Oceanography* 53(14-16): 1706-1719.

Baker, A. R., et al. (2006b). Trends in the solubility of iron, aluminium, manganese and phosphorus in aerosol collected over the Atlantic Ocean. *Marine Chemistry* 98(1): 43-58.

Barbeau, K., et al. (1996). Role of protozoan grazing in relieving iron limitation of phytoplankton. *Nature* 380(6569): 61-64.

Bonnet, S. and Guieu, C. (2004). Dissolution of atmospheric iron in seawater. *Geophysical Research Letters* 31(3).

Bonnet, S., et al. (2005). Effect of atmospheric nutrients on the autotrophic communities in a low nutrient, low chlorophyll system. *Limnology and Oceanography* 50(6): 1810-1819.

Buck, C. S., et al. (2006). Aerosol iron and aluminium solubility in the northwest Pacific Ocean: Results from the 2002 IOC cruise. *Geochemistry Geophysics Geosystems* 7(4): Q04M07.

Caquineau, S., et al. (2002). Mineralogy of Saharan dust transported over northwestern tropical Atlantic Ocean in relation to source regions. *Journal of Geophysical Research-Atmospheres* 107(D15).

Carrasco, N., et al. (2007). Low Concentrations of Surfactants Enhance Siderophore-Promoted Dissolution of Goethite. *Environmental Science & Technology* 41(10): 3633-3638.

Chavagnac, V., et al. (2007). Anti-Atlas Moroccan Chain as the source of lithogenic-derived micronutrient fluxes to the deep Northeast Atlantic Ocean. *Geophysical Research Letters* 34(21).

Chen, Y., et al. (2006). Comparison between pure-water- and seawater-soluble nutrient concentrations of aerosols from the Gulf of Aqaba. *Marine Chemistry* 101(1-2): 141-152.

Chen, Y., et al. (2007). Estimates of atmospheric dry deposition and associated input of nutrients to Gulf of Aqaba seawater. *Journal of Geophysical Research-Atmospheres* 112(D4).

Chiapello, I., et al. (1995). An additional low layer transport of Sahelian and Saharan dust over the North-Eastern Tropical Atlantic. *Geophysical Research Letters* 22(23): 3191 - 3194.

Chiapello, I., et al. (1997). Origins of African dust transported over the northeastern tropical Atlantic. *Journal of Geophysical Research-Atmospheres* 102(D12): 13701-13709.

Darwin, C. (1846). An account of the Fine Dust which often falls on Vessels in the Atlantic Ocean. *Quarterly Journal of the Geological Society* 2(1-2): 26-30.

Desboeufs, K. V., et al. (2005). Dissolution and solubility of trace metals from natural and anthropogenic aerosol particulate matter. *Chemosphere* 58(2): 195-203.

Dobson, M. and Fothergill, J. (1781). An Account of the Harmattan, a Singular African Wind. *Philosophical Transactions of the Royal Society of London* 71: 46-57.

Eglinton, T. I., et al. (2002). Composition, age and provenance of organic matter in NW African dust over the Atlantic Ocean. *Geochemistry Geophysics Geosystems* 3(8): 1050.

Engelstaedter, S., et al. (2006). North African dust emissions and transport. *Earth-Science Reviews* 79(1-2): 73-100.

Hand, J. L., et al. (2004). Estimates of atmospheric-processed soluble iron from observations and a global mineral aerosol model: Biogeochemical implications. *Journal of Geophysical Research-Atmospheres* 109(D17).

Herut, B., et al. (2002). The role of dust in supplying nitrogen and phosphorus to the Southeast Mediterranean. *Limnology and Oceanography* 47(3): 870-878.

Herut, B., et al. (2005). Response of East Mediterranean surface water to Saharan dust: On-board microcosm experiment and field observations. *Deep Sea Research Part II: Topical Studies in Oceanography* 52(22-23): 3024-3040.

Jickells, T. (1995). Atmospheric inputs of metals and nutrients to the oceans: their magnitude and effects. *Marine Chemistry* 48(3-4): 199-214.

Jickells, T. D. (1999). The inputs of dust derived elements to the Sargasso Sea; a synthesis. *Marine Chemistry* 68(1-2): 5-14.

Jickells, T. D., et al. (2005). Global Iron Connections Between Desert Dust, Ocean Biogeochemistry, and Climate. *Science* 308(5718): 67 - 71.

Journet, E., et al. (2008). Mineralogy as a critical factor of dust iron solubility. *Geophysical Research Letters* 35(7): 5.

Kaufman, Y. J., et al. (2002). A satellite view of aerosols in the climate system. *Nature* 419(6903): 215-223.

Mackie, D. S., et al. (2005). Simulating the cloud processing of iron in Australian dust: pH and dust concentration. *Geophysical Research Letters* 32(6): L06809.

Mahowald, N. M., et al. (2005). Atmospheric global dust cycle and iron inputs to the ocean. *Global Biogeochemical Cycles* 19(4).

Martin, J. H. and Gordon, M. R. (1988). Northeast Pacific iron distributions in relation to phytoplankton productivity. *Deep Sea Research Part A. Oceanographic Research Papers* 35(2): 177-196.

Mills, M. M., et al. (2004). Iron and phosphorus co-limit nitrogen fixation in the eastern tropical North Atlantic. *Nature* 429: 292 - 294.

Moore, C. M., et al. (2009). Large-scale distribution of Atlantic nitrogen fixation controlled by iron availability. *Nature Geoscience* 2(12): 867-871.

Muhs, D. R., et al. (2010). Geochemical and mineralogical evidence for Sahara and Sahel dust additions to Quaternary soils on Lanzarote, eastern Canary Islands, Spain. *Terra Nova* 00(0): 1-12.

Prospero, J. M. and Lamb, P. J. (2003). African Droughts and Dust Transport to the Caribbean: Climate Change Implications. *Science* 302(5647): 1024-1027.

Ridame, C. and Guieu, C. (2002). Saharan input of phosphate to the oligotrophic water of the open western Mediterranean Sea. *Limnology and Oceanography* 47(3): 856-869.

Schroth, A. W., et al. (2009). Iron solubility driven by speciation in dust sources to the ocean. *Nature Geoscience* 2(5): 337-340.

Sedwick, P. N., et al. (2005). Iron in the Sargasso Sea (Bermuda Atlantic Time-series Study region) during summer: Eolian imprint, spatiotemporal variability, and ecological implications. *Global Biogeochemical Cycles* 19(4).

Sedwick, P. N., et al. (2007). Impact of anthropogenic combustion emissions on the fractional solubility of aerosol iron: Evidence from the Sargasso Sea. *Geochemistry Geophysics Geosystems* 8.

Spokes, L. J. and Jickells, T. D. (1995). Factors controlling the solubility of aerosol trace metals in the atmosphere and on mixing into seawater. *Aquatic Geochemistry* 1(4): 355-374.

Wu, J., et al. (2007). Dissolution of aerosol iron in the surface waters of the North Pacific and North Atlantic oceans as determined by a semicontinuous flow-through reactor method. *Global Biogeochemical Cycles* 21(4).

2. Methodology

2.1 Overview

This chapter is divided into three sections: aerosol sample collection, sample processing to obtain solutions containing total and readily soluble fractions, and the analytical methods used with the dust samples and extract solutions. Methods associated with the measurement of nanomolar concentrations of nitrate and phosphate are dealt with in Chapters 3 and 4.

2.2 Aerosol Sample Collection

2.2.1 Approach

Atmospheric aerosols (total suspended particles – TSP) were collected onto 47 mm diameter, polypropylene filters (0.45 µm nominal pore-size, Sterlitech) and polycarbonate filters (0.4 µm pore-size, Nuclepore). The polypropylene filters were used for leaching experiments (using deionised water and seawater), while the polycarbonate filters were used to measure total chemical composition (via total acid digestion) and mineralogical composition (XRD analysis). The polycarbonate filters were cleaned before use by soaking in ca. 1 M HCl solution (Romil, SpA grade) overnight then rinsing thoroughly with deionised water. The cleaned filters were dried under a class-100 laminar flow cabinet before being re-packed in their original packaging ready for use.

2.2.2 Cape Verde Atmospheric Observatory

Low volume aerosol sampling was undertaken at the Cape Verde Atmospheric Observatory (CVAO) between 2 July 2007 and 1 September 2009; however due to insufficient time for sample analysis, only data between 2 July 2007 and 11 July 2008 will be presented in this thesis. Situated on the north-west coast of the island of São Vicente (Figure 2.1), around 800 km from the west-African coast in an area of high dust deposition, the CVAO is an ideal location to study dust inputs to the

ocean. Due to a very stable north-easterly wind direction at the site (Figure 2.2), the air sampled has not crossed land for hundreds of kilometres since leaving the African mainland, resulting in virtually negligible contamination from potential local aerosol sources.

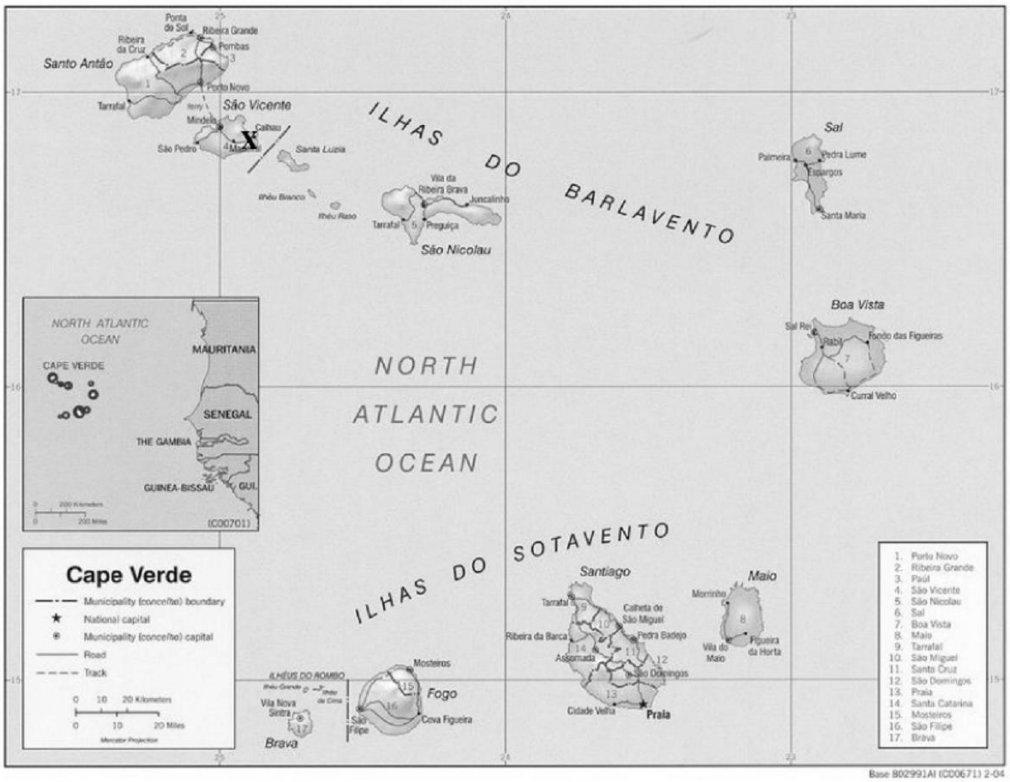

Figure 2.1 A map of the Cape Verde Islands. The position of the Cape Verde Atmospheric Observatory is indicated by a cross.

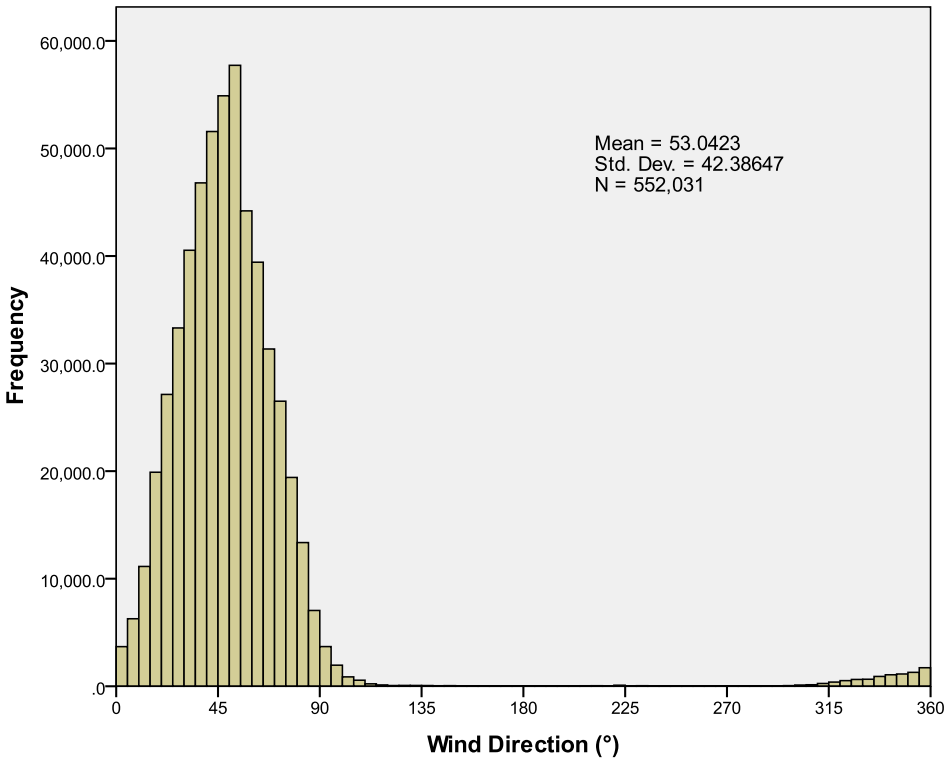

Figure 2.2 Histogram of wind direction recorded at the CVAO from 2 July 2007 to 11 July 2008. The wind direction is between 350° and 110° for 98.6% of the time.

2.2.3 Sampler – Cape Verde

A low-volume aerosol sampler was built to be installed at the top of the 30-metre sampling tower at the CVAO. The system comprised two rotary vane vacuum pumps (Piccolino VTE 8, Gardner Denver Thomas) drawing air through two pairs of 47 mm filters (two polycarbonate and two polypropylene filters). Two thermal mass flow meters (Top Trak 826, Sierra Instruments) monitored the flow rate of air through each pair of filters. A data logger (built in-house by Nigel Eastwood, SOES) monitored the analogue electrical signal from the mass flow meters and recorded the data on a Compact Flash memory card. For each pair of sample lines, the same type of filter was used in order to achieve an even division of flow between the two filters. A household gas meters and analogue pressure gauge was included in each of the four lines to monitor for any imbalances in the division of the air flow (Figure 2.3, Figure 2.4).

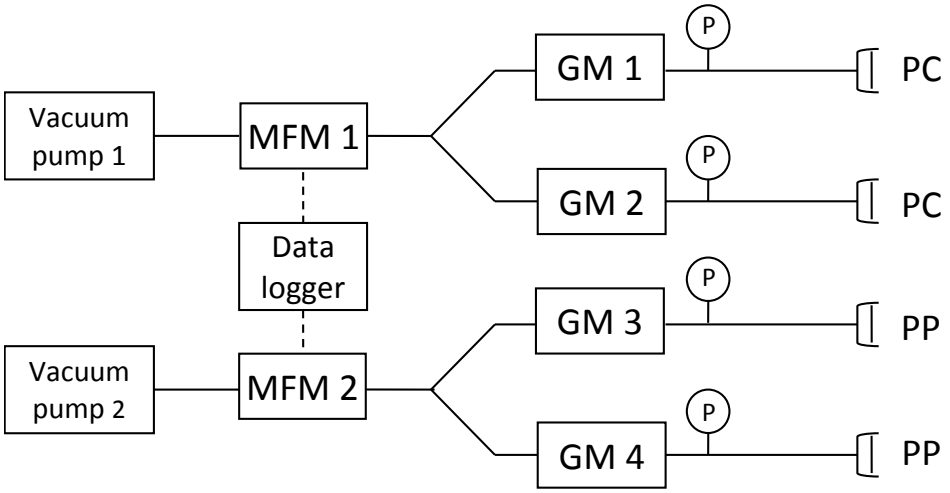

Figure 2.3 Diagram of low-volume aerosol Sampler installed at the Cape Verde Atmospheric Observatory, indicating arrangement of vacuum pumps, mass flow meters (MFM), gas meters (GM), pressure gauges (P) and polypropylene (PP) and polycarbonate (PC) filters.

Typical flow rates through each filter were around 30 standard $L.min^{-1}$, but this decreased as the filters became heavily loaded with dust, particularly for the polycarbonate filters. Local technicians changed the filters generally three times per week (more often during intense dust events) and stored the filters in a standard freezer (-20 °C) prior to shipment to the UK and analysis at NOCS. Filter freezing was deemed necessary due to reports that sample solubility decreases with storage time at room temperature, but not when filters were stored frozen (Buck et al., 2006)

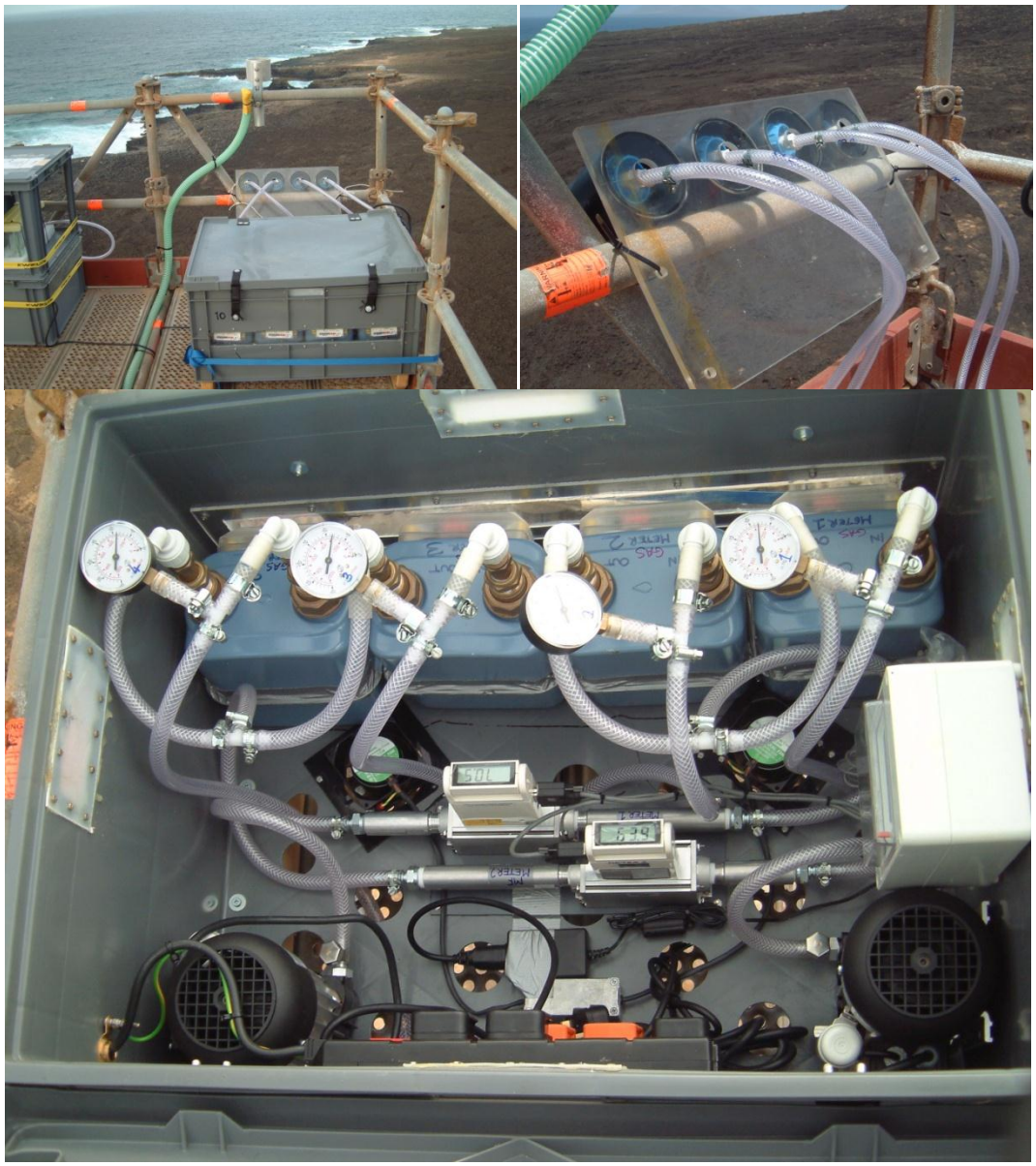

Figure 2.4 Photographs of the aerosol sampling system installed at the Cape Verde Atmospheric Observatory (CVAO).

2.2.4 Research cruise aboard RRS Discovery (D326)

Aerosol samples were also taken during a research cruise aboard the RRS Discovery in the tropical and subtropical eastern North Atlantic. A total of 29 sets of samples were collected in the period between 8 January and 4 February 2008. The area covered during the cruise is shown in the cruise track in Figure 2.5.

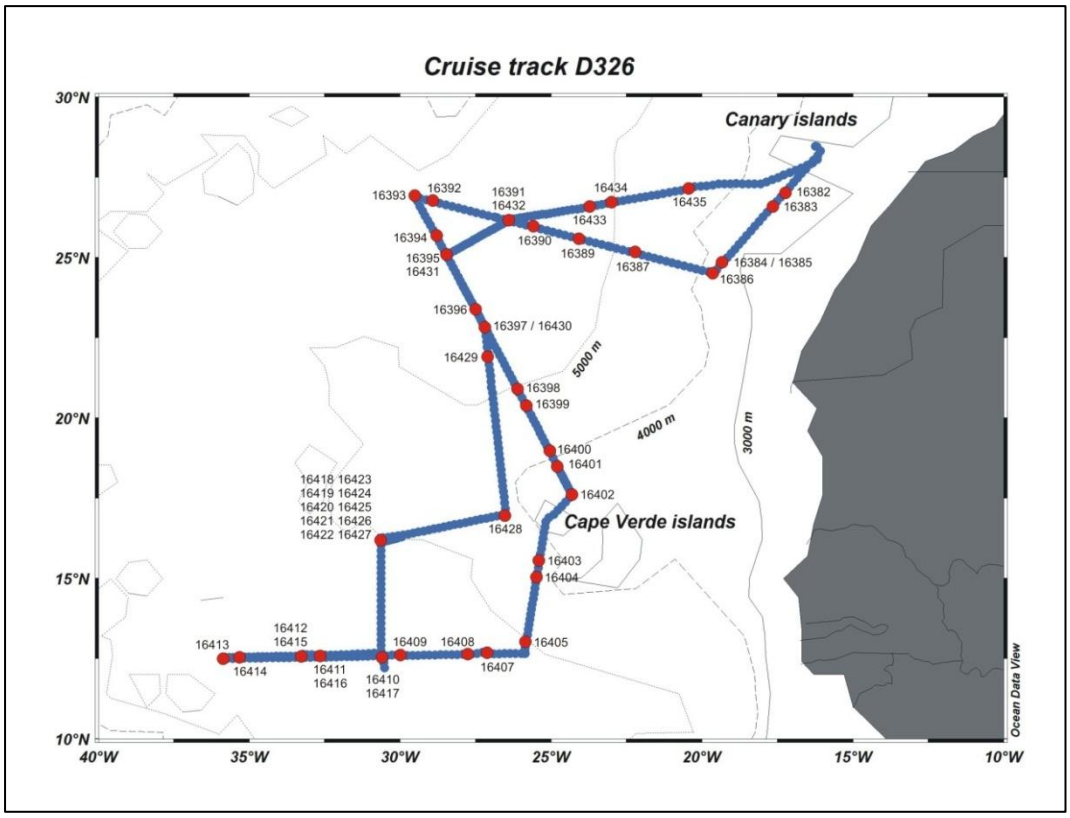

Figure 2.5 Cruise track for D326 aboard RRS Discovery from 8 January – 4 February 2008. Stations are marked in red together with their station numbers.

2.2.5 Ship-board aerosol sampler

A low volume sampler similar to the system installed at the CVAO was constructed for ship-board use. This system contained four MFMs, one per filter line, greatly simplifying the measurement of individual sample volumes in comparison with the CVAO-based sampler (see Figure 2.3). A schematic diagram of the system is shown in Figure 2.6 and photographs of the system in Figure 2.7.

In order to reduce the risk of sample contamination from the ship and to minimise the quantity of sea spray reaching the filters, the sampler was located on the deck above the bridge: as near to the bow and as high above the sea surface as practicable. In addition, a Perspex shield surrounding the filter holders was used to reduce the quantity of sea-spray reaching the filters. During periods of rainfall, the sampler was switched off to avoid contaminating the filters. To reduce further the risk of contamination from the ship's diesel exhaust, an automatic control system

was included to prevent sampling when the wind direction came from the stern or the wind speed dropped below a threshold value. This control system monitored an input from a digital wind vane and anemometer. When the wind speed and direction was outside specified limits (> ±90° from the bow; < 2 $m.s^{-1}$), four solenoid valves were engaged to cut off air flow to the pumps and to release any residual vacuum in the sample lines. The pumps were also switched off if conditions remained unsuitable for sampling for more than 5 minutes. The control and data logging system was built by Nigel Eastwood (School of Ocean and Earth Science) and the system was operated and stored data was transferred by simple commands over an RS232 link.

It was possible to change the filters more frequently during a cruise than at the CVAO due to more available personnel. Filters were generally changed every 24 hours and more frequently during a dust event. The samples were stored frozen (at -20°C) until analysis.

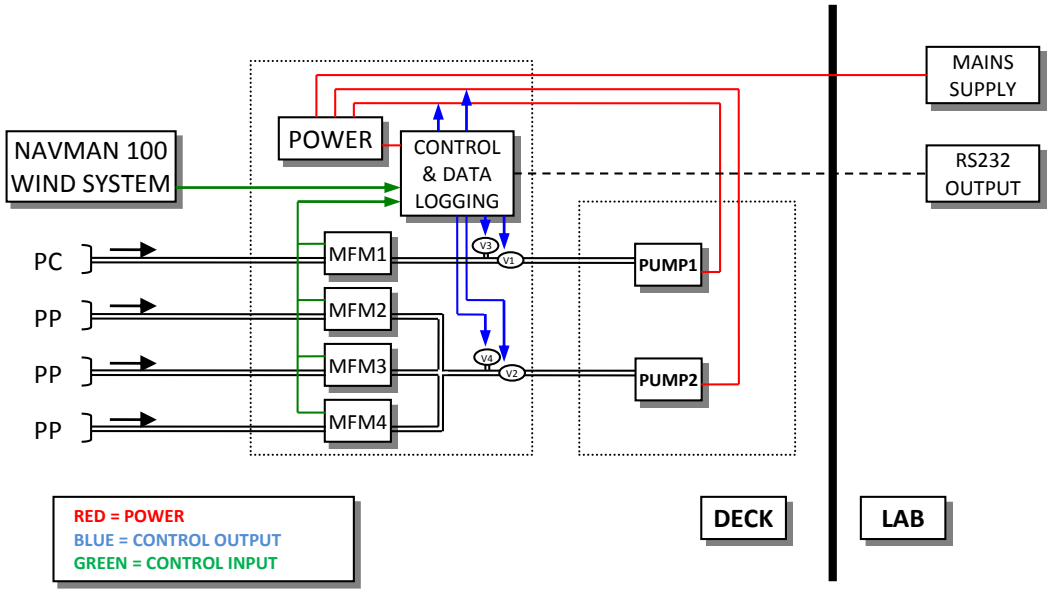

Figure 2.6 Diagram of ship-board low-volume aerosol sampler, indicating physical arrangement of components and connections to the control systems. MFM = mass flow meter, V = solenoid valve, PC = polycarbonate filter, PP = polypropylene filter.

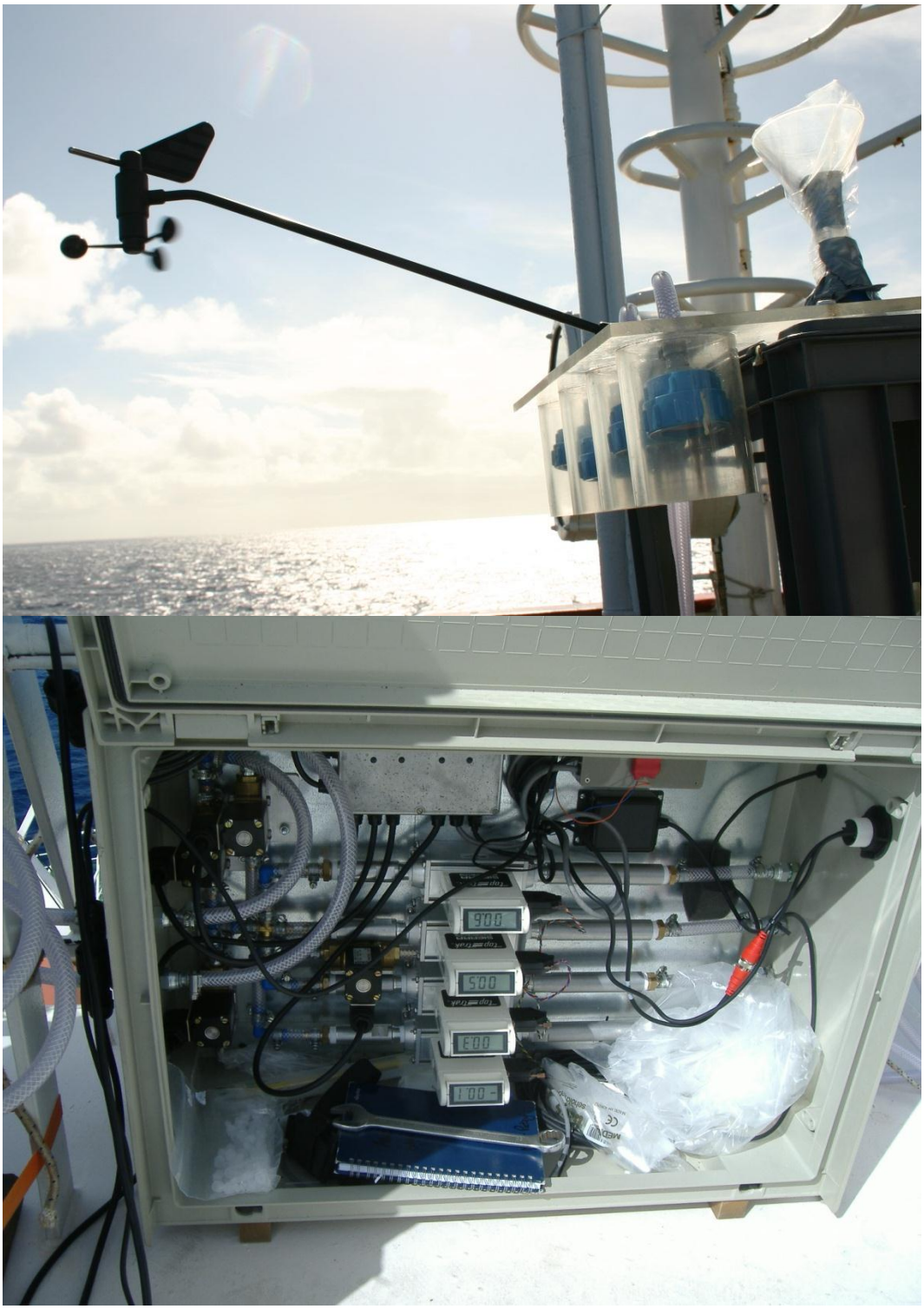

Figure 2.7 Photographs of the ship-board sampler showing the four sample lines with wind vane and anemometer (upper) and the control box showing mass flow meters, solenoid valves, and control and data logging equipment. The two pumps are in a separate box (not shown).

2.3 Sample processing

2.3.1 Total Acid Digestion

In order to measure total metal concentrations within the dust samples, a microwave-assisted acid digestion procedure was used to completely dissolve the aerosol samples together with the polycarbonate filter material, producing a solution suitable for ICP-MS analysis. A method by N. M. Hassan was adapted for this work (Hassan et al., 2007). Due to the number of positions available in the microwave system the work was carried out in batches of fifteen samples / reference solutions. A clean filter was digested with each batch to verify the cleanliness of the procedure and to provide a filter blank for the procedure. To verify the effectiveness of the digestion procedure, 20 mg of two different reference materials was included with every batch of samples. To minimise contamination, all work was carried out in a class-100 clean laboratory, with the exception of the perchloric acid step, which was conducted in a small laminar flow cabinet with the air outlet going directly into a fume cupboard in a routine chemistry laboratory. All Teflon digestion vessels were cleaned before use by soaking overnight in a large beaker of 50% v/v (ca. 6 M) HCl (analytical reagent grade) placed on top of a hot-plate set to ca. 150°C. The Teflon-ware was subsequently rinsed with deionised water before soaking overnight in a large beaker of 50% v/v (ca. 8 M) HNO_3 (analytical reagent grade) heated on a hot-plate at 150 °C. The apparatus was rinsed thoroughly and dried in a clean-air drying cabinet.

A whole filter was folded and placed in a microwave digestion vessel (for samples collected using the ship-board system, the filter was cut in half with ceramic scissors in order to conserve sample for subsequent analyses). To this was added 3 ml concentrated HCl (sub-boiling distilled), 3 ml concentrated HNO_3 (sub-boiling distilled) and 2.5 ml concentrated HF (SpA grade, Romil). The digestion vessels were allowed to stand for 30 – 60 minutes to allow any gases that may have formed to escape, before being sealed and loaded into the microwave. An Anton Paar Multiwave 3000 digestion system rated at 1400 W with a 16-position 16MF100

rotor was used. One position was taken up by the reference vessel, which contained a sapphire temperature and pressure probe, used by the instrument as a feed-back to allow precise control of the power delivered to the samples. This vessel was filled with 3 ml concentrated HCl + 3 ml concentrated HNO_3 together with a polycarbonate filter; its contents were discarded once the digestion programme was complete. Table 2.1 details the operating programme used. Maximum pressures reached during digestion were typically 18 – 19 bar.

Table 2.1 Digestion programme used with Anton Paar Multiwave 3000 digestion system.

Time	Target temp. (°C)
0	N/A
15	160
20	160
50	175
60	175
60 - 85	Allow to cool

Following digestion, the samples were transferred from the microwave vessels into 30 ml Teflon pots; the microwave vessels were washed with 2% v/v (ca. 0.3 M) HNO_3 (sub-boiling distilled) and this solution was also transferred to the Teflon pots. The solutions in the Teflon pots were then evaporated overnight on a hot-plate set to 140 °C. The samples were removed when only 0.5 – 1 ml of solution remained and 0.25 ml concentrated $HClO_4$ (Romil SpA) was added. Evaporation was continued at 140°C until all water had evaporated and white perchloric acid vapours were produced. At this stage the temperature of the hot-plate was increased to 170°C; after about 30 minutes of heating at this temperature, and when only a tiny bead of liquid remained in the bottom of each pot, a further 0.25 ml concentrated $HClO_4$ was added. All solutions were then evaporated to complete dryness with the hot-plate set to 170°C. The residues were then re-dissolved in 2% v/v HNO_3 (sub-boiling distilled) before being transferred to pre-weighed, acid-washed 30 ml low-density

polyethylene (LDPE) bottles. The samples were diluted to give a total volume of approximately 20 ml and then weighed.

2.3.2 Digestion reference material

It is important to verify the efficacy of the digestion procedure by digestion of a suitable reference material under the same conditions used for the sample digestions. Ideally the composition of this material should closely match the composition of the sample. Other researchers studying mineral-rich aerosol samples have used a variety of reference materials such as marine sediments (e.g. Guieu et al., 2002) and coal fly-ash (Trapp et al., 2010). Due to a lack of availability of some of the commonly used reference materials and to a desire to use an aerosol-based reference material, a reference material derived from aerosol material collected in an urban environment was chosen for this work (standard reference material 1648a; urban particulate matter, NIST, USA). However, we came to realise that while this material contains many highly refractory components and is therefore useful as an indicator of digestion efficiency, it is not very representative of the atmospheric dust collected in our study region. For this reason 20 mg of an additional uncertified, but well characterised reference material was also included with each batch of samples. This material is a finely ground loess sediment that was used for GeoPT13, a large inter-laboratory inter-comparison exercise organised by the International Association of Geoanalysts. Its composition has been determined accurately using a wide variety of digestion and spectroscopic techniques and the consensus values are made available on the internet (Potts et al., 2003).

2.3.3 Ultra-pure water and seawater leaching

To investigate the readily soluble fraction of metals and nutrients within the samples, a simple leach procedure was used analogous to that used by Bill Landing's group at Florida State University (Buck et al., 2006). Using a standard laboratory vacuum filtration unit, 100 ml of ultra-pure water (Milli-Q water; ≥ 18.2 MΩ.cm) or 0.2 µm-filtered surface seawater (taken from the tropical Northeast Atlantic Ocean)

was passed through the polypropylene dust-loaded filter using a small vacuum pump. The filtrate was then transferred immediately into several bottles for subsequent analysis (see Figure 2.8):

- ICP-MS – a 30 ml acid-cleaned LDPE containing 20 µl concentrated HNO_3 (UpA grade, Romil) was filled to the shoulder.
- Amino acids & TDN/DOC – 20ml was taken to fill a polypropylene tube (amino acids) and a glass ampoule (TDN/DOC) were filled for subsequent analysis by Pornsri Mingkwan; work which will not be discussed further in this thesis.
- Ion Chromatography – 5 ml of filtrate was decanted into a polypropylene sample tube, capped and stored in a refrigerator before analysis the following day.
- Nutrients – the remaining solution (about 40 ml) was transferred to an acid-washed 60 ml LDPE bottle. A 10 ml aliquot was immediately pipetted into a 30 ml polystyrene container (Fisher Scientific) for ammonium analysis. The remaining solution was frozen for NO_3^- / PO_4^{3-} analysis at a later date.

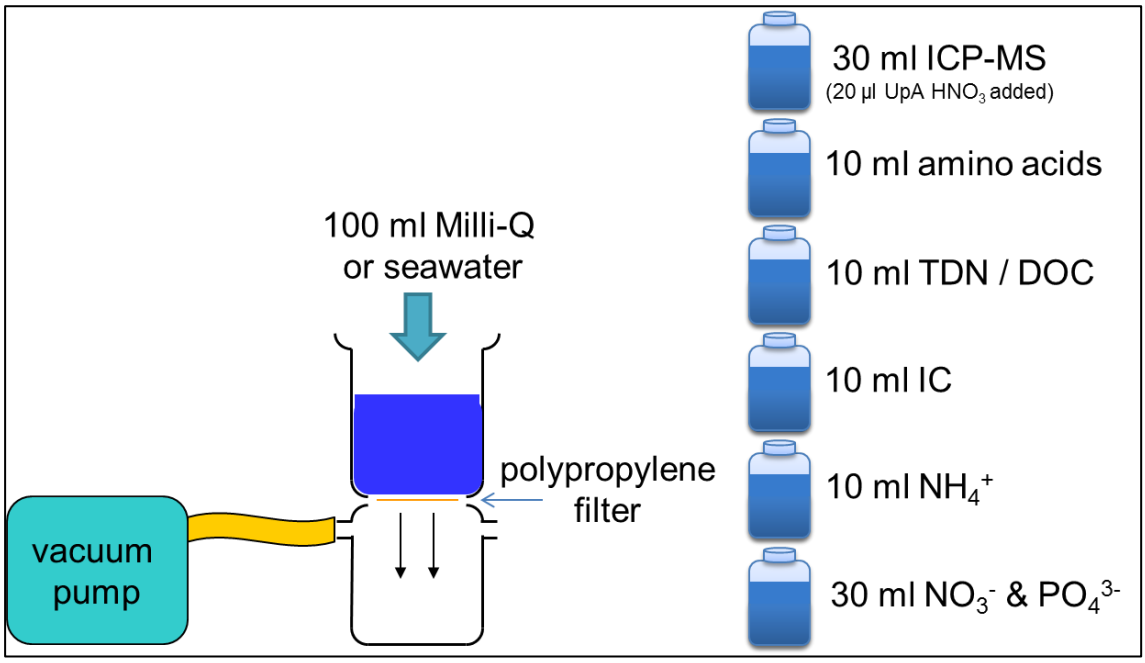

Figure 2.8 Schematic diagram of ultrapure water and seawater leaching experiments

All apparatus was soaked in 1 M HCl and rinsed thoroughly with ultrapure water before use and in-between samples. LDPE bottles for ICP-MS analysis were cleaned by soaking in 6 M HCl for one week, then transferred to a 8 M HNO_3 acid bath for a further week before being rinsed thoroughly with ultrapure water and allowed to dry in a clean air cabinet in the clean laboratory. LDPE bottles for nutrient analysis were cleaned by soaking in 1 M HCl overnight before being rinsed with ultrapure water and allowed to dry in the same way as the sample bottles for ICP-MS analysis.

With the seawater leaches, samples for ion chromatography were not taken. The bottle for trace metal analysis was still filled, but measurement for Fe and Al was carried out using flow injection analysis (FIA).

2.4 Analytical Techniques

2.4.1 Micromolar nutrient analysis

Analysis for micro-molar concentrations of nitrate + nitrite (NO_2^- + NO_3^-) and phosphate (PO_4^{3-}) in seawater and ultra-pure water leaches was made using a Seal Analytical QuAAtro autoanalyser. This is a standard nutrient autoanalyser, which uses the long-established principles of segmented continuous flow analysis (SCFA) and colourimetric chemistry (Hansen and Koroleff, 1999). With regards to reagent preparation and instrument flow rates, the manufacturer's recommendations were followed. Standard solutions were prepared from analytical reagent grade KNO_3 and KH_2PO_4. The accuracy of the instrument was verified by including a certified standard (OSIL limited) with each analytical run. Ultra-pure deionised water (Milli-Q water) was used as the standard matrix and wash solution when measuring deionised water leach samples, while a 40 $g.l^{-1}$ solution of NaCl (analytical reagent grade) was used for the standards and wash solution when analysing seawater leach samples.

2.4.2 Ammonium Analysis

For the measurement of dissolved ammonium in seawater and ultra-pure water leaches, the OPA (ortho-pthalaldehyde) fluorescence method described by Holmes

was used (Holmes et al., 1999). Standard solutions were prepared from analytical reagent grade NH_4Cl. Sample solutions were diluted from 10 ml to 20 ml and standard solutions were prepared to the same volume and in the concentration range (0.25 – 5 µM NH_4^+). Two millilitres working reagent was added to each of the sample and standard solutions before they were sealed, covered in aluminium foil and stored in the dark until analysis the following day. Fluorescence was measured using a Perkin Elmer LS55 spectrofluorometer, measuring the emission of the samples at 422 nm after excitation at 330 nm. It was necessary to dilute some samples further to bring the measurement to within the calibrated range of ≤ 5 µM.

2.4.3 Ion Chromatography

Major anions (Cl^-, Br^-, NO_3^-, SO_4^{-2}) in samples from ultra-pure water leaches were determined using a Dionex IC25 ion chromatography system. Details of the system configuration are given in Table 2.2. Working standard solutions were prepared using stock solutions obtained from Fisher Scientific. To verify the accuracy of the system, a combined 7-anion standard, diluted from a stock solution from Dionex was included in every analytical run.

Table 2.2 System parameters used for ion chromatographic analysis

System	DIONEX IC25
Pump	Isocratic IS25 DIONEX pump (0 - 5000 psi)
Flow rate	1 $mL.min^{-1}$
Operating pressure	1800 psi
Sample loop	250 µl
Sample injection	Autosampler AS40
Injection valve	Rheodyne 6-way valve
Columns	Guard column: AG14 4x50 mm Analytical column: AS14 4x250 mm
Eluent	8 mM $NaHCO_3$/ Na_2CO_3
Suppressor	ASRS ultra II 4-mm Self regenerating (Electrolysis of MQ water by applying 100 mA DC current)
Analysis time	20 min
Detector	CD 20 Conductivity cell (0 – 1000 µS/cm)
Software	Chromeleon 6.2 Integrator and Data management system

2.4.4 ICP-MS analysis

ICP-MS analysis was used to measure trace metals in ultra-pure water leaches and total acid digestion samples. An X-SERIES 2 ICP-MS (Thermo Fisher Scientific, Bremen, Germany) was setup in the standard configuration using an ASX-510 autosampler (Cetac, Omaha, Nebraska, USA). A total of 42 elements were determined simultaneously. A summary of the elements measured, together with instrumental detection limits (defined as 3 times the standard deviation of a clean acid blank) is given in Table 2.4. Standard solutions were prepared from 5 international rock reference materials. However for certain elements where the reference values for the rock standards were poorly defined (Ga, Ag, Cd, Sn, Hf and Hg), separate synthetic standards were prepared using certified single-element standard solutions from Romil. To correct for instrumental drift, all sample and standard solutions were spiked with an internal standard solution containing Be, In and Re to give a final concentration of 50 $\mu g.L^{-1}$ Be and 20 $\mu g.L^{-1}$ In and Re.

The instrument was tuned for optimum sensitivity, stability and low oxide formation using a 10 ppb multi-element tuning solution. A summary of the instrumental operating parameters is presented in Table 2.3. Using the ICP-MS operating software, an experiment was constructed containing Ba and REE interference correction solutions, blanks, calibration standards together with the unknown samples. Data were then acquired for the isotopes of interest in peak-jumping mode (4 x 40 second repeats per sample). After each sample analysis, a wash solution containing 2% HNO_3 was run until background levels were achieved (typically <3 minutes). The data quality was monitored throughout the run by examination of the statistics produced after each analysis. Within run reproducibility was typically better than 2% RSD for the 4 repeats. Any anomalous results were noted and re-run at the end of the procedure. The data handling procedure included the following steps: Correction for Ba and REE oxide and hydroxide formation, internal correction using Be, In and Re, blank correction, calibration against 5 rock standards and synthetic standards and dilution correction.

Table 2.3 System parameters used for ICP-MS analysis

System	Thermo Fisher X-Series II
RF Power	1.40kW Forward, <1W Reflected.
Sample Introduction System	Concentric nebulizer with low-volume impact bead spraychamber
Torch	Standard one-piece quartz torch with Plasma Screen
Interface	Standard Xt (Ni sample/Ni Skimmer)
Cool Gas Flow	13 $L.min^{-1}$
Auxiliary Gas Flow	0.8 $L.min^{-1}$
Nebuliser Gas Flow	0.85 - 0.90 $L.min^{-1}$
Sample Uptake Rate	Approx. 0.4 $mL.min^{-1}$
Detector	Simultaneous pulse/analogue
Wash Time	Monitored, minimum 100 seconds, maximum 300 seconds
Main Runs per sample:	4
Peak jumping mode:	
- Number of Points per peak	1
- Dwell Time/Point	20 ms
- Number of Sweeps/Replicate	100

Table 2.4 Average instrumental blank concentrations (dilute HNO3; n = 13 measurements), average filter blanks for ultra-pure water (MQ) leaches (n = 20) and total acid digestions (n = 18), and mean % recovery (± 1 standard deviation) from CRMs in total acid digestions. All blank values are in µg.L^{-1}.

Element	Instrumental Blank Mean	MQ Filter Blank Mean	Digestion Blank Mean	LOESS CRM % recovery		NIST1648a % recovery	
Na	< 0.5	2.3	10	109%	± 8%	108%	± 7%
Mg	0.65	1.4	2.0	109%	± 8%	102%	± 6%
Al	< 0.3	1.0	7.2	107%	± 9%	105%	± 7%
K	1.9	< 1.7	7.4				
Ca	< 2.1	9.0	16	110%	± 8%	106%	± 7%
Sc	< 0.008	< 0.008	< 0.008				
Ti	< 0.2	< 0.2	2.3	103%	± 11%	100%	± 9%
V	< 0.01	< 0.01	0.15	101%	± 13%	104%	± 13%
Cr	< 0.01	< 0.01	1.4	101%	± 12%	96%	± 11%
Mn	< 0.01	< 0.01	0.030	105%	± 8%	101%	± 6%
Fe	< 0.2	0.20	2.7	107%	± 11%	105%	± 11%
Co	< 0.002	< 0.002	< 0.002	103%	± 11%	101%	± 13%
Ni	< 0.01	0.015	0.14	96%	± 11%	89%	± 10%
Cu	< 0.025	0.028	0.10	96%	± 9%	87%	± 7%
Zn	< 0.1	0.43	0.52	97%	± 9%	82%	± 9%
Ga	< 0.003	0.0039	< 0.0034				
Rb	< 0.005	< 0.005	0.008	101%	± 9%	88%	± 9%
Sr	< 0.005	0.011	0.10	103%	± 8%	96%	± 9%
Y	< 0.0005	< 0.0005	0.17	85%	± 8%		
Nb	< 0.002	< 0.002	0.015				
Ag	< 0.002	< 0.002	0.007				
Cd	< 0.001	0.0022	0.002				
Sn	< 0.005	0.12	0.27				
Cs	< 0.0004	< 0.0004	0.001	101%	± 4%	93%	± 3%
Ba	< 0.01	0.033	0.059				
La	< 0.0004	< 0.0004	0.002	105%	± 12%	93%	± 4%
Ce	< 0.001	< 0.001	0.008	105%	± 12%	95%	± 4%
Pr	< 0.0002	< 0.0002	0.001	107%	± 13%		
Nd	< 0.001	< 0.001	0.002	105%	± 13%		
Sm	< 0.0006	< 0.0006	< 0.0006	104%	± 12%	89%	± 4%
Eu	< 0.0002	< 0.0002	< 0.0002	101%	± 8%		
Gd	< 0.0003	< 0.0003	0.0004	115%	± 11%		
Tb	< 0.0001	< 0.0001	< 0.0001	97%	± 8%		
Dy	< 0.0001	< 0.0001	0.0003	86%	± 7%		
Ho	< 0.00004	< 0.00004	0.0001	81%	± 7%		
Er	< 0.0001	< 0.0001	0.0002	79%	± 6%		
Tm	< 0.00002	< 0.00002	0.00002	81%	± 6%		
Yb	< 0.0001	< 0.0001	0.0001	75%	± 6%		
Lu	< 0.00002	< 0.00002	0.00002	74%	± 6%		
Pb	< 0.0003	< 0.0003	0.002	110%	± 11%	102%	± 5%
Th	< 0.001	0.011	0.04	100%	± 19%		
U	< 0.0001	< 0.0001	0.001	91%	± 14%		

2.4.5 Flow Injection Analysis – Dissolved Iron

Dissolved Fe in the seawater leach samples was measured using an automated flow injection chemiluminescence system, following the method of Obata (Obata et al., 1997; de Jong et al., 1998), with some modifications (Nielsdottir, 2009). Calibration standard solutions up to 5 nM Fe were prepared and samples were diluted in order to give a signal within the calibrated range. The accuracy of the technique was verified by measuring a reference material (seawater sample D2 from the SAFe inter-comparison programme; measured value 0.98 ± 0.05 nM; reference value 0.91 ± 0.17 nM (Johnson et al., 2007)). The detection limit of the system was typically in the range 0.009 to 0.06 nM Fe and the analytical blank in the range 0.017 to 0.042 nM Fe.

2.4.6 Back trajectory Calculation

Each sample was interpreted in terms of air-mass source by calculating five-day isentropic air-mass back-trajectories using the HYSPLIT (**HY**brid **S**ingle-**P**article **L**agrangian **I**ntegrated **T**rajectory) model (Draxler and Rolph, 2003; Rolph, 2003) with the GDAS meteorological dataset. Trajectories were calculated for arrival heights of 30, 750, 1500, 2000, 2500 and 3000 m above the sampling location. In the case of the samples collected at the CVAO, trajectories were calculated for every 12 hours, finishing at 1200 and 0000 GMT. For samples collected during cruise D326, trajectories were calculated for the start and end of every sampling period, and if the sampling period was greater than 18 hours, a third trajectory was calculated for the middle of the sampling period.

2.5 References

Buck, C. S., et al. (2006). Aerosol iron and aluminium solubility in the northwest Pacific Ocean: Results from the 2002 IOC cruise. *Geochemistry Geophysics Geosystems* 7(4): Q04M07.

de Jong, J. T. M., et al. (1998). Dissolved iron at subnanomolar levels in the Southern Ocean as determined by ship-board analysis. *Analytica Chimica Acta* 377(2-3): 113-124.

Guieu, C., et al. (2002). Chemical characterization of the Saharan dust end-member: Some biogeochemical implications for the western Mediterranean Sea. *Journal of Geophysical Research* 107.

Hansen, H. P. and Koroleff, F. (1999). Determination of Nutrients.in: *Methods of seawater analysis*. K. Grasshoff, K. Kremling and M. Ehrhardt. Weinheim, Germany Wiley-VCH**:** 159-228.

Hassan, N. M., et al. (2007). Analysis of environmental samples using microwave-assisted acid digestion and inductively coupled plasma mass spectrometry: Maximizing total element recoveries. *Water Air and Soil Pollution* 178(1-4): 323-334.

Holmes, R. M., et al. (1999). A simple and precise method for measuring ammonium in marine and freshwater ecosystems. *Canadian Journal of Fisheries and Aquatic Sciences* 56(10): 1801-1808.

Johnson, K. S., et al. (2007). Developing Standards for Dissolved Iron in Seawater. *Eos, Transactions, American Geophysical Union* 88(11): 131-132.

Nielsdottir, M. C. (2009). Iron Biogeochemistry in (Sub-) Polar Waters. *School of Ocean and Earth Science*. Southampton, University of Southampton. PhD**:** 136.

Obata, H., et al. (1997). Fundamental studies for chemical speciation of iron in seawater with an improved analytical method. *Marine Chemistry* 56(1-2): 97-106.

Potts, P. J., et al. (2003). GEOPT13 - An international proficiency test for analytical geochemistry laboratories - report on round 13 / July 2003. available from http://www.geoanalyst.org/geopt/GeoPT13Report.pdf.

Trapp, J. M., et al. (2010). Temporal variability of the elemental composition of African dust measured in trade wind aerosols at Barbados and Miami. *Marine Chemistry* 120(1-4): 71-82.

3. Determination of nitrate and phosphate in seawater at nanomolar concentrations

3.1 Overview

This chapter has been published in *Trends in Analytical Chemistry* (Vol. 27, No. 2, 2008, p. 169-182). It provides an overview of the methods currently available for nM nitrate and phosphate analysis in seawater, before going on to describe a system constructed in our laboratory for the measurement of nitrate and phosphate at nM concentrations. This instrument was deployed during a research cruise in the tropical and sub-tropical eastern North Atlantic aboard the FS Poseidon in January and February 2006 and surface nutrient concentrations from this cruise are presented. With the exception of Figure 3.1, all data presented in this chapter are the work of this author.

3.1.1 Nitrate and phosphate in marine waters

All living organisms require the nutrients nitrogen and phosphorus for their growth, metabolism and reproduction. Nitrogen is a component of amino acids, nucleic acids and other cell components, while phosphorus is found primarily in nucleic acids, phospholipids and adenosine triphosphate (ATP). Research has demonstrated that phytoplankton productivity in the surface ocean is often limited by the amount of available fixed inorganic nitrogen (i.e. dissolved forms other than molecular nitrogen) (Falkowski et al., 1998) and, in some cases, available phosphorus (Wu et al., 2000; Krom et al., 2005).

Nitrogen is present in the marine environment in various forms. Nitrate is the principal form of fixed dissolved inorganic nitrogen assimilated by organisms, although certain organisms can utilise nitrite, ammonium or even dissolved molecular nitrogen. Orthophosphate (predominantly HPO_4^{2-}) is considered the most important phosphorus species in seawater that is immediately biologically available.

Dissolved inorganic nutrients are usually the preferred substrates for phytoplankton, since organic sources of nitrogen and phosphorus generally require enzymatic remineralisation. However, some photosynthetic organisms can access dissolved organic nutrients, and there is growing interest in dissolved organic nitrogen (DON) and dissolved organic phosphorus (DOP) cycling in marine ecosystems. DON (or DOP) concentrations are determined indirectly as the difference between total dissolved nitrogen (or phosphorus) and inorganic dissolved nitrogen (or phosphorus). Since DON and DOP measurements contain the errors of two or more analytical measurements, accurate and precise measurements of nitrate and phosphate are essential (Bronk, 2002; Karl and Björkman, 2002).

Large temporal and spatial variations in nutrient concentrations exist in the oceans because of physical and biological processes. In surface waters, biological uptake depletes nitrate and phosphate. In highly stratified oligotrophic surface waters, with low nutrient inputs, nitrate and phosphate are typically at nanomolar (nM) concentrations. Approximately 40% of the world's oceans fall into this category. Nitrate and phosphate concentrations increase to micromolar concentrations with depth, as remineralisation of sinking particulate matter returns dissolved nutrients to the water column. Figure 3.1 shows an example of a vertical profile of nitrate and phosphate concentrations in the North Atlantic Ocean.

The high spatio-temporal variability of nitrate and phosphate in oceanic surface waters, combined with severe problems associated with storage of samples containing nM nutrient concentrations, poses a need for ship-based measurements. This puts further demands on the method, which needs to be rugged, portable, easy to operate, and with a high sample throughput (Hanrahan et al., 2002).

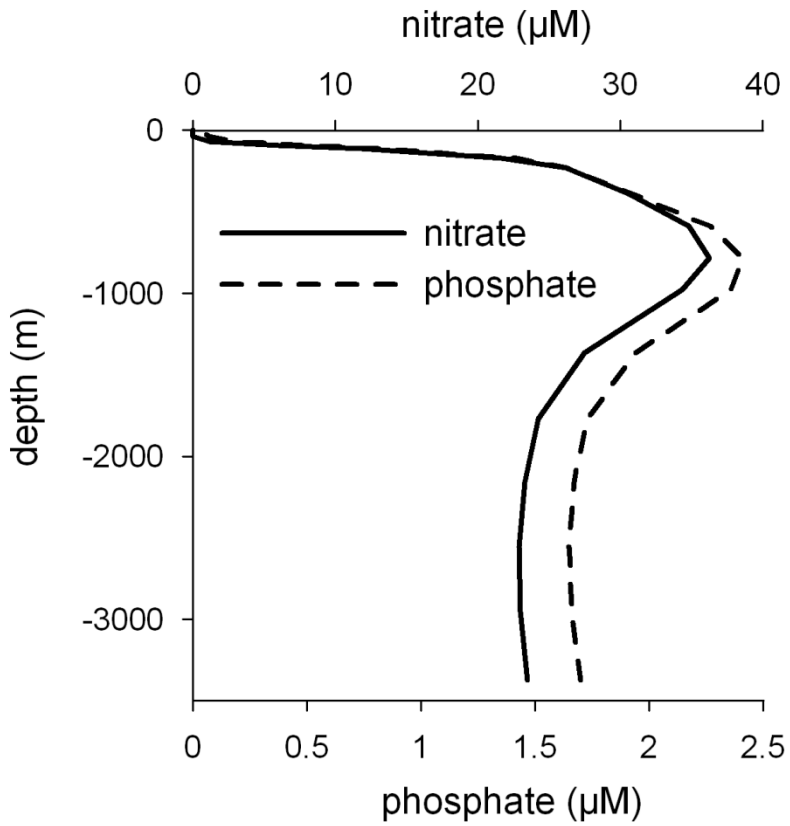

Figure 3.1 Vertical profile of nitrate and phosphate in the tropical North-East Atlantic at 17°N, 24°W, determined on 9 February 2006 during a research cruise aboard the FS Poseidon. Analysis was carried out using a conventional segmented-flow autoanalyser.

3.1.2 Conventional techniques

A variety of methods has been used to determine nitrate and phosphate in seawater. These methods can be divided into three broad categories:

1. manual methods, where each sample is treated individually;
2. automated methods, which are usually based on flow analysis; and,
3. sensors, which, upon contact with the seawater, monitor a signal that is indicative of the analyte concentration (Hansen and Koroleff, 1999).

Sensors would represent the ideal way to quantify nutrients in the marine environment, but do not yet show sufficient sensitivity or precision and often suffer interference from the high concentrations of ions present in seawater. For example, sensors are available that measure in-situ nitrate concentrations directly by

monitoring UV absorbance at 220 nm (Finch et al., 1998; Johnson and Coletti, 2002). They can provide instantaneous, near-continuous in-situ measurements in the oceans. However, the lowest reported limit of detection (LOD) is 0.21 µM (Finch et al., 1998), which limits its use in many surface waters. Interferences from organic matter and other anions, such as bromide and carbonate, also pose problems.

Flow analysis is a common technique used to automate chemical analyses. Typically, peristaltic pumps precisely mix sample with reagents in flow-through tubes or capillaries, while reaction products are continuously monitored using a flow-through detector. Various forms of flow analysis exist, including segmented continuous flow analysis (SCFA), flow-injection analysis (FIA) and sequential injection analysis (SIA). Automation, together with high sample throughput, high analytical precision and a reduced risk of sample contamination, has resulted in the widespread use of flow analysis for nutrient measurements in natural waters. Several recent reviews provided comprehensive overviews of the use of flow analysis for nitrate and phosphate (Miro et al., 2003; Estela and Cerda, 2005; Motomizu and Li, 2005; Gray et al., 2006).

The most widely used method for the analysis of nitrate involves reduction of nitrate to nitrite, usually using a copperised cadmium column. Nitrite is then determined spectrophotometrically (at 540 nm) following formation of a highly coloured dye through diazotisation with sulphanilamide and coupling with N-(1-naphthyl)-ethylenediamine dihydrochloride (NED) (Hansen and Koroleff, 1999). This analytical method determines the sum of the nitrate (NO_3^-) and nitrite (NO_2^-) concentrations; to calculate the nitrate concentration, it is necessary to measure nitrite separately in the sample (by omitting the reduction step) and subtract it from the combined NO_2^- + NO_3^- measurement. The technique is robust, sensitive and suffers from no known interferences in oxygenated seawater (Hansen and Koroleff, 1999; Moorcroft et al., 2001).

For the analysis of phosphate, Murphy and Riley's molybdenum blue (MB) method (Murphy and Riley, 1962) forms the basis for most methods. It involves reaction of the orthophosphate with ammonium molybdate under acidic conditions to form 12-

molybdophosphate, a yellow-coloured complex. This complex is reduced by either ascorbic acid or stannous chloride in the presence of antimony to give a phosphor-MB complex, which is determined at 660–880 nm, depending on reaction conditions. Antimony is not essential for the formation of the phosphor-MB complex, but its inclusion results in faster formation of the final product, which incorporates the element in a 1:2 P:Sb ratio (Drummond and Maher, 1995). Unfortunately, this reaction is not completely specific for orthophosphate; silicic acid (SiO_4^{4-}) and arsenate (AsO_3^{3-}) also form MB complexes, although formation of the former can be minimised with optimised reaction conditions (Zhang et al., 1999). Arsenate interference can be eliminated by reduction to arsenite (AsO_3^{3-}) (Johnson, 1971; Johnson and Pilson, 1972), but the precipitation of colloidal sulphur limits the usefulness of the procedure (Tsang et al., 2007), so field measurements are very rarely corrected for arsenate. Furthermore, the acidic reaction conditions employed in the method hydrolyse pyrophosphate ($P_2O_7^{4-}$) and selected organic-P compounds, resulting in the overestimation of orthophosphate concentrations. For this reason, the fraction measured by the MB procedure is termed soluble reactive phosphate (SRP).

These well-established techniques provide analyses with a precision of around 1% RSD and are relatively simple to perform. Their main limitation is that the LOD is approximately 0.1 µM nitrate and 0.03 µM phosphate, which means that variations in nM nitrate and phosphate concentrations will pass unobserved in oligotrophic ocean regions where these nutrients control primary production. In recent decades, researchers have developed a range of methods to determine nitrate and phosphate in seawater at nM concentrations. This chapter outlines the various approaches, with particular emphasis put on the analytical challenges associated with the methods and their suitability for field analysis.

Table 3.1 Overview of reported methods for nanomolar phosphate analysis in seawater.

Detection	Chemistry	Technique	Figures of Merit	Comments	Ref.
colorimetry	phospho-molybdenum blue	SCFA 2 m LWCC used as flow-cell	DL: 0.8 nM P: 4.8% (at 10 nM) R: 0.8 – 600	+ adapted from established standard technique + automated and requires no sample pre-treatment + simultaneous parallel measurement of nitrite/nitrate ~ 4 min per analytical cycle	this study
colorimetry	phospho-molybdenum blue - cetyltrimethylammonium bromide (PMB-CTAB)	FIA PMB-CTAB ion-pair complex pre-concentrated onto a C18 SPE cartridge 2 cm flow-cell	DL: 1.6 nM P: 4.5% (at 32.4 nM) R: 3.2 – 48.5 nM	+ automated system - accurate measurement of sample volume required; reagents are added directly to sample bottle by FIA system - slow formation of ion-association complex ~ 30 min per analytical cycle	(Liang et al., 2007)
CL	12-molybdophosphate – cetyltrimethylammonium bromide (MP-CTAB)	FIA MP-CTAB ion-pair complex pre-concentrated onto a C18 SPE cartridge	DL: 2 nM P: 4.7% (at 97 nM) R: 5 – 194 nM	- accurate measurement of sample volume required, since reagents are added directly to sample bottle -2-step rinse of SPE cartridge required to remove all traces of sample matrix, which interferes with CL reaction ~10 min per analytical cycle	(Liang et al., 2006)
colorimetry	12-molybdophosphate - malachite green, surfactant	manual sample preparation 10 cm quartz cell	DL: 8 nM P: 3.4% (at 50 nM) R: 10 – 400 nM	+ uses less acidic reaction conditions than previous MG methods, although pH still lower than for PMB methods - 40 min to develop colour	(Huang and Zhang, 2006)
colorimetry	phospho-molybdenum blue	manual sample preparation MAGIC 25 x pre-conc factor 10 cm cell	DL: 0.8 nM P: 102% (at 2 nM) R: 0.8 – 200 nM	+ improved version of the MAGIC procedure with reduced analysis time (~60 min) - samples pre-filtered to reduce turbidity	(Rimmelin and Moutin, 2005)
colorimetry	phospho-molybdenum blue	manual sample preparation HPLC analysis with C8 column	DL: 1 nM P: 5.6% (at 1 nM) R: 3 – 300 nM	- purification of reagents necessary for concentrations below 10 nM ~15 min HPLC injection interval	(Haberer and Brandes, 2003)
colorimetry	phospho-molybdenum blue	SCFA 2 m LWCC used as flow-cell	DL: 0.5 nM P: 2% (at 10 nM) R: 0.5 – 200	+ adapted from established standard technique + automated and requires no sample pre-treatment ~ 2 min per analytical cycle	(Zhang and Chi, 2002)
CL	vanadomolybdophosphate - dodecylpyridinium bromide (VMP-DDPB)	manual sample preparation VMP-DDPB ion-pair complex extracted onto paper filters and measured in a CL photometer	DL: 0.6 nM P: 14% (at 0.97 µM) R: 2 – 55 nM	+ does not require organic solvents unlike other filter pre-concentration methods ~25 min per sample	(Zui and Birks, 2000)

Detection	Chemistry	Technique	Figures of Merit	Comments	Ref.
colorimetry	phospho-molybdenum blue	manual sample preparation $Mg(OH)_2$-induced co-precipitation to concentrate PO_4^{3-} (MAGIC) 100 x pre-conc factor 10 cm cell	DL: 0.2 nM P: 10% (at 2 nM) R: NR	+ requires only a centrifuge + reagents added after pre-concentration step so blanks lower - long procedure (~90 min) with multiple steps	(Wu et al., 2000)
colorimetry	phospho-molybdenum blue	manual sample preparation n-hexanol liquid-liquid extraction 10 cm cell	DL: 4 nM P: NR R: 0 – 300 nM	+ requires no specialised equipment - contains several steps and uses significant volumes of organic solvents ~ 20 min sample preparation	(Hansen and Koroleff, 1999)
colorimetry	12-molybdophosphate-malachite green	manual sample preparation MP-MG ion-pair complex concentrated by extracting onto a cellulose nitrate filter	DL: 2 nM P: 0.57% (at 97 nM) R: 2 – 600	~20 min per analytical cycle	(Susanto et al., 1995)
colorimetry	phospho-molybdenum blue	manual sample preparation 60 cm capillary cell with standard LED source and photodiode detector	DL: 1 nM P: 6% (at 8 nM) R: 1 – 500 nM	+ standard LED and photodiode detection - Non-linearity and attenuation of light in cell ~ 40 min per analytical cycle	(Ormaza Gonzalez and Statham, 1991)
colorimetry	phospho-molybdenum blue - dodecyltrimethylammonium bromide (PMB-DTAB)	manual sample preparation PMB-DTAB ion-pair complex concentrated onto a 25 mm 0.45 µm cellulose nitrate filter, followed by dissolution in DMF	DL: 0.6 nM P: 2.2% (at 34 nM) R: 32 – 4500 nM	+ uses less solvent than liquid-liquid extraction ~ 25 min sample preparation	(Taguchi et al., 1985)
colorimetry	12-molybdophosphate - malachite green	manual sample preparation toluene/methylpentan-2-one liquid-liquid extraction 10 cm cell	DL: 3 nM P: 1.1% (at 139 nM) R: NR	+ requires no specialised equipment - contains several steps and uses significant volumes of organic solvents	(Motomizu et al., 1984)
colorimetry	phospho-molybdenum blue	manual sample preparation 1m capillary cell	DL: 0.2 nM P: 5% (at 1.6 nM) R: 0.2 – 323 nM	- non-linearity and attenuation of light in cell - Specialised optics and laser light source used ~ 30 min per analytical cycle	(Lei et al., 1983)
TL colorimetry	phospho-molybdenum blue	manual sample preparation 1cm cell with high-powered laser and specialised optics	DL: 0.2 nM P: 11.6% (at 3 nM) R: 0.2 – 16 nM	- complex and bulky equipment required ~ 30 min per analytical cycle	(Fujiwara et al., 1982b)

Methods are listed in order of the year they appeared in the literature, with the most recent listed first. CL, Chemiluminescence; FIA, Flow-injection analysis; SPE, Solid-phase extraction; TL, Thermal lensing; LED, Light-emitting diode; SCFA, Segmented continuous flow analysis; LWCC, Liquid-waveguide-capillary cell; LOD, Limit of detection; P, Precision (RSD); NR, Not reported; R, Range of concentrations for which method is reported to be suitable.

3.2 Nanomolar phosphate methods

There are, in principle, three ways to lower the LOD of a chemical analysis:

1. optimise the chemistry so that, for example, the reaction produces a more easily detected product;
2. pre-concentrate the analyte prior to analysis; or,
3. use a more sensitive instrument to detect the reaction product.

Most methods centre on pre-concentration and/or detector sensitivity. Table 3.1 shows an overview of the reported methods, their LODs, precision, and concentration range for the analysis of phosphate in seawater at nM concentrations.

3.2.1 Optimising the chemistry

There are only limited options to improve the LOD of phosphate analysis by altering the chemistry. The MB method has been in use since the 1920s and numerous improvements have been made over the years (Karl and Björkman, 2002). Colour development is rapid and pH and reagent concentrations have been optimised to increase specificity for orthophosphate. It seems unlikely that further significant improvements will be made with this method. Using a more highly coloured chromophore is another option but, in general, the molar absorptivities of dyes are of the same order of magnitude. Malachite green, a cationic dye, is one alternative that has received significant attention. When combined with 12-molybdophosphate, the dye forms a highly coloured ion-pair complex with a molar absorptivity coefficient around five times that of the phosphor-MB complex. Historically, malachite green methods have suffered from poor reagent stability, chromophore stability and poor selectivity, the last being due to acidic reaction conditions resulting in more hydrolysis of organic phosphorus compounds compared with phosphor-MB. There has been some recent work on this method, which has addressed the principal limitations (Huang and Zhang, 2006). However,

colour development takes around 40 min, which limits its suitability for automated analysis.

3.2.2 Pre-concentration approaches

Perhaps the most widely used method for determining nM concentrations of phosphate is the magnesium-induced co-precipitation (MAGIC) method, developed by Karl and Tien (Karl and Tien, 1992). It involves addition of sodium hydroxide to the water sample to induce precipitation of brucite ($Mg(OH)_2$). Orthophosphate is quantitatively removed from solution by adsorption to the precipitate, which is collected by centrifugation and dissolved in a small volume of dilute acid. Phosphate is then determined using the standard MB protocol. Unlike other pre-concentration techniques, most of the reagents are added after the concentration step, resulting in low blank values. The pre-concentration factor (the ratio between the volume of the initial sample and the re-dissolved precipitate) can be altered to allow the determination of different concentration ranges, and LODs as low as 0.2 nM PO_4^{3-} have been reported (Wu et al., 2000). Low LODs and high precision, combined with a requirement for only basic laboratory instrumentation, have resulted in the widespread adoption of the technique. Nonetheless, the MAGIC procedure comprises several manual steps and is therefore susceptible to contamination, time consuming and inconvenient for the analyses of large numbers of samples at sea. It also requires relatively large sample volumes (up to 250 ml) in order to achieve a high pre-concentration factor.

It is also possible to concentrate the analyte after formation of the chromophore. One approach is to use an immiscible organic solvent, such as hexane, to extract and concentrate the MB (Hansen and Koroleff, 1999) or 12-molybdophosphate malachite-green ion-pair complex (Motomizu et al., 1984). Alternatively, the coloured compound can be concentrated by extraction onto an acetate or cellulose nitrate filter, followed by dissolution of the filter in a small volume of organic solvent prior to spectrophotometric analysis (Taguchi et al., 1985; Susanto et al., 1995). While LODs as low as 0.6 nM have been reported (Taguchi et al., 1985), all of these methods involve several manual steps and require the use of organic

solvents. More recent efforts have included an automated FIA system, which concentrates an ion-pair complex of phosphor-MB and cetyltrimethylammonium bromide (CTAB), a cationic surfactant, onto a C18 SPE cartridge (Liang et al., 2007). An LOD of 1.6 nM was reported, but slow ion-pair formation resulted in low sample throughput.

Analogously, in a reported HPLC method, the phosphor-MB complex is concentrated onto a C8 column (Haberer and Brandes, 2003). This method uses manual sample derivatisation prior to HPLC analysis, so it is more labour intensive than the FIA approaches.

A general disadvantage of all the methods in which the chromophore is concentrated is that the reagents are also concentrated, resulting in increased blank values. In many cases it is necessary to purify the reagents prior to use, or to purchase very pure reagents.

3.2.3 Enhancing the detection technique

Another way to determine nM phosphate concentrations is to use a method of detection that is more sensitive than conventional spectrophotometry. Chemiluminescence offers superior sensitivity to spectrophotometry, because the signal is determined against a low background, so it is often applied in trace analysis. The oxidation of luminol (3-aminophthalhydrazide) results in the chemiluminescent emission of blue light (λ ~ 440 nm) and is the basis of several methods for phosphate analysis. Since Mg^{2+}, Ca^{2+} and other metal cations present in seawater can also facilitate luminol oxidation, the technique is combined with a pre-concentration step, which removes the sample matrix and concentrates the analyte. A recent example is a luminol-based FIA system, in which the ion-pair complex between CTAB and 12-molybdophosphate is extracted onto a C18 SPE cartridge (Liang et al., 2006). In this approach, the cartridge required rinsing with both water and ethanol to remove traces of sea-salt matrix, and this, along with the need to buffer the luminol reaction at high pH, made the injection programme somewhat complicated. The approach provided an LOD of 2 nM PO_4^{3-}, but the

precision (12% RSD at 42 nM PO_4^{3-}) was low in comparison with other available methods.

Electrochemical methods for the analysis of phosphate are also available. Ortho-phosphate is electrochemically inactive and therefore requires derivatisation in order to be detectable. Many reported electrochemical techniques for phosphate analysis rely on the reduction of 12-molybdophosphate or the oxidation of phosphor-MB. Electrochemical techniques have advantages over spectro-photometric methods:

1. they suffer less interference from dissolved silicon or turbidity; and,
2. they do not suffer from refractive index (Schlieren) effects in high-salinity samples.

However, the LOD of these techniques is typically of the order of 0.1–5 µM (Udnan et al., 2005), so it is necessary to combine them with analyte pre-concentration. To date, there have been no reports of an electrochemical method suitable for the determination of nM phosphate in seawater.

In absorbance spectrophotometry, lower LODs can be achieved with thermal lensing colorimetry. This uses high-power lasers to increase the signal-to-noise ratio. This has been applied to molybdenum phosphate analysis, giving an LOD of 0.2 nM (Fujiwara et al., 1982b), but it requires complex, expensive and bulky equipment and is not amenable to field applications.

A simpler way to improve the sensitivity of spectrophotometry is to increase the optical path length of the measurement cell. Initially, glass capillaries were coated with aluminium paint or foil to make them internally reflective, but these suffered from non-linearity (Lei et al., 1983) and attenuation of the light source (Lei et al., 1983; Ormaza Gonzalez and Statham, 1991).

More recently, coiled quartz capillaries coated with fluoropolymer Teflon AF have been developed (Dallas and Dasgupta, 2004), allowing the total internal reflection of light within the capillary and creating a long absorbance cell. These liquid-

waveguide-capillary cells (LWCCs) are compact, available in various lengths up to 5 m, and do not suffer from the same attenuation or the non-linearity problems associated with early glass capillaries. One of the biggest advantages of using LWCCs is that the simplicity of standard spectrophotometric analysis is maintained, while achieving very low LODs. It is also possible to combine an LWCC with a standard SCFA to create an automated system capable of measuring nM phosphate concentrations with high sample throughput (Zhang and Chi, 2002). LODs are of the order of 0.5–1 nM, and data from a number of field studies using this type of approach have been published (Zhang and Chi, 2002; Krom et al., 2005).

3.2.4 Alternative approaches

With the chemical techniques discussed above, sufficiently low LODs are achieved to allow the determination of phosphate concentrations in the majority of surface ocean waters. However, as already mentioned, the reaction conditions employed for SRP measurements result in an overestimation of the true orthophosphate concentration. This overestimation is particularly significant in waters where orthophosphate concentrations are very low. Biological radiolabelled phosphate uptake assays use the ambient microbial community in seawater to determine the true bio-available phosphate concentration. In a bioassay approach used in marine waters, very precise measurements of phosphate concentrations as low as 1 nM have been reported in conjunction with SRP measurements made by long path-length LWCC photometry (Zubkov et al., 2007). Comparison of the two techniques revealed that the bioassay measurements gave values 7–55% of the SRP determinations. An alternative method has been used successfully in freshwaters to determine phosphate down to concentrations of several 10s of pM, but the technique has not yet been applied to marine samples (Hudson and Taylor, 2005). While these techniques provide the most specific measure of nutrient concentrations, they are laborious and unsuitable for routine analysis.

3.3 Nanomolar nitrate methods

Almost all available methods for the analysis of nitrate in seawater rely on its reduction to the more reactive nitrite anion prior to determination. For this reason, methods for the analysis of nitrate and nitrite must be considered together. Table 3.2 shows an overview of the reported methods, their LODs, precision, and concentration range for the analysis of nitrate/nitrite in seawater at nM concentrations.

3.3.1 Pre-concentration approaches

In contrast with trace phosphate, there have been few reports detailing analyte pre-concentration for nitrate analysis. One example uses concentration of the azo-dye product of the standard sulphanilamide and NED procedure on an anion-exchange resin prior to spectrophotometric analysis (Wada and Hattori, 1971). This approach yielded an LOD of 1–2 nM NO_2^-; however, the method was sensitive to atmospheric contamination, and large sample volumes (up to 1000 ml) were required. Combined with a prior reduction step, required for nitrate analysis, the procedure would become extremely lengthy and vulnerable to sample contamination.

HPLC has also been applied to determine low concentrations of nitrite. The method relies on the reaction of nitrite with 2,4-dinitrophenylhydrazine to form an azide, which is chromatographically separated from interfering compounds and quantified by light absorption at 307 nm. Concentrations as low as 0.1 nM NO_2^- can be detected (Kieber and Seaton, 1995). Although highly sensitive, the method is labour intensive, and requires extremely pure reagents. Any adaptation of this method for nitrate analysis would increase its complexity and the risk of sample contamination, making it unsuitable for shipboard analysis.

3.3.2 Enhancing the detection technique

A number of fluorometric methods are available for the trace analysis of nitrate and nitrite, but interferences from other ions and background fluorescence from dissolved organic matter (DOM) hamper their application to seawater. A recently

reported fluorescence approach utilises reverse FIA (rFIA) to reduce interferences (Hudson and Taylor, 2005). In rFIA, the sample acts as the carrier solution, while a fixed volume of reagent is injected into the sample stream. A background fluorescence reading is determined prior to the fluorescence peak, which results from the reagent addition. The reported rFIA technique is capable of simultaneous analysis of NO_2^- and NO_2^- + NO_3^- (using an in-line copper-cadmium column) using diazotisation of nitrite with aniline (Masserini and Fanning, 2000). Using data correction for background fluorescence and reagent fluorescence, the approach yielded low LODs (6.9 nM NO_3^-) and generated results in good agreement with a chemiluminescence-based reference technique. The analytical method is capable of 18 analytical measurements per hour, and was applied successfully at sea.

Chemiluminescence-based approaches for nitrate determination have been reported, but, as with fluorometric methods, other ions present in seawater often interfere. Gas-phase chemiluminescence based on the reaction between NO and ozone offers a convenient way of removing matrix effects, and gives a high sensitivity (Garside, 1982). The reduction of nitrite with acidified KI liberates gaseous NO from the solution, which is subsequently channelled into an NO analyser, where it is reacted with ozone. This reaction produces nitrogen dioxide in an excited state, which decays via the emission of photons. A strong reductant, typically Ti(III), can be used for simultaneous determination of nitrate and nitrite. The main drawbacks of this approach include its technical complexity and the high temperatures (600°C) required to sustain NO concentrations prior to NO reaction with ozone. In addition, the precision of NO_3^- at low levels is impaired, because of the difficulty of precisely controlling the reduction of NO_3^- to NO (Aoki et al., 1997). The LOD for the method is ca. 10 nM NO_3^- , with a precision of 6.7% at this concentration.

Several groups have developed sensitive ion-exchange chromatographic (IEC) methods for nitrate in seawater (Hu et al., 1999; Maruo et al., 2006). With direct UV detection, it is a simple procedure and one of the few techniques that measures nitrate separately from nitrite. Generally, LODs are relatively high, due to the poor shape of the nitrate peak and the tendency of nitrate to co-elute with bromide, and

long elution times of 30 min or more are required. LODs as low as 8 nM NO_3^- have been reported (Hu et al., 1999), but, during sea trials, Maruo et al. (2006) obtained a lower sensitivity than in the laboratory due to motion of the ship.

Table 3.2 An overview of reported methods for nanomolar nitrate analysis in seawater.

Detection	Chemistry	Technique	Figures of Merit	Comments	Ref.
colorimetry	sulphanilamide-NEDD	SCFA 2 m LWCC used as flow cell	DL: 1.5 nM P: 1.7% (at 20 nM) R: 1.5 – 600 nM	+ adapted from established standard technique + automated and requires no sample pre-treatment + simultaneous parallel measurement of phosphate ~ 4 min per analytical cycle	this study
UV Abs	none	ion exchange chromatography	DL: 40 nM NO3- P: 0.6% (at 60 µM NO3-) R: 1 – 60 µM NO3-	+ direct NO3- detection - adversely affected by ship's motion ~ 40 min per analytical cycle	(Maruo et al., 2006)
FLQ	tetra-substituted amino aluminium phthalocyanine	manual sample preparation followed by analysis in a standard fluorometer. Cu-Cd column used to measure nitrate	DL: 7 nM NO2- P: 3.2% (at 350 nM NO2-) R: 21 – 840 nM NO2-	method performance in seawater only assessed for nitrite ~15 min sample preparation and analysis	(Zhan et al., 2001)
Fluorescence	aniline	rFIA system λex / λem = 610 nm / 686 nm	DL: 6.9 nM NO3- P: 50% (at 6.9 nM NO3-) R: NR	+ Fully automated system - corrections made for background fluorescence and reagent blank ~ 3 min per analytical cycle	(Masserini and Fanning, 2000)
colorimetry	sulphanilamide-NEDD	SCFA 2 m LWCC used as flow cell	DL: 2 nM P: 2.9% (at 10 nM) R: 2 – 250 nM	+ adapted from established standard technique + automated and requires no sample pre-treatment ~ 2 min per analytical cycle	(Zhang, 2000)
UV Abs	None	ion exchange chromatography	DL: 8 nM NO_3^- P: < 1.2% (conc NR) R: NR	+ direct NO_3^- detection - adversely affected by ship's motion ~ 40 min per analytical cycle	(Hu et al., 1999)
colorimetry	sulphanilamide-NEDD	manual sample preparation 4.5 m LWCC	DL: 1.5 nM NO_3^- P: 8% (at 10 nM NO_3^-) R: 1.5 – 50 nM NO_3^-	~ 20 min sample preparation and analysis	(Wensheng Yao, 1998)
CL	Ti^{III}, I^-, O_3	manual sample preparation followed by analysis in a CL analyser	DL: 80 nM NO_3^- P: 5% (conc NR) R: 80 – 4 000 nM NO_3^-	- complex and bulky equipment required - difficult to control NO_3^- reduction 5 ml sample volume; a smaller volume can be used to analyse higher concentration samples ~ 5 min sample preparation and analysis	(Cox, 1980)
colorimetry	2,4-DNPH	NO2- method manual sample preparation HPLC analysis with C1 column	DL: 0.1 nM NO2- P: 4% (conc NR) R: 0.5 – 1 000 nM NO2-	- purification of reagents is required ~10 min HPLC injection interval	(Kieber and Seaton, 1995)

Detection	Chemistry	Technique	Figures of Merit	Comments	Ref.
TL colorimetry	sulphanilamide-NEDD	manual sample preparation	DL: 0.2 nM NO_2^- P: 0.2% (conc NR) R: 0.2 – 50 nM NO_2^-	- complex and bulky equipment required method could, in principle, be applied to NO_3^- analysis	(Fujiwara et al., 1982a)
CL	Fe^{II}/MoO_4^{2-}, O_3	manual sample preparation followed by He purging of sample and NO released fed into a CL analyser	DL: 2 nM nM NO_3 P: 1% (full scale) R: 2 – 20 000 nM NO_3	+ varied sample vol. for diff sample concs - complex equipment - difficult to maintain temperature of sample for NO production ~5 – 6 min per analytical cycle	(Garside, 1982)
CL	Ti^{III}, I^-, O_3	FIA system	DL: 10 nM NO_3^- P: 6.7% (at 10 nM NO_3^-) R: 100 – 10 000 nM NO_3^-	- complex and bulky equipment required - difficult to control NO_3^- reduction ~ 3 min per analytical cycle	(Aoki et al., 1997)
colorimetry	sulphanilamide-NEDD	NO_2^- method Manual sample preparation Anion exchange pre-concentration 5 cm cell used	DL: 1 – 2 nM NO_2^- P: 6.6% (at 4 nM NO_2^-) R: 1 – 100 nM NO_2^-	- 500 – 1000 ml sample required - multiple steps involved - sensitive to atmospheric contamination ~ 40 min per sample	(Wada and Hattori, 1971)

A number of nitrite methods are included, since these form the basis of most methods for analysis. Where methods are described for both nitrite and nitrate, figures of merit for nitrate only are listed. Methods are listed in order of the year they appeared in the literature, with the most recent listed first. 2,4-DNPH, 2,4-dinitrophenylhydrazine; NEDD, N-naphthylethylenediamine dihydrochloride; FLQ, Fluorescence quenching; UV Abs, UV absorption spectrophotometry; CL, Chemiluminescence; TL , Thermal lensing; rFIA, Reverse flow-injection analysis; SCFA, Segmented continuous flow analysis; LWCC, Liquid-waveguide-capillary cell; LOD, Limit of detection; P, Precision (RSD); NR, Not reported; R, Range of concentrations for which method is reported to be suitable.

As with phosphate, thermal lensing has been applied to the standard colorimetric analysis of nitrite (Fujiwara et al., 1982a), but this approach has not been widely used due to the complexity and cost of the equipment.

Again, in parallel with phosphate analysis, LWCCs have been used to enhance the sensitivity of the standard colorimetric nitrate (and nitrite) analysis. At first, sample and reagents were mixed manually prior to introduction into the flow cell (Yao et al., 1998).

More recently, Zhang (2000) combined a segmented continuous flow autoanalyser with a 2-m LWCC to produce an automated instrument capable of detecting 0.1 nM NO_2^- and 2 nM NO_3^- with a throughput of 30 samples per hour. The inherent simplicity of long-path-length spectrophotometry has enabled its successful application to nitrate analysis at sea (Zhang, 2000; Zhang et al., 2001; Krom et al., 2005).

3.3.3 SCFA combined with LWCCs

An analytical instrument capable of simultaneous analysis of nitrate (plus nitrite) and phosphate at nM concentrations has been constructed in our laboratory. The system is capable of measuring 15 samples per hour with high precision, and has an LOD (3 x σ of blank) of 0.8 nM PO_4^{3-} and 1.5 nM NO_2^- plus NO_3^-. The instrument comprises a purpose-built, 2-channel SCFA system connected to two 2-m LWCCs (WPI Inc, USA) (Figure 3.2). A peristaltic pump continuously mixes the reagents with the sample stream, and the coloured products form in the glass mixing coils. Two tungsten-halogen light sources (LS1-LL, Ocean Optics Inc., USA) are used and two miniaturised USB spectrophotometers with fibre-optic connections (USB2000 VIS-NIR, Ocean Optics Inc., USA) continuously monitor the absorbance at appropriate wavelengths in the LWCC flow-cells. Four SMA-terminated fibre-optic cables (Ocean Optics Inc., USA) transmit light to and from the LWCCs. Samples are introduced into the instrument manually or using an autosampler. Analytical reagent-grade chemicals are used throughout, with the exception of the nitrate standard, which is

prepared from high-purity KNO_3. Reagents and stock standard solutions are prepared in de-ionised water (Milli-Q, Millipore; resistivity ≥18.2 MΩcm).

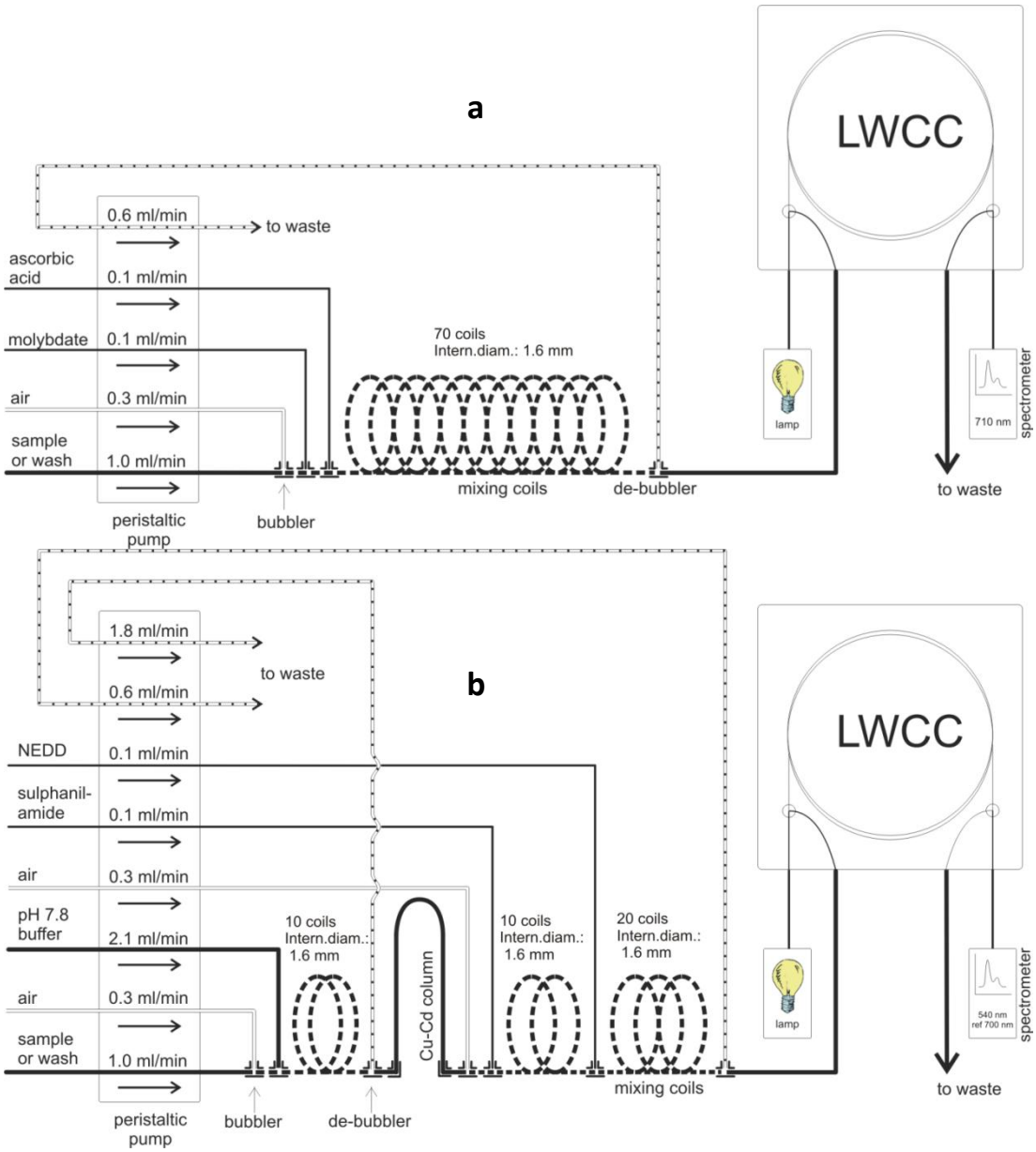

Figure 3.2 Phosphate and nitrate+nitrite SCFA-LWCC systems in use in our laboratory. The system design is based on Zhang (2000) and Zhang and Chi (2002). The glass coils used are 1.6-mm ID and larger than the 1-mm ID components used by Zhang, which may account for the lower analytical throughput achieved with the systems in our laboratory. a) Phosphate SCFA-LWCC system showing flow rates in ml/min. b) Nitrate+nitrite SCFA-LWCC system, showing flow rates in ml/min.

Refractive index changes (Schlieren effect) caused by differences in salinity between samples, standards and wash solution can cause baseline instability and lead to errors in peak-height determination. For this reason, it is important to match the salinity of wash solution and standards to the salinity of the sample (Hansen and Koroleff, 1999). Low-nutrient surface seawater is ideal for this purpose. In the case of phosphate analysis, it is possible to prepare phosphate-free seawater: 1M NaOH is added to seawater at a ratio 1:40 v/v, the phosphate-containing precipitate is allowed to settle overnight and the overlying solution is siphoned off (Karl and Tien, 1992; Zhang and Chi, 2002). However, there is no convenient way to remove nitrate from seawater, so it is necessary to analyse nitrate standards prepared in deionised water for seawater-sample calibration. Fortunately, with the nitrate method, the dilution of the sample with the buffer solution (in our case it is diluted ~3-fold with a 0.06 M imidazole buffer at pH 7.8) usually results in minimal ionic strength differences between seawater sample and standards in the final mixture (Hansen and Koroleff, 1999; Zhang, 2000).

The instrument uses the sulphanilamide/NED reaction for nitrate analysis (incorporating a copperised cadmium column for reduction of NO_3^- to NO_2^- and the MB reaction for phosphate (Zhang, 2000; Zhang and Chi, 2002). For the nitrate chemistry, the detection wavelength is 540 nm. A reference wavelength of 700 nm is used to compensate for light intensity fluctuations resulting from various sources including variations in lamp intensity, micro-bubbles within the flow cell, or Schlieren effect, and this approach hence enhances the signal-to-noise ratio.

The standard wavelength for the phospho-MB procedure is 880 nm or 885 nm. However, the transmission of light of these wavelengths in a 2-m LWCC is negligible, due to the absorption of far-red wavelengths by water. This phenomenon precludes the use of long-pathlength LWCC spectrophotometry with aqueous solutions at wavelengths greater than approximately 750 nm. For this reason, phospho-MB is determined using a slightly less intense absorption wavelength of 710 nm. Another general limitation of the phospho-MB flow-analysis techniques is the lack of a suitable reference wavelength to correct for intensity fluctuations. The analysis of phosphate is therefore more strongly affected by the formation of micro-bubbles

within the flow cell and the Schlieren effect, resulting in a lower signal-to-noise ratio compared with the nitrate system, for which a suitable reference wavelength exists. However, broadly similar LODs are obtained for both analytical nutrient techniques since the nitrate method requires dilution of the sample with a buffer solution. The influence of the Schlieren effect on the phosphate analysis also means that it is important to match the salinity of wash solution to that of standard and sample solutions.

Figure 3.3 shows the output of the phosphate instrument during calibration and the corresponding calibration curve. With SCFA, analyte contamination in the reagent solutions does not contribute proportionally to the analytical blanks. This is because the reagents are continuously pumped through the analyser and the resulting baseline signal is usually set to zero. However, it is still desirable to use reagents containing minimal concentrations of the analyte of interest, since this will lower the baseline, give an improved LOD and increase the linear dynamic range of the method.

3.3.4 Analytical challenges

Sample contamination is a major issue when determining nM nutrient concentrations. For this reason, it is preferable to use bottles, volumetric flasks and other apparatus made from plastics that are easy to clean, such as polyethylene or polypropylene. All vessels and instruments that make contact with sample or standard solutions should be thoroughly cleaned in acid. Soaking equipment in 1M HCl overnight, followed by three rinses with deionised water is sufficient to remove traces of nutrients. Cleaning protocols involving nitric acid, common in trace-metal analysis, risk introducing nitrate contamination and are unsuitable for trace-nitrate analysis.

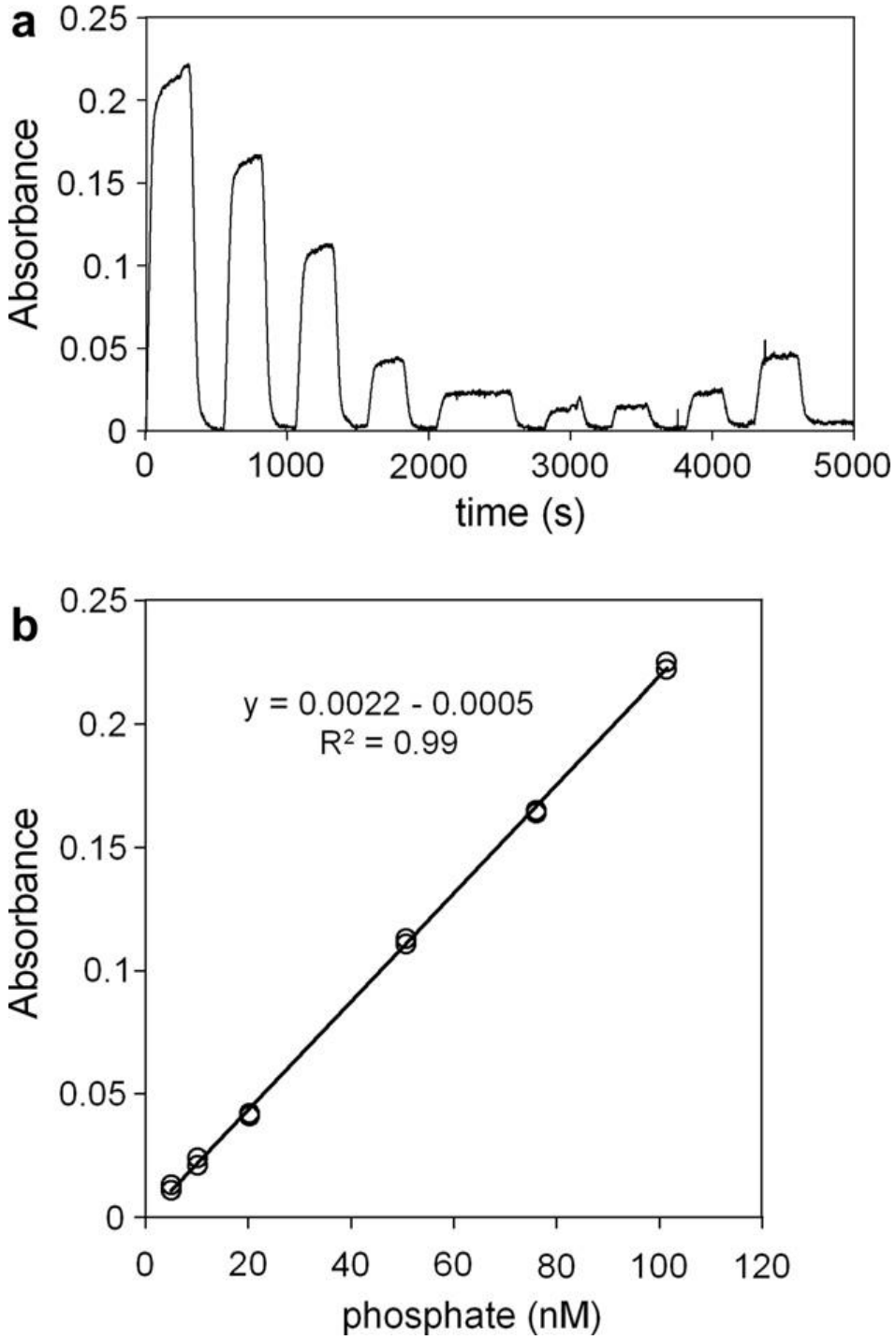

Figure 3.3 (a) Example of phosphate instrument output during a calibration. Samples were introduced manually, rather than using the autosampler, resulting in varying peak widths. The peaks represent (in chronological order) 100, 75, 50, 20, 10, 5, 5, 10 and 20-nM PO_4^{3-}. (b) Linear regression resulting from the instrumental trace shown in Fig. 3(a). Additional 50, 75 and 100-nM standard peaks included later in the analytical run have been included in the plot, but are not shown in Fig. 3(a).

Atmospheric contamination from oxides of nitrogen and air-borne particles poses a significant risk during low-level nitrate analysis. Yao et al. (1998) noted that sample blanks left open to the atmosphere overnight, developed nitrite concentrations of between 73 and 170 nM. Zafiriou et al. (1992) noted a similar effect with their nM nitrite measurements. In our laboratory, care is taken to avoid obvious sources of atmospheric contamination, such as bottles of nitric acid. However, it is still necessary to keep samples and wash solutions sealed until immediately before introduction into the instrument.

Sample and standard stability forms another potential challenge. Our approach is to dilute working standards immediately prior to analysis. Samples are stored in low-density polyethylene (LDPE) bottles in a refrigerator and analysed as soon as is practicable and preferably within 3 hours of sampling. However, there are no reported studies of the stability of seawater samples containing nM nutrient concentrations. One comparison of results from the analysis of frozen samples with samples that were analysed immediately after sampling demonstrated that the samples containing lower concentrations of nutrients were poorly preserved (Krom et al., 2005).

Contamination of the wash solution is common. Since concentrations are calculated from the height of the sample peak above the baseline, any contamination of the wash solution will increase the absorbance of the baseline and may lead to an underestimation of sample concentrations. This is more likely to occur when samples are introduced manually by moving the sample line between sample or standard solutions and the wash solution. Refreshing the wash solution minimises the contamination risks, and analysis of one or two standards at regular intervals during sample runs will help to spot any irregularities.

Micro-bubbles, which can form from dissolved air in the sample and reagent lines within the instrument, can also pose a major challenge. These micro-bubbles have a tendency to attach to the internal surfaces of the LWCC, resulting in erroneously high and fluctuating absorbance readings. The large internal surface-area-to-volume ratio of the LWCC makes this much more of a problem compared with smaller

conventional flow-cells. One solution is to de-gas reagent and sample solutions prior to their introduction into the instrument. Vacuum de-gassing or sparging with a low-solubility gas, such as helium, is commonly used in FIA, but is not easily applied to SCFA, since this approach involves the deliberate introduction of bubbles into the flow stream. In-line degassers with very small internal volumes are now commercially available. As with LWCCs, they contain Teflon AF capillaries, but here use is made of the exceptionally high gas permeability of Teflon AF rather than its special optical properties. The use of such a degasser inserted between a nitrate FIA system and an LWCC has recently been reported (Zhang, 2006), and significant improvements in signal-to-noise ratio were demonstrated. However, Teflon AF degassers are relatively expensive and not currently in widespread use. Alternatively, the tendency of micro-bubbles to attach to the walls of the LWCC can be reduced by maintaining the cell in a clean state. In our laboratory, the LWCC is cleaned thoroughly before and after use according to the manufacturer's instructions, and this approach has been found to be effective.

3.3.5 Field study

The SCFA-LWCC instrument was deployed during a research cruise on the FS Poseidon (PS332) to the tropical and sub-tropical North-East Atlantic Ocean in January–February 2006. Surface samples (ca. 3 m depth) were collected using a towed fish, which allowed contamination- free sampling within a clean laboratory container. Over a 4-week period, 170 samples were collected and analysed for nitrate (+ nitrite) and phosphate using the instrument. Figure 3.4 shows the spatial distributions of nitrate (+ nitrite) and phosphate, respectively, in the study region. The observed nutrient concentrations were low because of active biological uptake. Surface nitrate (+ nitrite) concentrations in surface waters were in the range <1.5 – 165 nM, with the lowest concentrations in thermally stratified waters (mixed layer depth ca. 60 m) in the western and southern areas of the study region, and higher concentrations in the northern areas with deeper mixed layers (ca. 120 m). Surface-phosphate concentrations were in the range 10 – 90 nM, with the lowest concentrations in thermally stratified waters in the western and southern areas of the study region. The highest phosphate concentrations were observed in the area

between 18°N and 22°N as a result of upwelling of nutrient-rich deep waters and horizontal advection of nutrient-rich waters from the Northwest African upwelling region. These results revealed low nutrient concentrations, which strongly influence primary productivity in the study region and are undetectable with conventional methods of analysis.

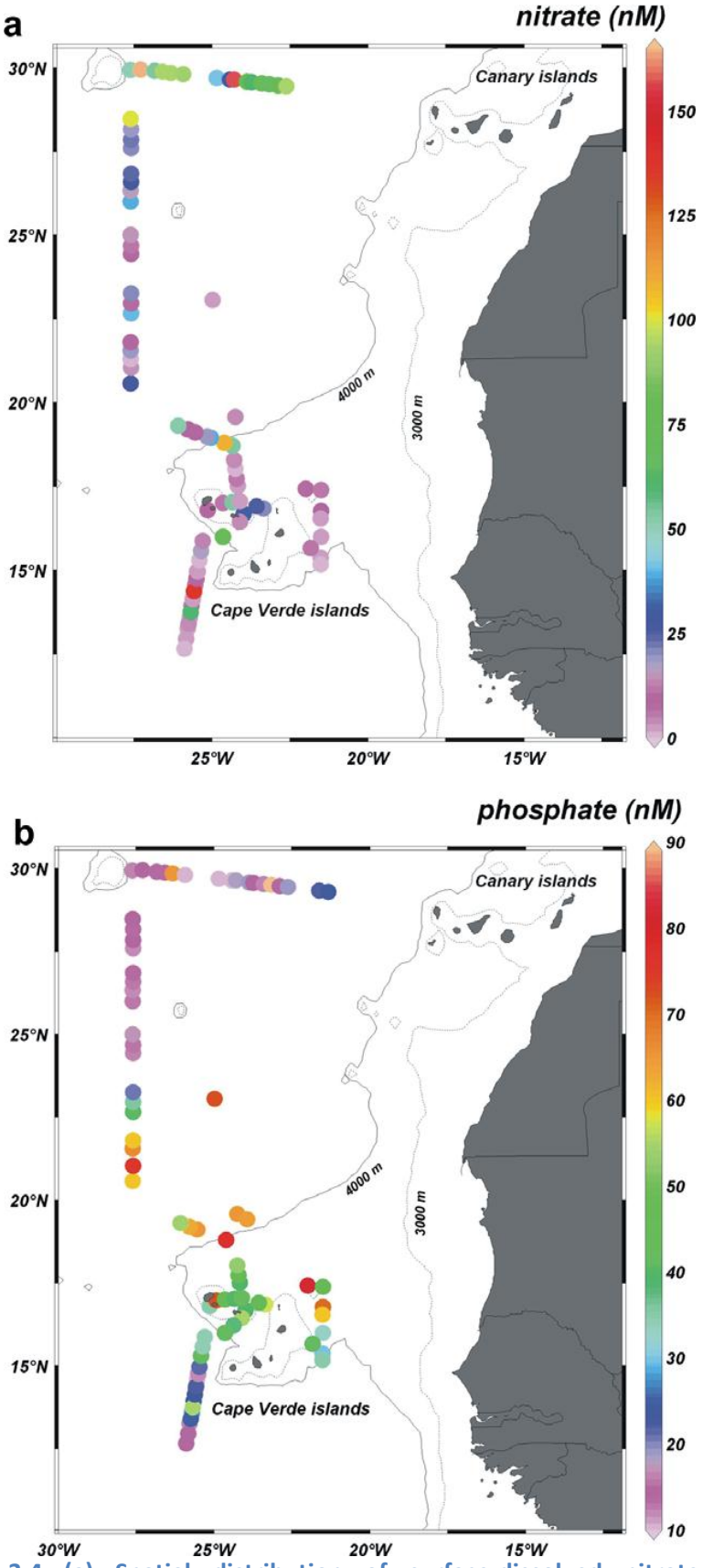

Figure 3.4 (a) Spatial distribution of surface-dissolved nitrate+nitrite concentrations in the Cape Verde Islands region during January to February 2006. (b) Spatial distribution of surface-dissolved phosphate concentrations in the Cape Verde Islands region during January to February 2006.

3.4 Conclusions

Nitrate and phosphate are nutrients of key importance in marine ecosystems and the measurement of their dissolved concentrations remains one of the most fundamental and routine measurements made by chemical oceanographers. Accurate knowledge of their concentrations is essential in order to understand many features and functions of marine ecosystems, including controls on the rate of phytoplankton growth and carbon cycling. However, surface nutrient concentrations in oligotrophic ocean regions are usually well below the limit of detection of conventional methods of analysis. Oligotrophic marine environments represent around 40% of the world's oceans, and are of significant importance to global nutrient and carbon cycling. This poses a sizeable challenge to chemical oceanographers, for whom nutrient analysis techniques have changed little since the 1960s.

Over the last three decades, a wide variety of techniques have been developed to determine nM concentrations of nitrate and phosphate in seawater and other natural waters. However, due to the technical challenges associated with these measurements, nanomolar nutrient measurements have been beyond the reach of most oceanographers until recently. Even today, nanomolar techniques are not yet routinely employed and instruments capable of nanomolar nutrient measurements are not yet commercially available. Of the many techniques described in this chapter, only the MAGIC method for phosphate has achieved widespread acceptance, but this method is labour intensive and not amenable to automation.

More recently, techniques employing LWCC flow cells have become more popular. Long path length spectrophotometry is an attractive option to those looking for a simple way to measure very low nutrient concentrations. LWCC cells can be added to existing flow-analysis-based instruments with relative ease to give nM LODs. Flow-analysis systems are generally rugged, portable, automated and capable of high sample throughput with minimised risk of sample contamination, which makes them ideally suited for shipboard analysis.

3.4.1 Future directions

Various challenges still need to be addressed in nM nutrient analysis which is still a relatively new field. As mentioned previously, corrections for interference from arsenate are rarely applied to phosphate measurements. Measurements of relatively high concentrations of phosphate contain only a small error, due to the low concentrations of arsenate present in seawater (10–30 nM (Johnson, 1971; Ormaza Gonzalez and Statham, 1991; Hansen and Koroleff, 1999)). However, now that it is possible to analyse phosphate concentrations of several nM, the interference from arsenate may be significant. There is a pressing need for a new method for the elimination of arsenate interference that is compatible with flow analysis.

Another challenge is the lack of any certified seawater standards containing zero or very low nutrient concentrations. It is possible to prepare standards by dilution from higher concentration solutions into low-nutrient seawater, but corrections are often required for salinity differences and low concentrations of nutrients in the standard matrix. Furthermore, the lack of any common standards makes verification of results from different studies difficult. Since solutions containing nM nutrient concentrations are unstable and easily contaminated, it is currently not feasible to produce such standards. Very few studies have investigated the stability of solutions containing nM concentrations of nutrients, yet such studies are essential in order to move forwards in this area.

At present, there is a drive to automate and to miniaturise analytical systems with a view to make them submersible (Gray et al., 2006; Miro et al., 2006). Such in-situ analysers could potentially be attached to frames lowered from research vessels or left on moorings for months at a time. A submersible nitrite system containing an LWCC has been reported (Adornato et al., 2005). Such an approach will eliminate sample handling and storage issues and provide data at much higher resolution than is possible with traditional sampling methodologies.

3.5 References

Adornato, L. R., et al. (2005). Continuous in situ determinations of nitrite at nanomolar concentrations. *Deep-Sea Research Part I-Oceanographic Research Papers* 52(3): 543-551.

Aoki, T., et al. (1997). Rapid flow injection analysis method for successive determination of ammonia, nitrite, and nitrate in water by gas-phase chemiluminescence. *Analytica Chimica Acta* 349(1-3): 11-16.

Bronk, D. A. (2002). Dynamics of DON.in: *Biogeochemistry of Marine Dissolved Organic Matter*. D. A. Hansell and C. A. Carlson. California, London, Elsevier**:** 153-247.

Cox, R. D. (1980). Determination of nitrate and nitrite at the parts per billion level by chemiluminescence. *Analytical Chemistry* 52(2): 332-335.

Dallas, T. and Dasgupta, P. K. (2004). Light at the end of the tunnel: recent analytical applications of liquid-core waveguides. *Trac-Trends in Analytical Chemistry* 23(5): 385-392.

Drummond, L. and Maher, W. (1995). Determination of phosphorus in aqueous solution via formation of the phosphoantimonylmolybdenum blue complex. Re-examination of optimum conditions for the analysis of phosphate. *Analytica Chimica Acta* 302(1): 69-74.

Estela, J. M. and Cerda, V. (2005). Flow analysis techniques for phosphorus: an overview. *Talanta* 66(2): 307-331.

Falkowski, P. G., et al. (1998). Biogeochemical controls and feedbacks on ocean primary production. *Science* 281(5374): 200-206.

Finch, M. S., et al. (1998). A low power ultra violet spectrophotometer for measurement of nitrate in seawater: introduction, calibration and initial sea trials. *Analytica Chimica Acta* 377(2-3): 167-177.

Fujiwara, K., et al. (1982a). Determination of phosphorus at the parts per trillion level by laser-induced thermal lensing colorimetry. *Analytical Chemistry* 54(12): 2026-2029.

Fujiwara, K., et al. (1982b). Thermal Lensing Colorimetry of Nitrite Ion with Single-Laser System. *Applied Spectroscopy* 36(2): 157-161.

Garside, C. (1982). A chemiluminescent technique for the determination of nanomolar concentrations of nitrate and nitrite in seawater. *Marine Chemistry* 11(2): 159-167.

Gray, S., et al. (2006). Flow analysis techniques for spatial and temporal measurement of nutrients in aquatic systems. *Environmental Chemistry* 3(1): 3-18.

Haberer, J. L. and Brandes, J. A. (2003). A high sensitivity, low volume HPLC method to determine soluble reactive phosphate in freshwater and saltwater. *Marine Chemistry* 82(3-4): 185-196.

Hanrahan, G., et al. (2002). High temporal and spatial resolution environmental monitoring using flow injection with spectroscopic detection. *Trac-Trends in Analytical Chemistry* 21(4): 233-239.

Hansen, H. P. and Koroleff, F. (1999). Determination of Nutrients.in: *Methods of seawater analysis*. K. Grasshoff, K. Kremling and M. Ehrhardt. Weinheim, Germany Wiley-VCH**:** 159-228.

Hu, W., et al. (1999). Direct Determination of Bromide, Nitrate, and Iodide in Saline Matrixes Using Electrostatic Ion Chromatography with an Electrolyte as Eluent. *Analytical Chemistry* 71(8): 1617-1620.

Huang, X. L. and Zhang, J. Z. (2006). Surfactant-sensitized malachite green method for trace determination of orthophosphate in aqueous solution. *Analytica Chimica Acta* 580(1): 55-67.

Hudson, J. J. and Taylor, W. D. (2005). Rapid estimation of phosphate at picomolar concentrations in freshwater lakes with potential application to P-limited marine systems. *Aquatic Sciences* 67(3): 316-325.

Johnson, D. L. (1971). Simultaneous Determination of Arsenate and Phosphate in Natural Waters. *Environmental Science & Technology* 5(5): 411-414.

Johnson, D. L. and Pilson, M. E. Q. (1972). Spectrophotometric determination of arsenite, arsenate, and phosphate in natural waters. *Analytica Chimica Acta* 58(2): 289-299.

Johnson, K. S. and Coletti, L. J. (2002). In situ ultraviolet spectrophotometry for high resolution and long-term monitoring of nitrate, bromide and bisulfide in the ocean. *Deep Sea Research Part I: Oceanographic Research Papers* 49(7): 1291-1305.

Karl, D. M. and Tien, G. (1992). Magic - a Sensitive and Precise Method for Measuring Dissolved Phosphorus in Aquatic Environments. *Limnology and Oceanography* 37(1): 105-116.

Karl, D. M. and Björkman, K. M. (2002). Dynamics of DOP.in: *Biogeochemistry of Marine Dissolved Organic Matter*. D. A. Hansell and C. A. Carlson. California, London, Elsevier**:** 249-366.

Kieber, R. J. and Seaton, P. J. (1995). Determination of Subnanomolar Concentrations of Nitrite in Natural Waters. *Analytical Chemistry* 67(18): 3261-3264.

Krom, M. D., et al. (2005). Nutrient cycling in the south east Levantine basin of the eastern Mediterranean: Results from a phosphorus starved system. *Deep-Sea Research Part II-Topical Studies in Oceanography* 52(22-23): 2879-2896.

Lei, W., et al. (1983). Determination of phosphorus in natural waters by long-capillary-cell absorption spectrometry. *Analytical Chemistry* 55(6): 951-955.

Liang, Y., et al. (2006). Flow injection analysis of ultratrace orthophosphate in seawater with solid-phase enrichment and luminol chemiluminescence detection. *Analytica Chimica Acta* 571(2): 184-190.

Liang, Y., et al. (2007). Flow injection analysis of nanomolar level orthophosphate in seawater with solid phase enrichment and colorimetric detection. *Marine Chemistry* 103(1-2): 122-130.

Maruo, M., et al. (2006). Onboard determination of submicromolar nitrate in seawater by anion-exchange chromatography with lithium chloride eluent. *Analytical Sciences* 22(9): 1175-1178.

Masserini, R. T. and Fanning, K. A. (2000). A sensor package for the simultaneous determination of nanomolar concentrations of nitrite, nitrate, and ammonia in seawater by fluorescence detection. *Marine Chemistry* 68(4): 323-333.

Miro, M., et al. (2003). Application of flowing stream techniques to water analysis. Part I. Ionic species: dissolved inorganic carbon, nutrients and related compounds. *Talanta* 60(5): 867-886.

Miro, M., et al. (2006). The potentials of the third generation of flow injection analysis for nutrient monitoring and fractionation analysis. *Environmental Chemistry* 3(1): 26-30.

Moorcroft, M. J., et al. (2001). Detection and determination of nitrate and nitrite: a review. *Talanta* 54(5): 785-803.

Motomizu, S., et al. (1984). Solvent extraction-spectrophotometric determination of phosphate with molybdate and malachite green in river water and sea-water. *Talanta* 31(4): 235-240.

Motomizu, S. and Li, Z. H. (2005). Trace and ultratrace analysis methods for the determination of phosphorus by flow-injection techniques. *Talanta* 66(2): 332-340.

Murphy, J. and Riley, J. P. (1962). A modified single solution method for the determination of phosphate in natural waters. *Analytica Chimica Acta* 27: 31-36.

Ormaza Gonzalez, F. I. and Statham, P. J. (1991). Determination of Dissolved Inorganic Phosphorus in Natural-Waters at Nanomolar Concentrations Using a Long Capillary Cell Detector. *Analytica Chimica Acta* 244(1): 63-70.

Rimmelin, P. and Moutin, T. (2005). Re-examination of the MAGIC method to determine low orthophosphate concentration in seawater. *Analytica Chimica Acta* 548(1-2): 174-182.

Susanto, J. P., et al. (1995). Determination of Micro-Amounts of Phosphorus with Malachite Green Using a Filtration-Dissolution Preconcentration Method and Flow-Injection Spectrophotometric Detection. *Analyst* 120(1): 187-191.

Taguchi, S., et al. (1985). Application of organic solvent-soluble membrane filters in the preconcentration and determination of trace elements: spectrophotometric determination of phosphorus as phosphomolybdenum blue. *Talanta* 32(5): 391-394.

Tsang, S., et al. (2007). Determination of phosphate/arsenate by a modified molybdenum blue method and reduction of arsenate by S2O42. *Talanta* 71(4): 1560-1568.

Udnan, Y., et al. (2005). Evaluation of on-line preconcentration and flow-injection amperometry for phosphate determination in fresh and marine waters. *Talanta* 66(2): 461-466.

Wada, E. and Hattori, A. (1971). Spectrophotometric determination of traces of nitrite by concentration of azo dye on an anion-exchange resin : Application to sea waters. *Analytica Chimica Acta* 56(2): 233-240.

Wensheng Yao, R. H. B. a. R. D. W. (1998). Determination of Nanomolar Concentrations of Nitrite and Nitrate in Natural Waters Using Long Path Length Absorbance Spectroscopy. *Environmental Science & Technology* 32(17): 2646-2649.

Wu, J., et al. (2000). Phosphate Depletion in the Western North Atlantic Ocean. *Science* 289(5480): 759-762.

Yao, W., et al. (1998). Determination of Nanomolar Concentrations of Nitrite and Nitrate in Natural Waters Using Long Path Length Absorbance Spectroscopy. *Environmental Science & Technology* 32(17): 2646-2649.

Zafiriou, O. C., et al. (1992). Trace Nitrite in Oxic Waters. *Deep-Sea Research Part a-Oceanographic Research Papers* 39(7-8A): 1329-1347.

Zhan, X. Q., et al. (2001). A sensitive fluorimetric method for the determination of nitrite and nitrate in seawater by a novel red-region fluorescence dye. *Analytical Letters* 34(15): 2761-2770.

Zhang, J.-Z. (2000). Shipboard automated determination of trace concentrations of nitrite and nitrate in oligotrophic water by gas-segmented continuous flow analysis with a liquid waveguide capillary flow cell. *Deep Sea Research Part I: Oceanographic Research Papers* 47(6): 1157-1171.

Zhang, J. Z., et al. (1999). Optimization of performance and minimization of silicate interference in continuous flow phosphate analysis. *Talanta* 49(2): 293-304.

Zhang, J. Z., et al. (2001). Enhanced new production observed from the diurnal cycle of nitrate in an oligotrophic anticyclonic eddy. *Geophysical Research Letters* 28(8): 1579-1582.

Zhang, J. Z. and Chi, J. (2002). Automated Analysis of Nanomolar Concentrations of Phosphate in Natural Waters with Liquid Waveguide. *Environmental Science & Technology* 36(5): 1048-1053.

Zhang, J. Z. (2006). Enhanced sensitivity in flow injection analysis using a long pathlength liquid waveguide capillary flow cell for spectrophotometric detection. *Analytical Sciences* 22(1): 57-60.

Zubkov, M. V., et al. (2007). Microbial control of phosphate in the nutrient-depleted North Atlantic subtropical gyre. *Environmental Microbiology* 9(8): 2079-2089.

Zui, O. V. and Birks, J. W. (2000). Trace Analysis of Phosphorus in Water by Sorption Preconcentration and Luminol Chemiluminescence. *Analytical Chemistry* 72(7): 1699-1703.

4. Interferences in the analysis of nanomolar concentrations of nitrate and phosphate in oceanic waters

4.1 Overview

This chapter has been published in *Analytica Chimica Acta* (Vol. 673, 2010, p. 109-116). It reports on investigations into interferences with the measurements of nanomolar nitrate + nitrite and soluble reactive phosphate (SRP) in oceanic surface seawater using a segmented continuous flow (SCFA) autoanalyser interfaced with a liquid waveguide capillary flow-cell (LWCC). The interferences of silicate and arsenate with the analysis of SRP, the effect of sample filtration on the measurement of nanomolar nitrate + nitrite and SRP concentrations, and the stability of samples during storage are described.

4.1.1 Introduction

Oligotrophic surface waters cover ca. 40% of the world's oceans and exhibit extremely low (nanomolar) inorganic nutrient concentrations and a low primary productivity (Falkowski et al., 1998). Our ability to study nutrient biogeochemistry in these waters has been hampered by significant analytical challenges involved in the determination of low nutrient concentrations. Over the past few decades a wide variety of analytical approaches has been applied to this challenge, but instruments capable of measuring nutrients at nanomolar concentrations that are sufficiently robust and portable for routine ship-board (Gimbert et al., 2007; Patey et al., 2008) and in-situ analysis (Adornato et al., 2007) have only become available in recent years.

Increased sensitivity for nutrient analysis has in general been achieved by improvement of the long-established chemical analyses. Today, popular methods to

obtain nanomolar phosphate detection include the magnesium-induced co-precipitation (MagIC) technique, which works by pre-concentrating phosphate in seawater samples prior to conventional analysis (Karl and Tien, 1992; Rimmelin and Moutin, 2005). Furthermore, the use of long path-length absorption spectroscopy, usually with a liquid-waveguide capillary-cell (LWCC) connected to an automated flow analysis-based system, has been reported for nanomolar nitrate or phosphate analysis (Yao et al., 1998; Zhang, 2000; Zhang and Chi, 2002; Dallas and Dasgupta, 2004; Anagnostou and Sherrell, 2008).

The Murphy and Riley molybdenum blue (MB) method forms the basis for the majority of phosphate methods applied to natural waters (Murphy and Riley, 1962). Orthophosphate (PO_4^{3-}) reacts with ammonium molybdate under acidic conditions and is subsequently reduced to produce the intensely coloured phospho-molybdenum blue complex, which is determined by absorption spectrophotometry. The method is simple, sensitive and amenable to automation, and consequently has been adopted widely. The MB phosphate method does, however, suffer from a number of interferences. A hypothetical, perfect method for measuring dissolved phosphate concentrations would be entirely specific for dissolved orthophosphate, a fraction commonly referred to as the dissolved inorganic phosphate (DIP), which is the biologically relevant nutrient. With the MB method, the acidic reaction conditions also hydrolyse pyrophosphates ($P_2O_7^{4-}$) and some organic phosphorus compounds. In addition arsenate (AsO_4^{3-}) and dissolved silicon ($Si(OH)_4$) also form MB complexes (Johnson, 1971), which results in an overestimation of orthophosphate concentrations. As a result of this, the operational term “soluble reactive phosphate” (SRP) is used to describe the fraction measured by the MB method (Karl and Björkman, 2002). Throughout this chapter, the term SRP is used to refer to this measured fraction, while DIP is used to refer to orthophosphate alone.

These interferences are more likely to be significant when orthophosphate is present at nanomolar concentrations, since arsenate is present at similarly low concentrations in seawater (typically ca. 20 nM in the open ocean (Johnson, 1971; Ormaza Gonzalez and Statham, 1991; Karl and Tien, 1997)). Furthermore, whilst

dissolved silicon is often present in the marine environment at micromolar concentrations, optimisation of the MB reaction conditions limits the silicon interference effect in the measured SRP signal to several nM (Zhang et al., 1999). Interference from other forms of dissolved phosphorus are also more significant at low orthophosphate concentrations, when these interfering forms are present at similar or greater concentrations than orthophosphate (Karl and Björkman, 2002). Arsenate interference can be overcome by reduction of arsenate (AsO_4^{3-}) to arsenite (AsO_3^{3-}) with thiosulphate. However, the MagIC method is the only nanomolar phosphate technique in which this approach is routinely employed (Karl and Tien, 1992; Rimmelin and Moutin, 2005), since the increase in reaction time and precipitation of colloidal sulphur associated with this additional step significantly limits its usefulness in automated analysis (Tsang et al., 2007). Most reported phosphate measurements, particularly those made using automated techniques, include no correction for interference effects (Karl and Björkman, 2002). This creates uncertainty when comparing datasets, especially at low phosphate concentrations.

Nitrate and nitrite are usually measured with a technique involving the diazotisation reaction of nitrite with sulphanilamide, followed by coupling with N-(1-naphthyl)-ethylenediamine dihydrochloride (NED) to form a pink dye that is determined spectrophotometrically (Hansen and Koroleff, 1999). Nitrate can be determined using this approach following reduction to nitrite, which is typically undertaken using a copperised cadmium column. Consequently, whilst the sulphanilamide-NED approach without reduction yields nitrite, the analysis following reduction yields nitrate + nitrite and therefore it is possible to calculate the nitrate concentration from the difference. However, nitrite concentrations in oceanic surface waters are typically very low (for example 0.4-1 nM in the Caribbean and Southwest Sargasso sea (Zafiriou et al., 1992)) and it is therefore common to report nitrate + nitrite concentrations only. This method for nitrate / nitrite analysis is not subject to any known interferences in oxygenated seawaters.

Sample handling and storage constitute important procedures in nutrient studies. A considerable amount of literature has been published on the storage of nutrient

samples (see, for example (Kotlash and Chessman, 1998; Gardolinski et al., 2001)), but this deals almost exclusively with higher concentration samples that have been analysed using conventional nutrient techniques. As a result of poor solution stability, there is currently no common, widely distributed reference nutrient standard available containing zero or nanomolar nutrient concentrations in seawater or any other matrix. Such a standard would enable a more accurate determination of the concentration of the blank (a problem with many nanomolar nutrient analyses) and also facilitate comparison of data obtained in different locations and by different methods.

It is common to measure open ocean nutrient samples without prior filtration since particulate nitrogen and phosphorus do not react rapidly enough to significantly increase the result, at least for samples containing micromolar nutrient concentrations (Hansen and Koroleff, 1999). For nanomolar measurements, the literature contains reports of data measured on both filtered (for example Pulido-Villena et al. (2010)), and unfiltered samples (for example Li et al. (2008)). To date there has been only one report of the effect of filtration on nanomolar SRP measurements, in which decreases of several nM in the filtered solutions were observed (Li and Hansell, 2008). The authors ascribed these decreases to both the removal of particulate phosphate from the sample (some of which would otherwise dissolve and react with the MB reagents) and to adsorption of DIP onto the filter material. We are not aware of any published work on the effects of filtration and sample stability on nanomolar level nitrate / nitrite determinations. There is a clear need for more understanding of nutrient stability and the effects of sample handling procedures, such as filtration, at nanomolar concentrations, since small differences in concentration at this level are often significant.

This chapter reports on arsenate and dissolved silicon interferences for the nanomolar phosphate long path-length absorption spectroscopy technique. In addition, the influence of sample filtration and storage is addressed with respect to nanomolar phosphate and nitrate + nitrite analyses, as obtained during ship-board experiments in the tropical and sub-tropical Northeast Atlantic Ocean. This work represents the first comprehensive investigation into interferences in the measurement of nanomolar nitrate and phosphate and highlights the need to consider these effects thoroughly when developing any new instrument.

4.2 Methods

4.2.1 Analytical system, reagents and standards

Nitrate (nitrate + nitrite; hereinafter nitrate) and phosphate measurements were made using a segmented continuous flow autoanalyser modified with a LWCC flow-cell, with a resolution of 0.25 nM/√Hz (nitrate) / 0.23 nM/√Hz (phosphate), resulting in a detection limit (defined as 3 x σ of repeated measurements of a very low standard) of 0.56 nM/√Hz (nitrate) / 0.51 nM/√Hz (phosphate) (see Table 4.1). The typical accuracy of the system (estimated as ± 2 standard errors of the sample estimate, derived from the standard errors of the calibration linear regression coefficients (see Miller and Miller (1993) for the formula used) is typically in the range ± 1 – 3 nM for both nitrate and phosphate, but depends on the quality of the calibration curve. A more detailed description of the instrument can be found in Chapter 3, so only a summary is given below.

The system comprised a purpose-built, 2-channel SCFA system connected to two 2-metre type II LWCCs (WPI Inc, USA) (Figure 4.1). These waveguides consist of a fused silica tube with its inner surface in contact with the sample and outer surface coated with a low refractive index material (Teflon AF).

Table 4.1 Instrument performance characteristics. Determined by 9 consecutive determinations of a low standard (phosphate free seawater for phosphate and low-nutrient seawater containing 6 nM nitrate/nitrite). Values have been scaled by the square root of the sampling time in order to facilitate comparison of different instruments.

	Std deviation σ (nM)	Sampling frequency (Hz)	Resolution (nM/√Hz)	Detection limit (3·σ) (nM/√Hz)
$NO_2^- + NO_3^-$	0.18	0.56	0.25	0.56
PO_4^{3-}	0.17	0. 51	0.23	0.51

A peristaltic pump continuously mixed the reagents with the sample stream, and the coloured products were formed in the glass mixing coils. Two tungsten-halogen lamps (LS1-LL, Ocean Optics Inc., USA) were used for the light source and two miniaturised USB spectrophotometers with fibre-optic connections (USB2000 VIS-NIR, Ocean Optics Inc., USA) continuously monitored the absorbance at the appropriate wavelengths in the LWCC flow-cells. Four SMA-terminated, 400 µm diameter fibre-optic cables (Ocean Optics Inc., USA) transmitted light to and from the LWCCs. Samples were introduced into the instrument manually at a rate of 15 samples.h^{-1}. All reagents were prepared using deionised water (Milli-Q, Millipore; resistivity ≥18.2 MΩcm) and all apparatus was cleaned by soaking in 1 M HCl overnight and rinsing thoroughly with deionised water. Reagents were prepared in accordance with the method described by Zhang and Chi (2002). All reagents were of analytical reagent grade and obtained from Fisher Scientific, unless stated otherwise.

Reagents for the phosphate method: ammonium molybdate ($(NH_4)_6Mo_7O_{24}.4H_2O$) solution was prepared by dissolving 3 g potassium antimonyl tartrate in 1 litre of deionised water. 50 mL of this solution was added to a solution containing 2.3 g ammonium molybdate dissolved in 192 mL of 2.5 M H_2SO_4 and diluted to 1 litre with deionised water. An ascorbic acid solution with added surfactant was prepared on a daily basis by dissolving 0.5 g ascorbic acid and 7 g sodium dodecyl sulphate (99% purity, Acros Organics) in 100 mL deionised water.

Reagents for the nitrate method: NED solution was prepared by dissolving 1 g N-1-naphthylethylenediamine hydrochloride in 1 litre of deionised water. Sulphanilamide solution was prepared from a stock solution of 10 g sulphanilamide dissolved in 1 litre of 1 M HCl. To reduce surface tension and improve the flow characteristics inside the autoanalyser and flow cell, a 25% aqueous solution of Brij-35 (Sigma-Aldrich) was added to this solution prior to analysis (250 µL Brij per 100 mL of stock solution). A buffer solution containing 3.4 g imidazole (ACS reagent grade, Sigma-Aldrich) in 1 litre of deionised water was adjusted to pH 7.8 with 4 M HCl.

Standard calibration solution preparation: nitrate stock standards (2 mM) were prepared from high-purity KNO_3 (99.999%, Acros Organics; pre-dried for 2 h at 60°C to remove residual moisture) and nitrite stock standards (2 mM) from $NaNO_2$ (also pre-dried for 2 h at 60°C). Orthophosphate stock standards (1 mM) were prepared from KH_2PO_4 (Analytical reagent grade, Fisher Scientific). These solutions were prepared in deionised water and were stored in the dark at 4°C. A silicate stock standard (4 mM) was prepared from Na_2SiF_6. An arsenate stock standard (1 mM) was prepared from $Na_2HAsO_4.7H_2O$ (Sigma-Aldrich). Working standards were prepared fresh each day by serial dilution of the stock standards with either low nutrient seawater (LNSW) for nitrate analysis or phosphate-free seawater (PFSW) for phosphate analysis.

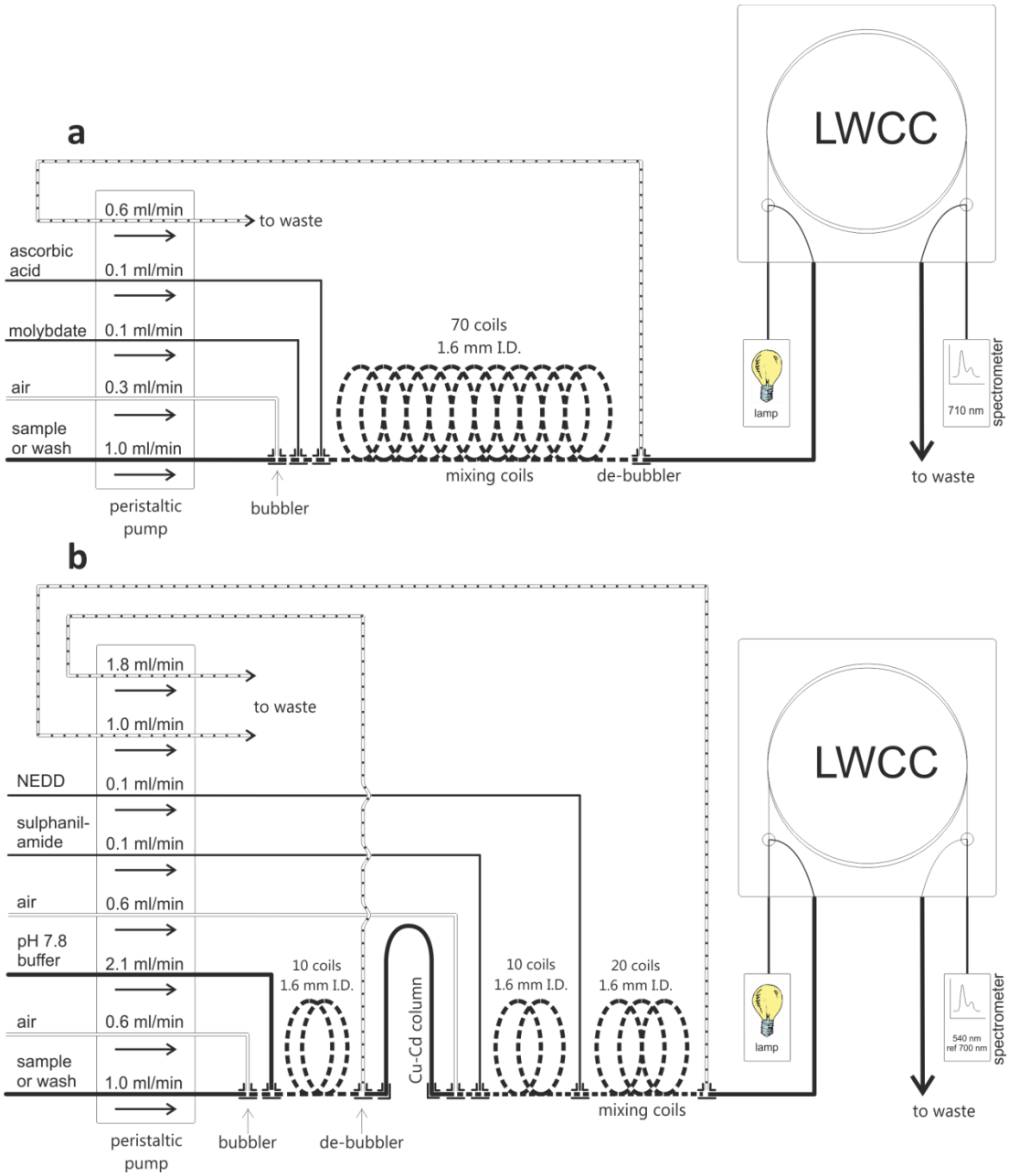

Figure 4.1 Schematic diagrams of (a) phosphate and (b) nitrate + nitrite SCFA-LWCC systems. Flow rates are shown in ml/min. The glass coils used are of 1.6 mm ID.

LNSW was collected from the tropical and sub-tropical Northeast Atlantic Ocean and filtered through a 0.2 µm cartridge filter (Sartobran 300, Sartorius). This seawater was used as a matrix for the dilute working standards and as a wash solution for the nitrate system. It is necessary to quantify and correct for the amount of nitrate in this seawater by analysing it against nitrate standards in a matrix of deionised water (assuming negligible nitrate in the deionised water and applying a correction for salt effect and refractive index (Zhang, 2000; Zhang and Chi, 2002)). Blank signals from the reagents can be set to zero during the analysis, since reagents are pumped through the system continuously. However, a high reagent blank reduces the linear dynamic range of the instrument and pump pulsing and flow fluctuations lead to reduced precision at high baseline levels. With our instrumental configuration and the absorbance set to zero with deionised water flowing through the LWCC, a typical reagent baseline (with deionised water as the wash solution) is ca 0.12 absorbance units.

Phosphate-free seawater was prepared by addition of 1 M NaOH to LNSW in a ratio of 1:40 v/v. After the magnesium hydroxide precipitate had been allowed to settle the overlying solution was siphoned off into acid-rinsed LDPE bottles. This phosphate stripped seawater was used as the matrix for working standard solutions and as a wash solution for the phosphate line of the analytical instrument. With reagents and deionised water flowing through the LWCC (with the cell filled with deionised water as a reference) the baseline is typically < 0.01 absorbance units with our system.

For the nitrate chemistry, a detection wavelength of 540 nm was used. To enhance the signal-to-noise ratio, a reference wavelength of 700 nm was used. This facilitated the compensation for light intensity fluctuations resulting from various sources including variations in lamp intensity, micro-bubbles within the flow cell, or the Schlieren effect, and this approach enhanced the signal-to-noise ratio (Dias et al., 2006). For the phosphate chemistry, a detection wavelength of 710 nm was used. The standard wavelength used for phosphate determinations with the MB method is 880 nm, but far red light absorption by water in long path-length LWCC

spectrophotometry precludes use of wavelengths greater than ca. 750 nm (Braun and Smirnov, 1993).

4.2.2 Arsenate interference experiments

Using PFSW as the solution matrix a series of AsO_4^{3-} standard solutions were prepared to give final concentrations of 0, 25, 50, 75 and 100 nM. To investigate the potential influence of phosphate on the arsenate interference effect, phosphate was added to the arsenate standards to give concentrations of 0, 5, 10, 20 and 50 nM PO_4^{3-}.

4.2.3 Silicate interference experiments

In oligotrophic open-ocean environments where SRP concentrations are in the nanomolar range, dissolved silicon concentrations are typically < 2.5 µM (see for example, World Ocean Atlas, 2005). The background concentration of dissolved silicon in the low nutrient seawater used for the experiments was 1.1 µM (measured with a standard colourimetric autoanalyser (Hansen and Koroleff, 1999)). Since the interference effect of dissolved silicon on the SRP measurement is relatively weak, fairly high concentrations of $Si(OH)_4$ were added to facilitate quantification of the interference. LNSW was spiked to give final additions of 2, 20, 40, 80 and 100 µM $Si(OH)_4$ above the background concentration.

4.2.4 Effect of sample filtration

The effect of sample filtration on nanomolar SRP and nitrate concentrations was investigated during a cruise in the tropical and sub-tropical Northeast Atlantic Ocean (*RRS Discovery* cruise 326, January – February 2008). Surface seawater samples were collected from a towed fish (towed at 3 – 4 m depth) using a Teflon diaphragm pump which pumped the surface seawater through acid-washed PVC tubing into a trace-metal clean chemistry laboratory. Samples were either collected unfiltered or filtered by diverting the flow through a filter capsule (Sartobran 300, Sartorius) containing a cellulose acetate membrane with a 0.2 µm cut-off. Samples were collected in acid-washed 60 mL LDPE bottles and stored in the dark at 4°C. To

observe differences between filtered and unfiltered samples, four samples were taken in quick succession (within 3 min); two filtered and two unfiltered, alternating between filtered and unfiltered samples in order to eliminate the possibility of differences arising from spatial changes in nutrient concentrations in the surface seawater. This experiment was carried out 5 times during the cruise.

4.2.5 Sample stability

Sample stability was also investigated during the *RRS Discovery* D326 cruise. Both filtered and unfiltered samples were tested. Twelve acid-washed 60 mL LDPE sample bottles were filled with surface seawater from a single Niskin (General Oceanics Inc.) sampling bottle collected during a depth cast. Bottles 1 – 9 were stored in the dark at 4°C; bottles 10 – 12 were frozen at -20˚C. Three of the refrigerated samples were analysed for nanomolar nutrients within a few hours of sampling; three further samples were removed and tested after 1 day of storage; and another three bottles were analysed after 2 days. Additionally, bottles 1-3 were retested at the one-day and two-day time-points to investigate whether concentrations in these individual bottles had remained stable. After 12 days, the frozen samples were defrosted and analysed.

4.3 Results and discussion

4.3.1 Arsenate interference of the nanomolar phosphate technique

Arsenate produces a MB complex with a comparable absorption spectrum to that formed with phosphate (Johnson, 1971). However, the formation of the arsenomolybdic complex is much slower than formation of the phosphomolybdic complex (ca. 90 min versus 5 min) (Johnson, 1971), and in addition the concentrations of arsenate in seawater are generally low (ca. 20 nM) (Johnson, 1971; Ormaza Gonzalez and Statham, 1991; Karl and Tien, 1997). Furthermore, the rate of arsenomolybdic complex formation is catalysed by phosphate ions (Hansen and Koroleff, 1999). The time allowed for phosphate colour formation following

addition of reagents in our autoanalyser is ca. 10 min, and consequently any arsenomolybdic complex formation is likely to be incomplete.

Positive correlations between arsenate concentrations and observed phosphate signals were observed for each set of seawater solutions containing fixed added phosphate concentrations in the range 0 to 50 nM (Figure 4.2), with the greatest arsenate interferences corresponding to the highest phosphate concentrations. When rates of change (i.e. the slopes of the regression lines in Figure 4.2) of interference with increasing phosphate are plotted (Figure 4.3), it is evident that As interferences are directly related with phosphate up to 50 nM phosphate. These observations confirm that phosphate catalyses the rate of formation of the arsenomolybdic complex. With no added phosphate, there was a small, yet measurable, interference (0.015 ± 0.004 nM phosphate increase per nM arsenate), while at 50 nM added phosphate there was an 8-fold increase in the effect of arsenate on the phosphate signal (0.121 ± 0.010 nM phosphate increase per nM arsenate). The relationship plotted in Figure 4.3 indicates that arsenate interference scales linearly with phosphate concentration. As the arsenate interference is catalysed by phosphate, the magnitude of the interference is a constant proportion of the phosphate concentration over the studied concentration range of 5 – 50 nM PO_4^{3-}. Using the relationship devised for our analytical system, and assuming that the intercept (see Figure 4.3) is positioned between zero and +0.002 (since a negative intercept would signify a reduction in SRP signal with increasing arsenate at very low phosphate concentrations), a typical seawater arsenate concentration of 20 nM would cause an overestimation of the SRP concentration and yield 5.23 ± 0.07 nM in a sample containing an actual phosphate concentration of 5.00 nM (an overestimation of 4.6 ± 1.4%). Furthermore, the overestimation would yield a concentration of 52.1 ± 0.5 nM in a sample containing an actual concentration of 50.0 nM (an overestimation of 4.2 ± 1.0%).

A number of other workers have investigated arsenate interference. Using an SCFA-LWCC method Li and Hansell (2008) analysed two natural seawater samples (containing 58.4 nM and 68.9 nM phosphate) before and after reduction of arsenate with KI and found no difference. Assuming their samples contained

measurable concentrations of arsenate, the different reagent set-up utilised (hydrazine was used instead of ascorbic acid, and potassium antimonyl tartrate was omitted) appeared to result in negligible arsenate interference. Another recently published method employed reversed flow injection analysis (rFIA) coupled to a LWCC, and reported the influence of arsenate concentrations of up to 53 nM on samples with phosphate concentrations of 0 and 82.5 nM and found no effect (Ma et al., 2009). The very short reaction time allowed for colour formation (2 min) by these authors may have resulted in negligible arseno-molybdic complex formation. On the other hand, with a sequential-injection, solid-phase-extraction (SI-SPE) based system, arsenate interference was found to be detectable at arsenate concentrations above 27 nM (Ma et al., 2008). The variety of results for different systems underlines the importance of evaluating arsenate interference for each analytical set-up for nanomolar phosphate analysis.

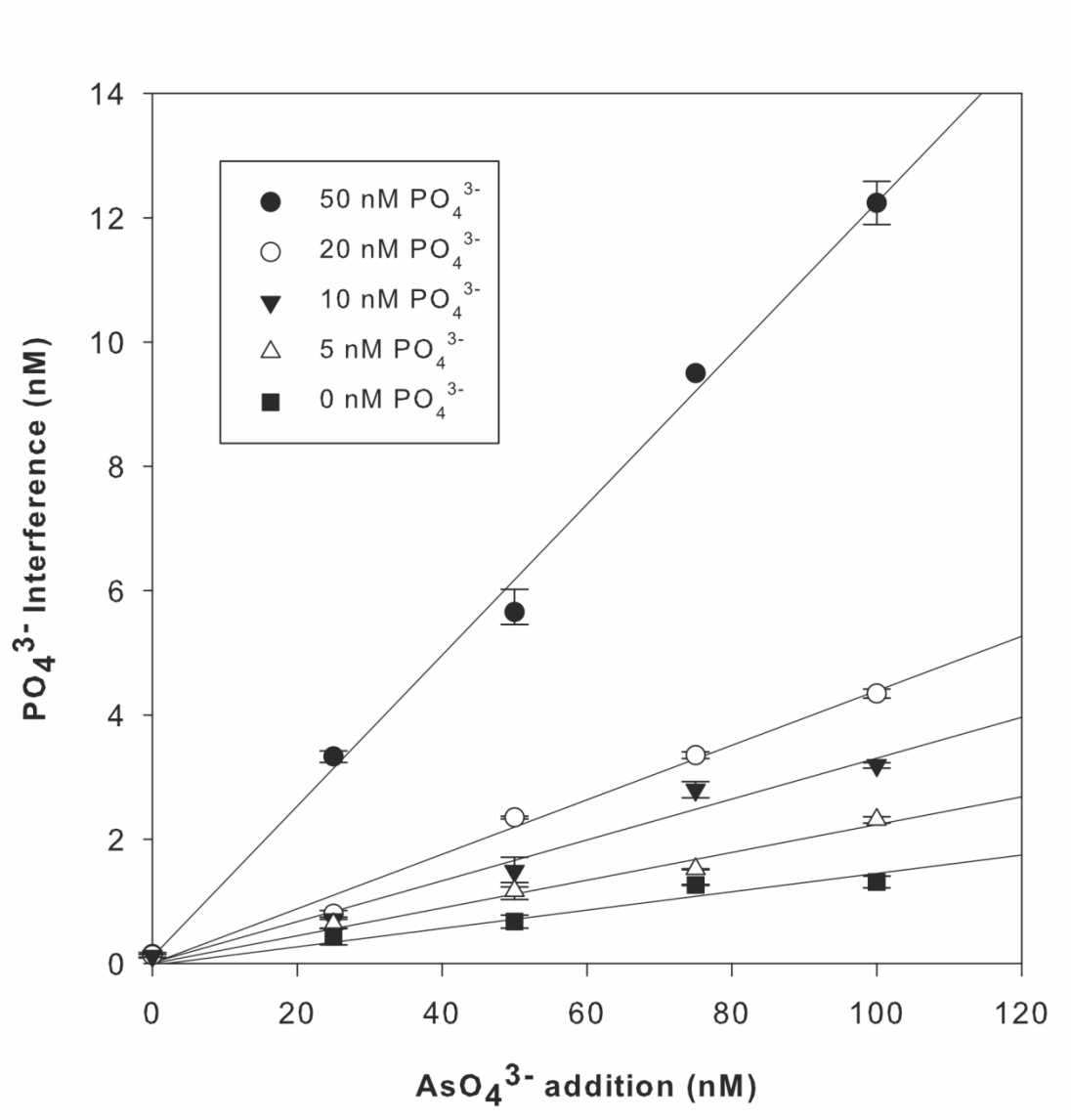

Figure 4.2 Effect of arsenate additions of up to 100 nM AsO_4^{3-} on phosphate concentrations measured in phosphate-free seawater spiked to contain phosphate at various concentrations up to 50 nM PO_4^{3-}. The concentration of phosphate added to the samples has been subtracted from the measured values. The markers represent the mean values and the error bars indicate the range of values obtained.

The regression coefficients (with uncertainties based on Student's t-values at 95% confidence) are:

0 nM PO_4^{3-}: [SRP] increase = (0.015 ± 0.004) x [AsO_4^{3-}] – (0.03 ± 0.24); R^2 = 0.908; n = 10
5 nM PO_4^{3-}: [SRP] increase = (0.023 ± 0.003) x [AsO_4^{3-}] – (0.01 ± 0.18); R^2 = 0.974; n = 10
10 nM PO_4^{3-}:[SRP] increase = (0.033 ± 0.005) x [AsO_4^{3-}] – (0.01 ± 0.30); R^2 = 0.960; n = 12
20 nM PO_4^{3-}:[SRP] increase = (0.044 ± 0.004) x [AsO_4^{3-}] + (0.01 ± 0.25); R^2 = 0.987; n = 10
50 nM PO_4^{3-}:[SRP] increase = (0.121 ± 0.010) x [AsO_4^{3-}] – (0.06 ± 0.60); R^2 = 0.988; n = 10

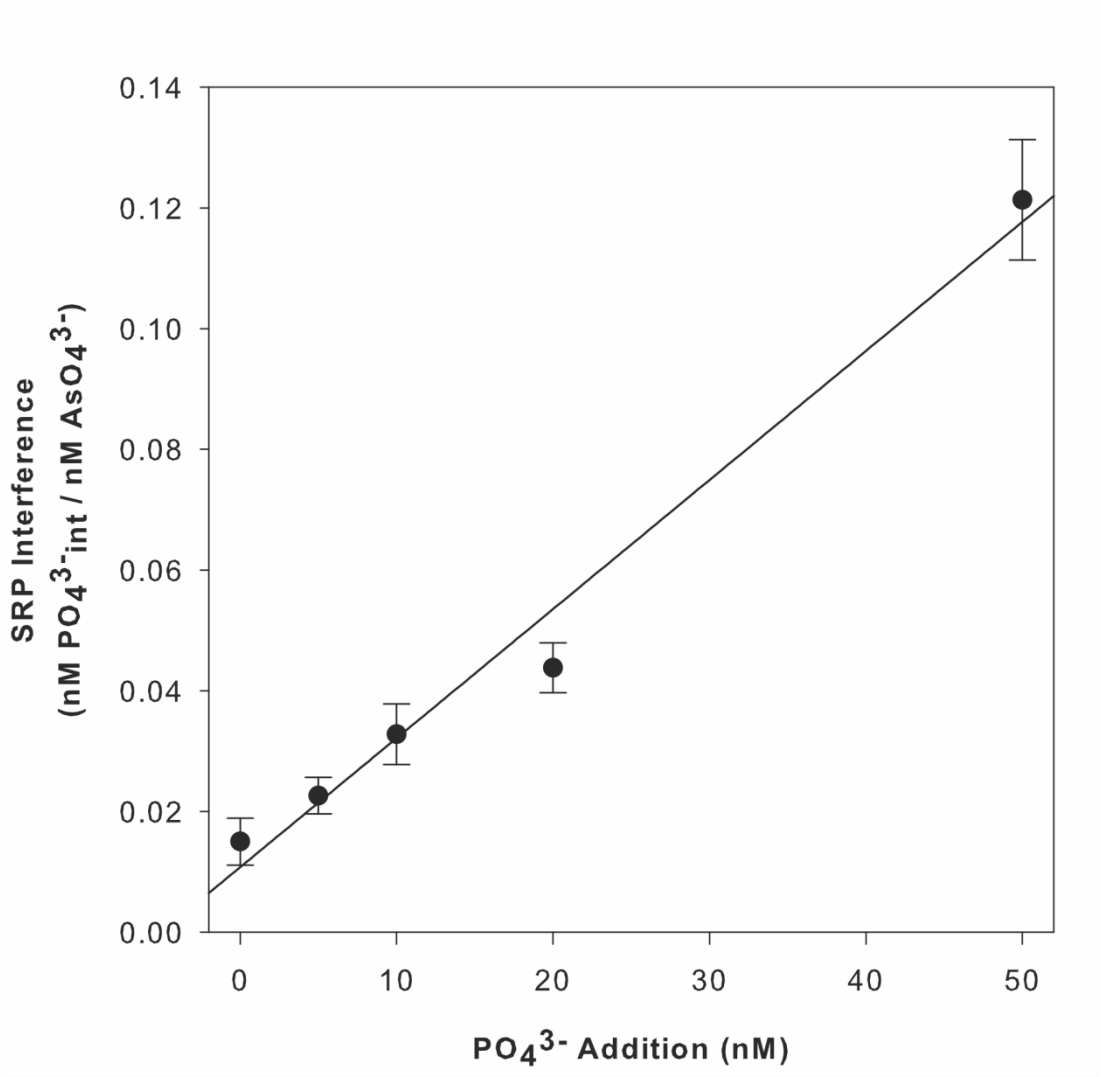

Figure 4.3 Slope of the linear regressions in Figure 4.2 plotted against phosphate concentration. The error bars show the 95% confidence intervals of the slope estimates. There is a linear increase in the extent of formation of the arsenomolybdic complex with phosphate concentration up to 50 nM phosphate. The regression coefficients (with uncertainties based on Student's t-values at 95% confidence) are:

SRP Interference = (0.0021 ± 0.0005) x $[PO_4^{3-}]$ – (0.011 ± 0.013); R^2 = 0.992; n = 5

4.3.2 Silicate Interference

A clear phosphate signal was apparent in the $Si(OH)_4$ standard additions, with the effect becoming non-linear at high added $Si(OH)_4$ concentrations (Figure 4.4). If the intercept in Figure 4.4 is ignored (since this corresponds to the SRP that would be

measured in the absence of interference from $Si(OH)_4$), the following relationship is obtained (uncertainties correspond to 95% confidence intervals):

$$[SRP]_{Si(OH)4} = (0.52 \pm 0.10) \times [Si(OH)_4] - (0.0016 \pm 0.0009) \times [Si(OH)_4]^2 \quad (4.1)$$

Using this relationship, a background dissolved silicon concentration of 100 µM would increase the measured SRP concentration by 36 ± 19 nM. During our D326 cruise in the tropical and sub-tropical Northeast Atlantic Ocean, surface water dissolved silicon concentrations ranged between 0.39 to 1.49 µM (with a precision of ± 0.5%, determined from the repeated determination of the same standard in every run of samples during the cruise). These concentrations of dissolved silicon would raise the measured SRP concentration by 0.20 ± 0.04 nM (at 0.39 µM $Si(OH)_4$) and by 0.78 ± 0.15 nM (at 1.5 µM $Si(OH)_4$). These interference estimates were relatively low compared with surface water phosphate concentrations that ranged between 2.1 ± 1.5 nM (n=2) and 99 ± 4 nM (n=1) (quoted errors are ± 2 standard errors, derived from the uncertainties in the calibration regression (Miller and Miller, 1993)). Thus, with our instrumental configuration, and in our study region, silicate interference would appear to have a relatively small effect on measured SRP concentrations, but may introduce a significant error for those samples containing the lowest phosphate concentrations. Nonetheless, it should be noted that in many freshwater environments it is common to find much higher dissolved silicon concentrations in conjunction with very low phosphate concentrations (Belz et al., 1999); hence the interference measured with our instrumental configuration could be very significant in certain measurement situations.

There are few publications describing silicate interference for nanomolar phosphate systems. The rFIA-LWCC approach of Ma et al. (2009) determined the effect of silicate concentrations up to 240 µM on samples containing 0 and 82.5 nM phosphate and found no effect (Ma et al., 2009). This finding may be due to the short reaction time allowed for colour development and the slower formation of the silicomolybdic complex relative to the phosphomolybdic complex (Hansen and Koroleff, 1999). An alternative SI-SPE-based phosphate system described by Ma et

al. (2009) also reported a lack of silicate interference at concentrations up to 160 µM, which again may be due to the short time allowed for colour development.

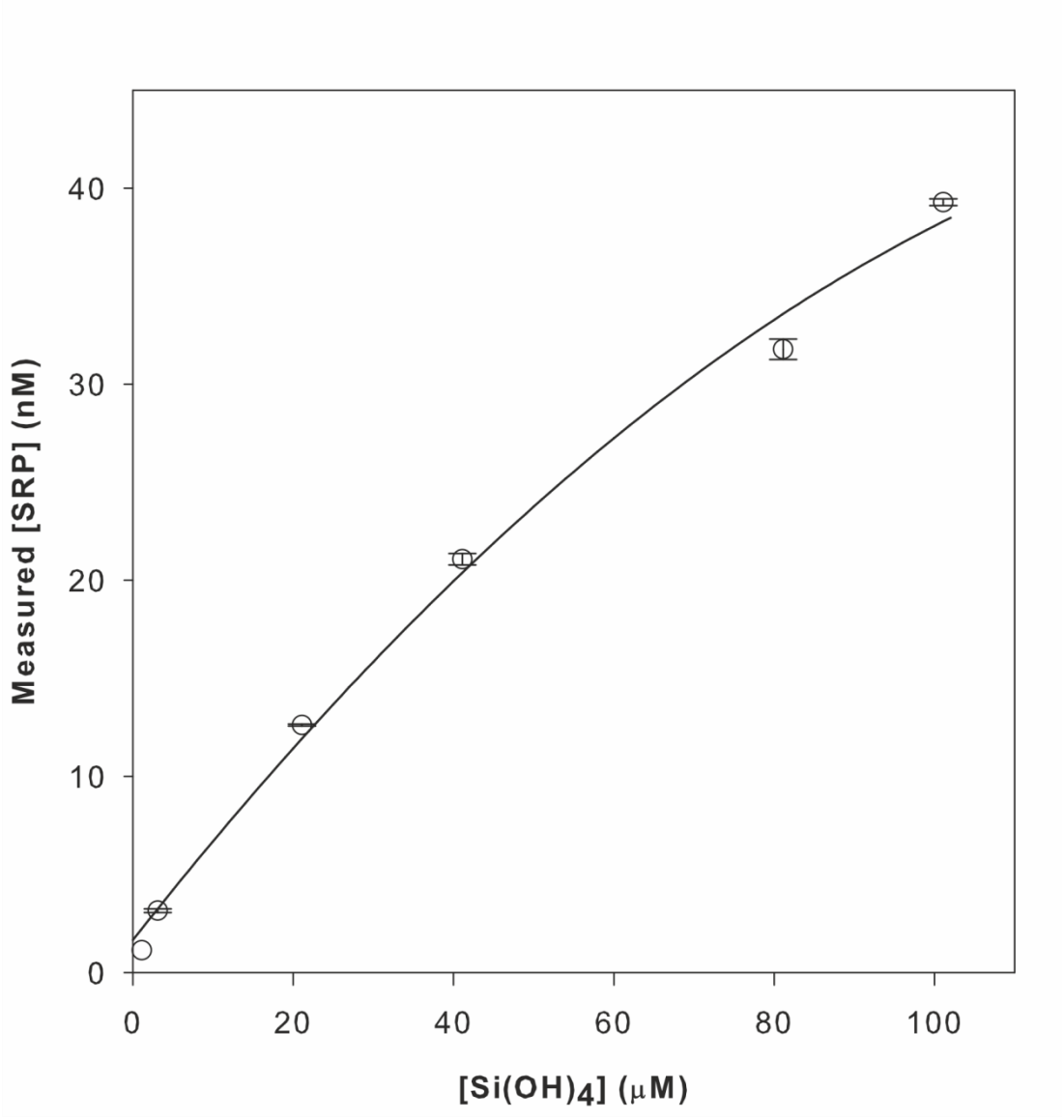

Figure 4.4 Effect on measured phosphate concentration of a sample of low nutrient seawater spiked with silicate concentrations of up to 100 µM. The error bars indicate the range of values obtained. A quadratic equation has been used to fit the data. The line (with uncertainties based on Student's t-values at 95% confidence) is given by: [SRP] = (1.6 ± 1.7) + (0.52 ± 0.10) x $[Si(OH)_4]$ – (0.0016 ± 0.0009) x $[Si(OH)_4]^2$; R^2 = 0.994; n = 11

Zhang et al. (1999) carried out a detailed analysis of silicate interference in phosphate analysis using standard SCFA analysis. They recommended optimal conditions in order to minimise silicate interference and maximise sensitivity to

phosphate. These recommendations included a final reaction solution pH of 1.00 (interference was greatest at pH 0.78), room temperature for the reaction and an $[H^+]/[Mo]$ ratio of around 70. The parameters for the analytical system used in this study were close to the recommendations by Zhang et al. (1999), with a final pH of 1.06 and an $[H^+]/[Mo]$ ratio of 74.

4.3.3 Effect of sample filtration

All five surface ocean seawater samples used in the sample filtration experiment contained very low concentrations of nitrate (6.3 – 11.2 nM in unfiltered samples), with filtration resulting in measured nitrate concentrations 0.1 to 1.7 nM less than in the unfiltered samples (Table 4.2). However, only for one of the samples (UT147, Table 4.2) was the difference greater than the precision of the instrument (± 0.6 nM). It is not possible to draw firm conclusions from just one significant result, but it seems that for some samples at least, filtration could result in a detectable decrease in the measured nitrate concentration. Since the nitrate and nitrite anions are highly soluble and not liable to be scavenged onto surfaces, lower concentrations could result from removal of particulate organic material from the samples, some of which may be solubilised under the acidic reaction conditions used for nitrite determination. We are not currently aware of any other published data on the effect of sample filtration on nanomolar nitrate + nitrate measurements in seawater.

Values of SRP determined in the five seawater samples presented in Table 4.2 showed a considerable concentration range (4.8 – 72.5 nM in unfiltered samples), yet the effect of filtration was a fairly uniform decrease of between 1.7 (± 0.7 nM) and 2.7 nM (± 0.5 nM) in the observed concentration, with the exception of one sample (UT147, Table 2), which increased by 2.8 nM (± 0.5 nM). These observations constituted a reduction in the SRP concentration by between 2.4 and 56% as a result of sample filtration, whilst for the sample showing a 2.8 nM increase in concentration the change was + 3.9%. Although phosphate is known to adsorb readily to surfaces, the in-line filters used for this study were in continuous use every day and considerable volumes (ca. 10 – 20 L) of water had been filtered prior

to sample collection for this experiment, and therefore it may be expected that the filters would be well equilibrated and adsorption effects minimised under these circumstances. Thus the observed reduction in SRP concentrations upon filtration may be due to the removal of particulate phosphorus from the seawater in material with sizes smaller than 0.2 µm. An alternative explanation is that light scattering within the LWCC by particles present in unfiltered samples is reduced by filtration. As a result of the broad absorption band of the phospho-molybdenum blue reaction product (Murphy and Riley, 1962), it is not possible to use a non-absorbing wavelength as a reference to correct for fluctuations in light intensity. For this reason the MB phosphate method should be more vulnerable to differences caused by light scattering from particles than the nitrate method.

Table 4.2 Effect of sample filtration on measured nitrate and SRP values of five underway samples taken during a cruise in the equatorial eastern North Atlantic. Four samples were taken simultaneously, of which two were filtered through a 0.2 µm Sartobran 300 in-line filter. The sample marked with an asterisk appears to be contaminated and has been excluded from the calculation of ΔSRP. Each value represents a single measurement. Since each set of samples was analysed at the same, quoted uncertainties are based on instrument precision (3 x s of repeated measurements of a low standard – see Table 4.1). Uncertainties for ΔSRP are calculated from the uncertainty (s) and number of repeated measurements (n) of the filtered (filt.) and unfiltered (unfilt.) samples according to: $s_{\Delta SRP} = \sqrt{\left(\frac{s_{filt.}}{\sqrt{n_{filt.}}}\right)^2 + \left(\frac{s_{unfilt.}}{\sqrt{n_{unfilt.}}}\right)^2}$

Sample ID	Sample Time	Sample Location	nitrate (nM)		Δnitrate (nM)	SRP (nM)		ΔSRP (nM)
			Unfiltered	Filtered		Unfiltered	Filtered	
UT138	28/1/2008 19.00	16.908 °N 26.978 °W	7.9 ± 0.6 7.8 ± 0.6	7.5 ± 0.6 7.6 ± 0.6	-0.3 ± 0.6	71.2 ± 0.5 71.5 ± 0.5	69.3 ± 0.5 69.9 ± 0.5	-1.7 ± 0.5
UT147	29/1/2008 19.05	20.096 °N 26.866 °W	11.2 ± 0.6 10.4 ± 0.6	9.1 ± 0.6 9.0 ± 0.6	-1.7 ± 0.6	71.8 ± 0.5 72.5 ± 0.5	75.3 ± 0.5 74.6 ± 0.5	+2.8 ± 0.5
UT155	30/1/2008 17.00	22.979 °N 27.286 °W	6.9 ± 0.6 7.1 ± 0.6	6.8 ± 0.6 6.8 ± 0.6	-0.2 ± 0.6	25.8 ± 0.5 25.2 ± 0.5	23.7 ± 0.5 23.8 ± 0.5	-1.7 ± 0.5
UT175	1/2/2008 17.00	26.309 °N 25.547 °W	6.5 ± 0.6 6.8 ± 0.6	6.6 ± 0.6 7.0 ± 0.6	-0.2 ± 0.6	6.0 ± 0.5 5.9 ± 0.5	7.7 ± 0.5 37.1 ± 0.5*	-1.7 ± 0.7
UT184	2/2/2008 19.00	26.806 °N 22.435 °W	6.3 ± 0.6 6.3 ± 0.6	6.2 ± 0.6 6.3 ± 0.6	-0.1 ± 0.6	4.8 ± 0.5 4.8 ± 0.5	2.2 ± 0.5 2.1 ± 0.5	-2.7 ± 0.5

It is not clear why for one of the samples in Table 4.2, the measured SRP concentration should increase upon filtration; one possibility is lysis of cells within the filter, releasing labile phosphate into the filtrate, although this might be expected to coincide with an increase in nitrate, which was not observed. Another explanation would be slight phosphate contamination of the filtered sample.

Li and Hansell recently reported the effect of filtration on SRP measured using a SCFA-LWCC system (Li and Hansell, 2008). Using six different types of filter and using both a solution of 50 nM phosphate in purified water and a natural seawater sample containing a similar SRP concentration, they found considerable differences between filter types. Their values of ΔSRP (SRP difference between filtered and unfiltered sample) in seawater for 0.45 µm cellulose nitrate membrane filters (ΔSRP = - 3.1 nM; -6.2%) and 0.45 µm cellulose ester membrane filters (ΔSRP = - 4.5 nM, -9%), are broadly comparable with the values presented here (using a 0.2 µm cellulose acetate filter). However these values cannot be interpreted and compared in any significant way without a detailed analysis of the various pools of phosphorus of the seawater samples (dissolved inorganic, dissolved organic phosphate and particulate phosphate). Moreover, the wide variety of filter types, pore sizes and membrane materials available from different vendors creates a challenge when comparing results from different studies, and a greater understanding of phosphate adsorption to different filters is needed.

4.3.4 Sample stability

4.3.4.1 Unfiltered samples

The sampling details and the observed nitrate and SRP concentrations in the sample stability experiments with the unfiltered samples from the towed fish supply are presented in Table 4.3. Nitrate concentrations in the refrigerated samples were stable (6.2 – 6.8 nM) over the two day storage period. In the frozen samples, the nitrate concentration were slightly higher (8.2 ± 0.5 nM) than the initial measurements, but the difference was not significant (Student's t-test; p = 0.28). Phosphate concentrations increased in the three bottles that were tested every day (bottles 1 – 3; from 12.0 ± 1.3 nM up to 15.6 ± 1.9 nM; an increase of 30% over the

two days), with a significant difference between the initial and 2-day time-points (Student's t-test; p = 0.03). However, in the samples that remained sealed prior to analysis (bottles 7 – 9, 13.6 nM ± 2.3 nM after 2 days) the difference from the initial measurement was insignificant (Student's t-test; p = 0.30) . There was a significant increase in phosphate concentrations in the samples that were frozen (14.7 ± 0.6 nM; a 22.5% increase over the initial value; Student's t-test: p = 0.02).

Table 4.3 Stability of samples of unfiltered surface seawater collected during *RRS Discovery* cruise D326. Sampled using CTD on 26 Jan 2008 15:30 h GMT from 4 m depth. Location: 16.2 °N 30.6 °W. Samples were stored in the dark at 4°C, except for bottles 10 – 12, which were frozen. Each value is the mean of 3 measurements (one from each bottle). Quoted uncertainties are ± 2 standard errors, calculated using the uncertainties in the calibration linear regression in accordance with Miller & Miller (Statistics for Analytical Chemistry, 1993). Values marked by an asterisk are statistically significant from the initial measurement (Student's t-test; p < 0.05).

Bottle Number	Initial (< 1 h after sampling)		One day (26 h)		Two days (51 h)		Frozen (12 days after sampling)	
	$[NO_3^-]$ (nM)	[SRP] (nM)	$[NO_3^-]$ (nM)	[SRP] (nM)	$[NO_3^-]$ (nM)	[SRP] (nM)	$[NO_3^-]$ (nM)	[SRP] (nM)
1 – 3	6.5 ± 2.6	12.0 ± 1.3	6.8 ± 0.7	13.0 ± 1.4	6.6 ± 0.7	15.6 ± 1.9*	--	--
4 – 6	--	--	6.3 ± 0.8	13.2 ± 1.4	--	--	--	--
7 – 9	--	--	--	--	6.2 ± 0.7	13.6 ± 2.3	--	--
10 – 12 (frozen)	--	--	--	--	--	--	8.2 ± 0.5	14.7 ± 0.6*

These results show that with the exception of slightly elevated SRP concentrations after 2 days in the samples that were measured repeatedly, there are no significant changes following storage for 2 days at 4°C. Since this increase in SRP concentrations was not observed in the samples that remained sealed and in the dark at 4°C for 2 days, it appears that the less optimal storage conditions of bottles 1-3 may have permitted slightly elevated levels of microbial activity. Elevated SRP concentrations following storage frozen are probably due to cell lysis during freezing.

4.3.4.2 Filtered samples

Seven filtered surface seawater samples from the towed fish supply were analysed twice: once on the day of sampling and then again the following day (stored at 4ºC). Table 4.4 lists the sampling details and the observed nitrate and SRP concentrations. As with the unfiltered samples, there was no detectable change in nitrate after 24 h; the calculated errors (± 2 std errors) for each pair of concentrations overlap. Phosphate values also showed no statistically significant changes following the 24 h storage period, with the exception of one sample (UT155, Table 4), which showed an increase of 11% (Student's t-test; p = 0.04).

Table 4.4 Stability of samples of 0.2 µm-filtered surface seawater collected during *RRS Discovery* cruise D326. The number of repeat measurements (n) is indicated below each concentration. Quoted uncertainties are ± 2 standard errors, calculated using the uncertainties in the calibration linear regression in accordance with Miller & Miller (1993). The two values marked by an asterisk are significantly different (Student's t-test; p = 0.04).

Sample ID	Sampling date / time	Sampling location	Initial measurement		Repeat measurement after 24 h	
			Nitrate (nM)	[SRP] (nM)	Nitrate (nM)	[SRP] (nM)
UT133	28/01/2008 09:05	16.57°N 28.70°W	7.1 ± 1.3 n = 1	53.3 ± 3.2 n = 1	7.3 ± 1.5 n = 2	48.4 ± 2.6 n = 2
UT134	28/01/2008 11:00	16.64°N 28.37°W	6.3 ± 1.3 n = 1	47.6 ± 3.2 n = 1	6.8 ± 2.1 n = 1	43.4 ± 3.6 n = 1
UT135	28/01/2008 13:00	16.71°N 28.03°W	6.4 ± 1.3 n = 1	11.8 ± 3.2 n = 1	6.7 ± 2.1 n = 1	10.7 ± 3.6 n = 1
UT136	28/01/2008 15:00	16.77°N 27.67°W	6.5 ± 1.3 n = 1	33.9 ± 3.2 n = 1	6.8 ± 2.1 n = 1	30.5 ± 3.6 n = 1
UT137	28/01/2008 17:18	16.85°N 27.27°W	25.8 ± 1.3 n = 1	84.2 ± 3.5 n = 1	25.6 ± 2.1 n = 1	76.8 ± 3.8 n = 1
UT155	30/01/2008 17:00	22.98°N 27.29°W	6.8 ± 2.1 n = 2	23.8 ± 0.9* n = 2	7.5 ± 1.1 n = 2	26.5 ± 0.5* n = 2
UT175	01/02/2008 17:00	26.31°N 25.55°W	6.6 ± 0.7 n = 4	5.9 ± 0.5 n = 4	6.6 ± 0.6 n = 2	4.8 ± 0.8 n = 2

A number of papers have been published on sample storage procedures for river and estuarine waters containing enhanced nutrient concentrations (e.g. Gardolinski et al., 2001), indicating the effectiveness of chloroform. Potential sample contamination precludes the use of this reagent for oceanic nanomolar nutrient work. To our knowledge there are, however, no reported studies that directly determined the stability of nanomolar nutrient concentrations in oceanic seawater

samples. One comparison of results from the analysis of frozen samples with samples that were analysed immediately after sampling demonstrated that the samples containing lower concentrations of nutrients were poorly preserved (Krom et al., 2005). A recent study found no significant change in SRP concentrations after storage of samples filtered and frozen, and then acidified before measurement, but measurements at the time of sampling were made using a conventional nutrient method, so it was not possible to determine the stability of samples containing the lowest phosphate concentrations (Pulido-Villena et al., 2010).

4.4 Conclusions

We have reported the effect of arsenate and dissolved silicon interferences on nanomolar SRP measurements using our SCFA-LWCC nanomolar phosphate system. The silicate interference was very low at the dissolved silicon concentrations that we encountered in the tropical and sub-tropical Northeast Atlantic Ocean, but dissolved arsenate showed a significant interference effect at the observed nanomolar phosphate concentrations. Our comparison of filtered and unfiltered samples showed measurable changes in SRP concentrations, indicating that caution should be exercised when comparing samples processed using different protocols. The limited investigation into sample stability suggested that for very low nutrient samples, storage in a fridge at 4°C for up to 24 hours is acceptable. However freezing produced measurable changes in both SRP and nitrate concentrations, at least for the unfiltered sample that we tested. A broader investigation into sample stability with a wider range of samples taken from different productivity regimes is required in order to draw firm conclusions about the optimum storage conditions and stability of nanomolar nutrient samples.

4.4.1 Future directions

Since the discovery of the important role played by iron in the oceans, considerable effort has focussed on the development of sampling techniques and instrumentation necessary to accurately measure the very low concentrations of dissolved Fe in seawater. Consequently analytical methods and sampling

procedures for the determination of trace metals in seawater are relatively well established and employed by a significant number of research groups around the world. Yet to fully understand phytoplankton dynamics and biogeochemical cycling it is necessary to have accurate measurements of macronutrient concentrations in addition to trace metals such as Fe. In oligotrophic surface waters, which cover around 40% of the global ocean, macronutrient concentrations are at nanomolar concentrations and cannot be measured using conventional instrumentation. Techniques for measuring nanomolar macro-nutrient concentrations, however, have until recently received much less attention and are less well developed. With relatively few laboratories currently equipped to measure nutrients at nanomolar concentrations, these measurements are still some way from becoming a standard procedure on research cruises in low nutrient waters. This situation is changing quickly, partly due to the advent of commercially available LWCC capillary cells and the relative simplicity of long path-length absorbance spectrophotometry rapidly, which has brought the attractive prospect of nM nutrient analysis within the reach of many researchers.

There is excellent potential for the application of nanomolar nutrient techniques to gain new insights into nutrient cycling in oligotrophic oceanic environments. While many nanomolar nutrient analysis methods are based heavily on the chemistry and instrumentation of the well-established micromolar techniques, the measurement of nanomolar nutrient concentrations brings up new challenges and it is important that any new methods are thoroughly tested for robustness and accuracy. Measurement interferences and artefacts that are insignificant when working with micromolar nutrient concentrations can become very significant when measuring at nanomolar levels. Poor solution stability and the ease of sample contamination are also major issues, and it is important to focus attention on the cleanliness of the sampling techniques used and to measure samples promptly after collection.

Measurement issues such as those raised in this chapter make the comparison of nanomolar nutrient datasets challenging, particularly at the lowest concentrations, and this is compounded by the lack of any certified reference material for low-level nutrient analysis. Therefore, when reporting new techniques or nanomolar nutrient

data it is extremely important to give be as detailed as possible in describing the sampling protocol and instrument used, and to give details of the validation of the analytical technique.

At this stage it seems appropriate to make some suggestions with regards to sampling and analytical protocols that should help to reduce analytical artefacts and aid inter-comparison of datasets from different research groups. With regards to sampling, it is essential that anything touching the sample is thoroughly cleaned. Sampling techniques do not require the same level of caution as is necessary for the measurement of e.g. Fe, but considerable care is still required. The use of polypropylene or polyethylene apparatus is recommended since these materials can be cleaned easily in acid. Soaking in dilute HCl (ca. 1M) for a few hours is effective at removing traces of nutrients from these plastics. If sampling on deck, eg from a CTD rosette, samples for nanomolar nutrients should be taken before less critical samples to reduce the risk of sample contamination. During sampling, the use of polyethylene or vinyl gloves is recommended to avoid contamination of, for example, niskin bottle taps. Nitrile gloves are perhaps best avoided since they contain nitrogen.

As illustrated in this chapter, whether the sample is filtered or not before analysis can make a significant difference to the result. While the need to filter samples may vary according to the research aims, it is important that in any publication it is explicitly stated whether or not the samples were filtered and if filtration was used, details of the exact filters used together with the type of filtration apparatus should be included. Until understanding of sample stability is more established, samples should be analysed as soon as possible after sampling and in any case within one day, while the frozen storage of samples should be avoided. To reduce bacterial activity in samples they should be kept refrigerated and in the dark. Risk of atmospheric contamination from oxides of nitrogen may be reduced by minimising the headspace in the bottles.

With regards to the analytical method used, there are a wide variety of approaches available, each with their own advantages and disadvantages, as discussed in

Chapter 3. It is important that when reporting data obtained with any new instrument that as much information as practicable is detailed about its analytical validation. Aspects particularly important for the facilitation of dataset inter-comparison include how any salt effect (refractive index) corrections were applied together with their approximate magnitudes, and assessments of AsO_4^{3-} and $Si(OH)_4$ interference for phosphate analysis. For the MB phosphate method, factors such as final solution pH, and the time allowed between reagent addition and spectrophotometric measurement have been shown to be important factors in AsO_4^{3-} and $Si(OH)_4$ interference (Zhang et al., 1999). The inclusion of detailed analytical information such as this may well be useful to future users of our data as they try to compare their data with measurements being made today.

4.5 References

Adornato, L. R., et al. (2007). High-Resolution In Situ Analysis of Nitrate and Phosphate in the Oligotrophic Ocean. *Environmental Science and Technology* 41(11): 4045-4052.

Anagnostou, E. and Sherrell, R. M. (2008). MAGIC method for subnanomolar orthophosphate determination in freshwater. *Limnology and Oceanography-Methods* 6: 64-74.

Belz, M., et al. (1999). Linearity and effective optical pathlength of liquid waveguide capillary cells.in: *Internal Standardization and Calibration Architectures for Chemical Sensors*. R. E. Shaffer and R. A. Potyrailo. Bellingham, Spie-Int Soc Optical Engineering. 3856**:** 271-281.

Braun, C. L. and Smirnov, S. N. (1993). Why is water blue? *Journal of Chemical Education* 70(8): 612-615.

Dallas, T. and Dasgupta, P. K. (2004). Light at the end of the tunnel: recent analytical applications of liquid-core waveguides. *Trac-Trends in Analytical Chemistry* 23(5): 385-392.

Dias, A. C. B., et al. (2006). A critical examination of the components of the Schlieren effect in flow analysis. *Talanta* 68(4): 1076-1082.

Falkowski, P. G., et al. (1998). Biogeochemical controls and feedbacks on ocean primary production. *Science* 281(5374): 200-206.

Gardolinski, P., et al. (2001). Comparison of sample storage protocols for the determination of nutrients in natural waters. *Water Research* 35(15): 3670-3678.

Gimbert, L. J., et al. (2007). Determination of nanomolar concentrations of phosphate in natural waters using flow injection with a long path length liquid waveguide capillary cell and solid-state spectrophotometric detection. *Talanta* 71(4): 1624-1628.

Hansen, H. P. and Koroleff, F. (1999). Determination of Nutrients.in: *Methods of seawater analysis*. K. Grasshoff, K. Kremling and M. Ehrhardt. Weinheim, Germany Wiley-VCH**:** 159-228.

Johnson, D. L. (1971). Simultaneous Determination of Arsenate and Phosphate in Natural Waters. *Environmental Science & Technology* 5(5): 411-414.

Karl, D. M. and Tien, G. (1992). Magic - a Sensitive and Precise Method for Measuring Dissolved Phosphorus in Aquatic Environments. *Limnology and Oceanography* 37(1): 105-116.

Karl, D. M. and Tien, G. (1997). Temporal variability in dissolved phosphorus concentrations in the subtropical North Pacific Ocean. *Marine Chemistry* 56(1-2): 77-96.

Karl, D. M. and Björkman, K. M. (2002). Dynamics of DOP.in: *Biogeochemistry of Marine Dissolved Organic Matter*. D. A. Hansell and C. A. Carlson. California, London, Elsevier**:** 249-366.

Kotlash, A. R. and Chessman, B. C. (1998). Effects of water sample preservation and storage on nitrogen and phosphorus determinations: Implications for the use of automated sampling equipment. *Water Research* 32(12): 3731-3737.

Krom, M. D., et al. (2005). Nutrient cycling in the south east Levantine basin of the eastern Mediterranean: Results from a phosphorus starved system. *Deep-Sea Research Part II-Topical Studies in Oceanography* 52(22-23): 2879-2896.

Li, Q. P. and Hansell, D. A. (2008). Intercomparison and coupling of magnesium-induced co-precipitation and long-path liquid-waveguide capillary cell techniques for trace analysis of phosphate in seawater. *Analytica Chimica Acta* 611(1): 68-72.

Li, Q. P., et al. (2008). Underway monitoring of nanomolar nitrate plus nitrite and phosphate in oligotrophic seawater *Limnology and Oceanography: Methods* 6: 319-326.

Ma, J., et al. (2008). Sequential injection analysis of nanomolar soluble reactive phosphorus in seawater with HLB solid phase extraction. *Marine Chemistry* 111(3-4): 151-159.

Ma, J., et al. (2009). Reverse flow injection analysis of nanomolar soluble reactive phosphorus in seawater with a long path length liquid waveguide capillary cell and spectrophotometric detection. *Talanta* 78(1): 315-320.

Miller, J. C. and Miller, J. N. (1993). Statistics for analytical chemistry. New York, Ellis Horwood PTR Prentice Hall.

Murphy, J. and Riley, J. P. (1962). A modified single solution method for the determination of phosphate in natural waters. *Analytica Chimica Acta* 27: 31-36.

Ormaza Gonzalez, F. I. and Statham, P. J. (1991). Determination of Dissolved Inorganic Phosphorus in Natural-Waters at Nanomolar Concentrations Using a Long Capillary Cell Detector. *Analytica Chimica Acta* 244(1): 63-70.

Patey, M. D., et al. (2008). Determination of nitrate and phosphate in seawater at nanomolar concentrations. *TrAC Trends in Analytical Chemistry* 27(2): 169-182.

Pulido-Villena, E., et al. (2010). Transient fertilizing effect of dust in P-deficient LNLC surface ocean. *Geophysical Research Letters* 37.

Rimmelin, P. and Moutin, T. (2005). Re-examination of the MAGIC method to determine low orthophosphate concentration in seawater. *Analytica Chimica Acta* 548(1-2): 174-182.

Tsang, S., et al. (2007). Determination of phosphate/arsenate by a modified molybdenum blue method and reduction of arsenate by S2O42. *Talanta* 71(4): 1560-1568.

Yao, W., et al. (1998). Determination of Nanomolar Concentrations of Nitrite and Nitrate in Natural Waters Using Long Path Length Absorbance Spectroscopy. *Environmental Science & Technology* 32(17): 2646-2649.

Zafiriou, O. C., et al. (1992). Trace Nitrite in Oxic Waters. *Deep-Sea Research Part a-Oceanographic Research Papers* 39(7-8A): 1329-1347.

Zhang, J.-Z. (2000). Shipboard automated determination of trace concentrations of nitrite and nitrate in oligotrophic water by gas-segmented continuous flow analysis with a liquid waveguide capillary flow cell. *Deep Sea Research Part I: Oceanographic Research Papers* 47(6): 1157-1171.

Zhang, J. Z., et al. (1999). Optimization of performance and minimization of silicate interference in continuous flow phosphate analysis. *Talanta* 49(2): 293-304.

Zhang, J. Z. and Chi, J. (2002). Automated Analysis of Nanomolar Concentrations of Phosphate in Natural Waters with Liquid Waveguide. *Environmental Science & Technology* 36(5): 1048-1053.

5. Elemental composition and variability of atmospheric dust over the eastern tropical and sub-tropical North Atlantic

5.1 Overview

This chapter focuses on the total elemental composition (as determined through complete acid digestion followed by ICP-MS analysis) of atmospheric dust samples collected at the Cape Verde Atmospheric Observatory (CVAO) between July 2007 and July 2008, and aboard the RRS Discovery during a research cruise (D326) in the tropical and subtropical eastern North Atlantic during January-February 2008.

5.2 Introduction

Recognition of the importance of aeolian dust as an important source of iron to certain ocean regions (Duce and Tindale, 1991; Jickells et al., 2005) has stimulated a significant amount of research into the production, transport and deposition of dust to the oceans. Over the last two decades, satellite measurements have proved invaluable in evaluating dust sources and making estimates of deposition. However, while they provide unparalleled spatial and temporal coverage of dust transport, it is hard to extract quantitative information from satellite data and in-situ aerosol measurements are essential in order to obtain accurate measurements of aerosol concentrations and composition (Mahowald et al., 2005). Due to the sporadic nature of dust transport, long-term measurements of aerosols such as those made at Bermuda (Prospero and Lamb, 2003) are essential in order to build up a picture of average dust fluxes and composition.

Small changes in the chemical composition and mineralogy of transported dust can be used to identify the original source of the dust. For example, through a combination of mineralogical and geochemical techniques, Chavagnac et al. (2007)

traced the source of mineral dust particles collected in sediment traps in the Northeast Atlantic to the Anti-Atlas Moroccan mountain area, while Muhs et al. (2010) identified mineral particles originating from both the Sahara and Sahel desert regions in the soils of the Canary Islands. Recent research suggesting the importance of dust composition and mineralogy for trace metal solubility (Aguilar-Islas et al., 2010) highlights the need for linking dust composition to specific sources.

Tracing individual dust outbreaks of Saharan dust to specific source regions is complicated by several factors. First, desert dust undergoes a continual process of uplift and deposition, mixing the soils and smoothing out differences between the original source rocks (Schütz and Sebert, 1987). Further homogenisation occurs during long-range transport of the dust, resulting in the composition of the transported dust reflecting the average composition of a large source region (Guieu et al., 2002). In addition, air-masses from densely populated or industrialised areas often mix with the mineral aerosol, further altering its chemical composition (Chester et al., 1999).

Analyses of dust samples collected at long-term monitoring sites in Barbados and Miami show a high degree of homogeneity, suggesting that African dust is thoroughly mixed by the time it has crossed the Atlantic Ocean (Trapp et al., 2010). However measurements made closer to the African continent, interpreted with the aid of air-mass back trajectory calculations, have detected distinct signatures from dust originating from different desert regions. Chiapello et al. (1997) collected samples over a 3-year period on the island of Sal (Cape Verde archipelago) and allocated them to one of three African source regions (see Figure 5.1). Distinct Fe/Ca, K/Ca, Si/Al and Ca/Al ratios were found for dust originating from each of these regions due higher amounts of Ca and Si/Al ratios in northern Saharan dust (Chiapello et al., 1997). Futher work on this dataset found that the ratio of the clay minerals illite / kaolinite was a good indicator of origin, since Kolinite is much more abundant in the Sahel and southern Sahara (Caquineau et al., 1998).

In this chapter, emphasis is placed on interpreting the variability in elemental composition of dust collected at the CVAO and during research cuise D326 in terms of mineral dust concentration and air-mass source region. Any trends in the variability of dust identified will form a useful starting point from which to interpret the solubility measurements discussed in Chapter 6.

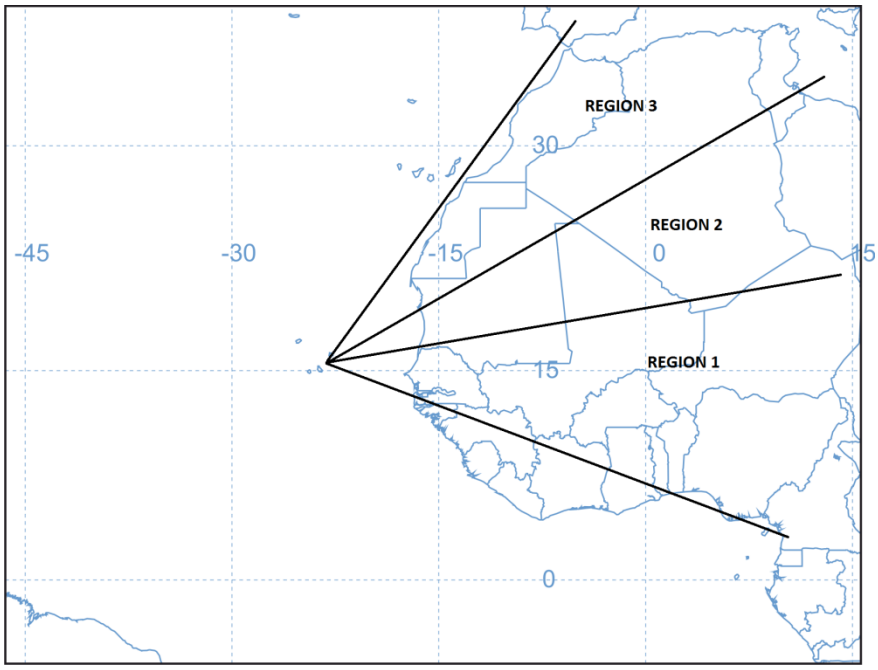

Figure 5.1 Scheme used by Chiapello et al. (1997) to classify air-masses originating from the African continent. Region 1: Sahel; Region 2: South and Central Sahara; Region 3: North and West Sahara.

Table 5.1 Summary of atmospheric concentrations of trace elements in dust sampled at the CVAO from 2 July 2007 to 11 July 2008 and during a research cruise D326 aboard RRS Discovery from 8 January to 4 February 2008. Values less than the blank are indicated by n.d.; Ga was not measured for the samples from D326.

Element		CVAO July 2007 – July 2008					RRS Discovery (D326) - January 2008				
		Min	Max	Arithmetic mean	Geometric mean	Standard deviation	Min	Max	Arithmetic mean	Geometric mean	Standard deviation
Na	(µg/m^3)	0.61	12.3	3.93	3.51	1.90	n.d.	11.7	5.41	4.82	2.67
Mg	(µg/m^3)	0.11	9.57	0.99	0.76	1.03	n.d.	5.16	2.13	1.47	1.58
Al	(µg/m^3)	0.01	66.9	2.89	0.76	6.99	n.d.	36.2	10.5	2.24	11.3
K	(µg/m^3)	0.04	10.7	0.77	0.36	1.37	0.001	6.06	1.99	0.81	1.91
Ca	(µg/m^3)	0.06	15.3	1.38	0.74	1.99	n.d.	9.22	3.27	1.56	3.08
Sc	(ng/m^3)	0.003	11.6	0.54	0.16	1.24	0.01	6.37	1.86	0.47	1.99
Ti	(µg/m^3)	0.0001	3.78	0.16	0.04	0.40	n.d.	1.95	0.60	0.13	0.62
V	(ng/m^3)	0.12	80.7	5.33	2.82	8.78	n.d.	41.4	13.9	4.94	13.4
Cr	(ng/m^3)	0.39	64.0	4.09	2.42	6.75	n.d.	34.8	11.2	5.18	10.9
Mn	(ng/m^3)	0.12	606	25.8	7.11	63.5	n.d.	307	93.3	22.3	98.2
Fe	(µg/m^3)	0.01	33.4	1.58	0.45	3.61	n.d.	18.5	5.38	1.25	5.72
Co	(ng/m^3)	0.01	14.5	0.69	0.22	1.56	n.d.	7.98	2.41	0.64	2.53
Ni	(ng/m^3)	0.04	29.3	2.06	1.22	3.03	n.d.	15.6	5.06	2.13	4.92
Cu	(ng/m^3)	0.02	23.6	1.44	0.65	2.66	n.d.	13.6	4.23	1.81	4.18
Zn	(ng/m^3)	0.36	52.7	6.31	4.32	6.95	n.d.	61.0	11.1	6.16	12.3
Ga	(ng/m^3)	0.04	5.43	1.22	0.74	1.24	n/a	n/a	n/a	n/a	n/a
Rb	(ng/m^3)	0.02	63.8	2.83	0.86	6.55	n.d.	31.0	9.42	2.71	9.89
Sr	(ng/m^3)	0.74	194	13.8	7.24	23.7	n.d.	133	36.7	17.4	37.4
Y	(ng/m^3)	0.01	25.2	1.48	0.46	3.20	n.d.	12.7	4.60	1.88	4.16
Nb	(ng/m^3)	0.002	14.6	0.61	0.19	1.52	n.d.	6.57	2.06	0.89	2.00

Element		CVAO July 2007 – July 2008					RRS Discovery (D326) - January 2008				
		Min	Max	Arithmetic mean	Geometric mean	Standard deviation	Min	Max	Arithmetic mean	Geometric mean	Standard deviation
Ag	**(pg/m^3)**	0.15	256	23.0	10.0	33.6	n.d.	115	40.0	19.1	33.6
Cd	**(pg/m^3)**	0.77	169	24.8	17.2	21.7	n.d.	165	40.8	27.7	35.2
Sn	**(ng/m^3)**	0.001	3.18	0.30	0.17	0.42	n.d.	2.46	0.60	0.37	0.60
Cs	**(pg/m^3)**	0.85	2935	147	47.4	319	n.d.	1514	480	149	502
Ba	**(ng/m^3)**	0.03	434	21.1	5.43	48.2	n.d.	243	74.2	17.2	76.5
La	**(ng/m^3)**	0.01	37.6	1.54	0.42	3.91	n.d.	19.4	5.59	1.21	6.12
Ce	**(ng/m^3)**	0.01	80.3	3.25	0.83	8.34	n.d.	40.3	11.8	2.54	12.9
Pr	**(pg/m^3)**	1.14	8307	362	94.0	890	n.d.	4642	1361	288	1486
Nd	**(ng/m^3)**	0.004	34.6	1.38	0.35	3.53	n.d.	17.5	5.15	1.08	5.61
Sm	**(pg/m^3)**	0.66	6453	263	66.7	664	n.d.	3356	988	201	1078
Eu	**(pg/m^3)**	0.10	1446	59.1	14.7	149	n.d.	743	224	48.7	240
Gd	**(pg/m^3)**	0.87	6484	268	68.4	672	n.d.	3440	1026	215	1115
Tb	**(pg/m^3)**	0.07	828	34.4	8.82	86.1	n.d.	438	131	26.8	142
Dy	**(pg/m^3)**	0.39	4289	182	46.8	448	n.d.	2289	684	147	742
Ho	**(pg/m^3)**	0.09	810	34.6	8.96	84.7	n.d.	435	130	27.8	141
Er	**(pg/m^3)**	0.29	2385	101	26.2	249	n.d.	1285	384	81.2	416
Tm	**(pg/m^3)**	0.05	340	14.5	3.79	35.6	n.d.	183	54.9	11.7	59.5
Yb	**(pg/m^3)**	0.24	2191	93.1	24.3	228	n.d.	1193	355	76.0	386
Lu	**(pg/m^3)**	0.04	315	13.6	3.59	33.0	n.d.	172	51.6	11.2	56.0
Pb	**(ng/m^3)**	0.03	18.9	2.09	1.19	2.50	n.d.	17.6	4.28	2.24	3.98
Th	**(ng/m^3)**	0.001	8.92	0.37	0.10	0.92	n.d.	4.43	1.30	0.27	1.40
U	**(pg/m^3)**	0.80	2218	97.4	31.1	229	1.71	1102	333	91.0	355

5.3 Total metal concentrations and distribution

5.3.1 Atmospheric metal and inferred dust concentrations

A summary of the data from the two datasets (CVAO and D326) including the range of values, mean and standard deviation for each element is presented in Table 5.1. Previous studies have shown that aerosol datasets are log-normally distributed (Orif, 2007) and therefore the geometric mean is the more representative average to use when comparing datasets. Application of the Shapiro-Wilk test for normality to a log transform of the two datasets showed that the majority of elements were log-normally distributed (using a 95% confidence interval). A number of elements did not pass the test (Mg, K, Ca, Ti, V, Cr, Sr, Ag, Cd and Sn); however a visual inspection of the data suggested that the distributions for these elements were close to log-normal.

Al is frequently used as a tracer for mineral aerosol mass (e.g. Guieu et al., 2002; Hsu et al., 2010) due to its high crustal abundance of 8.04% (Taylor and McLennan, 1995) making it relatively easy to measure when little material has been collected, and due to its lack of any significant non-crustal sources. It is possible to use other elements with predominantly crustal sources instead of Al as a tracer, and this is easier with the lower detection limits of modern ICP-MS instrumentation. For example Trapp, Millero et al. (2010) found a stronger correlation with TSP (Total Suspended Particles – obtained by weighing the filters before and after sampling) for Mn than for Al in their data so opted to use Mn as a crustal tracer. No direct measurements of TSP were made during this study, and in the absence of any evidence that another element was better and to facilitate comparison with many previous studies, Al was chosen as a crustal tracer for this analysis presented in this chapter. Approximate atmospheric mineral particle concentrations calculated from Al concentrations have been included in Figure 5.2 and Figure 5.3.

5.3.2 Seasonal pattern of dust deposition at the CVAO

Figure 5.2 shows total atmospheric concentrations of Fe and Al over the course of one year at the CVAO, with aerosol concentrations derived from the Al data with an additional axis. Trace metals in the aerosol samples were present in measurable quantities throughout the year at the CVAO site, but a number of periods with elevated aerosol concentration are apparent in the dataset. In addition, the data indicates a marked difference between summer and winter concentrations. Periods of elevated aerosol concentrations are more frequent and more intense during the winter months, with the highest concentrations observed during December 2007 and January 2008.

This is in line with expectations based on seasonal changes in the meteorological conditions in this region and is very similar to findings reported by Chiapello et al. (1995; 1997) for aerosol samples collected in Cape Verde between 1991 and 1994.

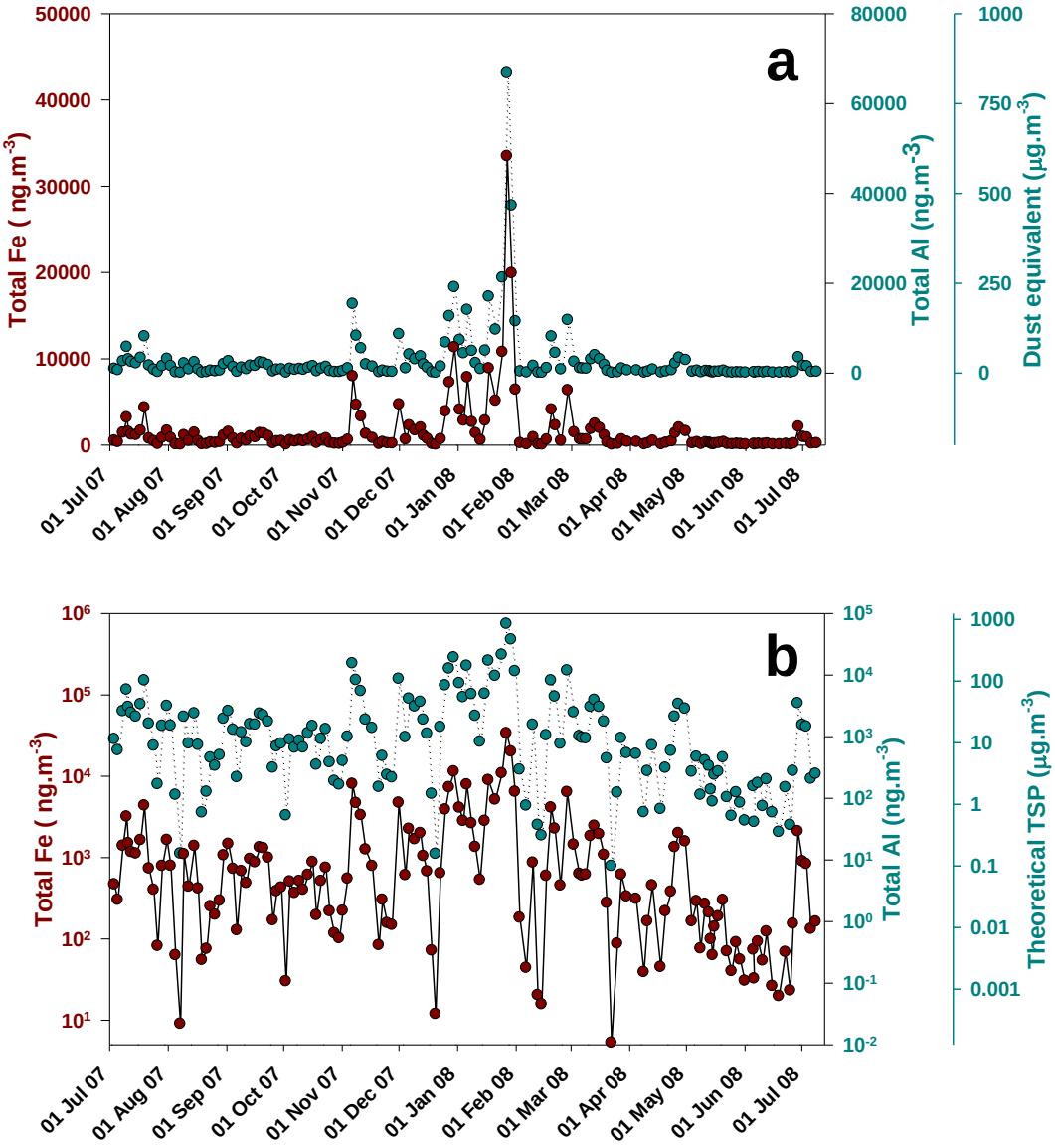

Figure 5.2 (a) Total Fe and Al atmospheric concentrations observed at the CVAO in the period between 2 July 2007 and 11 July 2008. Estimated mineral dust concentrations are indicated using Al concentrations, assuming 8.04 %wt. of Al in dust (Taylor and McLennan, 1995). (b) A log plot of the data in Figure 5.2 (a) to show the detail for lower concentration samples.

5.3.3 Dust events during research cruise D326

During the research cruise aboard the RRS Discovery, two periods with significant air-borne dust concentrations were encountered. The first event was in the period from 17 to 22 January 2008 and a second more intense and prolonged dust event was encountered between 25 January and 1 February 2008 (see Figure 5.3). An indication of the approximate location for the two events sampled during the research cruise is given in Figure 5.4. There is a notable similarity between the peaks in aerosol Al concentration recorded aboard RRS Discovery and the corresponding period measured at the CVAO (Figure 5.2), although higher Al concentrations were measured at the CVAO with peak concentrations (66.9 $\mu g.m^{-3}$ Al) almost twice the maximum shipboard values (36.2 $\mu g.m^{-3}$ Al). Mean Al concentrations for the two sets of measurements are more similar (10.5 $\mu g.m^{-3}$ Al D326 vs 15.0 $\mu g.m^{-3}$ Al CVAO).

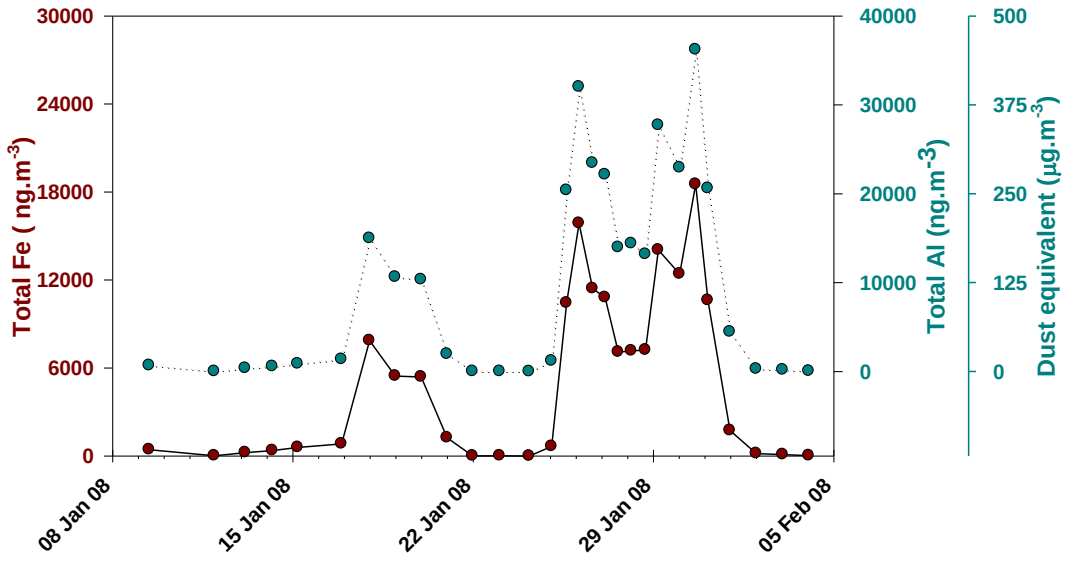

Figure 5.3 Total Fe and Al concentrations from samples collected aboard RRS Discovery during a research cruise (D326) in the eastern tropical and sub-tropical North Atlantic between 8 January and 4 February 2008. Estimated mineral dust concentrations are indicated using the Al data with the additional vertical axis.

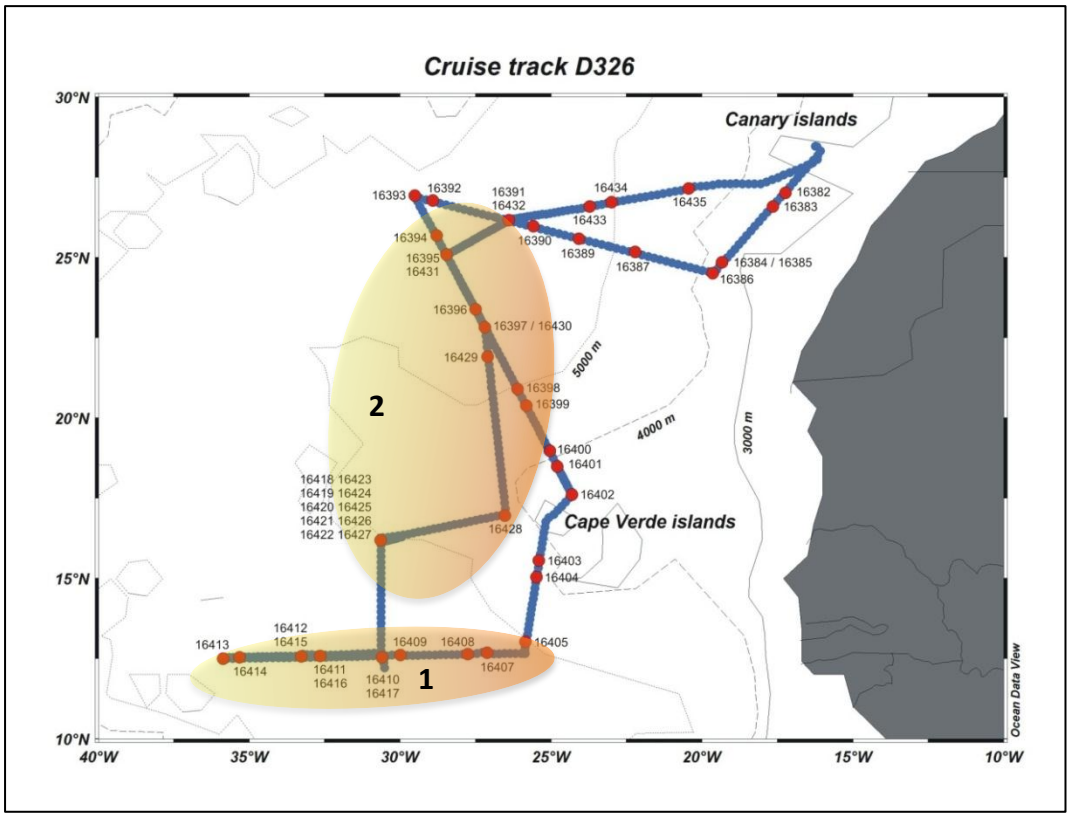

Figure 5.4 Cruise track for D326 indicating the approximate location of the two dust events that were sampled. Red circles mark the location of CTD stations with their associated station numbers. CTD stations 16405 – 16415 were during dust event 1, while stations 16419 – 16432 were sampled during the second period of dust deposition (see Figure 5.5)

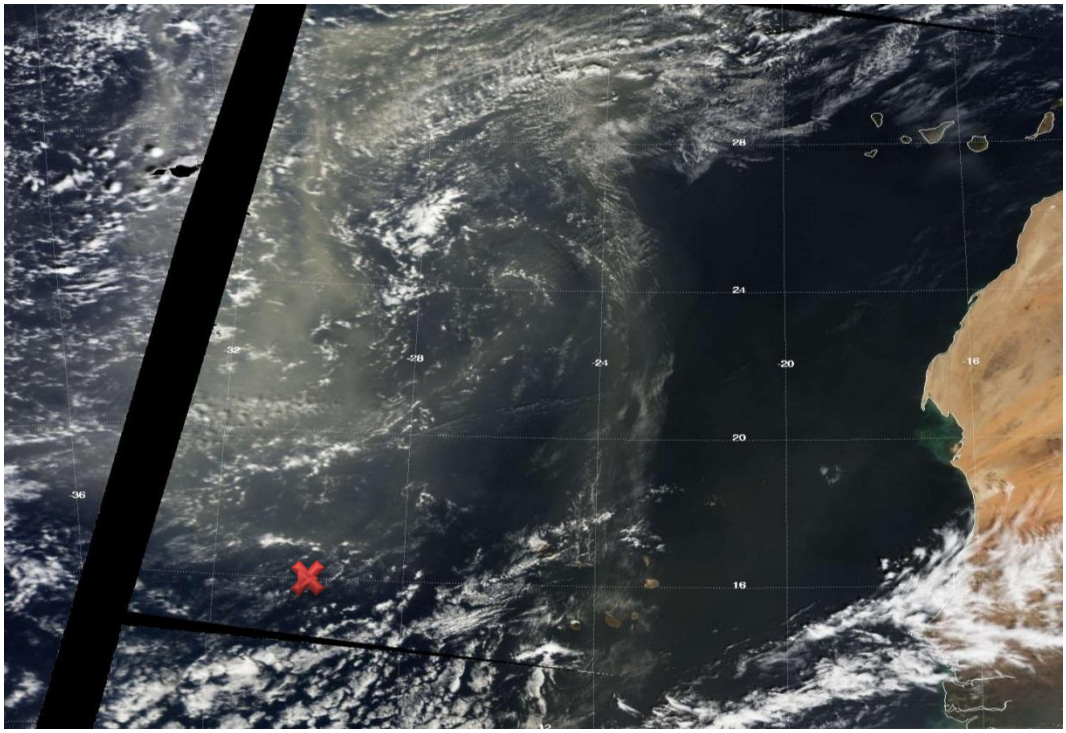

Figure 5.5 Satellite image showing atmospheric dust transport off the west African coast on 25 January 2008. The approximate location of the *RRS Discovery* on this date (16°N 30°W) is marked by a red cross.

5.4 Relative composition of aerosols

5.4.1 Relationship to upper crustal abundance

With the exception of a few elements, the overall composition of the aerosols collected at both CVAO and during cruise D326 closely follows mean upper crustal abundances (UCA) (see Figure 5.6). Elements with abundances significantly higher than UCA tend to be either major constituents of seawater (Na, Mg) or elements often associated with human activities (e.g. V, Cr, Ni, Zn, Cd, Pb).

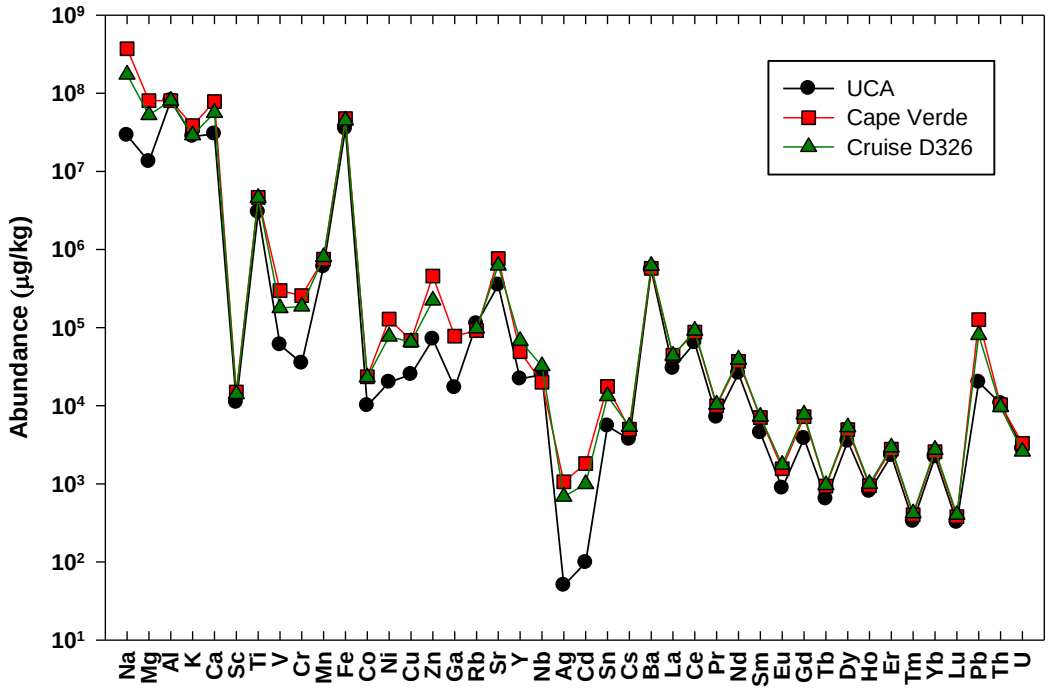

Figure 5.6 Mean composition of samples collected at CVAO and during cruise D326 plotted together with mean upper crustal composition (UCA) (Taylor and McLennan, 1995). All values have been normalised to 8.04% wt. Al.

Scatter plots of many of the elements determined simultaneously show strong correlations with aluminium, indicating that they share a common, crustal source. A Pearson correlation matrix diagram containing scatter plots and correlation coefficients (R) for each of the 42 elements determined by ICP-MS against every other element (Figure 5.7) shows that elements can be divided into two broad groups: the first group exhibiting a strong correlation with Al and the second group that is not highly correlated with Al (or any other metal).

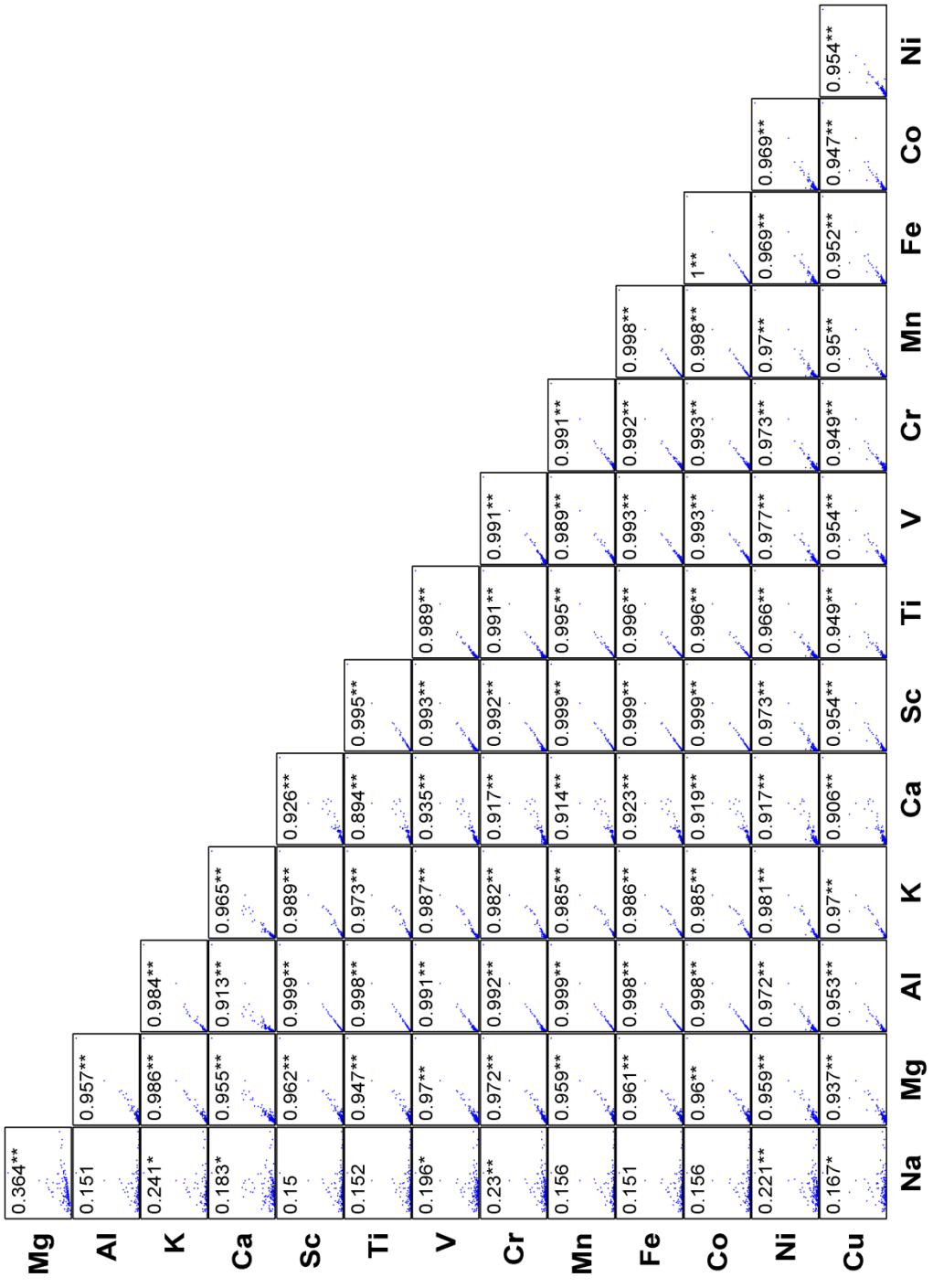

Figure 5.7 Matrix diagram showing the correlation between each of the 42 elements determined by total acid digestion / ICP-MS. Pearson correlation coefficients (R) are indicated for each plot and statistically significant correlations are indicated at the 5% (*) and 1% (**) confidence levels; see also further parts of the table on following pages.

Figure 5.7 continued

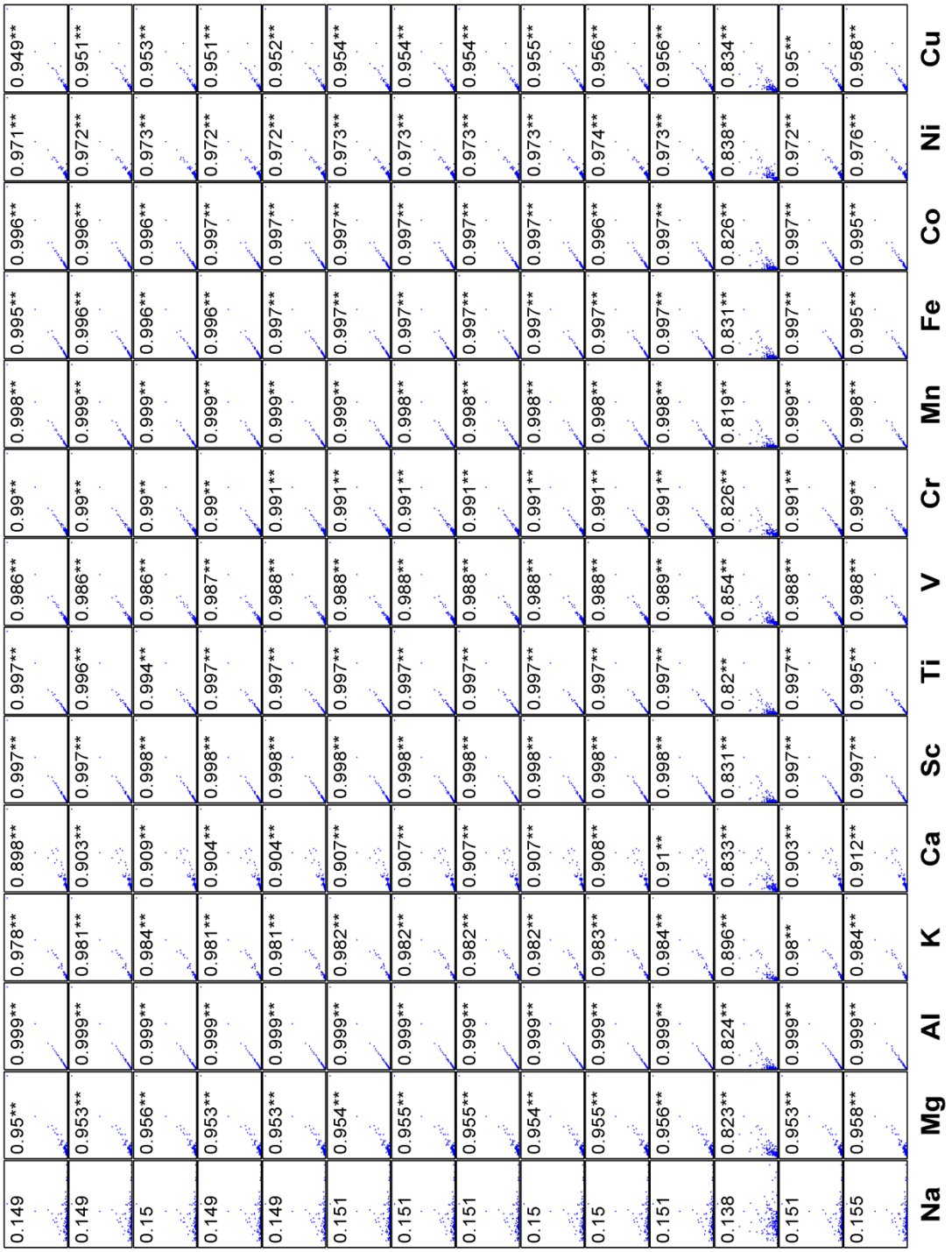

Figure 5.7 continued

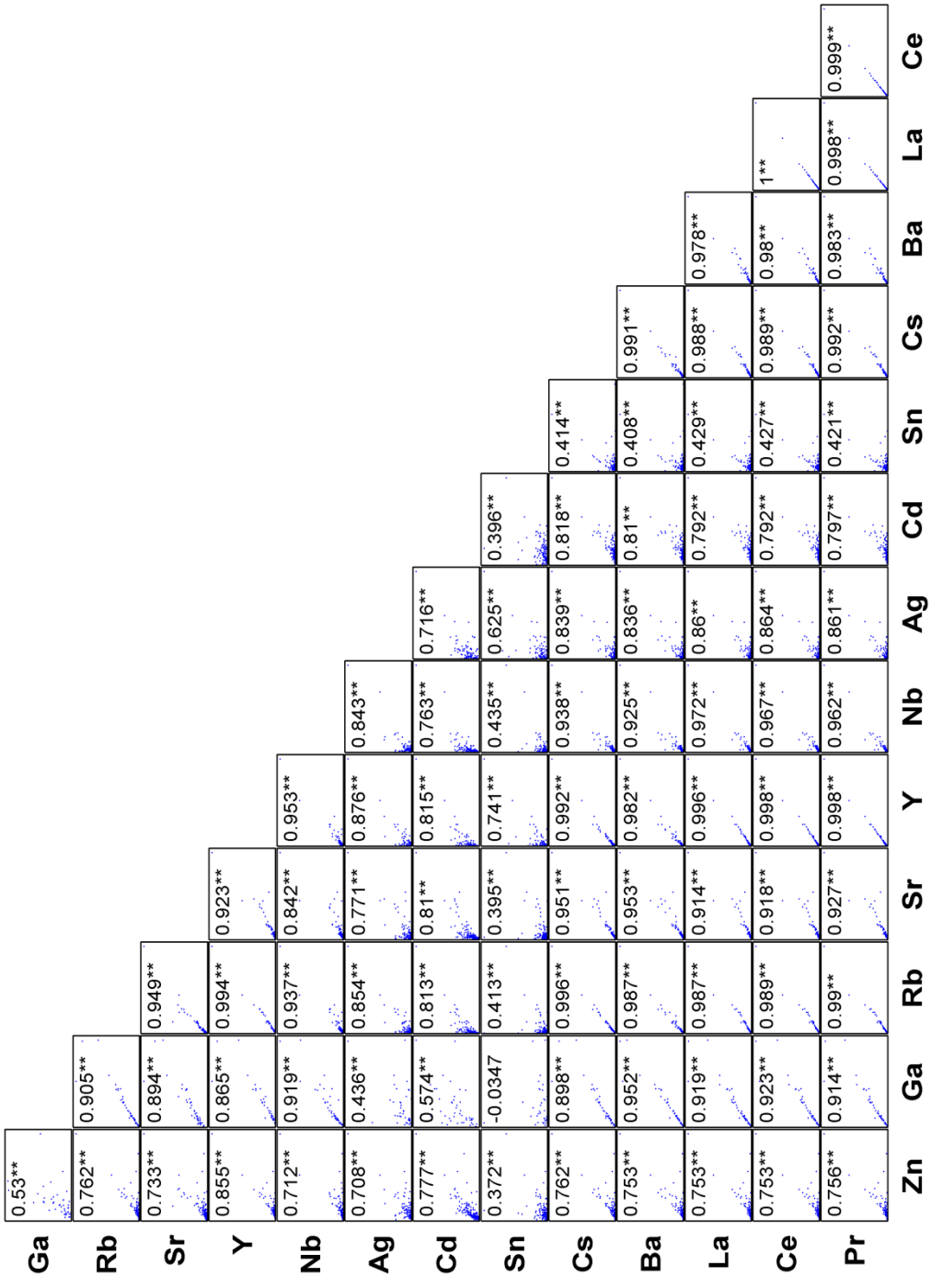

Figure 5.7 continued

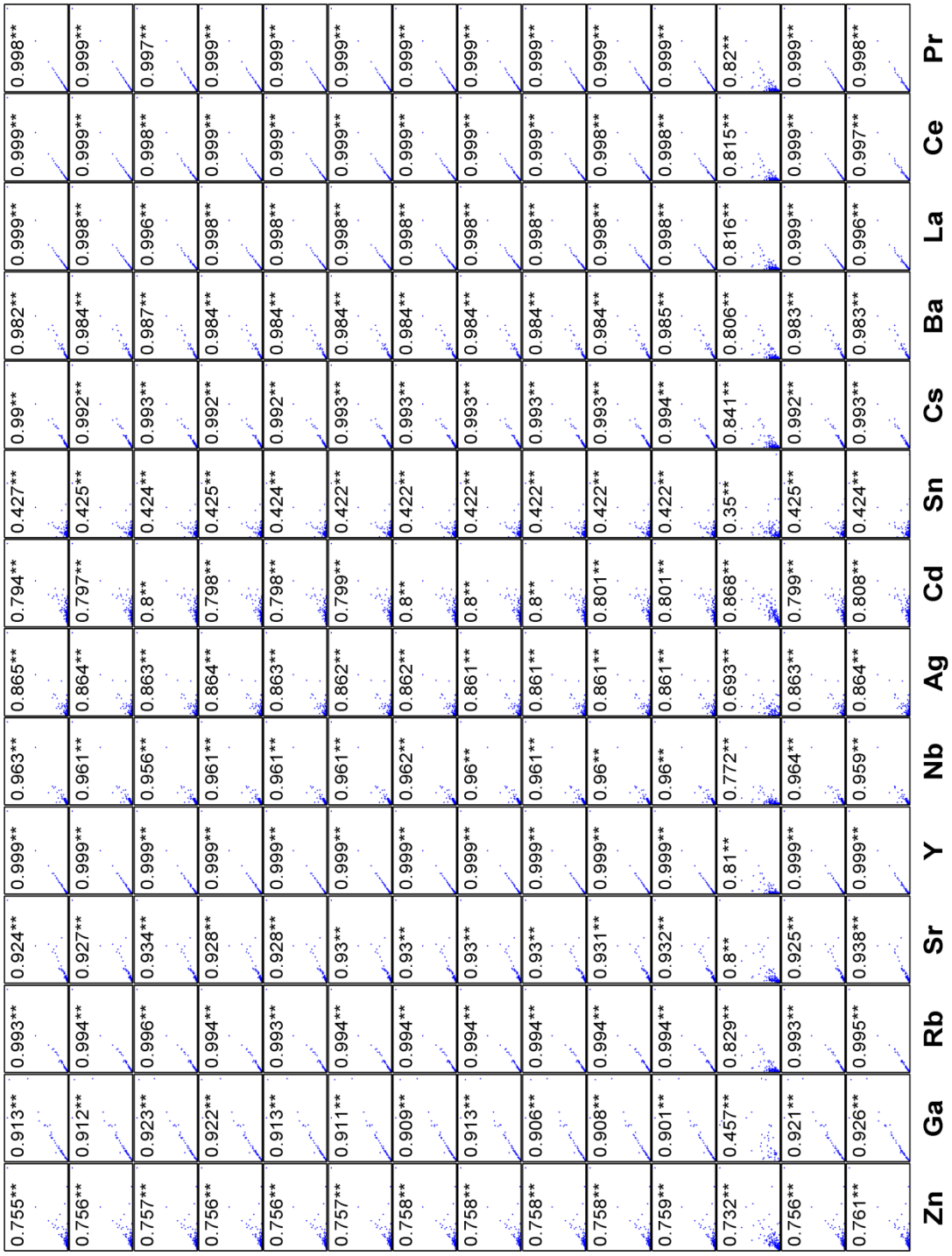

Figure 5.7 continued

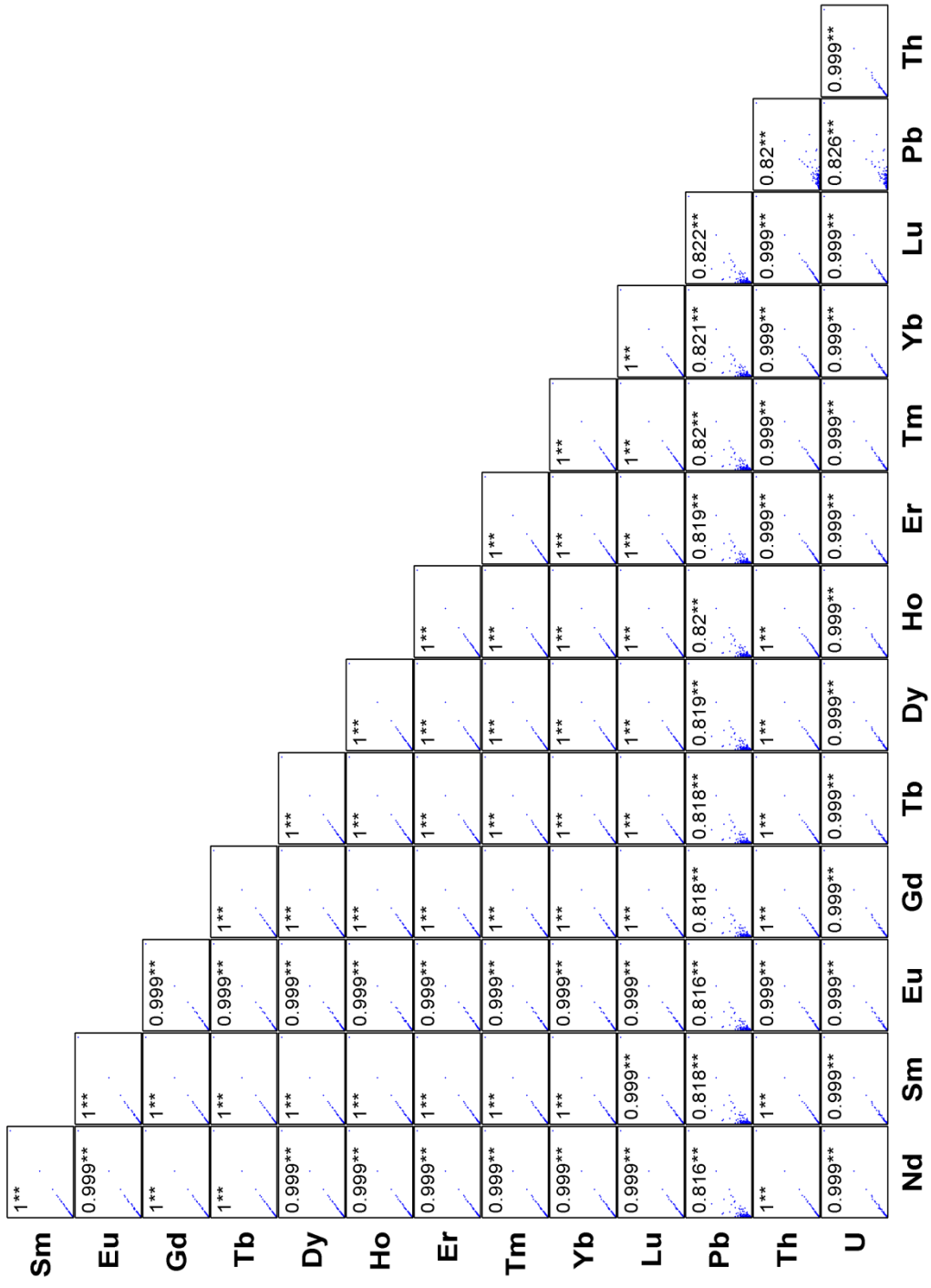

Figure 5.7 continued

Most of the 42 elements fall into the first group, for example Fe and U (Figure 5.8a, b) show strong correlations to Al. Although the ratio of these elements is close to typical crustal values (Taylor and McLennan, 1995), for many elements the ratio deviates slightly from the crustal value due to differences between the source rock composition and average crustal values and due to fractionation of the source material during uplift and transport (Schütz and Sebert, 1987).

A few elements do not show a strong correlation with Al, indicating they have a significant non-crustal contribution to the source. This group includes Na, a major component of sea salt (see Figure 5.8c) Ca, which is often associated with carbonate minerals, and elements which are often associated with oil combustion and other anthropogenic activities (Zn, Ag, Cd, Sn and Pb). Most of these elements associated with pollution sources showed considerable scatter, but with few, if any, points lying below the line of UCA, indicating that these elements also have a significant crustal contribution (see for example Pb, Figure 5.8d).

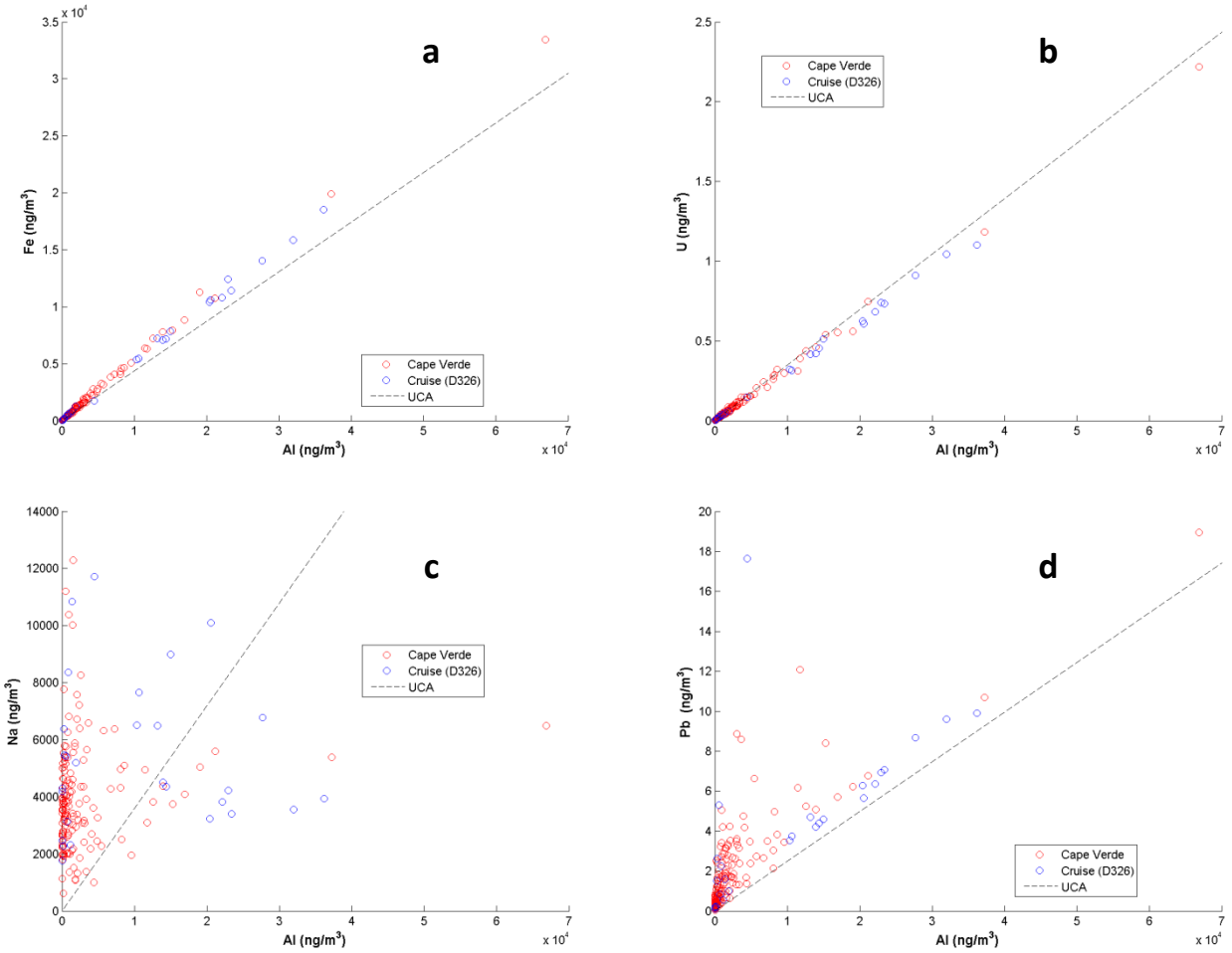

Figure 5.8 Relationship of total atmospheric concentrations of (a) Fe, (b), U, (c) Na, and (d) Pb with Al in dust collected at the CVAO and during cruise D326. Upper Crustal Abundance (UCA) (Taylor and McLennan, 1995) is indicated on each plot by a dashed line.

5.4.2 Enrichment Factors

When assessing whether specific elements are enriched or depleted relative to a specific source it is useful to calculate the enrichment factor (EF) (Chester et al., 1999; Herut et al., 2001). For marine aerosols the enrichment factor relative to crustal values is calculated using Equation 5.1:

$$\mathrm{EF} = \left(\frac{C_{xp}}{C_{Alp}}\right)/\left(\frac{C_{xc}}{C_{Alc}}\right) \quad (5.1)$$

Where C_{xp} and C_{Alp} are the concentrations of the trace metal of interest and Al in the aerosol sample, and C_{xc} and C_{Alc} are the concentrations of the same two elements in crustal material. An EF value > 10 is often taken to mean that a certain element is significantly enriched relative to typical crustal values and that a significant proportion of this element is derived from non-crustal sources.

shows mean crustal enrichment factors for the samples from the CVAO and from D326 arranged in order of increasing EF. Elements towards the left of the plot (e.g. Rb, Y) show little or no enrichment, have EF values close to 1 and a relatively small range of values. Towards the right of the plot, from Cu to Na, there are 11 elements that show clear enrichment relative to crustal values. They are all either major components of seawater (Na, Mg) or elements associated with anthropogenic activity (Cu, V, Pb, Ni, Cr, Zn, Sn, Ag and Cd). Enrichment factors for these elements also show considerable variability. By separating the CVAO dataset into quartiles based on total Al concentration and calculating mean crustal EF values for the upper and lower quartiles it becomes clear that the EF factors for elements with non-crustal sources vary strongly with mineral aerosol concentration (Figure 5.10). In the dustiest quartile of the CVAO dataset EF values for all elements are <10, while during less dusty periods the overall chemical composition of the aerosol load is greatly enriched in elements with non-crustal sources relative to UCA.

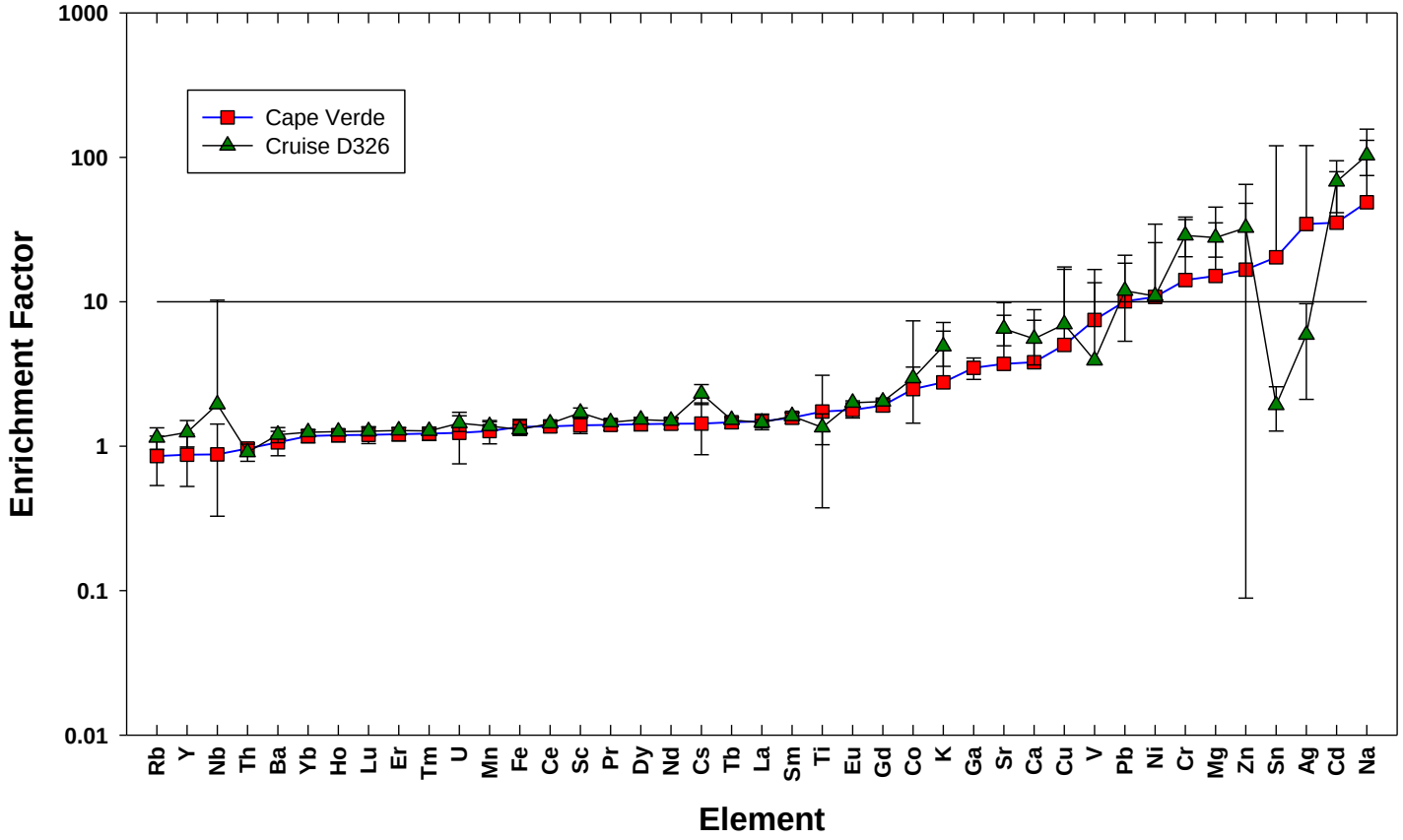

Figure 5.9 Mean crustal enrichment factors for total elemental concentrations determined at the CVAO and during cruise D326. Enrichment factors have been calculated by normalising to Al and using upper crustal concentrations from Taylor and McLennan (1995) as a reference – see Eqn. (5.1). The line at EF = 10 marks the arbitrary cut-off value, above which aerosols are said to be enriched relative to crustal values. Error bars are ± 1 standard deviation. Elements are in order of increasing crustal enrichment factors for CVAO dataset.

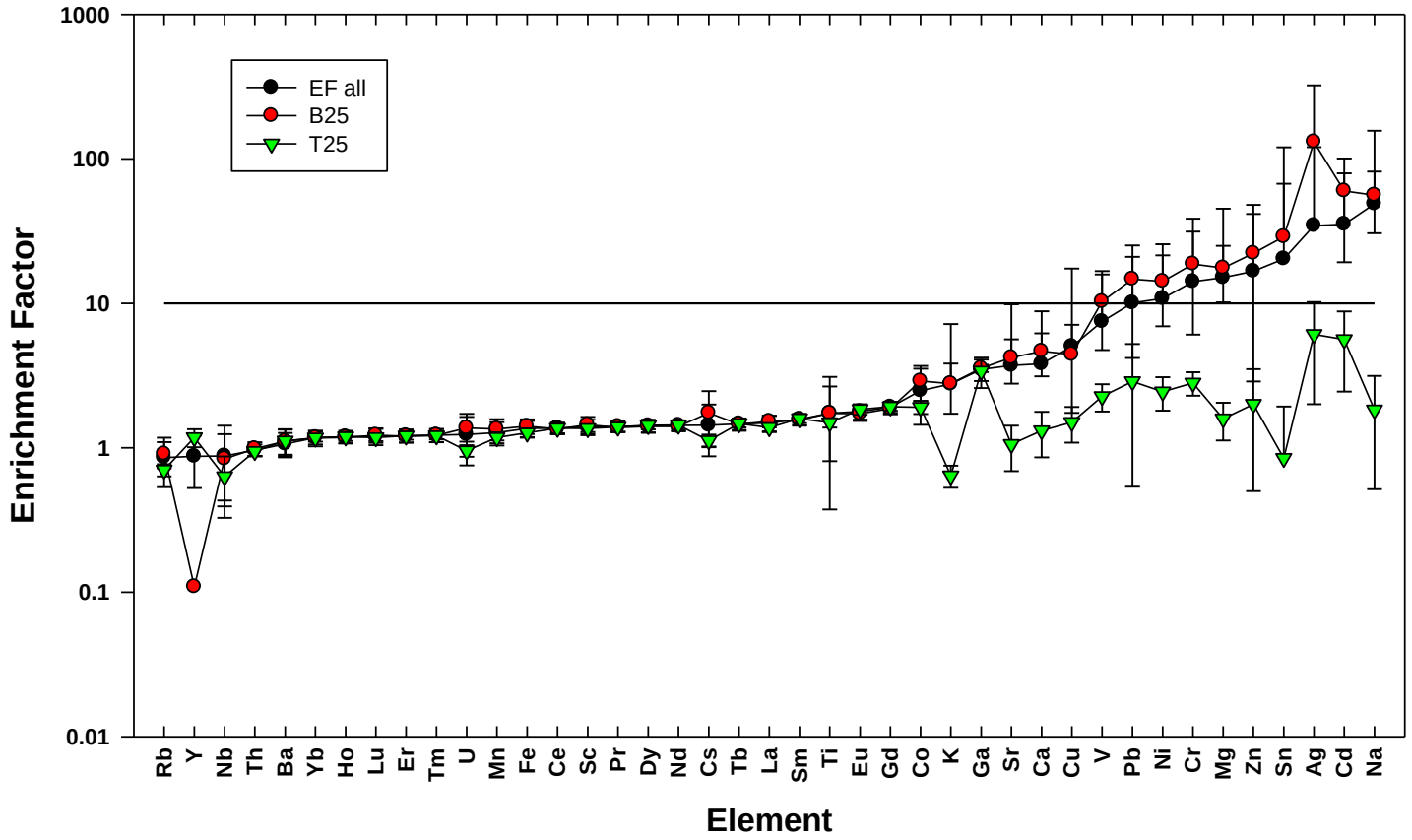

Figure 5.10 Mean crustal enrichment factors for total elemental concentrations determined at the CVAO, illustrating the difference in enrichment factors between the upper (T25) and lower (B25) quartiles of the dataset (ranked in order of atmospheric total Al concentration). Samples with < 1 µg.m^{-3} dust equivalent have been excluded from the calculations.

5.4.3 Trends in elemental composition associated with dust concentration

Statistical analysis was used to investigate further the differences between high dust and low dust conditions discussed in section 5.4.2 and illustrated in Figure 5.10. Initially the CVAO dataset was ranked in order of total atmospheric Al concentrations and any samples corresponding to dust concentrations of less than 1 $\mu g.m^{-3}$ were discarded to avoid using data close to the instrumental detection limit. Ca, Mg and K were corrected to remove the marine contribution using soluble Na concentrations determined from the ultrapure water leaching experiments (see Chapter 6) and seawater composition from Millero and Sohn (1992). Elemental concentrations were then normalised to Al (the ratios of K/Ca and Fe/Ca were also included as indicators of calcite (Chiapello et al., 1995)) before comparing the upper 25% of the ranked dataset then compared with the bottom 25%. Since the data were not normally distributed, the non-parametric Mann-Whitney U test was used to test for significant differences between the high and low concentration samples.

Significant differences ($p < 0.05$) were found for a number of elements (Table 5.2). As might be expected, based on the variability of EF values for enriched elements discussed in section 5.4.2 and shown in Figure 5.10, the pollution elements showed significant differences between the high and low aerosol concentrations. However a number of other elemental ratios also showed statistically significant differences in the distributions between the two groups of samples, including Fe/Al. The mean Fe/Al ratio during high atmospheric particle loadings (0.55) was lower than during periods with lower aerosol concentrations (0.61). However both values are within typical values reported for Saharan dust, e.g. 0.63 ± 0.14 (Guieu et al., 2002), 0.53 (Formenti et al., 2003), 0.58 (Kandler et al., 2007). Ca/Al ratios are also higher and much more variable in the lower quartile of the dataset, probably due to greater marine influence and consequently larger sea-salt corrections. This is supported by much larger and more variable Na/Al ratios in the lower quartile of the dataset. Care must be taken when interpreting the results of the Mann-Whitney test since it does not test the null hypothesis that the two means are statistically different; rather the test probes whether the two distributions are different.

Table 5.2 Mean elemental ratios in highest and lowest quartiles of dust at CVAO July 2007 – July 2008. Statistically different distributions are indicated in blue ($p < 0.05$)

Ratio	Bottom 25% N	Bottom 25% Mean (± 1 s.d.)	Top 25% N	Top 25% Mean (± 1 s.d.)	Mann-Whitney U	Sig.
Na/Al	34	20 ± 9	34	0.66 ± 0.47	0	< 0.001
$_{nss}$Mg/Al	22	0.93 ± 0.82	34	0.17 ± 0.05	62	< 0.001
$_{nss}$K/Al	18	0.36 ± 0.27	26	0.20 ± 0.03	155	0.059
$_{nss}$Ca/Al	32	0.95 ± 0.42	34	0.46 ± 0.16	173	< 0.001
Sc/Al (x 10^{-4})	34	2.0 ± 0.3	34	1.9 ± 0.1	412	0.042
Ti/Al	34	0.065 ± 0.035	34	0.056 ± 0.004	667	0.275
V/Al (x 10^{-4})	34	77 ± 41	34	17 ± 4	37	< 0.001
Cr/Al (x 10^{-4})	33	82 ± 55	34	12.3 ± 2.3	0	< 0.001
Mn/Al (x 10^{-4})	34	101 ± 17	34	88 ± 8	304	0.001
Fe/Al	34	0.61 ± 0.07	34	0.55 ± 0.04	260	< 0.001
Co/Al (x 10^{-4})	34	3.6 ± 1.0	34	2.4 ± 0.2	101	< 0.001
Ni/Al (x 10^{-4})	34	35 ± 18	34	6.1 ± 1.6	34	< 0.001
Cu/Al (x 10^{-4})	34	14 ± 8	34	4.7 ± 1.3	74	< 0.001
Zn/Al (x 10^{-4})	34	196 ± 171	34	18 ± 13	16	< 0.001
Rb/Al (x 10^{-4})	34	12.6 ± 2.6	34	9.8 ± 1.0	170	< 0.001
Sr/Al (x 10^{-4})	34	183 ± 62	34	46 ± 16	7	< 0.001
Nb/Al (x 10^{-4})	34	2.6 ± 1.3	34	2.0 ± 0.7	381	0.016
Ag/Al (x 10^{-4})	13	0.82 ± 1.19	34	0.04 ± 0.03	38	< 0.001
Cd/Al (x 10^{-4})	34	0.73 ± 0.50	34	0.07 ± 0.04	21	< 0.001
Sn/Al (x 10^{-4})	18	20 ± 26	33	0.6 ± 0.7	16	< 0.001
Cs/Al (x 10^{-4})	34	0.80 ± 0.33	34	0.52 ± 0.05	200	< 0.001
Ba/Al (x 10^{-4})	34	76.09 ± 16.04	34	76.42 ± 15.14	569	0.912
La/Al (x 10^{-4})	34	5.7 ± 0.5	34	5.2 ± 0.4	231	< 0.001
Ce/Al (x 10^{-4})	34	10.7 ± 0.8	34	10.9 ± 0.8	626	0.556
Pr/Al (x 10^{-4})	34	1.2 ± 0.1	34	1.2 ± 0.1	620	0.606
Nd/Al (x 10^{-4})	34	4.5 ± 0.3	34	4.6 ± 0.3	683	0.198
Sm/Al (x 10^{-4})	34	0.87 ± 0.08	34	0.89 ± 0.06	670	0.259
Eu/Al (x 10^{-4})	34	0.19 ± 0.02	34	0.20 ± 0.02	818	0.003
Gd/Al (x 10^{-4})	34	0.89 ± 0.08	34	0.91 ± 0.06	712	0.100
Tb/Al (x 10^{-4})	34	0.12 ± 0.01	34	0.12 ± 0.01	632	0.508
Dy/Al (x 10^{-4})	34	0.61 ± 0.06	34	0.62 ± 0.04	685	0.189
Ho/Al (x 10^{-4})	34	0.12 ± 0.01	34	0.12 ± 0.01	627	0.548
Er/Al (x 10^{-4})	34	0.34 ± 0.03	34	0.35 ± 0.02	611	0.686
Tm/Al (x 10^{-4})	34	0.05 ± 0.01	34	0.05 ± 0.00	603	0.759
Yb/Al (x 10^{-4})	34	0.32 ± 0.04	34	0.32 ± 0.02	623	0.581
Lu/Al (x 10^{-4})	34	0.049 ± 0.006	34	0.047 ± 0.003	458	0.141
Pb/Al (x 10^{-4})	34	37 ± 26	34	7.2 ± 5.8	47	< 0.001
Th/Al (x 10^{-4})	34	1.3 ± 0.1	34	1.3 ± 0.1	433	0.076
U/Al (x 10^{-4})	34	0.48 ± 0.09	34	0.33 ± 0.03	53	< 0.001
$_{nss}$K/$_{nss}$Ca	18	0.36 ± 0.23	26	0.46 ± 0.12	302	0.105
Fe/$_{nss}$Ca	32	0.85 ± 0.58	34	1.3 ± 0.5	879	< 0.000

5.4.4 Comparison of elemental composition at CVAO with cruise D326

A total of 11 samples collected at the CVAO between 8 January 2008 and 4 February 2008 enabled a direct comparison with samples collected aboard the RRS Discovery during January 2008. Elemental ratios were calculated as in section 5.4.3. Application of the Mann-Whitney U test revealed statistically significant differences ($p < 0.05$) between the two distributions in several cases, which are listed in Table 5.3. Comparatively higher nssMg/Al, Fe/nssCa and nssK/nssCa ratios were measured during the cruise than were measured at CVAO during the same period.

Table 5.3 Comparison of selected elemental ratios in dust samples collected during cruise D326 with samples collected at CVAO during the same period. Statistically different distributions are indicated in blue ($p < 0.05$). Quoted uncertainties are ± 1 s.d.

	D326		CVAO Jan - Feb 2008		Mann-Whitney U	Sig.
	N	Mean	N	Mean		
Yb/Al (x 10^{-6})	24	34 ± 1	11	32 ± 2	200	0.015
Lu/Al (x 10^{-6})	24	4.9 ± 0.2	11	4.7 ± 0.2	192	0.033
$_{nss}$Mg/Al	23	0.3 ± 0.4	11	0.15 ± 0.04	186	0.028
Fe/$_{nss}$Ca	23	2.4 ± 0.7	11	1.6 ± 0.6	205	0.004
$_{nss}$K/$_{nss}$Ca	23	1.1 ± 0.3	11	0.50 ± 0.15	253	< 0.001
$_{nss}$Ca/Al	24	0.44 ± 0.23	11	0.40 ± 0.16	139	0.804
$_{nss}$K/Al	23	0.26 ± 0.17	11	0.18 ± 0.03	179	0.053
Fe/Al	24	0.54 ± 0.07	11	0.55 ± 0.04	108	0.394

To investigate the possible sources of these differences, the air-mass back trajectories were inspected. Each sample was assigned to a category based upon the region(s) crossed by the back trajectories. Air-masses crossing the African continent were subdivided into three regions using the same scheme as Chiapello et al. (1997), depicted in Figure 5.1. Back trajectories for many of the samples suggested air-masses originated from more than one African Region, while for several samples from the cruise purely marine sources were indicated. On one occasion the air reaching the ship was calculated to have originated from North America.

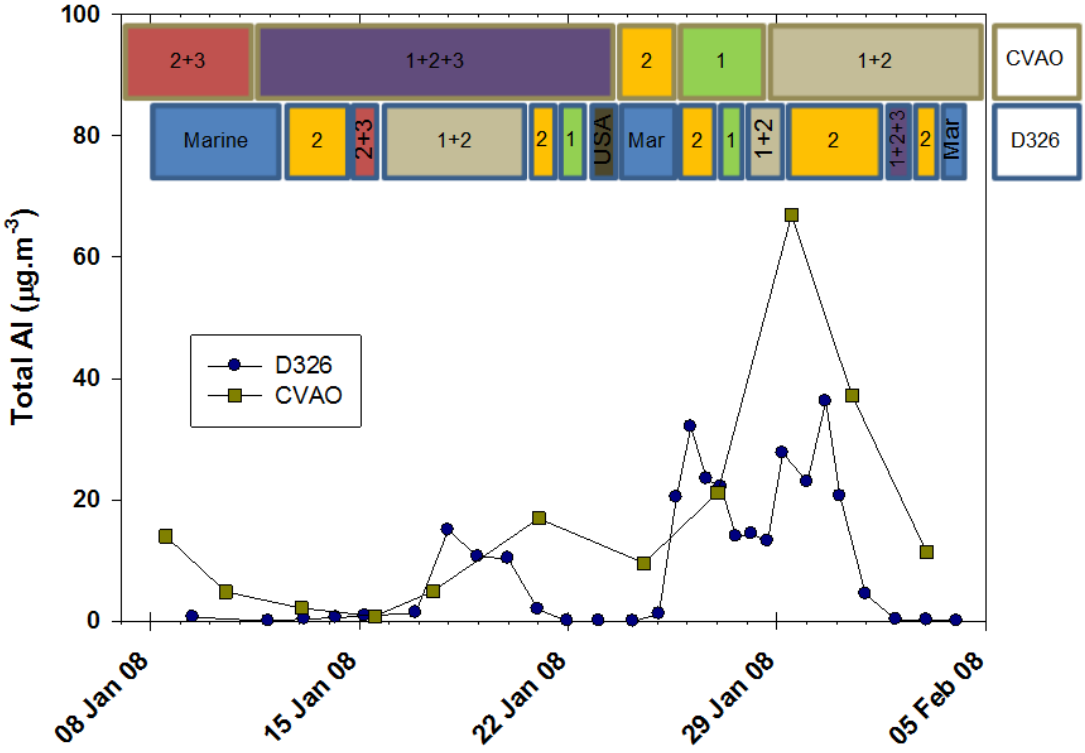

Figure 5.11 Classification of aerosol samples collected during D326 and of samples collected concurrently at the CVAO according to their 5-day air mass back trajectories together with total Al concentrations. "Mar or Marine" denotes air-masses with entirely marine origins. Back trajectories for one sample ("USA") indicated some influence from North America.

Figure 5.11 shows the source regions assigned to samples in the two sets of measurements together with the total Aluminium concentrations. Both sets of measurements are associated with similar source regions and a mixture of all three defined African regions contributing towards the atmospheric particles measured during the cruise period. In terms of sample source, the only significant difference between the CVAO and D326 data is the presence of several periods of "clean" air encountered during the research cruise, during which back-trajectories indicate air parcels that remained above the ocean for at least the preceding 5 days. A visual inspection of air-mass back trajectories finishing between 16 Jan and 23 Jan 2008 (a period covering the first dust event encountered during D326 – see Figure 5.4) reveals that for most of the period the air masses originating from the African continent come from roughly the same regions. Only on 21 and 22 Jan are the

trajectories notably different, with a change to air of predominantly marine origin reaching the ship while air reaching the CVAO is broadly the same as on 20 Jan. Thus, for both sets of measurements, back trajectories originating from the African continent cover a similar area. It seems probable that the differences in some ratios involving non-sea-salt Mg, Ca and K are due to an increased level of sea-salt in the cruise samples. While corrected to remove the marine component of these ratios, this correction was considerable when atmospheric Al concentrations during the cruise were low. These corrections during times of low atmospheric aerosol concentrations will have introduced errors into the ratios involving Mg, Ca and K. nssMg / Al concentrations for individual samples confirm this, with ratios increasing to 0.6 on 15 Jan 2008 and 1.7 on 1 Feb 2008, both coinciding with very low Al concentrations. During times of high Al, the nssMg / Al ratio decreases to about 0.15 – 0.2.

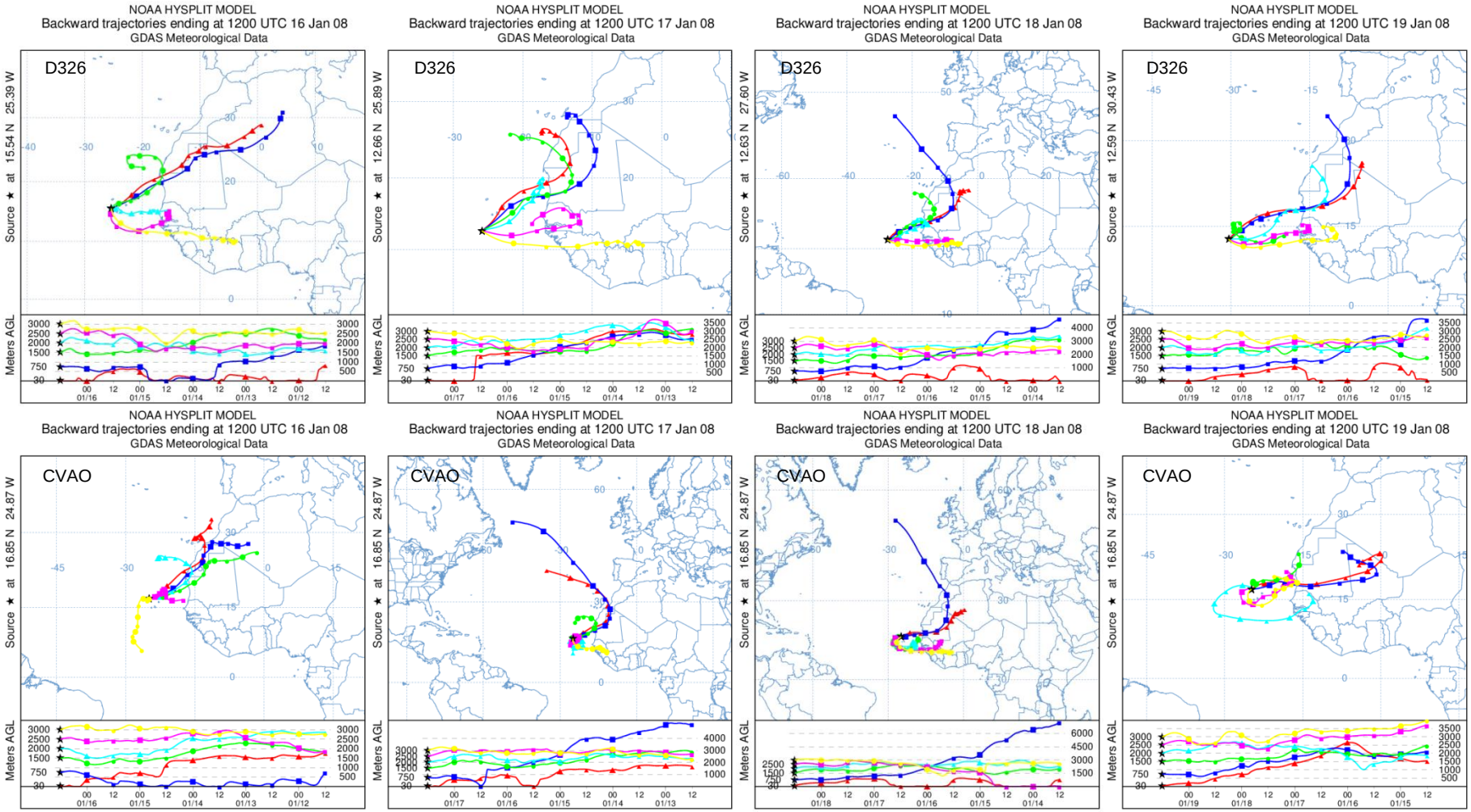

Figure 5.12 5-day air-mass back trajectories ending between 16 Jan – 23 Jan 2008 at the location of (top) RRS Discovery (cruise D326) and (bottom) the CVAO.

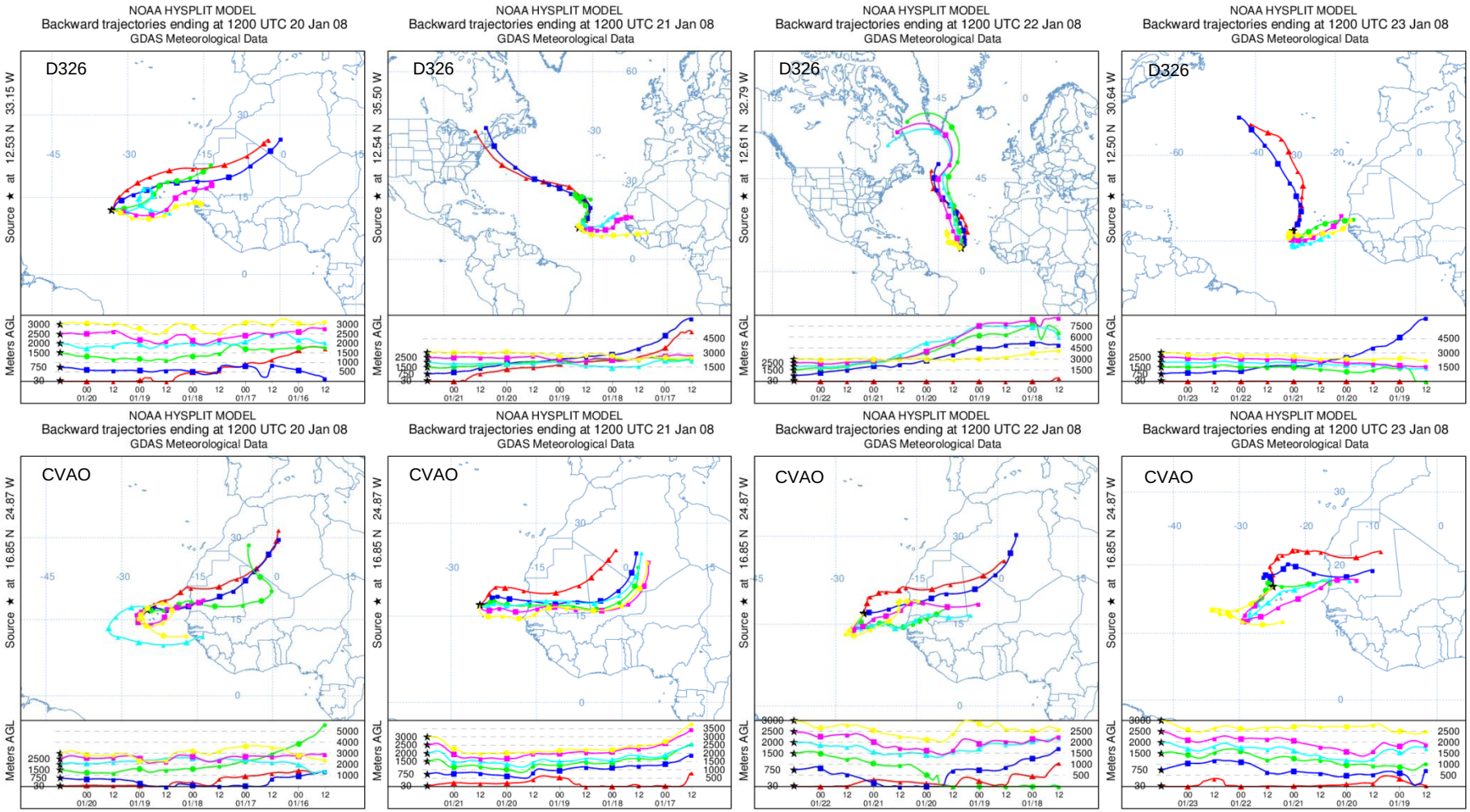

Figure 5.12 continued.

5.4.5 Seasonal changes in aerosol elemental composition at the CVAO in relation to source regions.

Meterological conditions can change relatively quickly, resulting in sharp changes in the source region(s) of dust arriving at the sampling location over the course of a few hours. Since in most cases the samples were collected for 2-3 days, a large proportion of the samples contained contributions from more than one Chiapello source region, which presents a challenge when trying to extract information about the characteristics of specific source regions. To look for clear differences within the CVAO dataset, a comparison was made between the climatologically distinct summer and winter periods at Cape Verde.

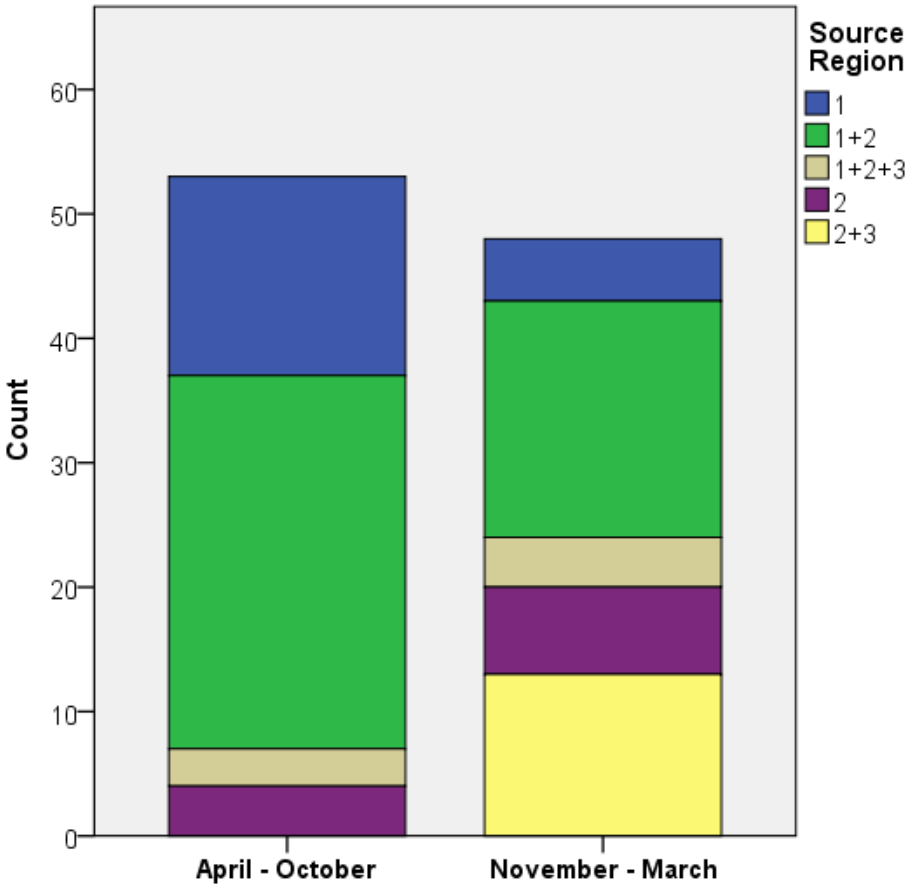

Figure 5.13 Air-mass origin classification at CVAO for samples with > 1 µgm^{-3} mineral dust (calculated from total Al) between July 2007 and July 2008.

Figure 5.13 shows the source region for dusty samples (Al equivalent to >1 $\mu g.m^{-3}$ TSP) between July 2007 and July 2008 separated into summer and winter periods. In the Cape Verde region, the winter climatological period is often considered to occur between October and March (Chiapello et al., 1995; Chiapello et al., 1997). However, based on aerosol Al concentrations measured in our dataset (see Figure 5.2) the winter period seems to begin a little later in early November 2007 with a sudden onset of intense dust events that continue until mid-March, so for this analysis samples collected between 1 November 2007 and 31 March 2008 were compared with those collected at other times. During the winter months (November to March), there are a significant number of samples with air-masses originating from a mixture of sectors 2 and 3 (south / central Sahara and north / west Sahara – see Figure 5.1), whereas no samples collected during the summer period are associated with these source regions. There is also a clear decrease in the number of samples originating from sector 1 (Sahel). To investigate this clear northward shift in sample source regions during the winter and any effect it had on elemental ratios, Mann-Whitney U tests were applied to the samples from both seasons. Samples with Al concentrations corresponding to less than 1 $\mu g.m^{-3}$ TSP equivalent were discarded. In total, 28 elemental ratios showed statistical differences between summer and winter at the $p < 0.05$ confidence level (see Table 5.4).

To investigate the possibility that these seasonal differences may be due to changes in dust source region, a number of ratios were investigated to see whether they varied according to source region. Ratios that have previously been shown to vary with source region and were chosen: nssMg/Al, nssK/Al, nssCa/Al, Fe/nssCa and nssK/nssCa. As far as possible, samples were selected with back trajectories indicating one of the three Chiapello source regions. Due to the lack of samples exclusively from Region 3, samples from Region 1, Region 2 and Regions 2 & 3 were compared.

Table 5.4 Mean elemental ratios in summer and winter at CVAO July 2007 – July 2008. Statistically different distributions are indicated in blue ($p < 0.05$) and uncertainties are ± 1 standard deviation

	October-March		April-September		Mann-Whitney	Sig.
	N	Mean	N	Mean	U	
Na/Al	54	3.7 ± 6.4	82	10 ± 10	916	< 0.001
nssMg/Al	48	0.20 ± 0.09	66	0.48 ± 0.59	1135	0.010
nssK/Al	45	0.18 ± 0.06	37	0.29 ± 0.20	491	0.001
nssCa/Al	54	0.50 ± 0.18	80	0.75 ± 0.38	1269	< 0.001
Sc/Al (x 10^{-4})	54	1.89 ± 0.14	82	1.90 ± 0.21	2266	0.817
Ti/Al	54	0.06 ± 0.01	82	0.06 ± 0.02	2124	0.689
V/Al (x 10^{-4})	54	26 ± 20	82	48 ± 35	1022	< 0.001
Cr/Al (x 10^{-4})	54	21 ± 20	81	45 ± 46	919	< 0.001
Mn/Al (x 10^{-4})	54	90 ± 7	82	92 ± 14	2460	0.274
Fe/Al	54	0.58 ± 0.05	82	0.58 ± 0.06	2258	0.845
Co/Al (x 10^{-4})	54	2.61 ± 0.49	82	2.95 ± 0.80	1617	0.008
Ni/Al (x 10^{-4})	54	11 ± 9	82	22 ± 16	906	< 0.001
Cu/Al (x 10^{-4})	54	6.2 ± 3.2	82	9.6 ± 6.7	1197	< 0.001
Zn/Al (x 10^{-4})	54	39 ± 58	82	104 ± 134	1020	< 0.001
Ga/Al (x 10^{-4})	7	6.8 ± 1.5	36	7.4 ± 1.0	101	0.411
Rb/Al (x 10^{-4})	54	9.9 ± 1.3	82	11 ± 2	1379	< 0.001
Sr/Al (x 10^{-4})	54	67 ± 44	82	109 ± 71	1147	< 0.001
Y/Al (x 10^{-4})	48	2.7 ± 1.0	46	2.1 ± 0.8	1607	< 0.001
Nb/Al (x 10^{-4})	54	2.2 ± 0.8	82	2.8 ± 1.1	1478	0.001
Ag/Al (x 10^{-4})	45	0.27 ± 0.71	50	0.15 ± 0.28	1038	0.517
Cd/Al (x 10^{-4})	54	0.17 ± 0.20	82	0.40 ± 0.42	1098	< 0.001
Sn/Al (x 10^{-4})	50	1.5 ± 1.6	55	7 ± 17	1021	0.023
Cs/Al (x 10^{-4})	54	0.53 ± 0.06	82	0.66 ± 0.25	1529	0.002
Ba/Al (x 10^{-4})	54	77 ± 15	82	70 ± 12	2851	0.005
La/Al (x 10^{-4})	54	5.3 ± 0.4	82	5.4 ± 0.5	1885	0.143
Ce/Al (x 10^{-4})	54	11.1 ± 0.9	82	10.7 ± 0.7	2832	0.006
Pr/Al (x 10^{-4})	54	1.3 ± 0.1	82	1.2 ± 0.1	2700	0.031
Nd/Al (x 10^{-4})	54	4.72 ± 0.38	82	4.54 ± 0.28	2831	0.006
Sm/Al (x 10^{-4})	54	0.90 ± 0.07	82	0.86 ± 0.06	2911	0.002
Eu/Al (x 10^{-4})	54	0.20 ± 0.02	82	0.19 ± 0.01	3039	< 0.001
Gd/Al (x 10^{-4})	54	0.92 ± 0.08	82	0.88 ± 0.05	2949	0.001
Tb/Al (x 10^{-4})	54	0.12 ± 0.01	82	0.11 ± 0.01	2808	0.008
Dy/Al (x 10^{-4})	54	0.62 ± 0.05	82	0.62 ± 0.05	2480	0.237
Ho/Al (x 10^{-4})	54	0.12 ± 0.01	82	0.12 ± 0.01	2329	0.609
Er/Al (x 10^{-4})	54	0.35 ± 0.03	82	0.34 ± 0.03	2468	0.259
Tm/Al (x 10^{-4})	54	0.050 ± 0.004	82	0.050 ± 0.004	2465	0.264
Yb/Al (x 10^{-4})	54	0.32 ± 0.03	82	0.32 ± 0.03	2336	0.587
Lu/Al (x 10^{-4})	54	0.047 ± 0.004	82	0.048 ± 0.004	2101	0.615
Pb/Al (x 10^{-4})	54	15 ± 13	82	22 ± 21	1711	0.025
Th/Al (x 10^{-4})	54	1.27 ± 0.10	82	1.29 ± 0.13	1916	0.185
U/Al (x 10^{-4})	54	0.36 ± 0.05	82	0.41 ± 0.09	1413	< 0.001
nssK/nssCa	45	0.41 ± 0.16	37	0.35 ± 0.18	1018	0.084
Fe/nssCa	54	1.3 ± 0.4	80	1.0 ± 0.8	3211	< 0.001

Table 5.5 shows the mean ratios for each of the three regions, together with the number of measurements, and their standard deviations. The values for the three regions are all very close and with relatively large standard deviations, particularly for Region 1. The sample origins may be too mixed (due to the long sampling duration) to be able to see distinct geochemical signatures that have been observed by others (Chiapello et al., 1997). Another complication seems to be that the samples contained significant quantities of sea salt. Large corrections were applied to Mg, K and Ca values (60%, 40% and 30% average corrections, respectively) to remove the marine component. This is probably the cause of a significant proportion of the variability in ratios involving these elements.

Table 5.5 Selected elemental ratios in samples originating from specific African regions. Mean values are given with uncertainties of 1 s.d.

	Sahel (Region 1)	**South / Central Sahara** (Region 2)	**North / West & South / Central Sahara** (Regions 2 & 3)
N° Samples	21	11	13
nssMg/Al	0.30 ± 0.19	0.17 ± 0.05	0.16 ± 0.04
nssK/Al	0.23 ± 0.06	0.20 ± 0.03	0.20 ± 0.03
nssCa/Al	0.57 ± 0.18	0.50 ± 0.23	0.52 ± 0.11
Fe/nssCa	1.1 ± 0.4	1.3 ± 0.5	1.2 ± 0.3
nssK/nssCa	0.48 ± 0.13	0.46 ± 0.13	0.39 ± 0.10
Fe/Al	0.58 ± 0.04	0.56 ± 0.05	0.58 ± 0.04

Thus it is not possible to explain the observed seasonal differences in elemental ratios in terms of changes in dust source regions, at least by using the elemental ratios in Table 5.5. Another possible explanation for the differences in Table 5.4 is the higher atmospheric particle concentrations during winter resulting in altered enrichment factors for many elements.

A comparison of the mean elemental ratios obtained with comparable values from the literature is presented in Table 5.6 and Table 5.7. There is reasonable agreement for many elemental ratios, although discrepancies are much higher for elements with non-crustal sources, such as Pb, for which results are much more varied.

Table 5.6 Comparison of total metal ratios in dust collected at CVAO with other reported values measured at or close to Cape Verde. Uncertainties, where quoted, are ± 1 s.d.

Reference	This work		Chiapello et al. (1997)			Johansen et al. (2000)	Formenti et al. (2003)
Sample Type	Aerosol		Aerosol			Aerosol	Aerosol (> ~1 µm)
Comments	30m sampling tower, on coast		25 m sampling tower at 100 m altitude, 5 km inland			Research cruise	Aircraft measurements
Location	São Vicente, Cape Verde		Sal, Cape Verde			Barbados - Cape Verde	Cape Verde Region
Date	Oct '07 - Mar '08	Jul–Sep '07; Apr–Jul '08	Winter periods '92-'94			Apr '96	Sep '00
Dust Source			Sahel	South/Central	North/West		
Na/Al	5 ± 7	10 ± 10	0.10			2.1	0.082 ± 0.004
nssMg/Al	0.21 ± 0.11	0.51 ± 0.63				0.39	0.15 ± 0.02
nssK/Al	0.18 ± 0.06	0.31 ± 0.20	0.18	0.21	0.24	0.26	0.21 ± 0.01
nssCa/Al	0.51 ± 0.18	0.79 ± 0.40	0.20 ± 0.05	0.36 ± 0.07	0.60 ± 0.19	0.44	0.36 ± 0.02
Sc/Al (x 10^{-4})	1.9 ± 0.2	1.9 ± 0.2				1.7	
Ti/Al	0.057 ± 0.009	0.061 ± 0.025				0.067	0.059 ± 0.002
V/Al (x 10^{-4})	32 ± 27	46 ± 34				17	14 ± 0.3
Mn/Al	90 ± 8	92 ± 15				110	590 ± 20
Fe/Al	0.58 ± 0.05	0.58 ± 0.06	0.54	0.52	0.54	0.54	0.54 ± 0.02
Ni/Al (x 10^{-4})	14 ± 14	21 ± 16					4.8 ± 0.9
Cu/Al (x 10^{-4})	7.7 ± 6.2	8.8 ± 5.5					3.8 ± 0.6
Zn/Al (x 10^{-4})	47 ± 67	108 ± 140				50	17 ± 1
Ga/Al (x 10^{-4})	7.1 ± 1.2	7.4 ± 1.1				4.3	
Sr/Al (x 10^{-4})	72 ± 48	111 ± 73					38 ± 0.1
Cs/Al (x 10^{-4})	0.54 ± 0.07	0.68 ± 0.27				0.52	14 ± 1
Pb/Al (x 10^{-4})	19 ± 20	19 ± 17				6.5	
Th/Al (x 10^{-4})	1.3 ± 0.1	1.3 ± 0.1				1.35	
nssK/nssCa	0.41 ± 0.16	0.35 ± 0.18	0.96 ± 0.21	0.62 ± 0.10	0.43 ± 0.11	0.60	0.58 ± 0.01
Fe/nssCa	1.26 ± 0.41	0.99 ± 0.84	2.71 ± 0.59	1.43 ± 0.32	0.90 ± 0.30	1.24	1.46 ± 0.05

Table 5.7 Comparison of total metal ratios in dust collected at CVAO with other reported values measured around northern Africa

Reference	This work		Guieu et al. (2002)[a]	Viana et al. (2002)[b]		Alastuey et al. (2005)[b]		Kandler et al. (2007)[b]	Formenti et al. (2008)			
Sample Type	Aerosol		Sieved Soil / rain	Aerosol (PM10)		Aerosol		Aerosol	Aerosol			
Location	São Vicente, Cape Verde		North Africa / Corsica	Canary Islands		Izaña Santa Cruz Tenerife		Izaña, Tenerife	Banizoumbou, Niger[c]	AMMA SOP0/DABEX[d]	DODO1[d]	DODO2[d]
Date	Oct '07-Mar '08	Jul–Sep '07; Apr–Jul '08	'85-'96	Feb '01	Jun '01	28-31 Jul '02		Jul-Aug '05	Jan-Feb '06	Jan-Feb '06	Feb '06	Feb '06
Dust Source			N/NW Sahara	Sahara	Sahel			N/NW Sahara				
Na/Al	5 ± 7	10 ± 10		0.40	3.84	0.14	1.2		0.05±0.04	0.06±0.03	0.5±0.7	0.3±0.6
nssMg/Al	0.21 ± 0.11	0.51 ± 0.63		0.32	0.60	0.17	0.33		0.14±0.03	0.2±0.1	0.3±0.1	0.2±0.1
nssK/Al	0.18 ± 0.06	0.31 ± 0.20		0.28	0.51	0.22	0.30	0.20	0.20±0.05	0.3±0.2	0.2±0.1	0.24±0.06
nssCa/Al	0.51 ± 0.18	0.79 ± 0.40		0.90	1.15	0.40	1.0	0.28	0.4±0.1	0.5±0.3	0.6±0.6	0.6±0.2
Sc/Al (x 10^{-4})	1.9 ± 0.2	1.9 ± 0.2				1.9	4.1					
Ti/Al	0.057 ± 0.009	0.061 ± 0.025		0.049	0.053	0.052	0.087		0.08±0.01	0.10±0.04	0.1±0.1	0.08±0.01
V/Al (x 10^{-4})	32 ± 27	46 ± 34		27	66	9.3	65					
Cr/Al (x 10^{-4})	23 ± 22	47 ± 49				7.1	14.5					
Mn/Al (x 10^{-4})	90 ± 8	92 ± 15		90	120	90	120					
Fe/Al	0.58 ± 0.05	0.58 ± 0.06	0.63±0.02	0.52	0.87	0.52	0.66	0.58	0.59±0.06	0.70±0.30	0.70±0.08	0.68±0.04
Co/Al (x 10^{-4})	2.7 ± 0.5	3.0 ± 0.8				1.5	3.3					
Ni/Al (x 10^{-4})	14 ± 14	21 ± 16				4.0	28					
Cu/Al (x 10^{-4})	7.7 ± 6.2	8.8 ± 5.5				6.5	55					
Zn/Al (x 10^{-4})	47 ± 67	108 ± 140				9.6	82					
Ga/Al (x 10^{-4})	7.1 ± 1.2	7.4 ± 1.1				2.9	3.4					
Rb/Al (x 10^{-4})	10.2 ± 1.6	11.2 ± 2.2				9.4	13.9					
Sr/Al (x 10^{-4})	72 ± 48	111 ± 73				36	58					
Y/Al (x 10^{-4})	2.5 ± 1.1	2.2 ± 0.7				1.6	2.1					
Nb/Al (x 10^{-4})	2.4 ± 0.9	2.7 ± 1.1				1.6	5.7					
Cd/Al (x 10^{-4})	0.25 ± 0.34	0.37 ± 0.39				0.19	0.19					

Table 5.7 continued.

Reference	This work		Guieu et al. (2002)[a]	Viana et al. (2002)[b]		Alastuey et al. (2005)[b]		Kandler et al. (2007)[b]	Formenti et al. (2008)			
Sample Type	Aerosol		Sieved Soil / rain	Aerosol (PM10)		Aerosol		Aerosol	Aerosol			
Location	São Vicente, Cape Verde		North Africa / Corsica	Canary Islands		Izaña Santa Cruz Tenerife		Izaña, Tenerife	Banizoumbou, Niger[c]	AMMA SOP0/DABEX[d]	DODO1[d]	DODO2[d]
Date	Oct '07-Mar '08	Jul–Sep '07; Apr–Jul '08	'85-'96	Feb '01	Jun '01	28-31 Jul '02		Jul-Aug '05	Jan-Feb '06	Jan-Feb '06	Feb '06	Feb '06
Dust Source			N/NW Sahara	Sahara	Sahel			N/NW Sahara				
Sn/Al (x 10^{-4})	3.1 ± 7.6	7 ± 17				1.3	6.5					
Cs/Al (x 10^{-4})	0.54 ± 0.07	0.68 ± 0.27										
Ba/Al (x 10^{-4})	75 ± 15	70 ± 13		72	163	75	81					
La/Al (x 10^{-4})	5.4 ± 0.4	5.4 ± 0.5				0.53	0.94					
Ce/Al (x 10^{-4})	11.1 ± 0.8	10.6 ± 0.8				1.4	1.1					
Pr/Al (x 10^{-4})	1.3 ± 0.1	1.21 ± 0.08				8.36	14					
Sm/Al (x 10^{-4})	0.90 ± 0.07	0.86 ± 0.06				0.19	8.6					
Eu/Al (x 10^{-4})	0.20 ± 0.02	0.19 ± 0.01				1.12	3.3					
Gd/Al (x 10^{-4})	0.92 ± 0.07	0.88 ± 0.05				0.40	2.1					
Pb/Al (x 10^{-4})	19 ± 20	19 ± 17	3.41 ± 1.16	36	87	3.5	19					
Th/Al (x 10^{-4})	1.3 ± 0.1	1.3 ± 0.1				1.3	1.7					
U/Al (x 10^{-4})	0.37 ± 0.06	0.40 ± 0.09				0.71	0.57					
nssK/nssCa	0.41 ± 0.16	0.35 ± 0.18		0.32	0.45	0.54	0.30					
Fe/nssCa	1.26 ± 0.41	0.99 ± 0.84		0.58	0.77	1.3	0.66					

[a] Proposed Saharan dust end-member, based on analysis of sieved soils from Morroco, Mauritania, Algeria and Tunisia and rain samples collected in Corsica. [b] Values calculated from values listed in original article. [c] Ground-based measurements in Niger. [d] Results from 3 aircraft campaigns based in Dakar, Senegal.

5.4.6 Rare earth element patterns

The rare earth elements (REEs) are a coherent group of elements with atomic number from 57 to 71. Due to their similar chemical properties and insolubility in water, REE concentrations in rocks form characteristic patterns which are usually compared by normalising the concentrations to a reference material (often chondritic meteorite or post-Archaen Australian average shale) (Taylor and McLennan, 1995). REEs are relatively immobile in sediments and are subjected to little fractionation during chemical and physical weathering, thus REE patterns in sediments represent a signature of igneous processes that occurred during the formation of the parent rock can be used as an indicator of the provenance of sedimentary materials (Muhs et al., 2007).

REE patterns were calculated for the data from the CVAO to see whether they could be used to distinguish different aerosol source regions. Absolute REE concentrations (µg/kg – calculated using total Al concentrations and assuming 8.04% w/w Al) were normalised to chondritic meteorite compositions (taken from Taylor and Gorton, 1977). Figure 5.14 contains REE patterns plotted using mean values for samples from five different source region categories according to air-mass back-trajectories. A very similar REEE pattern is obtained for samples from all regions, with light rare earth elements (LREE) significantly enriched relative to the heavy rare earth elements (HREE), a relatively flat and uniform HREE pattern and a marked depletion in Eu relative to its neighbouring elements, Sm and Gd. This pattern is typical of sedimentary materials derived from post-Archean continental crust and is found in sediments from around the world with remarkable uniformity (Taylor and McLennan, 1995). Profiles typically differ the most in the level of HREE enrichment and the degree of Eu depletion relative to the other REEs (termed a negative Eu anomaly), and a visual inspection of the CVAO data in Figure 5.14 shows that there is more variation in these two parts of the REE pattern.

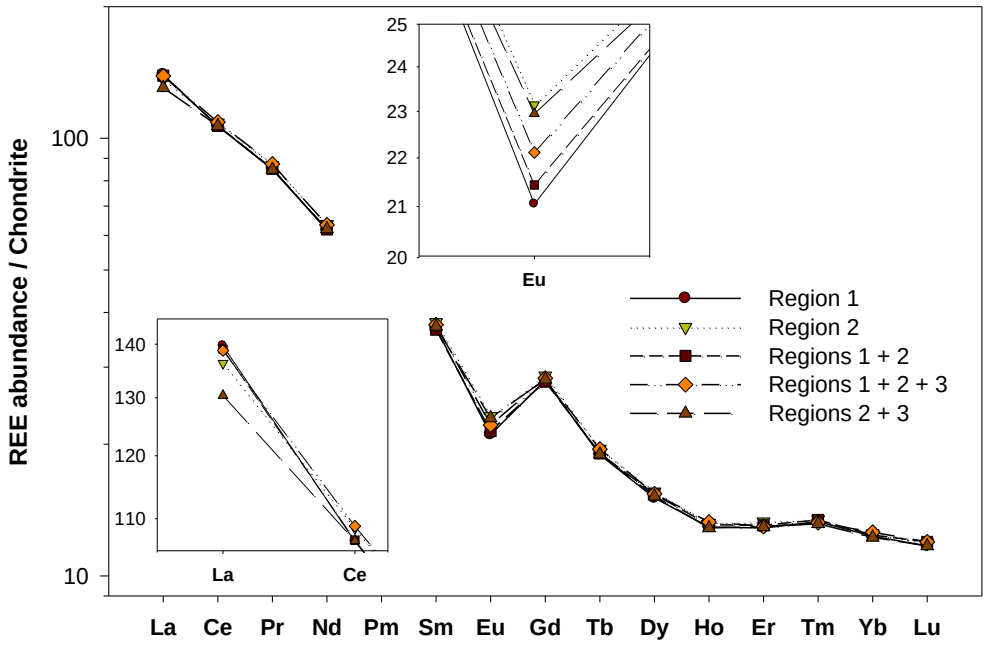

Figure 5.14 Chondrite normalised REE patterns for samples collected at the CVAO between 2 July 2007 and 11 July 2008. Mean values are plotted from 5 groups corresponding to different source regions identified from air-mass back-trajectories (labelled according to Chiapello et al., 1997). 16 samples containing very low concentrations (Al < 3.8 µg/filter) have been excluded.

To facilitate the comparison of REE data for source identification it is useful to calculate three parameters: Eu/Eu* is a measure of the Europium anomaly, where Eu is the Chondrite normalised Europium concentration (Eu_N) and Eu* is the expected Europium concentration based on Sm and Gd ($Eu^* = (Sm_N \times Gd_N)^{1/2}$). Eu/Eu* is < 1 for a negative Europium anomaly (Eu depleted relative to its neighbouring REEs) and <1 for a positive anomaly. La_N/Yb_N is a measure of the LREE enrichment relative to the HREE and is simply the ratio of the chondrite normalised values for La and Yb, with higher values indicating more LREE enrichment. Gd_N/Yb_N is a measure of HREE depletion, with higher values indicating more depletion of the heavier elements relative to Gd. Table 5.8 shows summary statistics for these parameters calculated for the samples from each of the five source regions shown in Figure 5.13.

Table 5.8 Summary of REE parameters calculated for 137 samples collected at the CVAO between 2 July 2007 and 11 July 2008 separated into groups according to source region. Sample groupings are the same as in Figure 5.14.

		Region 1	Region 2	Regions 1 + 2	Regions 1 + 2 + 3	Regions 2 + 3
Eu/Eu*	Min	0.57	0.65	0.54	0.66	0.66
	Max	0.72	0.75	0.76	0.74	0.77
	Mean	**0.66**	**0.70**	**0.67**	**0.68**	**0.71**
	Std. dev.	0.03	0.03	0.04	0.03	0.03
La_N/Yb_N	Min	9.31	10.09	8.67	10.15	9.81
	Max	13.61	12.39	14.98	12.04	11.70
	Mean	**11.40**	**10.95**	**11.29**	**11.05**	**10.68**
	Std. dev.	1.00	0.76	1.29	0.58	0.63
Gd_N/Yb_N	Min	1.98	2.03	1.87	2.14	2.04
	Max	2.62	2.43	2.74	2.34	2.39
	Mean	**2.28**	**2.30**	**2.25**	**2.25**	**2.30**
	Std. dev.	0.16	0.12	0.16	0.07	0.08
No. of samples		33	13	69	8	14

Muhs et al. (2007) describe approximate values for African dust as Eu/Eu* ~ 0.55 – 0.80; La_N/Yb_N ~ 5 – 12.5; and Gd_N/Yb_N ~ 1 – 2.5, and all of the CVAO data falls within or very close to this range. Gd_N/Yb_N values for all five source regions span a very similar range and have similar mean values, suggesting that there is little difference in the HREE values between the different source regions. La_N/Yb_N and Eu/Eu* values show more differences between the different regions, but again there is a large amount of overlap between the values for different regions. A plot of Eu/Eu* vs La_N/Yb_N is shown in Figure 5.15. The data for samples originating from a mixture of Regions 1 and 2 contain a large amount of scatter and have been excluded to improve the clarity of the figure. Despite the scatter a general trend can be made out, with samples from Region 1 (Sahel) tending towards higher La_N/Yb_N and lower Eu/Eu*, Regions 2 + 3 (Sahara) tending towards lower La_N/Yb_N and higher Eu/Eu* and Regions 2 (and samples with a mixture of Regions 1, 2 and 3) coming somewhere in between.

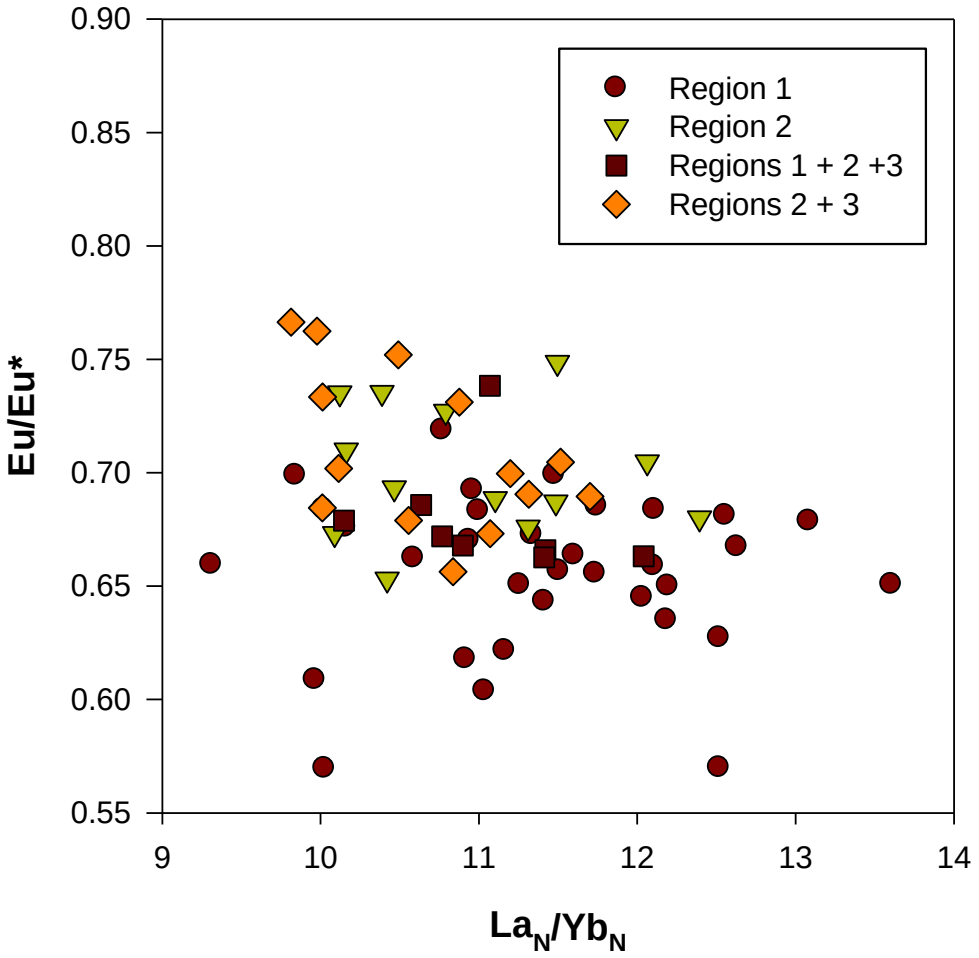

Figure 5.15 Plot of Eu/Eu* vs LaN/YbN for individual samples collected at the CVAO between 2 July 2007 and 11 July 2008. Samples associated with Regions 1 + 2, and with very low concentrations (Al < 3.8 µg/filter) have been excluded.

Our data is consistent with the findings of Moreno et al. (2006), who conducted a geochemical study of dust samples collected in various locations across the Sahel and Sahara and found only very small variations in REE concentrations. While some trends in the REE patterns from the CVAO dataset are perceptible, overall the variations appear to be too small for REE patterns alone to be used as an accurate indicator of aerosol source.

5.5 Non-crustal contributions to aerosol composition

5.5.1 Biomass burning

Biomass burning (BB) aerosols are produced primarily from the burning of agricultural waste, with the African continent one of the largest global sources. A plethora of chemical species are present in the gases and soot emitted by agricultural fires, including oxides of nitrogen, SO_2, NH_3, K, CN, Hg and many forms of organic carbon (Andreae and Merlet, 2001). As is the case with mineral dust, BB aerosols can be transported large distances and have an influence on global climate through alteration of the optical properties of the atmosphere (Johnson et al., 2008). A well-determined seasonal cycle in biomass burning aerosol emissions from western Africa has been established, with maximum emissions occurring between December and February (Hand et al., 2010).

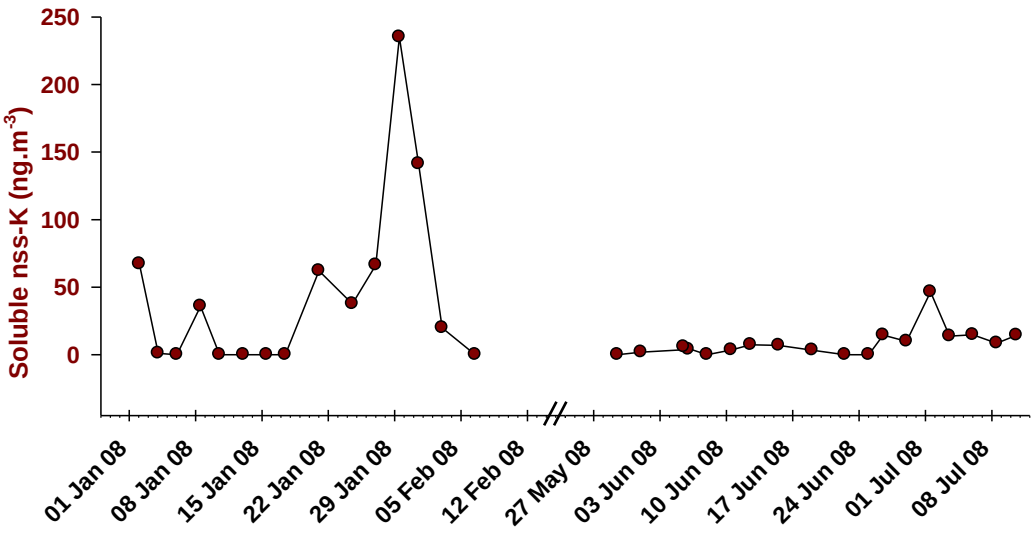

Figure 5.16 MQ Soluble K measured in samples collected at the CVAO. Data is available for two periods in Jan-Feb and June-July 2008. Values have been corrected for sea-salt K using MQ soluble Na concentrations.

Measuring organic carbon in aerosols requires sampling onto separate glass fibre filters and was beyond the scope of this study. However soluble K is often used as an indicator of BB aerosols since the combustion of plant matter, which is rich in potassium, releases large quantities of aerosol particles high in K (Pio et al., 2008). Water soluble K concentrations for the CVAO samples, as determined using the MQ leach procedure described in Chapter 2, are only available during two periods of about 6 weeks during January/February and June/July 2008. Figure 5.16 shows the MQ soluble K values (corrected for sea-salt K using MQ soluble Na concentrations). Although data are only available for two short periods and it is therefore not possible to draw conclusions about seasonal changes, K concentrations are consistent with the expected seasonal pattern, with several large spikes in K concentrations during the 6-week period in winter and relatively low and constant concentrations during the 6-week summer period. Another notable feature is that the spikes in soluble K during January/February 2008 coincide well with peaks in total Al (see Figure 5.3). Using energy dispersive X-ray analysis and scanning electron microscopy Hand et al. (2010) investigated the composition of particles in African aerosols and found a large degree of internal mixing between soot and mineral dust; that is, soot particles attached to mineral dust particles. The authors suggest that the large surface area of mineral dust particles may favour the condensation of secondary organic carbon. This is one possible explanation for the observed correlation between soluble nssK and total Al in the CVAO samples and this hypothesis is supported by a slight increase in % solubility of nssK (from close to 0% to 2% - data not shown) during the dust event between 17 January and 2 February 2008. If the enhanced soluble nssK concentrations were a result of the dissolution of crustal material, a decrease in the soluble fraction with increasing Al would be expected. Nonetheless, single particle analytical techniques would be required to confirm or refute this.

5.5.2 Anthropogenic activity

V, Ni, Cu, Zn and Pb are often associated with urban pollution and the burning of oil; however they are also present in nature in significant quantities, with mean UCA ranging from 20 ppm to 71 ppm (Taylor and McLennan, 1995). To assess the non-

crustal fractions of these elements the crustal values were subtracted from the measured concentrations. Crustal values were calculated using total Al concentrations and UCA values for the element in question (Taylor and McLennan, 1995). Excess atmospheric concentrations of the above five elements throughout the 1-year period at the CVAO are presented in Figure 5.17 together with total Al concentrations for comparison.

Despite the correction applied, excess V and Ni concentrations still show a strong correlation with total Al (R^2 = 0.90 and 0.75, respectively). This correlation suggests that V and Ni are present in the mineral component of the aerosol samples at concentrations higher than UCA. There are no significant V or Ni peaks in Figure 5.17 that do not correspond with elevated Al concentrations (except perhaps on 2 August 2007 for Ni), indicating that there are no significant non-crustal sources of these elements.

For excess Cu and Zn, there is no relationship with Al (R^2 = 0.17 and 0.04, respectively), but some peaks remain, indicating some non-crustal sources of these elements. Excess Pb shows a large number of peaks throughout the year with the most intense events occurring during the winter months (November to March). Although there is not a correlation between excess Pb and Al (R^2 = 0.05), nearly all of the significant peaks in excess Pb coincide with a peak in total Al. This is also apparent for the peaks in excess Cu and Zn. This is a similar result to that obtained for soluble K in Section 5.5.1 and suggests that mineral dust may be forming internal mixtures with these species. In addition to many industrial and local population centres on the African continent, pollutants from Europe can be rapidly transported to Africa where they are mixed with dust-laden air (Kallos et al., 1998). In this way, the large surface area of mineral dust may be acting to adsorb and concentrate particles of anthropogenic origin.

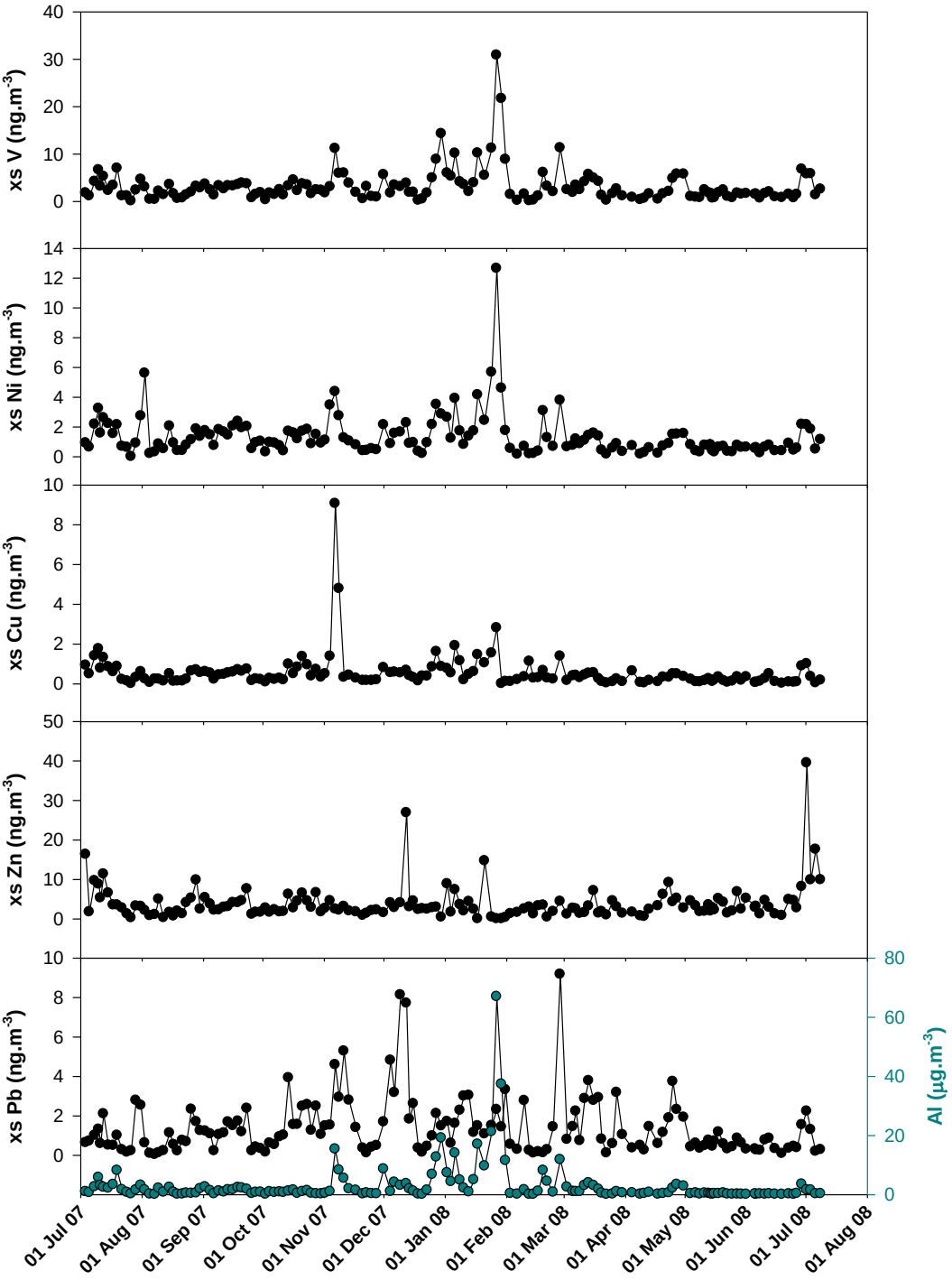

Figure 5.17 CVAO record of excess atmospheric concentrations of selected pollutant aerosol species. Values are excess concentrations, calculated by subtracting the crustal component from the value total digestion (using total Al concentrations and UCA for the element in question). Total Al concentrations (in cyan) are included for reference.

5.6 Discussion

Quantification of the production and transport of aerosols, their deposition to the oceans and the important role they play in biogeochemical cycles and in regulating climate is a major area of research involving scientists working in a wide range of disciplines including biology, oceanography, biogeochemistry, geochemistry, atmospheric chemistry and climate modelling. However, as is often the case with marine and ocean science, obtaining sufficient measurement coverage, both spatial and temporal, poses a great challenge to scientists. Satellite observations, with their unparalleled coverage, have been able to address this issue to some extent, but it remains very difficult to extract quantitative information from these observations. Direct measurements of aerosol particles are essential in order to get reliable estimates of aerosol concentrations and composition and to constrain model and satellite estimates (Mahowald et al., 2005).

Aerosol measurements over the tropical eastern North Atlantic are very limited in both spatial and temporal coverage, with observations limited to the occasional research cruise (Baker et al., 2006), some land-based observations from the Canary Islands (e.g. Neuer et al., 2004) and a few limited studies in Cape Verde (e.g. Chiapello et al., 1995; 1997). The aerosol dataset presented in this thesis represents the most comprehensive set of measurements to date covering a complete seasonal cycle in the eastern tropical and subtropical North Atlantic. It is distinctive also in that, during January and February 2008, independent measurements were made of similar air-masses at land and sea, enabling a glimpse of the spatial variability of aerosol concentrations. As such this work is a significant aid to filling gaps in knowledge of aerosol composition and sources, and to constraining estimates of aerosol concentration in the most dust impacted ocean region in the world.

Previously established seasonal variations in average aerosol concentrations (Chiapello et al., 1995) are clearly visible in our dataset, with numerous periods of elevated atmospheric Al concentrations during the winter period (November – March) and very low concentrations during the summer months (April – October).

An annual mean atmospheric Al concentration of 2.9 $\mu g.m^{-3}$ was measured at the CVAO between July 2007 and July 2008, while the average Al concentration between 4 January and 8 February 2008 (during cruise D326) at CVAO was 15.0 $\mu g.m^{-3}$. Using the UCA of Al, this monthly average value (CVAO January 2008) corresponds to a theoretical mineral dust concentration of 187 $\mu g.m^{-3}$. Chiapello et al. (1995) list maximum monthly average mineral dust concentrations as 120, 95 and 70 $\mu g.m^{-3}$, for 1992, 1993 and 1994, respectively. Mean shipboard concentrations measured during the same period (10.5 $\mu g.m^{-3}$ Al) corresponded to 131 $\mu g.m^{-3}$ mineral dust. Thus it appears that January 2008 was a particularly dusty month and it is fortuitous that shipboard aerosol measurements are also available for this period. Mean measured atmospheric Al concentrations measured at CVAO during the cruise period are around 50% greater than the shipboard measurements. The ship was typically a few hundred kilometres from the CVAO (see Figure 5.4), but this difference gives an illustration of the spatial variability of dust concentrations on this occasion.

Chemically, the samples show a high degree of uniformity. For most elements, very high correlations between their concentration values and total Al values shows that, to a large extent, they have a crustal source. Elements that do not show a correlation with Al have predominantly non-crustal sources. The use of Pearson correlation coefficients with Al, however, is a fairly crude way to extract information about the source of an element. Species with mixed crustal / non-crustal origin may show a strong correlation with Al due to the dominance of crustal material in samples with high Al. The comparison of crustal enrichment factors for elements under high Al and low Al conditions (see Figure 5.10) is a powerful technique to determine which elements are relatively enriched during low mineral dust conditions and therefore have other, non-crustal sources. This analysis reveals sea salt components as well as 9 transition elements to have non-crustal sources in addition to a crustal component (Cu, V, Pb, Ni, Cr, Zn, Sn, Ag and Cd). Plots of some of these transition elements with the theoretical crustal fraction removed (see Figure 5.17) suggest that for elements such as V and Ni this non-crustal fraction is very small. However for Cu, Zn and Pb there are clear signs of non-crustal inputs.

Elevated concentrations of these elements are often associated with emissions from industrial areas and cities. It is particularly interesting that peaks in these elements all coincide with elevated Al concentrations, albeit very small peaks in some cases. This appears to be evidence that atmospheric mineral dust particles may be collecting adsorbed pollutants during transport, although single particle analytical techniques would be required to prove this conclusively. It also suggests that there are no significant local sources of pollution, as elevated levels of Pb, Zn and Cu arrive only with episodes of mineral dust.

Limited evidence exists for biomass burning inputs in the CVAO samples, in the form of elevated soluble nss K concentrations during the winter (see Figure 5.16). Again nss K, a strong indicator of biomass aerosols, appears to be associated with elevated Al concentrations. Direct evidence of biomass burning aerosols adsorbed to mineral dust have already been reported (Hand et al., 2010). Our data supports these findings, although we do not have the analytical measurements necessary to investigate this further.

It has proven challenging to relate the chemical composition of particles to individual source regions. A division of the samples into three groups according to the source region(s) indicated by their air-mass back trajectory revealed did not show any real differences between the groups (see Table 5.5). It appears that relatively long sampling durations of 2-3 days resulted in many samples with mixed origins, which makes it harder to measure differences between the different groups. In addition, the coastal nature of the sight results in fairly high correction factors to remove the sea-salt component of elemental ratios involving Mg, K and Ca. Significant differences in many elemental ratios were found, however, when comparing samples collected in summer and winter (see Table 5.6). These differences must be related to the shifts in sample source region associated with seasonal changes in meteorological conditions. A future re-analysis of the data focussing on specific samples and / or dust events with more constrained source regions will hopefully prove more fruitful.

An analysis of REE patterns as a function of sample source region (in section 5.4.6) revealed some general trends in a plot of Eu / Eu* vs La_N/Yb_N (see Figure 5.15), but the differences are very small and there is a great deal of scatter. As with the elemental ratios above, it seems likely that a future reanalysis of the data focussing on a narrower range of samples and / or individual dust events will be able to extract useful relationships between a sample's origin and its REE pattern. Furthermore the use of clay ratios has been shown to be a powerful technique for distinguishing the source region of Saharan soil (Caquineau et al., 2002) and forthcoming results from XRD of some 40 samples the datasets described here is anticipated to be a useful aid to interpreting the geochemical data.

5.7 Conclusions

During the course of a one year period at the CVAO numerous dust events of varying size have been captured and the expected seasonal changes in aerosol concentration are clearly visible. There was a high level of consistency in the chemical composition of the samples, with many of the 42 elements determined by total acid digestion displaying a high level of correlation to Al. Statistically significant differences were found for the concentrations of many elements and trends in REE patterns are perceptible when comparing samples from climatologically different periods, but it is not possible at this stage to link these differences to changes in the dust source regions between different samples. Efforts to do this have been complicated by the relatively long sampling period of 2 – 3 days, which results in many samples containing material from a mixture of source regions, and also due to a relatively large amount of sea salt collecting on the filters, resulting in degraded measurement precision for Mg, K and Ca.

Dust events captured aboard RRS Discovery during a cruise D326 in the Cape Verde region were sampled simultaneously at the CVAO. The distance between the two sampling sites was only a few hundreds of kilometres and the chemical signature of the two sample sets was virtually indistinguishable; however mean atmospheric particle concentrations sampled aboard RRS Discovery were around 70% of those

measured at the CVAO, which gives some idea of the spatial variability of aerosol inputs during a period of significant large scale atmospheric dust transport.

Enrichment factors suggest that elements typically associated with anthropogenic activity (Cu, V, Pb, Ni, Cr, Zn, Sn, Ag and Cd) are relatively enriched when aerosol concentrations are low. However all of these elements show positive correlations with Al, and their concentrations are at their greatest during dust events. Cu, Zn and Pb show the highest levels of anthropogenic input, yet show a strong association with mineral dust, perhaps having become adsorbed to the surface of the dust during transport. There is also evidence from soluble nss K concentrations of significant biomass burning aerosols. As with Cu, Zn and Pb, there is a correspondence with mineral dust concentrations and this indicates possible internal mixing between mineral dust particles and biomass burning aerosols.

5.8 References

Aguilar-Islas, A. M., et al. (2010). Dissolution of aerosol-derived iron in seawater: Leach solution chemistry, aerosol type, and colloidal iron fraction. *Marine Chemistry* 120(1-4): 25-33.

Alastuey, A., et al. (2005). Characterisation of TSP and PM2.5 at Izana and Sta. Cruz de Tenerife (Canary Islands, Spain) during a Saharan Dust Episode (July 2002). *Atmospheric Environment* 39(26): 4715-4728.

Andreae, M. O. and Merlet, P. (2001). Emission of trace gases and aerosols from biomass burning. *Global Biogeochem. Cycles* 15(4): 955-966.

Baker, A. R., et al. (2006). Nutrients in atmospheric aerosol particles along the Atlantic Meridional Transect. *Deep Sea Research Part II: Topical Studies in Oceanography* 53(14-16): 1706-1719.

Caquineau, S., et al. (1998). Saharan dust: Clay ratio as a relevant tracer to assess the origin of soil-derived aerosols. *Geophysical Research Letters* 25(7): 983-986.

Caquineau, S., et al. (2002). Mineralogy of Saharan dust transported over northwestern tropical Atlantic Ocean in relation to source regions. *Journal of Geophysical Research-Atmospheres* 107(D15).

Chavagnac, V., et al. (2007). Anti-Atlas Moroccan Chain as the source of lithogenic-derived micronutrient fluxes to the deep Northeast Atlantic Ocean. *Geophysical Research Letters* 34(21).

Chester, R., et al. (1999). The trace metal chemistry of atmospheric dry deposition samples collected at Cap Ferrat: a coastal site in the Western Mediterranean. *Marine Chemistry* 68(1-2): 15-30.

Chiapello, I., et al. (1995). An additional low layer transport of Sahelian and Saharan dust over the North-Eastern Tropical Atlantic. *Geophysical Research Letters* 22(23): 3191 - 3194.

Chiapello, I., et al. (1997). Origins of African dust transported over the northeastern tropical Atlantic. *Journal of Geophysical Research-Atmospheres* 102(D12): 13701-13709.

Duce, R. A. and Tindale, N. W. (1991). Atmospheric Transport of Iron and Its Deposition in the Ocean. *Limnology and Oceanography* 36(8): 1715-1726.

Formenti, P., et al. (2003). Chemical composition of mineral dust aerosol during the Saharan Dust Experiment (SHADE) airborne campaign in the Cape Verde region, September 2000. *Journal of Geophysical Research-Atmospheres* 108(D18).

Formenti, P., et al. (2008). Regional variability of the composition of mineral dust from western Africa: Results from the AMMA SOP0/DABEX and DODO field campaigns. *Journal of Geophysical Research-Atmospheres* 113(D20).

Guieu, C., et al. (2002). Chemical characterization of the Saharan dust end-member: Some biogeochemical implications for the western Mediterranean Sea. *Journal of Geophysical Research* 107.

Hand, V. L., et al. (2010). Evidence of internal mixing of African dust and biomass burning particles by individual particle analysis using electron beam techniques. *Journal of Geophysical Research* 115(D13): D13301.

Herut, B., et al. (2001). Dry atmospheric inputs of trace metals at the Mediterranean coast of Israel (SE Mediterranean): sources and fluxes. *Atmospheric Environment* 35(4): 803-813.

Hsu, S.-C., et al. (2010). Sources, solubility, and dry deposition of aerosol trace elements over the East China Sea. *Marine Chemistry* 120(1-4): 116-127.

Jickells, T. D., et al. (2005). Global Iron Connections Between Desert Dust, Ocean Biogeochemistry, and Climate. *Science* 308(5718): 67 - 71.

Johansen, A. M., et al. (2000). Chemical composition of aerosols collected over the tropical North Atlantic Ocean. *Journal of Geophysical Research-Atmospheres* 105(D12): 15277-15312.

Johnson, B. T., et al. (2008). Aircraft measurements of biomass burning aerosol over West Africa during DABEX. *Journal of Geophysical Research* 113(D23): D00C06.

Kallos, G., et al. (1998). On the long-range transport of air pollutants from Europe to Africa. *Geophysical Research Letters* 25(5): 619-622.

Kandler, K., et al. (2007). Chemical composition and complex refractive index of Saharan Mineral Dust at Izaña, Tenerife (Spain) derived by electron microscopy. *Atmospheric Environment* 41(37): 8058-8074.

Mahowald, N. M., et al. (2005). Atmospheric global dust cycle and iron inputs to the ocean. *Global Biogeochemical Cycles* 19(4).

Millero, F. J. and Sohn, M. L. (1992). Chemical Oceanography. Boca Raton, CRC Press.

Moreno, T., et al. (2006). Geochemical variations in aeolian mineral particles from the Sahara-Sahel Dust Corridor. *Chemosphere* 65(2): 261-270.

Muhs, D. R., et al. (2007). Geochemical evidence for African dust inputs to soils of western Atlantic islands: Barbados, the Bahamas, and Florida. *Journal of Geophysical Research* 112(F2): F02009.

Muhs, D. R., et al. (2010). Geochemical and mineralogical evidence for Sahara and Sahel dust additions to Quaternary soils on Lanzarote, eastern Canary Islands, Spain. *Terra Nova* 00(0): 1-12.

Neuer, S., et al. (2004). Dust deposition pulses to the eastern subtropical North Atlantic gyre: Does ocean's biogeochemistry respond? *Global Biogeochemical Cycles* 18(4).

Orif, M. (2007). The impacts of atmospherically derived metals on coastal marine systems. *School of Earth, Ocean and Environmental Sciences*. Plymouth, University of Plymouth. PhD**:** 248.

Pio, C. A., et al. (2008). Chemical composition of atmospheric aerosols during the 2003 summer intense forest fire period. *Atmospheric Environment* 42(32): 7530-7543.

Prospero, J. M. and Lamb, P. J. (2003). African Droughts and Dust Transport to the Caribbean: Climate Change Implications. *Science* 302(5647): 1024-1027.

Schütz, L. and Sebert, M. (1987). Mineral aerosols and source identification. *Journal of Aerosol Science* 18(1): 1-10.

Taylor, S. R. and Gorton, M. P. (1977). Geochemical application of spark source mass spectrography--III. Element sensitivity, precision and accuracy. *Geochimica Et Cosmochimica Acta* 41(9): 1375-1380.

Taylor, S. R. and McLennan, S. M. (1995). The geochemical evolution of the continental crust. *Reviews of Geophysics* 33(2): 241-265.

Trapp, J. M., et al. (2010). Temporal variability of the elemental composition of African dust measured in trade wind aerosols at Barbados and Miami. *Marine Chemistry* 120(1-4): 71-82.

Viana, M., et al. (2002). Influence of African dust on the levels of atmospheric particulates in the Canary Islands air quality network. *Atmospheric Environment* 36(38): 5861-5875.

6. Soluble trace metals and nutrients in atmospheric dust over the eastern tropical North Atlantic

6.1 Overview

In this chapter, data will be presented for the soluble fraction of trace metals and nutrients in dust collected at the Cape Verde Atmospheric Observatory (CVAO) in the period between July 2007 and July 2008, and aboard the RRS Discovery during a research cruise (D326) in the (sub-)tropical eastern North Atlantic (January-February 2008).

6.2 Introduction

Over recent decades, considerable effort has gone into quantifying dust sources, transport and deposition of dust to the world's oceans (Mahowald et al., 2005). The atmosphere is an important source of Fe and other nutrients to the surface oceans and much effort has therefore been directed towards understanding the fraction of dust that is available for biological uptake following atmospheric deposition. The oligotropic ocean gyres form ca. 30-40% of the world's oceans and phytoplankton growth is limited by N and P availability. Iron is a key limiting nutrient in ca. 30-40% of the world's oceans, the so-called High Nutrient Low Chlorophyll (HNLC) regions including the Southern Ocean and Equatorial and Subarctic Pacific . Iron also plays a key role in the distribution of nitrogen fixers (diazotrophs) and their fixation rates, because of its central role in the enzyme nitrogenase (Moore et al., 2009). It is generally assumed that some proportion of the dust must first be released into solution in order to be available to organisms. However, to what extent dust is soluble, which factors control this extent of solubility, and how well the fraction measured by current techniques as "dissolved" corresponds with the fraction useful

to marine biota, remain unanswered and challenging questions for the marine and atmospheric scientific communities (Jickells et al., 2005).

6.2.1 Measuring dust dissolution

There is no widely accepted definition of the "dissolved" in environmental sciences. Solubility is an operationally defined term, with the fraction that will pass through a filter with a pore size of 0.4 or 0.2 µm usually considered to be dissolved. For highly soluble inorganic ions, such as nitrate and ammonium, the distinction is not significant. However, for the less soluble nutrients and for Fe in particular the distinction is important. Recently, the use of ultrafiltration techniques with pore sizes as small as 0.02 µm have shown that a significant proportion of "dissolved" Fe is actually in a colloidal form (Wu et al., 2001).

A wide range of approaches have been used to estimate Fe solubility (see Chapter 1), and these have produced a correspondingly wide variety of results. Calculations based on estimates of oceanic iron inventories relative to atmospheric dust inputs lead to estimates of global average fractional Fe solubility (that is, the fraction of Fe in the particle that dissolves) of about 1 – 2 % (Baker and Croot, 2010), while small scale laboratory and ship-board experiments have generated a much wider range of values, due to variations in the methodologies and differences in the sources and chemical and mineralogical characteristics of the dust. Although there is some overlap, small-scale experiments generally fall into the category of those which seek to understand the many processes occurring once the dust is suspended in the water column, and those which focus on the properties of the dust and how these relate to the relative solubility of the dust. The former category typically involves adding dust to bottles of seawater under varying conditions and monitoring the release of Fe and/or other nutrients over timescales of hours to days (e.g. Bonnet and Guieu, 2004), while the latter category of experiments involve exposing a dust sample to an extraction solution for a predetermined length of time and measuring the Fe extracted. The ultrapure water leaching technique employed in this study falls firmly into this second category of experiments.

6.2.2 Choice of dissolution medium

Due to the complex nature of the physical and chemical processes that occur during dust transport and deposition, there is no obvious choice of media solution that is suitable for all situations. Consequently, a variety of dissolution media have been used in solubility experiments, each with their own set of advantages and limitations (Canepari et al., 2010).

Natural seawater is an obvious choice for those interested in the solubility of dust in the ocean. It is the most environmentally relevant medium, particularly when considering the direct deposition of particles to the ocean by dry deposition. Seawater is often used to investigate the role of iron-binding ligands in dissolution processes (e.g. Wu et al., 2007; Aguilar-Islas et al., 2010). Organic metal binding ligands present in seawater are known to have a strong influence on the maximum solubility and rate of dust dissolution (e.g. Wagener et al., 2008; Baker and Croot, 2010) yet relatively little is known about composition of this organic material. There are two principal limitations with the use of natural seawater. Firstly, variability in its composition, particularly the dissolved organic fraction, creates an additional variable to consider when interpreting data and makes comparison between experiments challenging. For this reason, more reproducible dissolution media are typically used when the properties of the dust are of more interest than processes occurring in the water column. Secondly, the high ionic strength of seawater can create analytical difficulties. For example, seawater samples cannot be measured on an ICP-MS without first removing the sea-salt matrix using a chelating column, with isotope dilution techniques are often required where the extraction efficiencies of the chelating material are less than 100% (e.g. Barriada et al., 2007).

Table 6.1 Summary of leachable atmospheric concentrations (nmol.m^{-3}) of selected species as determined with ultrapure water leaches on samples collected at the CVAO between 2 July 2007 and 11 July 2008 and during a research cruise D326 aboard RRS Discovery from 8 January to 4 February 2008. Corrections for marine SO_4^{2-} (used to calculate Non-sea-salt sulphate - nssSO_4^{2-}) have been derived using soluble Na concentrations and seawater ratios from Millero and Sohn (1992). Ga was not measured for the samples from D326.

Element		CVAO July 2007 – July 2008					RRS Discovery (D326) - January 2008				
		Min	Max	Geometric mean	Arithmetic mean	Standard deviation	Min	Max	Geometric mean	Arithmetic mean	Standard deviation
Na	**(µmol/m^3)**	0.01	0.63	0.16	0.18	0.08	0.03	0.37	0.13	0.16	0.09
Mg	**(nmol/m^3)**	0.70	68	19	21	8.4	3.4	48	20	24	12
Al	**(nmol/m^3)**	0.02	8.6	0.80	1.5	1.4	< 0.04	48	7.2	18	15
K	**(nmol/m^3)**	2.1	9.2	3.9	4.1	1.4	0.36	16	5.9	7.6	4.1
Ca	**(nmol/m^3)**	1.0	78	13	18	15	1.0	76	17	29	23
Sc	**(pmol/m^3)**	< 0.2	1.2	0.11	0.21	0.23	< 0.7	5.8	1.1	2.3	1.9
Ti	**(pmol/m^3)**	< 3.9	176	8.1	17	22	< 16	144	42	59	40
V	**(pmol/m^3)**	0.73	46	13	15	8.7	< 0.9	55	14	20	12
Cr	**(pmol/m^3)**	< 0.2	5.4	1.3	1.5	0.90	< 0.9	26	5.4	9.5	8.1
Mn	**(pmol/m^3)**	0.75	510	47	83	83	1.7	964	112	351	328
Fe	**(pmol/m^3)**	0.003	3.5	0.27	0.50	0.49	< 0.01	16	2.3	5.5	4.7
Co	**(pmol/m^3)**	0.03	3.7	0.64	0.88	0.62	< 0.1	12	1.8	4.6	4.1
Ni	**(pmol/m^3)**	0.54	21	5.4	6.6	4.0	< 0.8	29	7.5	11	6.9
Cu	**(pmol/m^3)**	< 0.4	14	1.4	1.9	1.8	< 1.6	18	4.7	6.6	4.9
Zn	**(pmol/m^3)**	3.2	1114	42	71	123	< 6.8	64	31	35	16
Ga	**(pmol/m^3)**	< 0.04	9.7	1.4	2.2	1.9	n/a	n/a	n/a	n/a	n/a
Rb	**(pmol/m^3)**	0.12	6.2	1.4	1.7	1.0	< 0.25	18	3.6	6.9	5.9
Sr	**(pmol/m^3)**	3.9	333	55	68	51	6.2	441	79	121	97
Y	**(pmol/m^3)**	0.01	2.0	0.25	0.39	0.32	< 0.02	8.7	0.90	3.3	3.2
Nb	**(pmol/m^3)**	< 0.02	0.49	0.02	0.05	0.07	< 0.08	0.94	0.16	0.34	0.28
Cd	**(pmol/m^3)**	0.02	0.44	0.12	0.15	0.09	< 0.04	0.39	0.10	0.13	0.09

Element		CVAO July 2007 – July 2008					RRS Discovery (D326) - January 2008				
		Min	Max	Geometric mean	Arithmetic mean	Standard deviation	Min	Max	Geometric mean	Arithmetic mean	Standard deviation
Sn	(pmol/m^3)	0.38	5.3	1.0	1.1	0.79	3.0	14	6.5	7.2	3.2
Cs	(pmol/m^3)	< 0.003	0.090	0.018	0.023	0.016	< 0.01	0.58	0.08	0.17	0.16
Ba	(pmol/m^3)	0.15	63	7.8	13	12	< 0.4	205	26	70	64
La	(pmol/m^3)	0.01	1.3	0.20	0.30	0.24	0.01	7.8	0.69	2.5	2.5
Ce	(pmol/m^3)	0.01	3.6	0.46	0.75	0.64	< 0.02	19	1.5	6.2	6.2
Pr	(pmol/m^3)	< 0.001	0.39	0.051	0.084	0.070	< 0.01	2.1	0.18	0.70	0.70
Nd	(pmol/m^3)	< 0.01	1.6	0.21	0.34	0.29	< 0.03	8.2	0.68	2.8	2.8
Sm	(pmol/m^3)	< 0.004	0.32	0.042	0.072	0.060	< 0.02	1.6	0.23	0.64	0.57
Eu	(pmol/m^3)	< 0.001	0.077	0.010	0.016	0.014	< 0.004	0.39	0.039	0.14	0.14
Gd	(pmol/m^3)	< 0.002	0.27	0.038	0.062	0.051	< 0.01	1.61	0.15	0.61	0.58
Tb	(pmol/m^3)	< 0.0005	0.048	0.0052	0.0083	0.0071	< 0.002	0.20	0.024	0.077	0.071
Dy	(pmol/m^3)	< 0.001	0.19	0.026	0.042	0.034	< 0.003	0.95	0.084	0.35	0.35
Ho	(pmol/m^3)	< 0.0002	0.034	0.0047	0.0074	0.0061	< 0.001	0.17	0.017	0.062	0.062
Er	(pmol/m^3)	< 0.0005	0.095	0.012	0.019	0.016	< 0.002	0.44	0.043	0.17	0.17
Tm	(pmol/m^3)	0.0001	0.011	0.0016	0.0025	0.0022	< 0.001	0.058	0.010	0.023	0.020
Yb	(pmol/m^3)	< 0.0004	0.058	0.0095	0.015	0.012	< 0.002	0.34	0.033	0.13	0.12
Lu	(pmol/m^3)	< 0.0001	0.012	0.0014	0.0021	0.0018	< 0.0005	0.048	0.0063	0.018	0.016
Pb	(pmol/m^3)	0.1	12	1.4	2.2	2.0	0.25	28	2.2	3.9	5.7
Th	(pmol/m^3)	< 0.001	0.092	0.0038	0.0094	0.0133	< 0.003	0.22	0.03	0.07	0.06
U	(pmol/m^3)	< 0.0004	0.098	0.015	0.020	0.015	< 0.002	0.28	0.045	0.11	0.11
NO_3^-	(nmol/m^3)	0.1	69	18	20	9.0	5.7	33	17	18	7.0
PO_4^{3-}	(nmol/m^3)	< 0.02	1.3	0.11	0.18	0.18	< 0.08	1.2	0.24	0.45	0.39
NH_4^+	(nmol/m^3)	0.04	30	6.8	8.9	5.7	0.8	66	4.2	8.7	13
Cl^-	(µmol/m^3)	0.02	1.76	0.19	0.21	0.15	0.03	0.5	0.17	0.21	0.12
$nssSO_4^{2-}$	(nmol/m^3)	1.4	47	18	21	9.9	< 0.2	50	13	16	10.1

pH 4.7 ammonium acetate buffer solution is a popular choice of dissolution media for assessing trace metal solubility, particularly when a reproducible medium is required to compare aerosols with different sources (e.g. Baker et al., 2006b). While the use of chemical buffer solutions as dissolution media raises questions of environmental relevance, a significant advantage is produced by the minimisation of local pH changes brought about by the dissolution of species such as carbonate or sulphate. Dilute acid solutions, such as pH 2 HNO3 (e.g. Trapp et al., 2010) are also widely employed. Proponents argue that such acidic environments are encountered in clouds as acidic species such as nitric and sulphuric acid are dissolved in cloud droplets and that the use of these media therefore represents an upper limit on aerosol solubility. The use of acidic dissolution media also minimises external factors that can influence experimental results, such as buffering, and particle adsorption. However, the use of such low solution pH is likely to overestimate trace metal bio-availability and lead to less selectivity with regards to comparing aerosols with subtly different particle composition (Canepari et al., 2010).

Ultrapure water is another widely used dissolution media (e.g. Buck et al., 2006; Buck et al., 2010) and the one that has been used in this study. Purified water suffers the drawback that it is sensitive to external factors such as local pH changes, adsorption phenomena and metal complex formation. However, experiments using purified water have the significant advantage of simplicity and are relatively easy to reproduce. Purified water is also a comparatively natural medium and, although not directly to the study area for this work is sometimes compared with the process of wet deposition where particles are incorporated into falling rain drops.

For this work we chose to follow the approach taken by William Landing at Florida State University, USA, using a simple ultrapure water leaching protocol (Buck et al., 2006). This technique has the advantage that it is very simple and easily reproducible for a large number of samples. The ultrapure water leaches can also be analysed readily by ICP-MS and other techniques without prior sample processing and enable a broad suite of measurements from the same sample solution that would not be possible with other dissolution media.

6.3 Ultrapure water leaches

Table 6.1 presents summary statistics for the atmospheric concentrations of the various species extracted using the ultrapure water leaching protocol with samples collected at the CVAO between July 2007 and July 2008 and aboard RRS Discovery during cruise D326.

6.3.1 Samples collected at the CVAO

The data for soluble Fe are illustrated in Figure 6.1, together with total atmospheric concentrations of nutrients (NO_3^-, NH_4^+, PO_4^{3-}), calculated by dividing the quantity of analyte measured by the sample air volume. Total Al is included to give an indication of mineral dust inputs. There were numerous spikes in soluble Fe concentrations throughout the 12-month sample collection period, the majority of which coincided with dust events (peaks in total Al) of varying size. There did not, however, appear to be a strong relationship between the magnitude of the dust event (total Al concentration) and the concentration of soluble Fe. Despite the strong contrast between the summer and winter months in terms of total Al concentrations, the seasonal change in leachable Fe was much weaker, with some significant peaks in Fe resulting from relatively small dust events, even during the summer months.

Soluble phosphate concentrations in Figure 6.1 closely follow those of soluble Fe (R^2 = 0.81; n = 152), consistent with the two elements sharing a common source. Phosphorus in Saharan dust is predominantly in inorganic minerals such as apatite ($Ca_5(PO_4)_3X$, X = OH/F/Cl) and often associated with iron oxyhydroxides coated on clay minerals and quartz particles (Guieu et al., 2002; Singer et al., 2004).

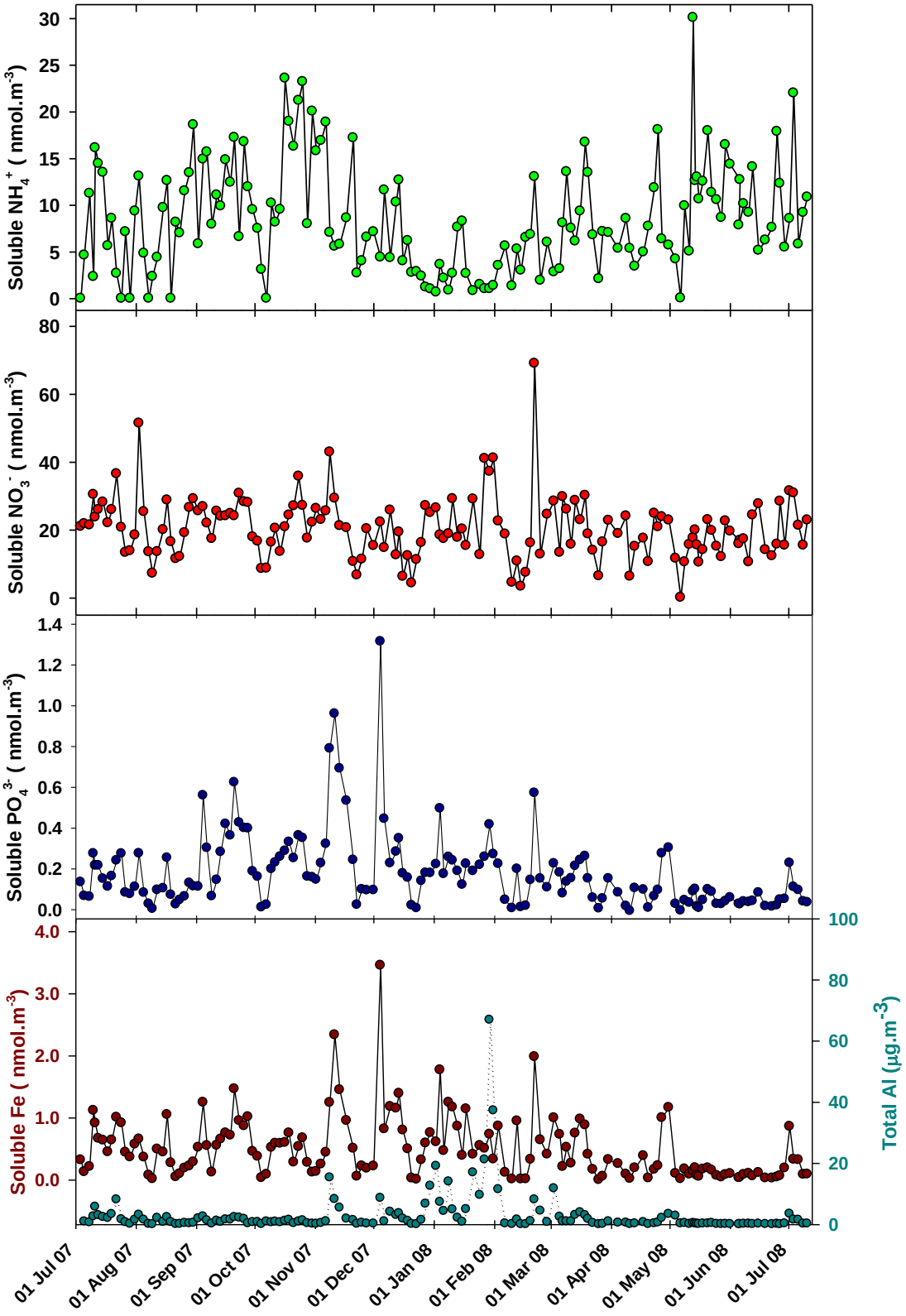

Figure 6.1 Soluble Fe and nutrient concentrations (as determined by ultrapure water leaches) between 2 July 2007 and 11 July 2008 at the CVAO. Total Al concentrations (determined by total acid digestion) are also shown to give an indication of dust inputs.

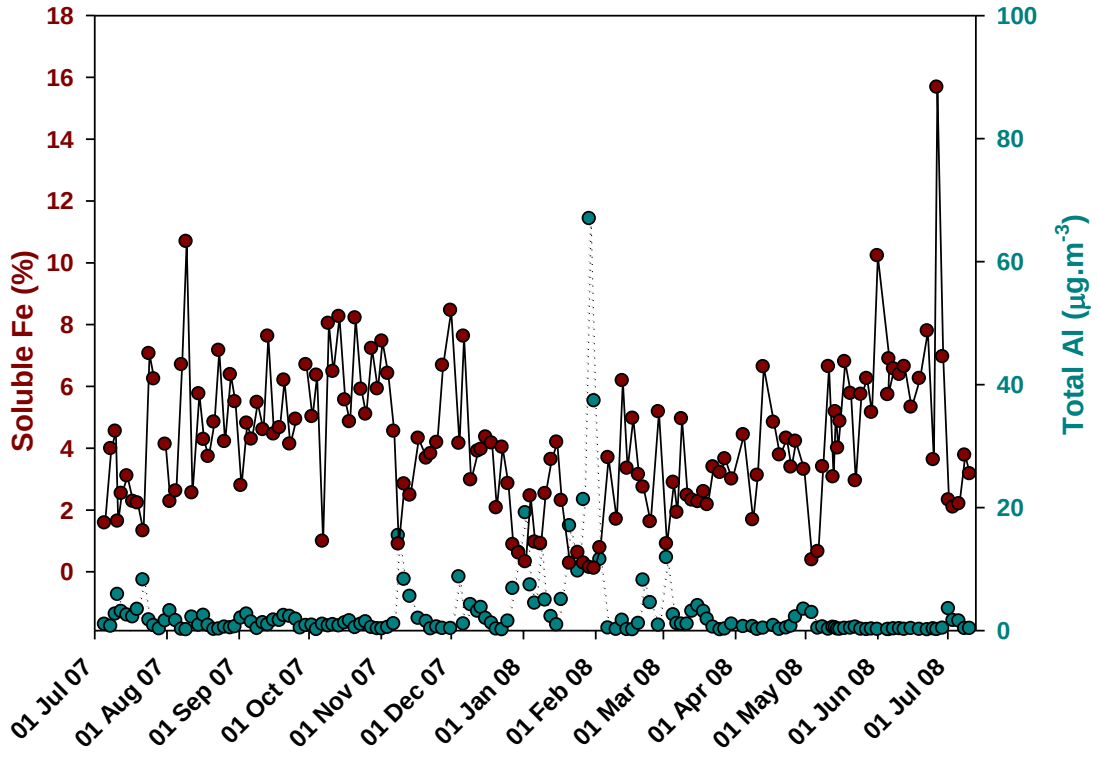

Figure 6.2 Fractional solubility of aerosol Fe (as determined by ultrapure water leaches) between 2 July 2007 and 11 July 2008 at the CVAO. Total Al concentrations (determined by total acid digestion) are shown in cyan.

Soluble inorganic nitrogen species (NO_3^- and NH_4^+) do not show a correlation with Fe or P (R^2 = 0.19, n = 154 for NO_3^- vs Fe; R^2 = 0.004, n = 148 for NH_4^+). Nitrate showed no overall seasonal pattern, with atmospheric concentrations typically ranging from 5 to 30 nmol/m^3, while ammonium concentrations were more variable, with concentrations up to 30 nmol/m^3 but showed a slight decrease in the winter compared with summer.

When leachable Fe is converted into fractional solubilities (the amount of Fe released as a proportion of the concentration determined by total acid digestion), the mean solubility was found to vary from 0.1% to 16%, with a mean value of 4.2% (Table 6.2). When compared with total Al concentrations obtained during the same period, an inverse relationship is perceptible, with peaks in Al coinciding with drops in the fractional Fe solubility and the lowest fractional solubility associated with the most intense dust event in late January 2008 (see Figure 6.2).

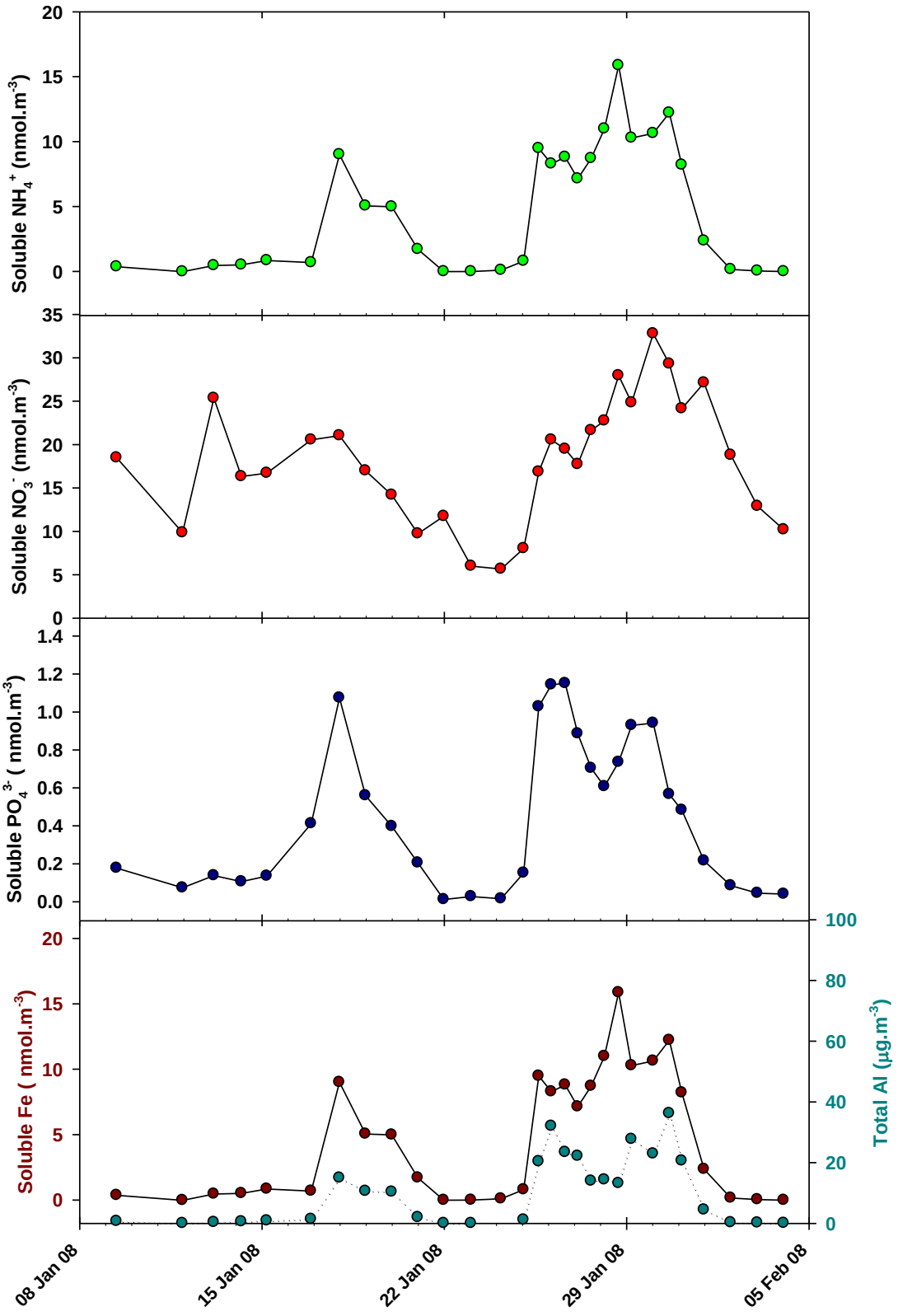

Figure 6.3 Soluble Fe and nutrient concentrations (as determined by ultrapure water leaches) during cruise D326. Total Al concentrations (determined by total acid digestion) are shown in cyan.

6.3.2 Samples collected during D326

Summary statistics for the results from ultrapure water leaches of samples collected during research cruise D326 indicate significantly higher concentrations than observed at the CVAO (Table 6.1) for many species. For example, with Fe and Al the geometric means of the two sets of measurements differed by almost a factor of 10. For leachable Mn and PO_4^{3-} the difference was more modest, with mean D326 concentrations 2 – 3 times those measured on samples from the CVAO, while for inorganic nitrogen and sulphate, the two sets of measurements were broadly comparable.

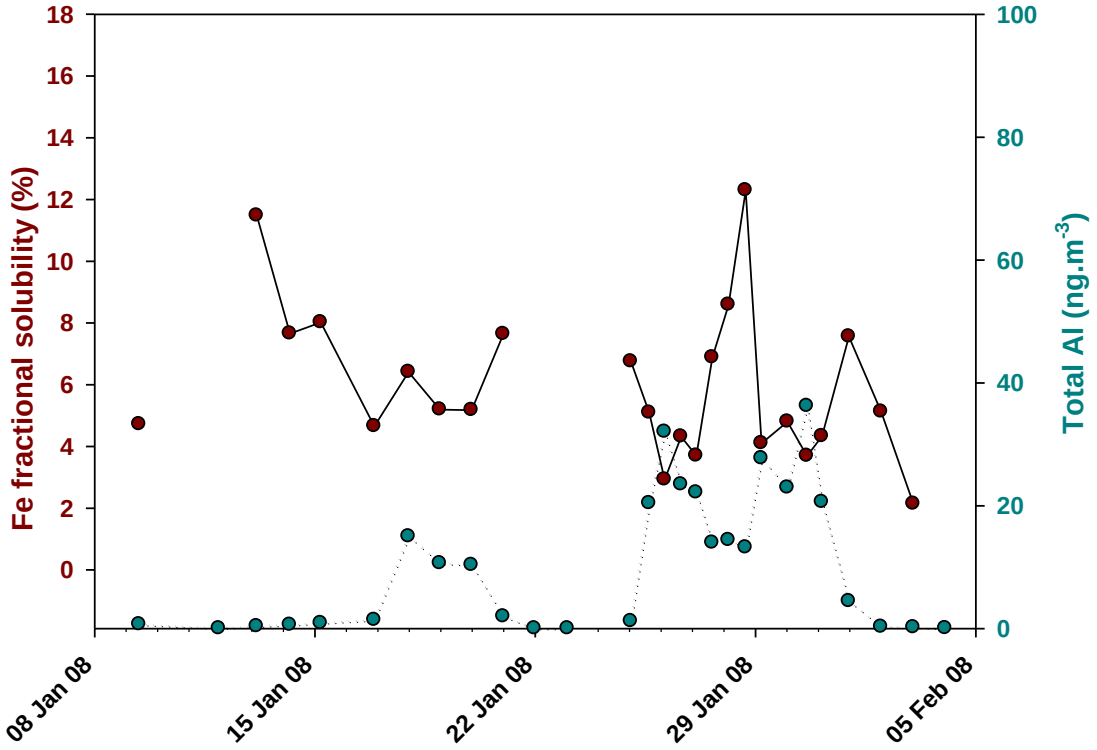

Figure 6.4 Fractional solubility of aerosol Fe in ultrapure water leaches of samples collected during cruise D326. Total Al concentrations (determined by total acid digestion) are shown in cyan.

Soluble Fe, PO_4^{3-}, NO_3^- and NH_4^+ concentrations, together with total Al measured from dust collected during D326 are plotted in Figure 6.3. Leached concentrations for all four species showed a similar pattern to total Al concentrations. For Fe, the

same inverse relationship between the fraction of total Fe released and total Al concentrations observed in the CVAO dataset, was also apparent in the D326 data (Figure 6.4). While significantly higher leachable Fe concentrations were measured for the D326 samples than at any point during the CVAO dataset, the overall fractional solubilities for the two datasets are broadly comparable, owing to significantly lower mean dust concentrations during the course of one year at the CVAO in comparison with observed dust concentrations during the cruise. Nonetheless, significantly higher fractional solubility was measured for the D326 samples, than for samples collected at the CVAO during the same period. Possible explanations for this discrepancy will be discussed in sections 6.4 and 6.5.

6.3.3 Relative solubility of different metals

Mean fractional solubility values for the 42 elements analysed by ICP-MS analysis are shown in Table 6.2, including values for both CVAO and D326 samples and listed in order of decreasing solubility of the CVAO samples. Comparing mean solubility values for D326 and the CVAO, values are similar for both sets of measurements and the order of solubility of elements for D326 is not significantly different to that for the CVAO samples.

To a first approximation, the order of solubility in the table appears to follow the intrinsic chemical properties of the elements, with very insoluble elements such as Ti and Th demonstrating the lowest solubility values, with Fe and Al also fairly insoluble near the bottom of the table. The REE, which share almost identical chemical properties, are all together with mean solubility varying from about 8% to 14%. Above the REE are most of the transition elements, and most soluble of all are the alkaline earth and alkaline metals. There also seems to be a relationship between aerosol source, as identified from principal component analysis (see Section 6.3.5), and relative solubility. Elements associated with anthropogenic activity (Zn, Pb, V, Ni and Cu) show relatively high solubility, with most more soluble than other transition elements in the table (e.g. Co, Rb, Y and Ga). Elements with a significant sea-salt source (Na and Mg) are among the most soluble elements in the table.

Table 6.2 Fractional solubility of 42 elements determined by ICP-MS in aerosols collected at the CVAO between 2 July 2007 and 11 July 2008 and collected aboard RRS Discovery during cruise D326. Elements are listed in order of decreasing mean solubility measured in the CVAO samples.

	CVAO			D236		
	Mean	Min	Max	**Mean**	Min	Max
Na_{sol} (%)	**75.92**	2.63	99.65	**61.12**	32.28	90.78
Ca_{sol} (%)	**66.24**	11.64	99.72	**46.60**	21.94	85.94
Sr_{sol} (%)	**61.00**	9.24	98.94	**43.24**	16.02	88.68
Mg_{sol} (%)	**59.61**	2.42	99.27	**37.91**	10.02	83.55
Cd_{sol} (%)	**57.03**	1.06	97.50	**44.51**	3.81	99.02
K_{sol} (%)	**38.40**	3.37	97.45	**26.05**	5.76	64.93
Zn_{sol} (%)	**47.21**	0.77	98.42	**33.20**	6.87	98.66
Sn_{sol} (%)	**40.95**	4.93	89.80	**40.91**	29.84	51.67
Mn_{sol} (%)	**41.17**	2.57	99.28	**35.25**	13.08	98.07
Pb_{sol} (%)	**32.91**	0.29	96.53	**28.01**	5.31	89.91
Ni_{sol} (%)	**32.25**	0.62	86.63	**25.34**	6.45	68.66
V_{sol} (%)	**31.64**	0.58	94.05	**18.36**	3.51	63.72
Ba_{sol} (%)	**22.93**	1.77	93.59	**20.04**	8.35	50.88
Co_{sol} (%)	**22.29**	0.65	90.09	**20.43**	7.14	55.20
Rb_{sol} (%)	**20.32**	0.51	73.60	**18.99**	3.98	96.32
Cu_{sol} (%)	**19.02**	0.73	80.20	**18.70**	5.78	52.07
Y_{sol} (%)	**13.68**	0.36	55.43	**12.14**	4.79	33.03
Ga_{sol} (%)	**18.60**	4.71	95.20	**-**	-	-
U_{sol} (%)	**16.11**	0.89	77.73	**16.22**	5.63	55.93
Eu_{sol} (%)	**13.79**	0.49	86.79	**13.69**	6.14	29.66
Sm_{sol} (%)	**12.89**	0.39	78.21	**11.75**	5.33	28.88
Dy_{sol} (%)	**12.17**	0.38	66.99	**12.30**	2.99	34.02
Tb_{sol} (%)	**12.01**	0.38	70.97	**11.81**	5.26	30.44
Ho_{sol} (%)	**11.80**	0.34	60.92	**13.47**	4.60	56.86
Gd_{sol} (%)	**11.66**	0.39	65.81	**12.21**	1.88	27.87
Nd_{sol} (%)	**11.36**	0.32	56.90	**11.69**	4.66	40.11
Er_{sol} (%)	**10.54**	0.33	51.08	**12.21**	4.57	38.19
Pr_{sol} (%)	**10.17**	0.32	52.95	**10.68**	4.21	22.71
Ce_{sol} (%)	**9.91**	0.30	53.78	**10.56**	4.32	25.69
Tm_{sol} (%)	**9.77**	0.31	50.98	**8.38**	4.12	24.27
Yb_{sol} (%)	**9.22**	0.26	48.10	**12.55**	4.96	84.16
Lu_{sol} (%)	**9.09**	0.25	53.41	**9.57**	3.33	38.30
La_{sol} (%)	**8.66**	0.24	43.34	**10.41**	3.65	42.42
Cs_{sol} (%)	**7.77**	0.11	33.69	**8.53**	2.57	23.10
Ag_{sol} (%)	**6.39**	0.01	32.19	**2.06**	1.33	2.78
Sc_{sol} (%)	**4.82**	0.03	80.28	**7.48**	2.88	27.97
Fe_{sol} (%)	**4.18**	0.09	15.66	**5.97**	2.14	12.29
Al_{sol} (%)	**3.68**	0.11	21.93	**4.85**	2.14	10.04
Cr_{sol} (%)	**3.30**	0.13	11.80	**6.43**	2.15	26.78
Nb_{sol} (%)	**2.25**	0.02	69.10	**1.96**	0.51	6.33
Th_{sol} (%)	**1.40**	0.05	13.73	**1.15**	0.16	2.89
Ti_{sol} (%)	**1.09**	0.02	7.66	**0.70**	0.19	2.02

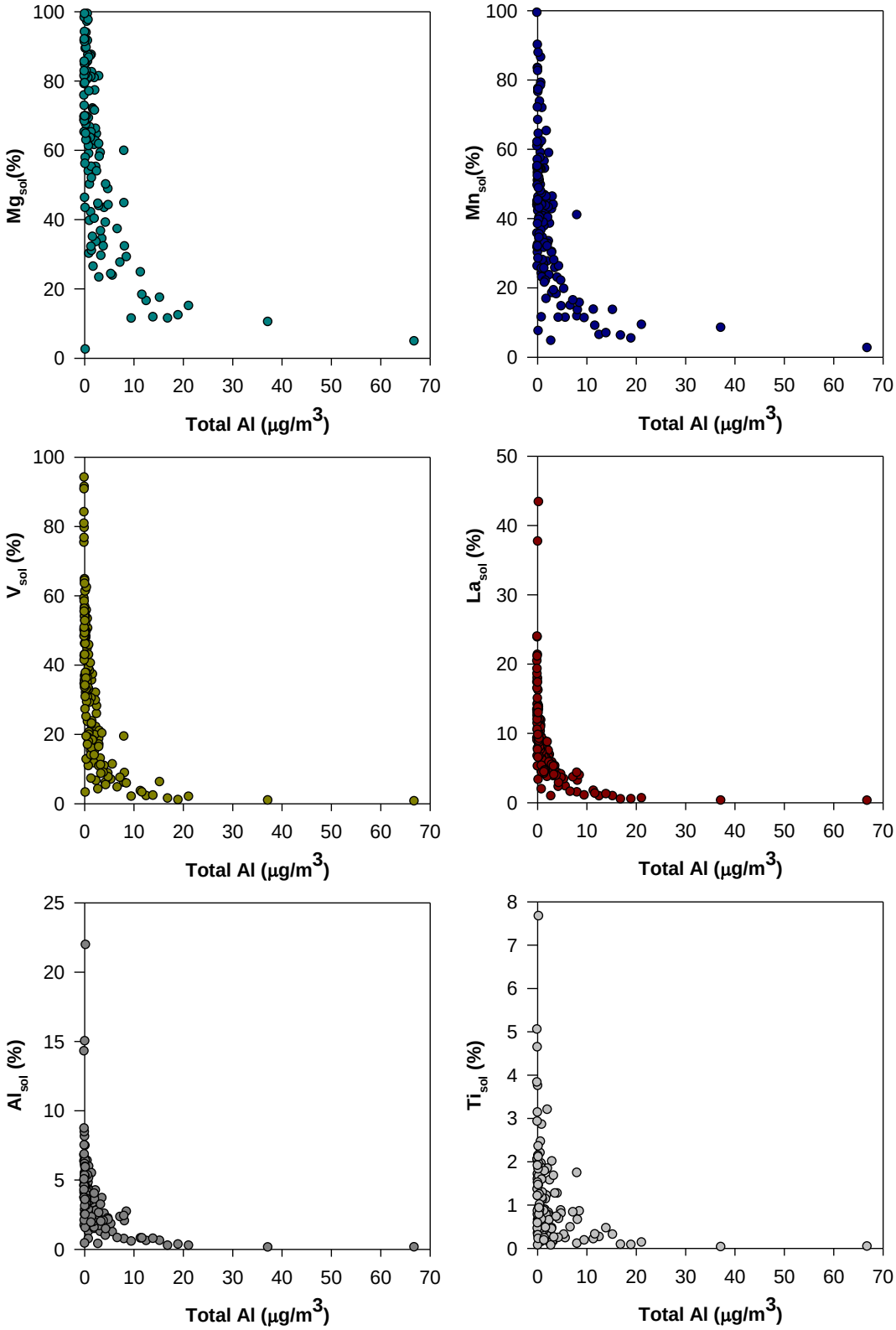

Figure 6.5 Examples of the inverse relationship between particle solubility and total Al concentrations exhibited by all 42 elements in Table 6.2. Examples are shown for elements with predominantly marine (Mg), anthropogenic (V), and crustal sources with varying intrinsic solubility (Mn, La, Al, Ti).

All 42 elements show the inverse relationship between fractional solubility and dust loading that appears to be ubiquitous in aerosol datasets. Figure 6.5 shows representative examples of this relationship for 6 elements with varying sources and mean solubility values. Atmospheric dust loading, therefore, appears to exert a strong influence on aerosol solubility on even some of the most soluble aerosol species.

6.3.4 Relationship of Fe to Al released in leaching experiments

A strong linear relationship between Fe and Al in the ultrapure water leaches seems to be a uniform feature of both samples collected at the CVAO and during the research cruise, D326 (see Figure 6.6). The mean Fe/Al mass ratio of 0.69 (molar ratio of 0.33) obtained for soluble Fe and Al from the regression line in Figure 6.6 is greater than the Fe/Al mass ratio of 0.51 (molar ratio of 0.25) in the bulk aerosol. The soluble Fe/Al ratio is comparable to those found by Buck et al. (2006; 2010) who, using the same aerosol collection and leaching techniques found a molar ratio of 0.26 in aerosols collected over the Atlantic Ocean (Buck et al., 2010) and 0.3 in aerosols collected over the Pacific Ocean (Buck et al., 2006).

The uniformity of these results and the difference between the Fe/Al ratio in the ultrapure water leaches and the bulk aerosol suggests that the dissolution process is dominated by one or more aluminosilicate mineral(s). The enrichment of Fe relative to Al in the ultrapure water leach solutions also indicates that Al may be associated more with refractory mineral phases than Fe.

.

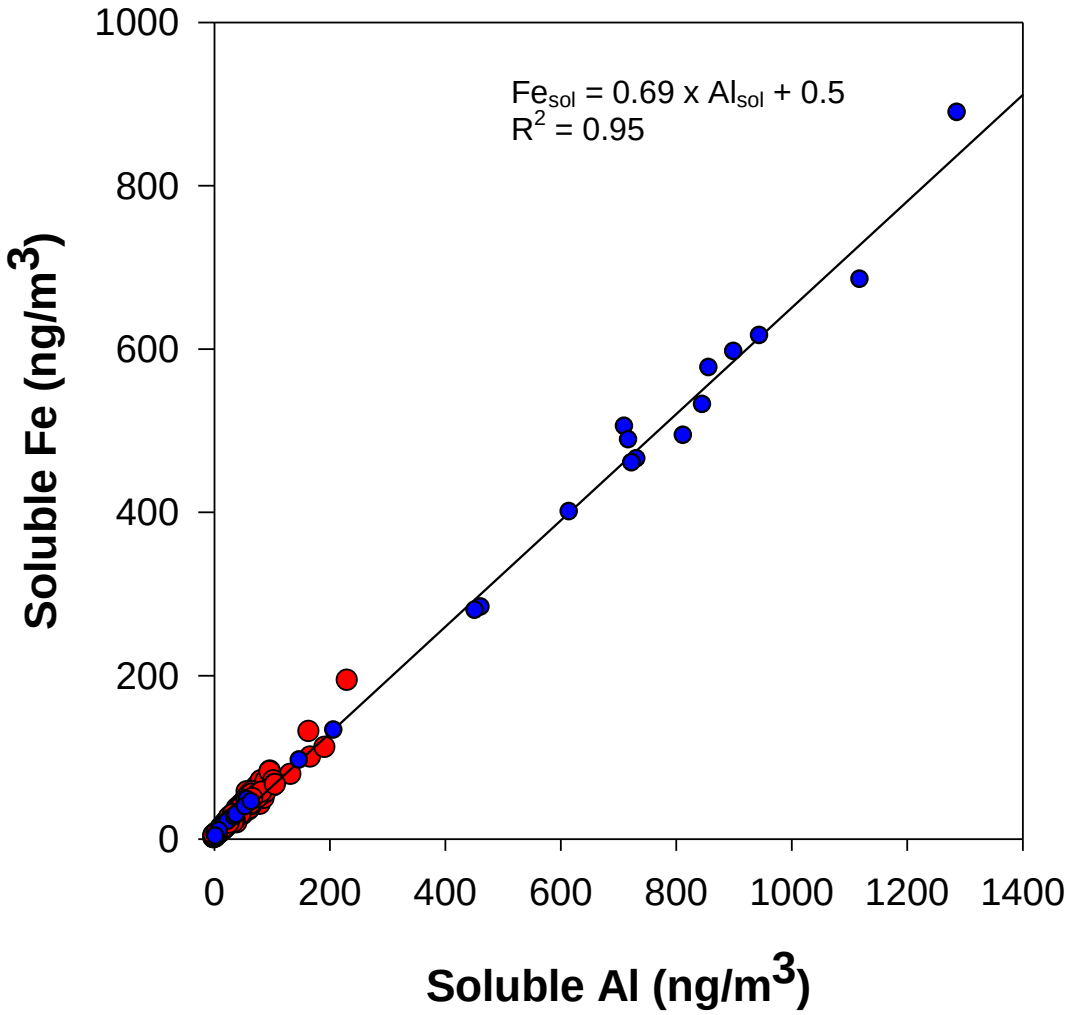

Figure 6.6 Relationship between soluble Fe and Al concentrations in ultrapure water leaches of samples collected during cruise D326 (blue circles) and at the CVAO between July 2007 and July 2008 (red circles).

6.3.5 Principal component analysis

A principal component analysis (PCA) was performed in order to explore in more detail the relationships between the various species determined in the ultrapure water leaches. A log transform was applied to the atmospheric concentrations so that the dataset was close to normally distributed. K, Ga, Ag, Cd and Sn were excluded from the analysis due to either a large number of missing values or a large number of values at or close to the detection limit.

From the PCA analysis, three components were extracted which accounted for a total of 84.2% of the variance in the dataset. The rotated principal component matrix is shown in Table 6.3 and shows that the three components have distinct crustal, anthropogenic and marine signatures. Component 1 is clearly correlated with elements characteristic of crustal rocks such as Al, Fe and Si. Included in this group are most transition elements, lanthanides and actinides and phosphate.

The second component correlates well with species often associated with human activities, including the transition elements V, Ni, Cu and Zn in addition to Pb, sulphate and ammonium. Component 3 corresponds well with the major constituents of seawater, showing high correlations with Na, Mg and Cl. Weaker correlations with minor components of seawater, Ca and Sr, which are more strongly correlated with Component 1 reflects the dual source of these elements. It is noteworthy that nitrate concentrations are associated with this third component. Atmospheric nitrate is predominantly anthropogenic in origin, derived from NO_x compounds, which are the product of the high temperature oxidation of nitrogen gas inside combustion engines and also from other industrial activities (Duce et al., 2008). NOx are subsequently oxidised in the atmosphere to HNO_3, which when mixed with marine air masses reacts with coarse mode sea-salt aerosols (Spokes et al., 2000; Baker and Croot, 2010). Consequently, this accounts for the observed correlation of nitrate with sea-salt in the principal component analysis.

Table 6.3 Varimax rotated principal component matrix for 43 species measured in ultrapure water leaches of dust samples collected at the CVAO. Each element is highlighted according to the main component with which it is correlated.

	Component		
	1 – Crustal	2 – Pollution	3 - Marine
Variance	62.0%	11.8%	10.3%
Na	-.069	.103	.924
Mg	-.007	.156	.931
Al	.978	.046	-.006
Ca	.754	-.166	.528
Sc	.675	-.242	-.163
Ti	.886	-.052	-.046
V	.107	.886	.233
Cr	.850	.301	.044
Mn	.911	-.070	.267
Fe	.954	.128	.012
Co	.863	.289	.246
Ni	.120	.897	.246
Cu	.199	.722	.172
Zn	-.249	.656	-.044
Rb	.900	-.001	.282
Sr	.674	-.247	.610
Y	.982	.024	.071
Nb	.751	-.120	-.117
Cs	.759	.372	-.044
Ba	.921	-.160	.196
La	.978	.092	.087
Ce	.983	.007	.062
Pr	.977	.073	.095
Nd	.975	.048	.096
Sm	.972	.055	.089
Eu	.973	.002	.080
Gd	.973	.040	.088
Tb	.974	.055	.081
Dy	.974	.061	.095
Ho	.977	.059	.073
Er	.962	.063	.095
Tm	.956	.025	.041
Yb	.963	.099	.055
Lu	.935	.025	-.042
Pb	.070	.788	-.196
Th	.726	-.287	-.129
U	.938	-.020	.162
Cl^-	-.099	-.029	.876
$nssSO_4^{2-}$	.384	.541	.449
NO_3^-	.362	.381	.676
$Si(OH)_4$	.860	-.116	.093
PO_4^{3-}	.809	.271	.077
NH_4^+	-.319	.842	-.080

6.4 Analytical aspects of the ultrapure water leach procedure

6.4.1 Proportion of labile metals and nutrients released

To determine the efficiency of the applied 100 ml ultrapure water leaching protocol, several samples were leached more than once. The proportion of selected metals and nutrients released by three successive 100 ml ultrapure water for ten individual samples is shown in Figure 6.7. Of the metals, Fe and Al, both with approximately 35 – 75% released by the first 100 ml, are substantially less labile than Mn, for which about 50 – 95% is released. For the other species in Figure 6.7, PO_4^{3-} shows a very similar pattern to Fe and Al, with ~ 35 – 75% released. NH_4^+ and SO_4^{2-} are highly soluble, with one 100 ml aliquot being sufficient to extract the readily soluble species (for several samples NH_4^+ concentrations are approaching the detection limit of 0.2 µM, which results in the efficiency of the leach appearing to be low for these samples). NO_3^- also appears highly soluble and with the exception of two samples, shows the first 100 ml to be efficient at leaching all the nitrate present.

The release of Fe after a single 100 ml leach measured here is lower than the 95% Fe release that has been reported by Buck et al. (2006). The reasons for this are not fully clear. Buck et al. did not describe the amount of dust present on the filter(s) that were used to determine the 95% Fe release value. However, broadly similar total Fe concentrations to this work were reported, and therefore the amount of dust on individual filters should be comparable. One possible explanation is that Buck et al. measured their samples within 7 days following sampling, whereas it was necessary to store our samples frozen for several months prior to analysis. During this time, it is possible that more soluble forms of Fe could have undergone transformation into more thermodynamically stable and less soluble forms. There are suggestions that storage of samples for several months unfrozen results in a large drop in soluble Fe (Buck et al., 2006). However a comprehensive study of Fe solubility and speciation variation with varying storage protocols is needed to properly assess this issue.

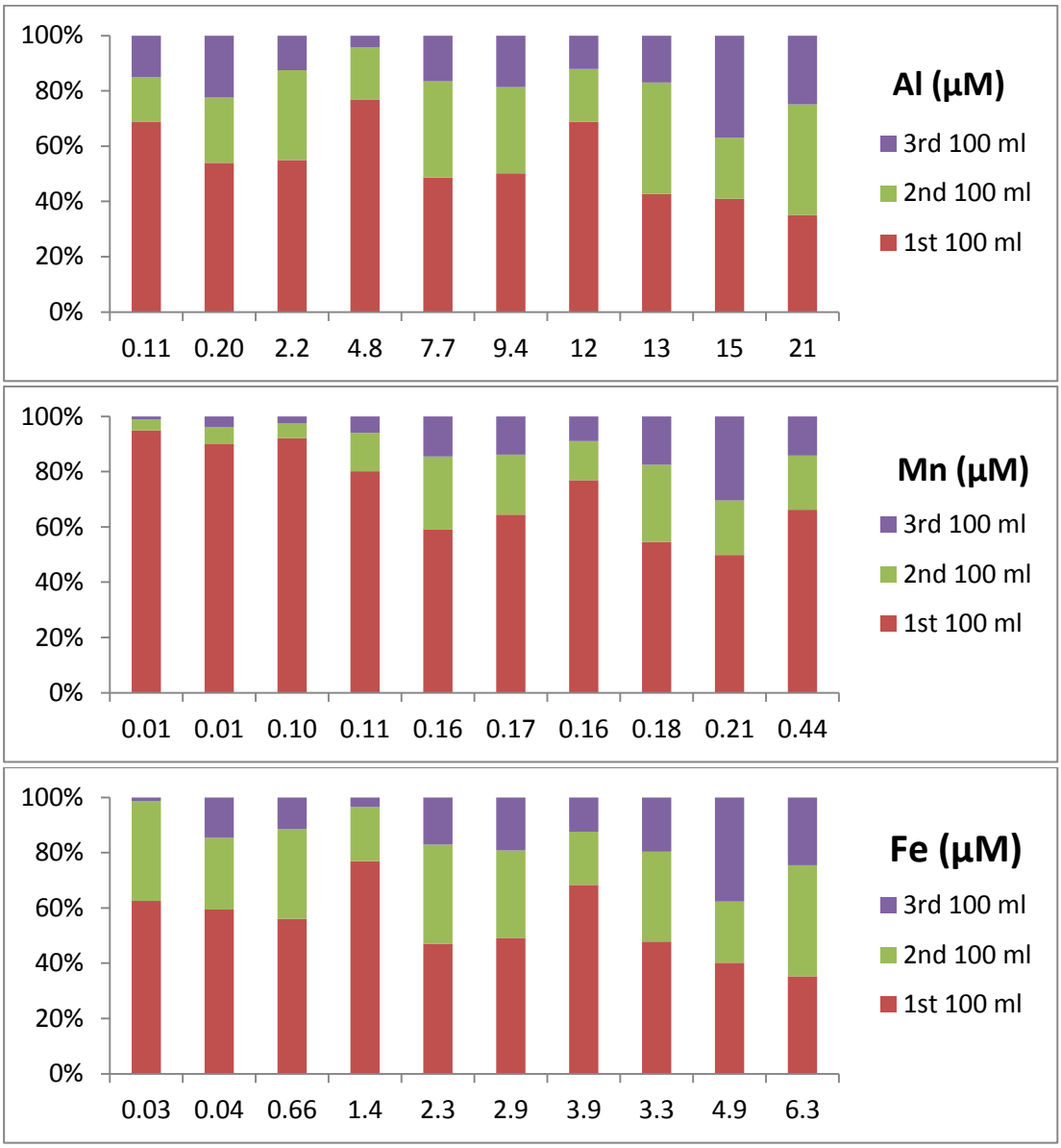

Figure 6.7 Quantity of selected metals and nutrients released into solution after the first and second 100 ml leaches (shown as a percentage of the cumulative total for 3 x 100 ml leaches). Ten filters were each leached three times using the ultrapure water leaching protocol. For all analytes, the ten samples are ordered from left to right in order of increasing concentration of Al leached. The total concentration leached is indicated by the value under each bar.

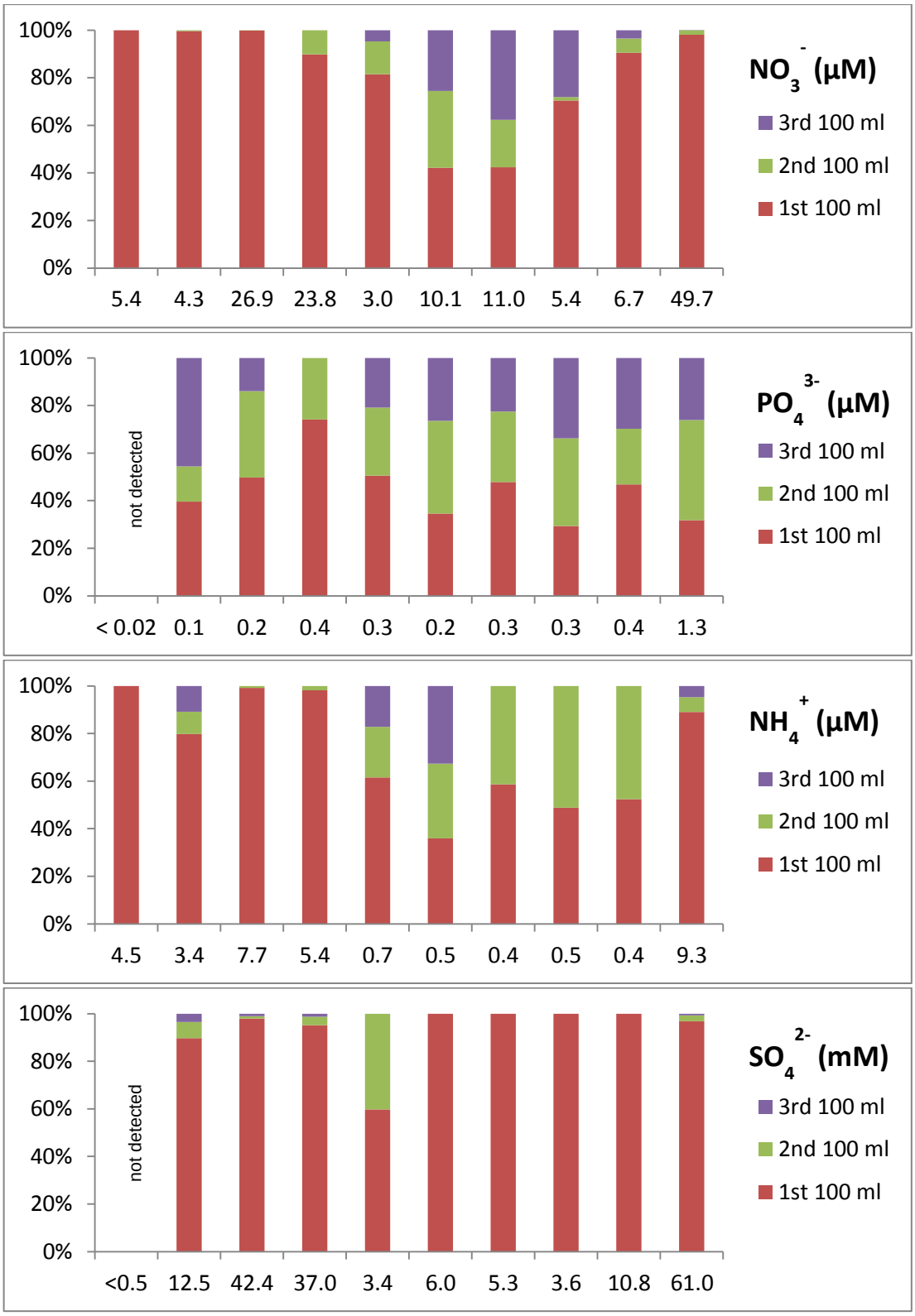

Figure 6.7 Continued

6.4.2 pH variation in leach solution

One potential limitation with using deionised water as a dissolution medium is that the extractable fraction of elements can be affected by spontaneous pH changes produced by the dissolution of the aerosol (Canepari et al., 2010). Since $CaCO_3$ is a fairly strong base and can make up a significant component of mineral dust from the Sahara, the possible influence of $CaCO_3$ dissolution on the release of Fe was investigated. Soluble nssCa (non-sea-salt Ca) concentrations were corrected for the marine component by using soluble Na concentrations and a Na/Ca seawater ratio taken from Millero and Sohn (1992). Theoretical solution pH values for the extract solutions were then calculated using the software package Visual MINTEQ (Jon Petter Gustafsson, KTH, Sweden). It was assumed that the system was in equilibrium with atmospheric CO_2, that all of the dissolved nssCa was the result of $CaCO_3$ dissolution and that $CaCO_3$ was the only component of the dust that might affect the resulting pH of the leach solution. Although simplistic, this approach should enable general conclusions to be drawn about the effect of pH.

Figure 6.8 shows the relationship between the theoretical pH values and the fractional Fe solubility values obtained. Up to about pH 9.5, there is no discernable correlation between pH and the percentage of Fe released in the leach. However, at higher pH values, there does seem to be a marked reduction in the fractional Fe solubility. There is also a marked difference between the samples collected during D326 (blue circles) and samples from the CVAO collected during the same period (green circles), with the D326 samples showing lower pH values and higher fractional Fe solubility than the corresponding samples from CVAO. Consequently, higher quantities of calcite on the filters collected at CVAO may explain, at least in part, the significant differences between the two sets of measurements made at the same time and in relative proximity.

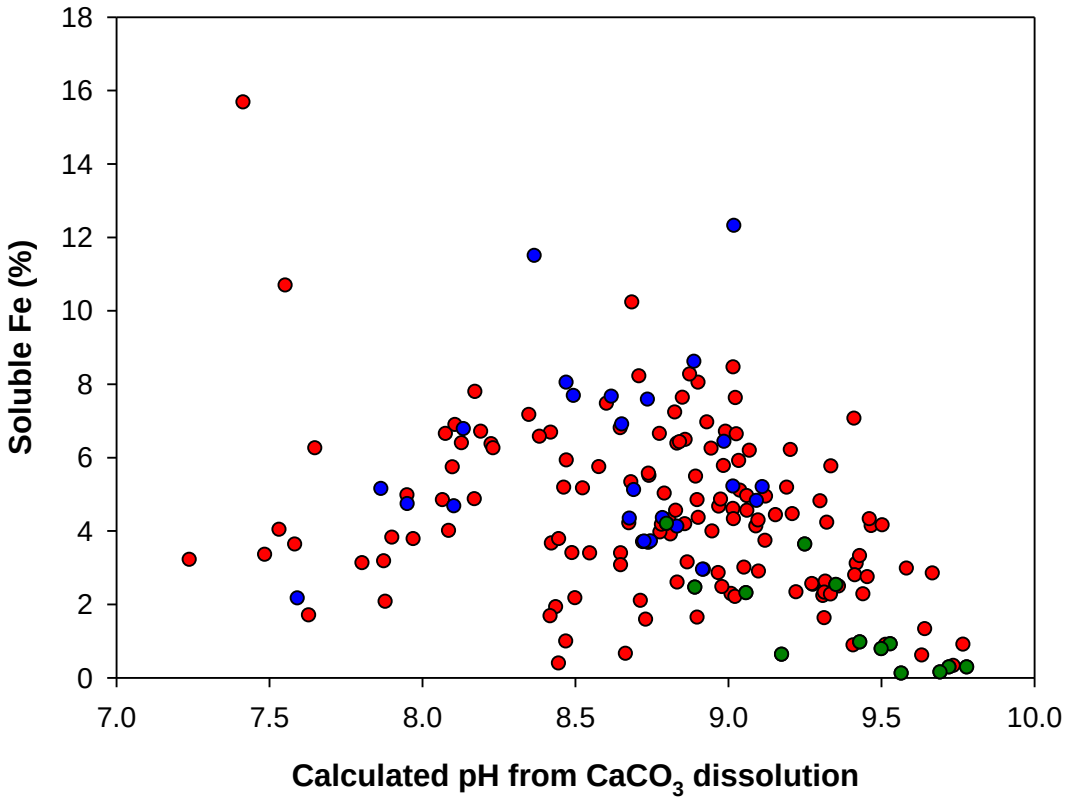

Figure 6.8 Fractional Fe solubility obtained from ultrapure water leaches versus calculated pH based on CaCO3 dissolution. Samples extracts from cruise D326 (blue circles), the CVAO during cruise D326 (January 2008) (green circles) and the CVAO during the rest of the year (July 2007 – July 2008) (red circles).

6.4.3 Comparison with seawater

For 22 filter samples, a seawater leach was carried out using one of the other replicate filters. Filtered (0.2 µm) surface seawater collected during D326 from the subtropical North Atlantic Ocean was used for this purpose. Figure 6.9 shows the observed concentrations of Fe, PO_4^{3-}, NO_3^- and NH_4^+ extracted in seawater with the corresponding values for the samples extracted in ultrapure water. Leachable Fe concentrations were found to be lower using seawater in place of ultrapure water. The seawater and ultrapure water Fe values obtained are significantly correlated (R^2 = 0.68), with Fe concentrations in seawater approximately 30% of the ultrapure water values. This difference was greater than that reported by Buck et al. (2010), who found seawater concentrations were about 85% of ultrapure water values.

Differences in NO_3^- and NH_4^+ between seawater and pure water leaches were smaller, with seawater concentrations around 85% (NO_3^-) and 73% (NH_4^+) of the values in ultrapure water, albeit with considerable scatter. For PO_4^{3-} the correlation between the results from seawater leaches with those from pure water leaches was weaker (R^2 = 0.47), but the overall trend indicated that seawater concentrations were only ~ 17% of the measurements made using ultrapure water as the extraction solution.

Some of the differences may have arisen from imbalances in air-flow between the two replicate filters durin aerosol sampling, but this does not account for the much greater solubility of PO_4^{3-} and Fe in pure water relative to seawater. In these cases it seems likely that the higher pH of seawater results in a less efficient extraction of P and Fe from the mineral components of the dust.

An alternative explanation for the differences in Fe dissolution is a difference in the iron binding capacity of the seawater used for the experiments. Freshly filtered surface seawater was used for the experiments described by Buck et al. (2006), whereas the water used in our experiments had been stored for several months prior to use. Fe binding ligands may degrade with time, resulting in lower Fe solubility in our experiments compared with those described by Buck et al. (2006). However, it takes only a few seconds for the extraction solution to pass through the dust-impregnated filter and it seems unlikely that significant equilibration of free Fe with organic Fe complexing ligands could occur with sufficient speed to enhance the amount of Fe released into solution.

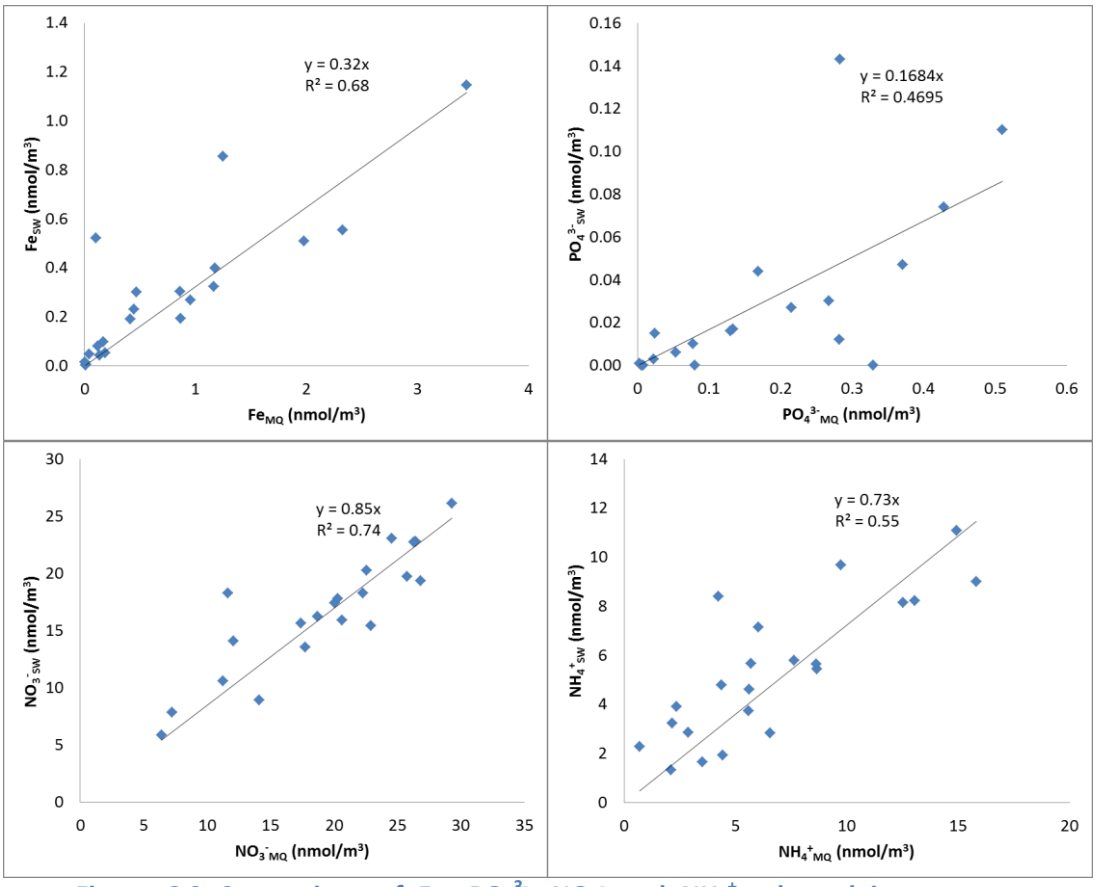

Figure 6.9 Comparison of Fe, PO_4^{3-}, NO_3^- and NH_4^+ released in seawater leaching experiments with Fe released using ultrapure water (n = 22; all concentrations in units of nmol analyte per m^3 of air sampled).

6.5 Factors controlling release of Fe

Various factors have been suggested to explain the large variations in fractional solubility of aerosol Fe that have been reported by workers (Baker and Croot, 2010). An important process that has been invoked invloves acid processing of aerosols, in which Fe solubility is enhanced by aerosol particles mixing with atmospheric acid species such as HNO_3 and H_2SO_4 (Spokes and Jickells, 1995). Differences in aerosol particle size distribution is considered to control Fe solubility (Baker and Jickells, 2006), with smaller particles exhibiting a higher surface-area-to-volume ratio and hence a higher Fe solubility. Furhermore, the mixing of anthropogenic aerosols with high intrinsic Fe solubility, with less soluble mineral aerosols may affect the overall solubility of the bulk aerosol mixture (Sholkovitz et al., 2009).

Attempts to link aerosol solubility to acid processing have focussed on investigating correlations between fractional Fe solubility and the concentration of acid species in

aerosols (Hand et al., 2004; Baker et al., 2006a; Baker et al., 2006b). However these studies have failed to find any strong link between these characteristics. Baker and Croot (2010) have highlighted a number of factors which complicate efforts to find a link between solubility and acid processing. First, bulk measurements cannot distinguish whether the aerosols are internally or externally mixed, that is whether or not there is physical contact between the acid species and the Fe-containing aerosol particles. In addition, acid species may be neutralised by $CaCO_3$, and nitric acid can react with NaCl in seasalt, resulting in a loss of HCl to the gas phase. In this way nitrate and sulphate concentrations are not a reliable indicator of aerosol acidity (Baker and Croot, 2010). Indeed, in our data there was no correlation between either soluble $nssSO_4^{2-}$ or NO_3^- concentrations with the fractional Fe solubility.

6.5.1 Dust loading and particle size

The hypothesis that aerosol particle size controls Fe solubility, due to the larger surface-area-to-volume ratio of smaller particles, stems from the observation of an inverse relationship of fractional Fe solubility with total aerosol concentration, which is a feature commonly observed in aerosol datasets (Baker and Jickells, 2006; Sholkovitz et al., 2009; Trapp et al., 2010). However, even with size-resolved measurements it is challenging to unambiguously confirm that particle size is the cause of this relationship, since size distribution is often a function aerosol transport and so other processes related to atmospheric transport are difficult to separate. In particular there is a shift in mineralogy with transport leading to dust becoming relatively enriched in clays relative to quartz (Glaccum and Prospero, 1980).

In our data from the CVAO and cruise D326 the inverse relationship between fractional Fe solubility and total Al (as a proxy for dust loading) is clearly apparent (see Figure 6.10). There is a marked difference between the data from the cruise and the CVAO. From the statistical calculations in section 6.4.2 it appears that the differences between the CVAO data and D326 data from the same period can be explained, at least in part, by local pH changes brought about by carbonate dissolution. It appears from the difference between the CVAO data and D326 data

in Figure 6.10 that atmospheric aerosol concentration alone cannot explain the observed Fe concentrations. Plotting fractional Fe solubility against the total mass of Al on each filter (see Figure 6.11) results in D326 values being much closer to the CVAO. This appears to demonstrate that there is a particle concentration effect with the ultrapure water leaches, with the higher concentrations on some filters resulting in saturation of the leaching solution. This is intertwined with the pH effect discussed in section 6.4.2, since the amount of carbonate on each filter will increase with the quantity of dust.

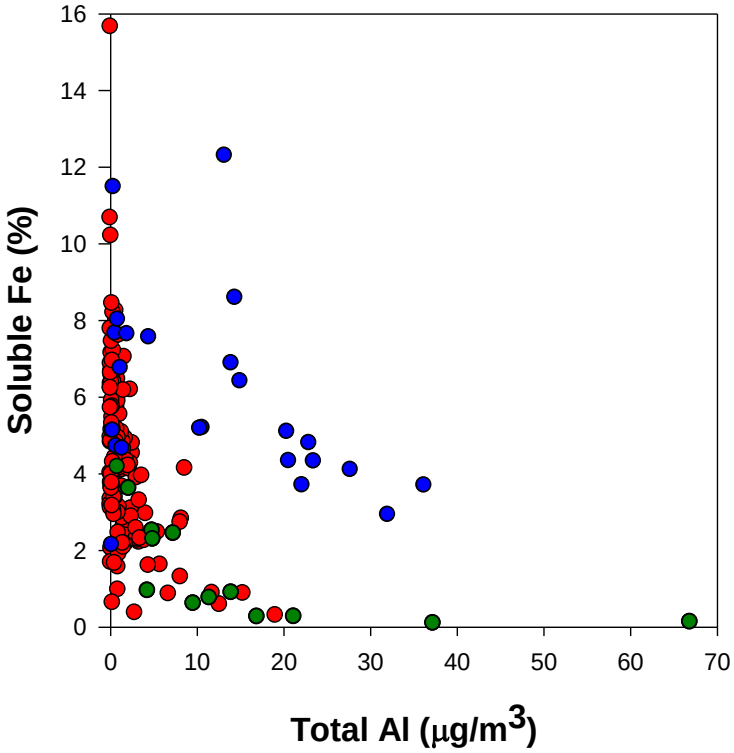

Figure 6.10 Soluble Fe versus total atmospheric Al concentrations in ultrapure water leach extracts. Data are from CVAO July 07 – July 08 (red), D326 (blue) and from the CVAO for samples collected at the same time as the D326 cruise sailed (green).

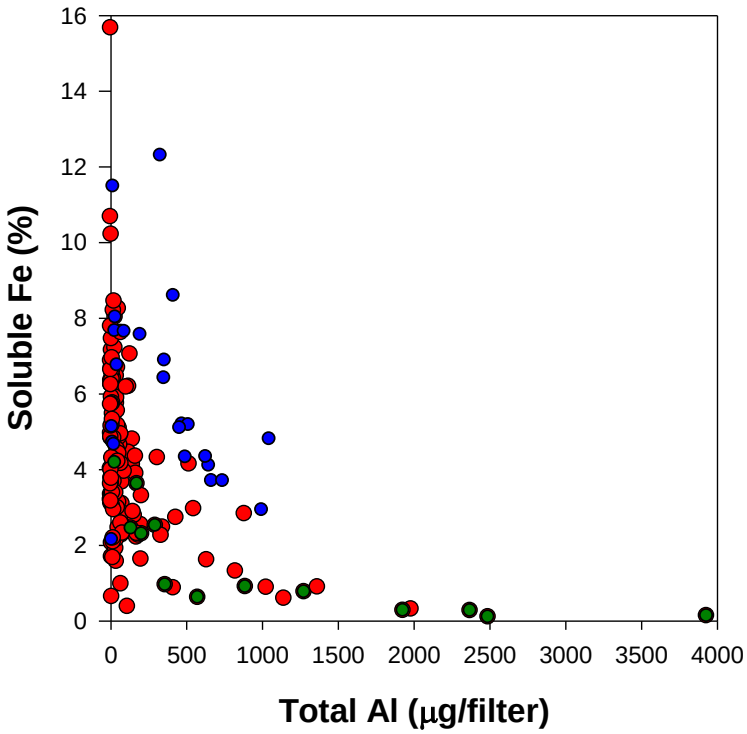

Figure 6.11 Soluble Fe versus quantity of dust on filter (as indicated by Al mass) used in ultrapure water leach extracts. Data are from CVAO July 07 – July 08 (red), D326 (blue) and from CVAO for samples collected at the same time as the D326 cruise sailed (green).

6.5.2 Aerosol Vanadium

Sholkovitz et al. (2009) proposed that the relative proportion of anthropogenic dust (which has a high intrinsic Fe solubility) to mineral dust (with relatively low Fe solubility) in a bulk dust sample is the controlling factor in Fe solubility. Using vanadium concentrations as a tracer of anthropogenic dust inputs they found a predictive relationship between V/Al ratios in the bulk elemental composition of the dust with fractional Fe solubility. With the data generated in this study there is no clear and predictive relationship between V concentrations and fractional Fe solubility (see Figure 6.12). Fe solubility values are in general higher at high V/Al, but high V/Al concentrations tend to occur at very low dust loadings (Al concentrations), hence it is not possible to confirm or rule out the potential role of anthropogenic Fe in controlling Fe dissolution in our samples.

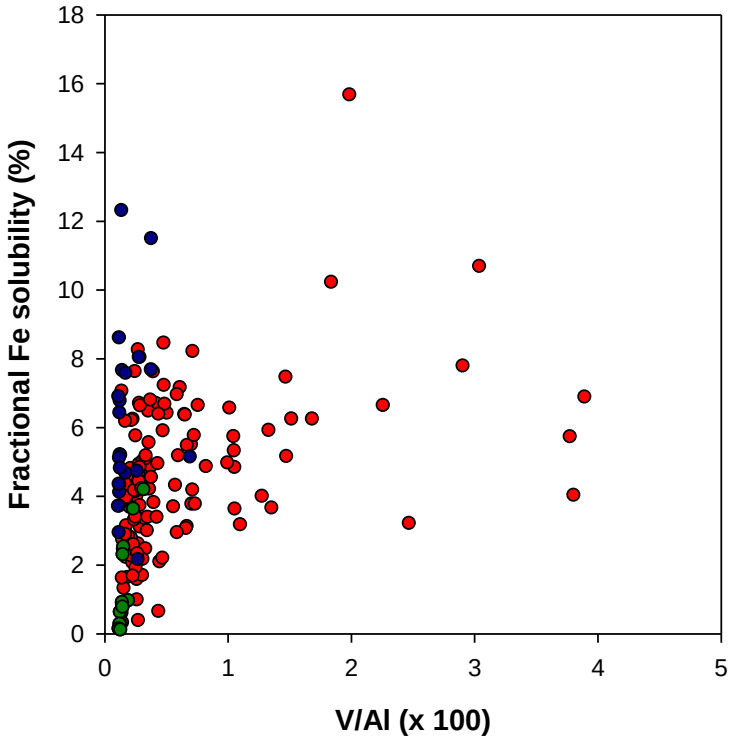

Figure 6.12 Fractional Fe solubility in ultrapure water leach extracts plotted against total V/Al ratio. Data are from CVAO July 07 – July 08 (red), D326 (blue) and from CVAO for samples collected at the same time as the D326 cruise sailed (green).

6.6 Soluble metal and nutrient fluxes

Calculations were made to estimate atmospheric fluxes of soluble nutrients to the ocean in our study region. Deposition occurs by both wet deposition (reaching the ocean by becoming incorporated into rain drops) and dry deposition (direct settling of the particles onto the ocean surface). Measurements and modelling studies indicate that overall, wet deposition may be more important with 30 – 95% of deposition occurring in this way, depending on the location (Hand et al., 2004; Jickells et al., 2005). In this thesis it is not possible to address wet deposition, since rain samples were not collected. However, in our study region the dry air exiting from western Africa results in very little rainfall, so it is likely that dry deposition is the dominant pathway (Baker et al., 2007). Dry deposition fluxes are calculated as the product of the atmospheric concentration (C_A) of the species of interest and its deposition velocity (v_d):

$$\mathrm{F^d = C_A^c v_d^c + C_A^f v_d^f} \qquad (6.1)$$

Values of v_d^c = 0.02 m.s^{-1} for coarse mode aerosols (> 1 µm diameter) and v_c^f = 0.001 m.s^{-1} for fine mode aerosols (< 1 µm diameter) was assumed (Duce et al., 1991). While the uncertainties in these deposition velocities are acknowledged to be large, these values have been widely applied as a first approximation where actual deposition velocities are unknown. Subsequent attempts to constrain deposition velocities have produced similar estimates (Mahowald et al., 2005). We have followed the approach of other workers with regards to the partition of individual species between coarse and fine mode particles (Spokes et al., 2000; Baker et al., 2003):

- Fe / Al — 100% coarse mode
- PO_4^{3-} — 40% coarse mode
- NO_3^- — 85% coarse mode
- NH_4^+ — 30% coarse mode

Table 6.4 shows the calculated dry deposition of soluble Al, Fe, inorganic N and P. There is about a two-fold enhancement in the flux of Fe, Al and P at the CVAO in

winter (Oct – Mar) in comparison with summer fluxes (Apr – Sep), whereas N deposition fluxes are similar in the two periods. There is also cleardifference in soluble Al, Fe and P fluxes between the shipboard (D326) values and the CVAO values from the same period (Jan 08). Again, soluble N inputs are broadly similar at the CVAO in January 2008 and during cruise D326.

Table 6.4 Mean dry deposition fluxes and elemental ratios for soluble Al, Fe, N and P determined from ultrapure water leach extracts of samples collected at the CVAO and during cruise D326.

CVAO:	Al $\mu mol.m^{-2}.d^{-1}$	Fe $\mu mol.m^{-2}.d^{-1}$	$NO_3^- + NH_4^+$ $\mu mol.m^{-2}.d^{-1}$	PO_4^{3-} $\mu mol.m^{-2}.d^{-1}$	Fe:N	Fe:P	N:P
Apr – Sep	1.8 ± 1.7	0.64 ± 0.62	36 ± 14	0.14 ± 0.14	0.018	4.6	256
Oct – Mar	3.4 ± 3.0	1.1 ± 1.0	35 ± 19	0.25 ± 0.23	0.032	4.4	138
Jul 07 – Jul 08	2.5 ± 2.5	0.86 ± 0.85	35 ± 19	0.25 ± 0.23	0.024	4.4	183
CVAO Jan 08	4.4 ± 1.8	1.3 ± 0.6	39 ± 16	0.25 ± 0.08	0.032	5.0	157
D326 Jan/Feb 08	30 ± 26	9.5 ± 8.1	32 ± 18	0.48 ±0.41	0.298	20	66

Elemental ratios in the fluxes can be compared with the Redfield ratios (Ho et al., 2003) to provide an initial comparison of the relative balance of nutrient inputs with the requirements of phytoplankton. Observed Fe:N and Fe:P ratios in the atmospheric deposition fluxes are all significantly higher than Redfield ratios (0.0005 - Fe:N; 0.0075 - Fe:P – Ho et al. (2003)), with observed N:P ratios also much higher than Redfield (16 – Ho et al. (2003)). These results show that atmospheric nutrient inputs are enriched in Fe and depleted in P relative to biological requirements. Nitrogen inputs are also enriched, although not to the same level as Fe. This relative enrichment of atmospheric Fe and N has also been observed by others working in this ocean region (Duarte et al., 2006; Baker et al., 2007), and has important consequences for diazotrophy in the study region (Mather et al., 2008; Moore et al., 2009).

In a recent article by Baker et al. (2010) dry deposition nutrient fluxes for our study area are reported. Based on ship-board measurements taken during longitudinal surveys of the Atlantic Ocean over several years they estimate dry deposition fluxes of inorganic nitrogen and soluble phosphorus to the tropical eastern North Atlantic to be 18 and 0.015 $\mu mol.m^{-2}.d^{-1}$, respectively. For the inorganic nitrogen flux, this is a two-fold difference, although still within the margins of error for the two

estimates. However for phosphate, the calculated flux by Baker et al. is an order of magnitude lower than the values listed in Table 6.4.

There appear to be two causes for this discrepancy. First, the average atmospheric phosphate concentrations reported by Baker et al. for the tropical eastern North Atlantic (0.06 nmol.m^{-3}) are around a third of the mean concentration measured at CVAO in Table 6.1 (0.18 nmol.m^{-3}). This difference could be explained by the much larger area represented by the average values used by Baker et al; average dust concentrations may diminish rapidly with distance from the coast resulting in lower mean values. Also, the measurements by Baker et al. may suffer from under-sampling. In their study, they include data from 6 cruises that passed through the study region during a 6-year period. Given the highly variable nature of atmospheric aerosol concentrations, this is unlikely to be sufficient sampling resolution to produce an accurate estimate of average atmospheric concentrations of soluble phosphorus.

The second cause for the discrepancy appears to be the deposition velocity values used. Baker et al. (2010) calculate dry deposition using a model which incorporates wind speed and the effect of relative humidity on particle growth. They report that their calculated deposition velocities fall in the range v_d^c = 0.0002 – 0.0003 m.s^{-1} and v_d^f = 0.006 – 0.012 m.s^{-1}, much lower than the estimated values used in this work (v_d^c = 0.02 m.s^{-1} and v_c^f = 0.001 m.s^{-1}). Using the mean atmospheric concentration from Baker et al. (0.06 nmol/m^3) and the higher deposition values give a flux estimate of 0.05 µmol.m^{-2}.d^{-1}, which is significantly closer to the value in Table 6.4.

This example highlights the huge uncertainty in calculating aerosol deposition fluxes, not just in terms of spatial and temporal coverage, but also from the huge uncertainty in the true deposition velocity. Values calculated from a model are likely to yield more accurate results than the simple approach used above. However calculating accurate deposition velocities is not trivial and requires detailed knowledge of particle size characteristics which is not available for this dataset (Baker et al., 2010).

6.7 Discussion

The quantification of atmospheric nutrient inputs into the oceans is limited by both a lack of measurements and a lack of understanding of the fundamental processes which affect aerosol solubility (Baker and Croot, 2010; Baker et al., 2010). The aerosol solubility measurements reported in this chapter represent a significant step towards addressing the paucity of measurement data in the tropical eastern North Atlantic, one of the most dust-affected ocean regions in the world. It also makes steps towards a better understanding of the factors that control dissolution due to the large number of measurements made over an entire seasonal cycle and the wide range of aerosol composition and concentration that has been sampled.

As discussed in Section 6.2, there is no perfect method for the measurement of aerosol dissolution and when choosing a technique compromises have to be made according to the research aims. In this chapter an assessment was made of some of the main drawbacks of the method chosen for this work, which will be a useful reference for future comparisons of solubility measurements made using ultrapure water leaches. The principal limitation of the ultrapure water leach procedure used in this research is the lack of buffering capacity of the dissolution medium. This experimental limitation appears to have resulted in reduced solubility of the material on a few of the most heavily laden filters due to carbonate dissolution (see Figure 6.8). Another limitation is that, due to local saturation effects, the labile fraction of less soluble aerosol components, such as Al and Fe, is not completely released by passing 100 ml of purified water through the sample (see Section 6.3.3). However, despite these limitations, an identical procedure was used for almost 200 samples, and this enables useful comparisons of aerosol solubility for a broad range of samples. In addition, the use of water as a dissolution medium enables the measurement of a wide range of species, which would otherwise be very time consuming and challenging.

In comparing solubility ultrapure water with seawater we attempted to address a key issue in relating solubility measurements to dissolved concentrations measured in the ocean, a problem that is particularly relevant when dry deposition is being

considered (Ridame and Guieu, 2002). There is relatively good agreement between concentrations measured in the two media for more soluble species such as NO_3^- and NH_4^+; however, for less soluble species such as Fe and Al, measured seawater concentrations are significantly lower than the corresponding pure water concentrations (see Figure 6.9). These results are similar to findings by Chen et al. (2006), who found an order of magnitude decrease in the solubility of Fe in seawater relative to pure water, but roughly similar concentrations of inorganic N obtained with both dissolution media. In contrast, Buck et al. (2006; 2010) found much smaller differences when comparing seawater and pure water dissolution. One possibility for this difference is due to differences in the properties of the seawater used. Fresh surface seawater was used by Buck et al., while stored surface seawater was used for the study by Chen et al. and in the work described in this chapter. Differences in the organic metal binding ligands present in the seawater are very likely and could conceivably lead to differences in observed solubility. Another explanation, and one which seems more plausible given the large discrepancies between the reported relationships, is due to the Fe concentrations measured. Fe released in the majority of samples measured by Buck et al. (2006; 2010) corresponded to atmospheric concentrations of < 0.2 $nmol.m^{-3}$, whereas in this work the corresponding values were up to 1.4 $nmol.m^{-3}$ and in the results reported by Chen et al. (2006) up to 1.2 $nmol.m^{-3}$. The presence of much higher quantities of Fe may accentuate the observed differences in solubility between seawater and ultrapure water.

One striking feature of our dataset is the strong inverse relationship between the soluble fraction measured and total Al that was observed for every species measured (see Figure 6.5). This is a ubiquitous feature present in virtually all aerosol datasets, and implies that the strongest control on the soluble fraction of aerosol particles is the concentration of the particles themselves. There is considerable debate in the literature as to the possible cause of this with three principal theories attributing it to either (a) a decrease in particle size associated with lower particle concentrations (Baker and Jickells, 2006), (b) an increasing proportion of more soluble anthropogenic particles present at low particle concentrations (Sholkovitz et

al., 2009), or (c) a shift in mineralogy to a higher proportion of more soluble minerals as particle concentrations decrease (Glaccum and Prospero, 1980; Journet et al., 2008). It is very difficult to determine which of these processes is the most important, since all three are likely to occur together. Our dataset does not yield much light on this since particle sizes were not measured and mineralogy data is not yet available. It has been suggested that V/Al ratios (as a proxy for the relative proportion of anthropogenic Fe in the sample) can be used to predict Fe solubility (Sholkovitz et al., 2009). No such relationship was found in our data (see Figure 6.12), but this neither proves nor disproves that anthropogenic Fe is the cause of the inverse solubility relationship since high V/Al ratios correspond to low total Al concentrations and vice versa.

A strong relationship between the concentration of dissolved Fe and Al was observed in the dissolution experiments using ultrapure water (see Figure 6.6). The soluble Fe/Al mass ratio (0.69) is higher than in the bulk material (0.51), reflecting a higher solubility of Fe relative to Al. It is possible that this relationship could result from un-dissolved particles passing through the 0.4 µm filter pores; however the low solubility values for of Ti (mean value 1%) suggests that this was not occurring to any significant extent. Further investigation is required to determine the cause of this relationship, which mineral(s) are involved and whether a similar relationship can be found in seawater. Dissolved Al concentrations in the ocean are a useful tracer of mineral dust inputs, since Al is not actively taken up by organisms (Measures and Brown, 1996). If a relationship between dissolved Al concentrations and aerosol-derived soluble Fe inputs to the ocean, it would represent a significant step forwards.

A major benefit of using ICP-MS analysis with aerosol solubility experiments is the ability to compare the solubility of a broad range of elements (Table 6.2). A basic analysis of their relative solubility appears to indicate that the primary factor affecting the relative solubility of the elements is their intrinsic chemical properties. Aerosol source also seems to play a role, with elements identified from a PCA analysis (See section 6.3.5) as having a non-crustal (presumably anthropogenic) source – Zn, Pb, V, Ni and Cu – all showing relatively high solubility.

This continuous 12-month dataset allows us to estimate mean atmospheric concentrations for a wide variety of biologically important species with much more accuracy than was previously possible. Conversion of these numbers to deposition fluxes, however, involves a lot of uncertainty. Comparison of the deposition fluxes with those derived by Baker et al. (2010) illustrates that, for any given atmospheric concentration of soluble phosphorus, the use of their calculated deposition velocities compared with the values used in this thesis results in flux estimates that differ by more than a factor of three. This demonstrates that caution should be exercised when using assumed values for the deposition velocity, as has been done in this thesis. Although detailed particle size information would be required for the most accurate estimates of the deposition velocity, our flux estimates can probably be improved by the use of a model incorporating wind speed data and other meteorology and an assumed particle size distribution in an analogous manner to Baker et al. (2010). Such work is necessary in order to obtain more reliable flux estimates and to construct a nutrient budget for the study area. Despite these issues, the calculated deposition fluxes show that the material is greatly enriched in Fe relative to P, in comparison with biological requirements. This relative enrichment has important consequences for nitrogen fixation and nutrient limitation in the study region (Mather et al., 2008; Moore et al., 2009).

6.8 Conclusions

Calculations of pH based on the amount of Ca dissolved indicate that for the most dust-laden filters local pH effects significantly lowered the solubility. This appears to result in the large difference between soluble metal concentrations measured during January 2008 at the CVAO and during cruise D326 during the same month. Whilst comparable dust concentrations were measured at both locations, the longer sampling period at the CVAO resulted in more dust on the filters and led to much lower solubility values being measured. The susceptibility of pure water to local pH changes is a limitation of using it as a dissolution medium. Nevertheless, during the rest of the year, total dust concentrations are much lower than in January 2008, so the saturation / pH effect should be less significant.

Multiple leaching of the same filter has shown that for less soluble species, such as Fe, Al and PO_4^{3-}, not all of the labile material is removed in the first 100 ml of leaching solution. The proportion removed decreases as the quantity of material on the filter increases, consistent with the dissolution media becoming saturated as it passes through the filter sample. Since the same quantity of leaching solution has been used throughout, useful comparisons across the dataset are still possible, but for more dust-laden samples soluble Fe concentrations will be reduced somewhat relative to soluble Fe concentrations from samples collected during less dusty periods.

A limited comparison of the ultrapure water leaches with seawater leaches demonstrated significant differences between the two, with the former showing higher levels of dissolution for nutrients and Fe. The difference was greatest for Fe, where solubility was approximately three times higher in ultrapure water, presumably because of the higher pH of seawater relative to pure water.

Overall, the dataset shows the same cycle in soluble trace metals as the total dust discussed in Chapter 5, although the seasonal difference is less. There is a high degree of correlation between soluble PO_4^{3-}, Fe and Al in the leach solutions, consistent with them sharing the same. PCA reveals more detailed information about correlations between the various species measured in the leach extracts, with three components representing the bulk of the variability within the dataset. These components have clear crustal, anthropogenic and marine influences. Estimates of dry deposition fluxes show that dust inputs supply relatively little P in comparison with Fe and inorganic nitrogen.

6.9 References

Aguilar-Islas, A. M., et al. (2010). Dissolution of aerosol-derived iron in seawater: Leach solution chemistry, aerosol type, and colloidal iron fraction. *Marine Chemistry* 120(1-4): 25-33.

Baker, A. R., et al. (2003). Atmospheric deposition of nutrients to the Atlantic Ocean. *Geophysical Research Letters* 30(24).

Baker, A. R. and Jickells, T. D. (2006). Mineral particle size as a control on aerosol iron solubility. *Geophysical Research Letters* 33(17).

Baker, A. R., et al. (2006a). Nutrients in atmospheric aerosol particles along the Atlantic Meridional Transect. *Deep Sea Research Part II: Topical Studies in Oceanography* 53(14-16): 1706-1719.

Baker, A. R., et al. (2006b). Trends in the solubility of iron, aluminium, manganese and phosphorus in aerosol collected over the Atlantic Ocean. *Marine Chemistry* 98(1): 43-58.

Baker, A. R., et al. (2007). Dry and wet deposition of nutrients from the tropical Atlantic atmosphere: Links to primary productivity and nitrogen fixation. *Deep Sea Research Part I: Oceanographic Research Papers* 54(10): 1704-1720.

Baker, A. R. and Croot, P. L. (2010). Atmospheric and marine controls on aerosol iron solubility in seawater. *Marine Chemistry* 120(1-4): 4-13.

Baker, A. R., et al. (2010). Estimation of atmospheric nutrient inputs to the Atlantic Ocean from 50°N to 50°S based on large-scale field sampling: Fixed nitrogen and dry deposition of phosphorus. *Global Biogeochemical Cycles* 24(3).

Barriada, J. L., et al. (2007). Dissolved silver measurements in seawater. *TrAC Trends in Analytical Chemistry* 26(8): 809-817.

Bonnet, S. and Guieu, C. (2004). Dissolution of atmospheric iron in seawater. *Geophysical Research Letters* 31(3).

Buck, C. S., et al. (2006). Aerosol iron and aluminium solubility in the northwest Pacific Ocean: Results from the 2002 IOC cruise. *Geochemistry Geophysics Geosystems* 7(4): Q04M07.

Buck, C. S., et al. (2010). The solubility and deposition of aerosol Fe and other trace elements in the North Atlantic Ocean: Observations from the A16N CLIVAR/CO2 repeat hydrography section. *Marine Chemistry* 120(1-4): 57-70.

Canepari, S., et al. (2010). Comparison of extracting solutions for elemental fractionation in airborne particulate matter. *Talanta* 82(2): 834-844.

Chen, Y., et al. (2006). Comparison between pure-water- and seawater-soluble nutrient concentrations of aerosols from the Gulf of Aqaba. *Marine Chemistry* 101(1-2): 141-152.

Duarte, C. M., et al. (2006). Aerosol inputs enhance new production in the subtropical northeast Atlantic. *Journal of Geophysical Research-Biogeosciences* 111(G4).

Duce, R. A., et al. (1991). The atmospheric input of trace species to the world ocean. *Global Biogeochem. Cycles* 5(3): 193-259.

Duce, R. A., et al. (2008). Impacts of Atmospheric Anthropogenic Nitrogen on the Open Ocean. *Science* 320(5878): 893-897.

Glaccum, R. A. and Prospero, J. M. (1980). Saharan aerosols over the tropical North Atlantic -- Mineralogy. *Marine Geology* 37(3-4): 295-321.

Guieu, C., et al. (2002). Chemical characterization of the Saharan dust end-member: Some biogeochemical implications for the western Mediterranean Sea. *Journal of Geophysical Research* 107.

Hand, J. L., et al. (2004). Estimates of atmospheric-processed soluble iron from observations and a global mineral aerosol model: Biogeochemical implications. *Journal of Geophysical Research-Atmospheres* 109(D17).

Ho, T. Y., et al. (2003). The elemental composition of some marine phytoplankton. *Journal of Phycology* 39(6): 1145-1159.

Jickells, T. D., et al. (2005). Global Iron Connections Between Desert Dust, Ocean Biogeochemistry, and Climate. *Science* 308(5718): 67 - 71.

Journet, E., et al. (2008). Mineralogy as a critical factor of dust iron solubility. *Geophysical Research Letters* 35(7): 5.

Mahowald, N. M., et al. (2005). Atmospheric global dust cycle and iron inputs to the ocean. *Global Biogeochemical Cycles* 19(4).

Mather, R. L., et al. (2008). Phosphorus cycling in the North and South Atlantic Ocean subtropical gyres. *Nature Geosci* 1(7): 439-443.

Measures, C. I. and Brown, E. T. (1996). Estimating dust input to the Atlantic Ocean using surface water aluminium concentrations.in: *The impact of desert dust across the Mediterranean*. S. Guerzoni and R. Chester. Netherlands, Kluwer Academic Publishers**:** 301-311.

Millero, F. J. and Sohn, M. L. (1992). Chemical Oceanography. Boca Raton, CRC Press.

Moore, C. M., et al. (2009). Large-scale distribution of Atlantic nitrogen fixation controlled by iron availability. *Nature Geoscience* 2(12): 867-871.

Ridame, C. and Guieu, C. (2002). Saharan input of phosphate to the oligotrophic water of the open western Mediterranean Sea. *Limnology and Oceanography* 47(3): 856-869.

Sholkovitz, E. R., et al. (2009). Influence of anthropogenic combustion emissions on the deposition of soluble aerosol iron to the ocean: Empirical estimates for island sites in the North Atlantic. *Geochimica Et Cosmochimica Acta* 73(14): 3981-4003.

Singer, A., et al. (2004). Properties of the non-soluble fractions of suspended dust over the Dead Sea. *Atmospheric Environment* 38(12): 1745-1753.

Spokes, L. J. and Jickells, T. D. (1995). Factors controlling the solubility of aerosol trace metals in the atmosphere and on mixing into seawater. *Aquatic Geochemistry* 1(4): 355-374.

Spokes, L. J., et al. (2000). Nitrogen deposition to the eastern Atlantic Ocean. The importance of south-easterly flow. *Tellus B* 52(1): 37-49.

Trapp, J. M., et al. (2010). Temporal variability of the elemental composition of African dust measured in trade wind aerosols at Barbados and Miami. *Marine Chemistry* 120(1-4): 71-82.

Wagener, T., et al. (2008). Dust iron dissolution in seawater: Results from a one-year time-series in the Mediterranean Sea. *Geophysical Research Letters* 35(16): 6.

Wu, J., et al. (2001). Soluble and Colloidal Iron in the Oligotrophic North Atlantic and North Pacific. *Science* 293(5531): 847-849.

Wu, J., et al. (2007). Dissolution of aerosol iron in the surface waters of the North Pacific and North Atlantic oceans as determined by a semicontinuous flow-through reactor method. *Global Biogeochemical Cycles* 21(4).

7. Conclusions and future directions

7.1 Overview

In order to assess the influence of aerosol derived nutrients on marine biogeochemical cycling it is necessary to bring together several scientific disciplines: geochemistry and meteorology to assess atmospheric particle sources, composition and transport; atmospheric chemistry and physics to understand how the properties of the particles are altered with transport; and chemical and biological oceanography to assess the fate of the particles once deposited to the oceans and to evaluate their importance relative to other sources of nutrients. The work presented in this thesis has focussed on two of these areas. Chapters 3 and 4 concerned the measurement nanomolar concentrations of nutrients; precise and highly sensitive measurements of nutrients are essential to understand nutrient cycling and assess the importance of aerosol inputs in ocean regions where surface nutrient concentrations are well below conventional limits of detection. In Chapters 5 and 6 we have presented an extensive dataset of aerosol composition and solubility measurements over the (sub)tropical North Atlantic Ocean, comprising one year of sample collection at the CVAO and samples collected during a four-week research cruise in the (sub-) tropical North Atlantic Ocean.

7.1.1 Nanomolar nutrient analysis

Nanomolar nutrient analysis is a relatively new capability for chemical oceanographers and the adoption of analytical systems with this capability is only beginning to enter mainstream activities. Chapter 3 presented a review of past and current used techniques for nitrate and phosphate analysis at nanomolar concentrations in seawater, highlighting the various approaches available and their relative drawbacks and merits. It has been published as a topical review in *Trends in Analytical Chemistry* (Patey et al., 2008). It was the first review of its kind and it is

anticipated that it will prove a useful overview for researchers looking to develop or acquire new instruments for laboratory or field-based use.

In our laboratory we have developed our own system for the simultaneous measurement of nitrate and phosphate with sub-nanomolar detection limits. This system has been used during two research cruises in the study area, generating high quality surface water nutrient data in an ocean region where, until recently, precise nutrient concentrations could not be measured.

In Chapter 4 we highlighted a number of analytical challenges associated with the measurement of nutrients at such low concentrations. Some of these are obvious, such as sample contamination, and others which are not immediately apparent and can easily be overlooked since many measurement artefacts and interferences have in the past been neglected as they are often negligible at the higher analyte concentrations that are routinely analysed with conventional instrumentation. At low concentrations the limitations of chemical methods of analysis become more apparent; in particular the overestimation of orthophosphate concentrations by the phospho-molybdenum blue technique can be very significant. Hydrolysis of organic P compounds and pyrophosphate present in natural waters, add to the SRP signal. In addition, arsenate and dissolved Si also form coloured molybdate complexes. For Si, we have determined that the interference is not significant in our study region, where $Si(OH)_4$ concentrations are relatively low; however, this may not be the case in all oceanographic environments. Arsenate interference was determined to be more significant in our study regions, with a 20 nM background concentration of AsO_4^{3-} resulting in a calculated increase in the measured SRP signal of ~5%. Due to the slow formation of the arsenomolybdic complex, it appears that the length of period between reagent addition and colourimetric analysis is a key parameter in reducing interference and this fact will be useful when designing any new system for nanomolar PO_4^{3-} analysis.

We have also reported preliminary investigations into the stability of samples containing nanomolar concentrations of nutrients and into the small, yet significant differences in observed concentrations as a result of sample filtration. To our

knowledge this is the first comprehensive investigation into interferences of this nature. It is hoped that its publication (Patey et al., 2010) will raise awareness of some of the issues with working at this concentration and will be of use to others designing new analytical systems.

7.1.2 Aerosol collection and analysis

Satellite observations provide unequalled temporal and spatial coverage of atmospheric particle transport. However, it is difficult to retrieve quantitative information from these observations, such as aerosol concentrations, composition and deposition rates, or at what height in the atmosphere the particles are being transported. There is a pressing need for more direct measurements of aerosols in remote ocean regions in order to complement satellite data and to help the modelling community to constrain their aerosol deposition models. Much of our knowledge of aerosols over the North Atlantic comes from just a few long-term monitoring stations, such as in Barbados and Miami (e.g. Prospero and Lamb, 2003), the Canary Islands (e.g. Neuer et al., 2004), occasional studies on the Cape Verde Islands (e.g. Chiapello et al., 1995) and data from various cruises which have taken place at various times of the year.

The dataset presented in this thesis represents one of very few sets of measurements covering a seasonal cycle in the tropical North Atlantic, including information on aerosol solubility. As such it is anticipated that it will be of great use to researchers aiming to model fluxes of aerosol-derived metals and nutrients to the ocean in this region.

Some issues were encountered with the solubility experiments. The ultrapure water leaching protocol used to investigate solubility was susceptible to over saturation and/or local pH fluctuations as a result of carbonate dissolution. Overall this resulted in a significant reduction of the amount of dissolution, particularly on the most heavily laden filters. It appeared to lead to a large discrepancy between the calculated solubility observed with samples collected during the research cruise (D326) and samples collected at the same time at the CVAO. The two sets of

samples appeared at least chemically similar, but XRD results should follow shortly and help to confirm to whether this is indeed the case.

Using our data, it was possible to examine seasonal patterns in concentrations of soluble nutrients and approximate fluxes to the oceans. A clear seasonal difference was observed for soluble Fe and P deposition, which share a predominantly crustal source, while inorganic N, which is mainly anthropogenic in origin, shows no seasonal trend in deposition fluxes. Elemental ratios were compared with the Redfield ratio and indicate that throughout the year soluble nutrient fluxes were comparatively rich in Fe, depleted in N and strongly depleted in P.

7.2 Future directions

7.2.1 Nanomolar nutrient analysis

Work in the field of nanomolar nutrient analysis is shifting from the development of bench-top systems towards miniaturised, in-situ instruments suitable for deployment in the oceans. Looking further ahead, the ultimate aim is a fully automated, self-contained instrument that can be left attached to a buoy or floating in the ocean for months at a time. There will however be significant challenges to overcome before this goal is reached. Apart from the engineering difficulties associated with creating a miniaturised, pressure-resistant, fully automated device that is efficient with power and reagents, there is the issue of bio-fouling, and the problem of calibration stability.

There is still no international reference standard for nanomolar nutrients due to poor solution stability. The forthcoming GEOTRACES programme plans to address this issue. If successful it will be the first laboratory inter-comparison study with nanomolar nutrient analysis techniques and may pave the way for more reliable nutrient measurements.

7.2.2 Aerosol measurements

Through this work, an extensive dataset has been generated and to this date, there has been insufficient time for but a preliminary analysis and overview of the main features of the dataset. There is a great amount of further information that will be obtained both through further analysis and interpretation of the data so far generated and with further analysis of the stored filter samples and digest solutions.

XRD spectra have recently been recorded for 40 filter samples representing every major dust episode and a wide variety of air-mass source regions during the 12-month period at the CVAO and aboard the RRS Discovery during cruise D326. Work is underway to process the spectra to generate quantitative estimates of the relative amounts of minerals present in each sample. This will provide valuable additional information with which to interpret the solubility information.

From the analysis shown in Chapter 5 it seems that the chemical composition signature is mixed between different regions. More specific information on the composition of individual dust events may enable improved comparisons of specific samples in terms of chemical and mineralogical composition and solubility, than the seasonal and other averages which have been presented.

Pb isotopic composition was measured as part of the ICP-MS analysis, the data has not yet been studied in detail. Pb isotopic composition may provide information on sources and relative contribution of anthropogenic pollution to the samples (Véron and Church, 1997), and this information may prove complementary to the techniques providing information on crustal sources. There are also plans to investigate Nd and Sr isotopes in the total acid digests using thermal ionization mass spectrometry (TIMS). This is another tool to provide information on the source and age of rocks contributing to the sample.

Long-term aerosol datasets such as the records at Barbados and Miami, which span over 4 decades, provide a wealth of information about dust transport patterns, seasonal changes, interactions with the climate system and long term trends. If a

similar time-series site at the CVAO were possible it would undoubtedly prove a valuable source of information to the marine and atmospheric science communities and, as time-series stations have done on several occasions, may even reveal something unexpected.

With regards to the measurement of aerosol solubility, it is widely acknowledged that the diversity of experimental methods and dissolution media used by different researchers contributes significantly to the large uncertainty in aerosol solubility, making it hard to compare solubility data from different sources and to draw conclusions about the relative solubility of different aerosol types. Baker and Croot (2010) have suggested that future experiments should be designed to probe atmospheric and oceanic controls on solubility separately. For experiments probing variations in atmospheric partial solubility, a leach procedure using a standardised dissolution medium that is not subject to solubility constraints, such as a buffered ammonium acetate solution could be used. To investigate oceanic controls on aerosol solubility, a standardised set of "aerosol" materials representative of major aerosol sources could be used. Depending on the nature of the experiment, this could be combined with standardised artificial seawater. Such a co-ordinated effort should facilitate not only easier comparison of different datasets, but also help to determine the relative importance of the various controls on solubility.

7.3 Planned publications

At least two articles are planned from the unpublished data presented in Chapters 5 and 6. The first will present the total elemental composition data for the 12-month time-series at the CVAO. It will comprise the general analysis of elemental aerosol composition and variability that was given in Chapter 5 together with the solubility values in Chapter 6. A detailed comparison of the solubility of different species will be included together with phosphate solubility, for which phosphate analysis of the total digestion samples is pending. A detailed analysis of sample composition and relative solubility according to source region will be carried out, including

mineralogy data. Individual dust events will be isolated to look for differences in mineralogy, geochemistry and solubility in relation to different source regions.

The second publication will investigate the biogeochemical significance of aerosol inputs to the tropical eastern North Atlantic Ocean. Using soluble aerosol concentrations measured at the CVAO and during D326, it is possible to calculate deposition fluxes more accurately and for many more species than was previously possible for this region. However, further investigations need to be made into the best way to calculate deposition velocities, as this is a key area of uncertainty in flux calculations. A large amount of surface nanomolar nutrient and dissolved Fe, primary productivity and nitrogen fixation rate measurements are available from two cruises (D326 in January – February 2008 and PO332 in January – February 2006). Using this information it should be possible to construct a nutrient budget for the region during these two months and gain insight into the relative importance of atmospheric nutrient inputs to primary productivity and nitrogen fixation.

7.4 References

Baker, A. R. and Croot, P. L. (2010). Atmospheric and marine controls on aerosol iron solubility in seawater. *Marine Chemistry* 120(1-4): 4-13.

Chiapello, I., et al. (1995). An additional low layer transport of Sahelian and Saharan dust over the North-Eastern Tropical Atlantic. *Geophysical Research Letters* 22(23): 3191 - 3194.

Neuer, S., et al. (2004). Dust deposition pulses to the eastern subtropical North Atlantic gyre: Does ocean's biogeochemistry respond? *Global Biogeochemical Cycles* 18(4).

Patey, M. D., et al. (2008). Determination of nitrate and phosphate in seawater at nanomolar concentrations. *TrAC Trends in Analytical Chemistry* 27(2): 169-182.

Patey, M. D., et al. (2010). Interferences in the analysis of nanomolar concentrations of nitrate and phosphate in oceanic waters. *Analytica Chimica Acta* 673(2): 109-116.

Prospero, J. M. and Lamb, P. J. (2003). African Droughts and Dust Transport to the Caribbean: Climate Change Implications. *Science* 302(5647): 1024-1027.

Véron, A. J. and Church, T. M. (1997). Use of stable lead isotopes and trace metals to characterize air mass sources into the eastern North Atlantic. *Journal of Geophysical Research* 102(D23): 28049-28058.

Appendix I

Determination of nitrate and phosphate in seawater at nanomolar concentrations.

Patey, M. D., M. J. A. Rijkenberg, P. J. Statham, M. C. Stinchcombe, E. P. Achterberg and M. Mowlem

TrAC Trends in Analytical Chemistry, 2008, vol. 27**,** pp 169-182

Appendix II

Interferences in the analysis of nanomolar concentrations of nitrate and phosphate in oceanic waters.

Patey, M. D., E. P. Achterberg, M. J. A. Rijkenberg, P. J. Statham and M. Mowlem

Analytica Chimica Acta, 2010, vol. 673, pp 109-116